http://www.nap.edu/catalog/1992.html

We ship printed books within 1 business day; personal PDFs are available immediately.

Material Fluxes on the Surface of the Earth

Panel on Global Surficial Geofluxes, Board on Earth Sciences and Resources, National Research Council

ISBN: 0-309-56863-3, 190 pages, 8.5 x 11, (1994)

This PDF is available from the National Academies Press at: http://www.nap.edu/catalog/1992.html

Visit the National Academies Press online, the authoritative source for all books from the National Academy of Sciences, the National Academy of Engineering, the Institute of Medicine, and the National Research Council:

- Download hundreds of free books in PDF
- Read thousands of books online for free
- Explore our innovative research tools – try the "Research Dashboard" now!
- Sign up to be notified when new books are published
- Purchase printed books and selected PDF files

Thank you for downloading this PDF. If you have comments, questions or just want more information about the books published by the National Academies Press, you may contact our customer service department toll-free at 888-624-8373, visit us online, or send an email to feedback@nap.edu.

This book plus thousands more are available at http://www.nap.edu.

THE NATIONAL ACADEMIES
Advisers to the Nation on Science, Engineering, and Medicine

i

STUDIES IN GEOPHYSICS

Material Fluxes on the Surface of the Earth

Board on Earth Sciences and Resources
Commission on Geosciences, Environment, and Resources
National Research Council

NATIONAL ACADEMY PRESS
Washington, D.C. 1994

ii

Printed in the United States of America

Panel on Global Surficial Geofluxes

WILLIAM W. HAY, University of Colorado *and* GEOMAR, KIEL, Germany, *Chairman*
JOHN T. ANDREWS, University of Colorado
VICTOR R. BAKER, University of Arizona
JACK DYMOND, Oregon State University
LEE R. KUMP, Pennsylvania State University
ABRAHAM LERMAN, Northwestern University
W. R. MARTIN, Woods Hole Oceanographic Institution
MICHEL MEYBECK, Universite Pierre et Marie Curie
JOHN D. MILLIMAN, Virginia Institute of Marine Studies
DAVID K. REA, University of Michigan
F. L. SAYLES, Woods Hole Oceanographic Institution

Staff

THOMAS M. USSELMAN, Associate Director
JUDITH ESTEP, Administrative Assistant

iv

Geophysics Study Committee[*]

BYRON D. TAPLEY, University of Texas, *Chairman*
RICHARD T. BARBER, Monterey Bay Aquarium Research Institute
ROBIN BRETT, U.S. Geological Survey
RALPH J. CICERONE, University of California, Irvine
RANA A. FINE, University of Miami
LYNN W. GELHAR, Massachusetts Institute of Technology
NORMAN F. NESS, University of Delaware
GEORGE C. REID, National Oceanic and Atmospheric Administration
ROBERT S. YEATS, Oregon State University

Staff

THOMAS M. USSELMAN, Associate Director
JUDITH ESTEP, Administrative Assistant

---

[*] Membership of the Geophysics Study Committee during most of the conduct of the report. The committee is no longer active.

Board on Earth Sciences and Resources

LALLY A. ANDERSON, Staff Assistant
CHARLENE E. ANDERSON, Administrative Assistant
JUDITH ESTEP, Administrative Assistant
SHELLEY MYERS, Project Assistant

Commission on Geosciences, Environment, and Resources

M. GORDON WOLMAN, The Johns Hopkins University, *Chairman*
PATRICK R. ATKINS, Aluminum Company of America
PETER S. EAGLESON, Massachusetts Institute of Technology
EDWARD A. FRIEMAN, Scripps Institution of Oceanography
W. BARCLAY KAMB, California Institute of Technology
JACK E. OLIVER, Cornell University
FRANK L. PARKER, Vanderbilt University
RAYMOND A. PRICE, Queen's University at Kingston
THOMAS C. SCHELLING, University of Maryland
LARRY L. SMARR, University of Illinois at Urbana-Champaign
STEVEN M. STANLEY, The Johns Hopkins University
VICTORIA J. TSCHINKEL, Landers and Parson
WARREN WASHINGTON, National Center for Atmospheric Research
EDITH BROWN WEISS, Georgetown University Law Center

Staff

STEPHEN RATTIEN, Executive Director
STEPHEN D. PARKER, Associate Executive Director
MORGAN GOPNIK, Assistant Executive Director
JEANETTE SPOON, Administrative Officer
SANDI FITZPATRICK, Administrative Associate
ROBIN ALLEN, Senior Project Assistant

Studies in Geophysics *

ENERGY AND CLIMATE
Roger R. Revelle, *panel chairman,* 1977, 158 pp.
ESTUARIES, GEOPHYSICS, AND THE ENVIRONMENT
Charles B. Officer, *panel chairman,* 1977, 127 pp.
CLIMATE, CLIMATIC CHANGE, AND WATER SUPPLY
James R. Wallis, *panel chairman,* 1977, 132 pp.
THE UPPER ATMOSPHERE AND MAGNETOSPHERE
Francis S. Johnson, *panel chairman,* 1977, 168 pp.
GEOPHYSICAL PREDICTIONS
Helmut E. Landsberg, *panel chairman,* 1978, 215 pp.
IMPACT OF TECHNOLOGY ON GEOPHYSICS
Homer E. Newell, *panel chairman,* 1979, 136 pp.
CONTINENTAL TECTONICS
B. Clark Burchfiel, Jack E. Oliver, and Leon T. Silver, *panel co-chairmen,* 1980, 197 pp.
MINERAL RESOURCES: GENETIC UNDERSTANDING FOR PRACTICAL APPLICATIONS
Paul B. Barton, Jr., *panel chairman,* 1981, 119 pp.
SCIENTIFIC BASIS OF WATER-RESOURCE MANAGEMENT
Myron B. Fiering, *panel chairman,* 1982, 127 pp.
SOLAR VARIABILITY, WEATHER, AND CLIMATE
John A. Eddy, *panel chairman,* 1982, 104 pp.
CLIMATE IN EARTH HISTORY
Wolfgang H. Berger and John C. Crowell, *panel cochairmen,* 1982, 198 pp.

---

* Published to date.

FUNDAMENTAL RESEARCH ON ESTUARIES: THE IMPORTANCE OF AN INTERDISCIPLINARY APPROACH
L. Eugene Cronin and Charles B. Officer, *panel co-chairmen,* 1983, 79 pp.
EXPLOSIVE VOLCANISM: INCEPTION, EVOLUTION, AND HAZARDS
Francis R. Boyd, *panel chairman,* 1984, 176 pp.
GROUNDWATER CONTAMINATION
John D. Bredehoeft, *panel chairman,* 1984, 179 pp.
ACTIVE TECTONICS
Robert E. Wallace, *panel chairman,* 1986, 266 pp.
THE EARTH'S ELECTRICAL ENVIRONMENT
E. Philip Krider and Raymond G. Roble, *panel co-chairmen,* 1986, 263 pp.
SEA-LEVEL CHANGE
Roger Revelle, *panel chairman,* 1990, 217 pp.
THE ROLE OF FLUIDS IN CRUSTAL PROCESSES
John D. Bredehoeft and Denis L. Norton, *panel co-chairmen,* 1990, 170 pp.
MATERIAL FLUXES ON THE SURFACE OF THE EARTH
William W. Hay, *panel chairman,* 1994, 192 pp.

Preface

This report is part of a series, *Studies in Geophysics,* that has been carried out over the past 14 years to provide (1) a source of information from the scientific community to aid policymakers in decisions on societal problems that involve geophysics and (2) assessments of emerging research topics within the broad scope of geophysics. An important part of such reports is an evaluation of the adequacy of current geophysical knowledge and the appropriateness of current research programs in addressing needed information.

The study *Material Fluxes on the Surface of the Earth* is designed to report on the state of knowledge of the major fluxes and pathways by which materials are transferred from one site to another on the surface of the earth. The purpose of the study is to

1. present the state of knowledge of modern and late Pleistocene process rates and fluxes, including the last glaciation and during the deglaciation, on a global scale;
2. evaluate the variability inherent in process rates and fluxes in these young geologic times;
3. assess the extent to which modern measurements of fluxes already incorporate anthropogenic effects;
4. express variability of natural processes and fluxes in terms of fluctuations and changes occurring on different time scales;
5. identify gaps in the understanding of the natural variability of surficial processes and material fluxes; and
6. suggest how the natural variability could be incorporated into the baselines of modern processes to be used in models of future change.

The topic was initiated by the Geophysics Study Committee in consultation with the liaison representatives of the federal agencies that support the committee, relevant boards and committees within the National Research Council, and members of the scientific community. While this report was being completed, the Geophysics Study Committee

ceased operations and its parent Board on Earth Sciences and Resources assumed the responsibility for the completion of this report.

The preliminary scientific findings of the authored background chapters were presented at a symposium during the 28th International Geological Congress in July 1989 in Washington, D.C. In completing their chapters, the authors had the benefit of discussions at this symposium as well as the comments of several scientific referees. Ultimate responsibility for the individual chapters, however, rests with the authors.

The Overview of the study summarizes the highlights of the chapters and formulates conclusions and recommendations. In preparing the Overview, the panel chairman had the benefit of meetings that took place at the symposium, comments of the panel, and the comments of scientists, who reviewed the report according to procedures established by the National Research Council's Report Review Committee. Responsibility for the Overview rests with the Board on Earth Sciences and Resources and the chairman.

Contents

Overview

Rapidly occurring changes in the global environment have become a major concern for policymakers and scientists alike. In assessing the nature and course of these changes for the Earth as a system, we need to differentiate between those that can be managed by altering policies, such as control of atmospheric and hydrologic inputs from human activities, and those that represent a progression of natural events, which may not be controllable. Although natural variability is inherent in the system, humans have become a major factor in inducing environmental change. In order to determine the directions and magnitudes of anthropogenic changes, it will be necessary to understand the natural dynamic processes that have brought the environment to its present condition.

The principal conclusion of this study is that a better understanding is necessary of the natural fluxes and pathways by which materials are transferred from one site to another on the surface of the Earth. This knowledge is critical to evaluating the impact of anthropogenic changes. There is a common misconception among the general public and much of the scientific community that processes and fluxes on the surface of the Earth were in a steady state prior to the industrial revolution and that preindustrial rates are well known. It is assumed that the environment has been increasingly perturbed from that base level by human activity. In fact, although there have been major recent efforts to study natural systems, there remain many uncertainties about the base level of surficial processes and fluxes and their natural variability.

Specifically, this study examines the following:

- The state of knowledge of some of the most important processes, rates, and fluxes for Recent, Holocene, and late Pleistocene times;
- the variability inherent in these processes, rates, and fluxes in relatively recent geologic times;
- the extent to which modern measurements of these fluxes already incorporate anthropogenic effects;

- the variability of natural processes and fluxes in terms of fluctuations and changes occurring on different time scales;
- gaps in the understanding of the natural variability of surficial processes and material fluxes; and
- how the natural variability might be incorporated into the modern process "baselines" to be used in models of future change.

This study concentrates on fluxes that move material on the surface of the Earth and are continuous or occur frequently. We have not attempted to evaluate the rate of fluxes of material associated with volcanic eruptions and mass wastage that are discontinuous and are infrequent. We recognize that, in the long term, catastrophic events might have a cumulative impact of the same order of magnitude as the more frequent and continuous processes, but the historical record contains an inadequate sampling of such events. Neither have we attempted to evaluate fluxes of volcanic gases, hydrothermal fluids, or the fluids expelled from sediments along subsection zones. Studies of these fluxes are still in their infancy, and their variability in time and space is poorly known. Preliminary extrapolations indicate that for some materials, these fluxes may be of the same order of magnitude as those from better-known sources.

Although we are concerned primarily with natural fluxes of surficial materials, human influence is important. For example, because of modern agricultural and construction practices, many river particulate loads measured over the past 30 years probably do not reflect natural processes. The storage-transport processes that are important today may not be those important on either shorter or longer time scales. For dissolved materials, humans are already a very effective geologic agent. They increase sources through construction, mining, deforestation, and agricultural activity, including fixation of atmospheric nitrogen. Human activity modifies the sinks for detritus through dam, reservoir, and coastal construction, and for nutrients through the induced eutrophication of lakes. These changes make determination of the roles of natural processes in the modern biogeochemical cycles increasingly difficult.

The natural fluxes of materials on the surface of the Earth are a function of the rates of weathering of rocks and sediments, transport, and deposition. "Weathering" originally referred to the alteration of rocks exposed to atmospheric agents; in recent years it has taken on a broader meaning to include the effects of all processes operating at the interface between the solid earth and the atmosphere, hydrosphere, and cryosphere. Transport is effected by gravity and by moving water, air, or ice. Deposition is a result of gravitational, chemical, or biological processes, or a combination of these processes acting on the transported materials. Weathering is typically very slow; characteristic rates are those of soil formation — on the order of thousands to hundreds of thousands of years. Transport is typically rapid, operating on the scale of minutes to years for gravitational movement, hours to days for eolian transport, days to months for fluvial transport, and decades to millennia for glacial transport. Transport need not be direct from the site of weathering to the site of ultimate deposition, but materials may
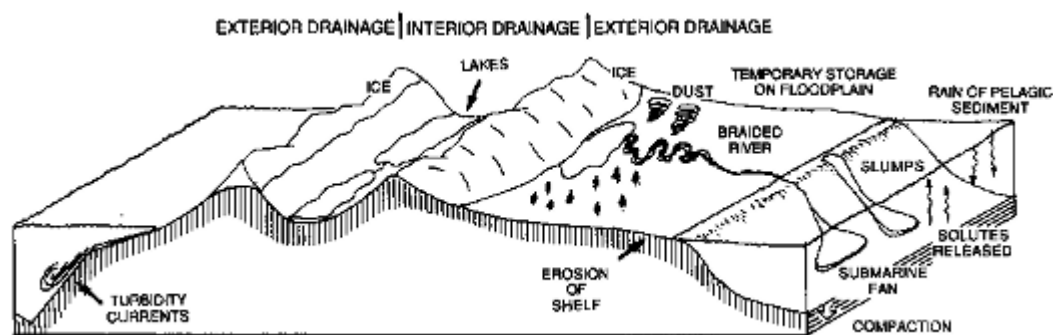
FIGURE 1 Some erosional and depositional environments during a glacial lowstand of sea level.

be stored for indefinite periods along the transport route. Deposition of solid material from air and water is generally rapid, occurring in a matter of hours to days at the depositional site, but ions carried in solution may remain in solution for thousands or even millions of years.
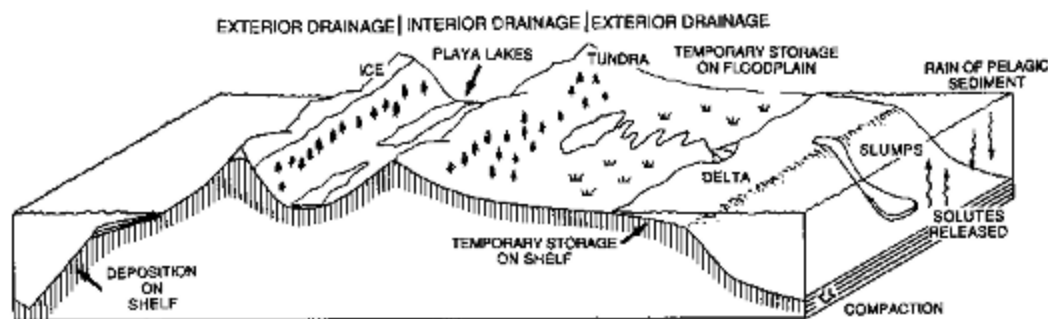
FIGURE 2 Some erosional and depositional environments during an interglacial highstand of sea level.

The processes of weathering, transport, and deposition of sediments and rocks are sensitive to changes in climate, the biological environment, and tectonic activity. Some of the changes that have occurred as a result of a transition from a glacial to an interglacial state are shown in Figures 1 and 2.

The surficial fluxes of ions in solution vary as a function of the volume flows and residence times of water on the continents, areal exposure of different rock types, reaction rates between minerals and the surface-water and groundwater solutions, neutralization of acidity from the atmosphere and that produced within the soil and weathering zone, and temperature. The weathering process also results in the formation of secondary minerals that temporarily store ions. Many of these secondary minerals are sensitive to climate change and may release the stored ions in response to changes in the environment.

KNOWLEDGE OF THE PRESENT FLUX RATES OF GEOLOGIC MATERIALS

The present knowledge of rates of regional and global fluxes of geologic materials is imperfect and uneven, as summarized in Table 1. Estimates of the amounts of material carried by many geologic agents rest on extrapolations of instantaneous fluxes or averages of long-term deposition rates. These may or may not be representative of the transport system. Regular monitoring of river loads is carried out in a few countries, but for many rivers, the seasonal and interannual variability is not well known (see Milliman and Syvitski, Chapter 5, this volume). Estimates of global flux and process rates rely on incomplete observations made mostly in small, intensively studied regions, and on measurements made at isolated stations on land or at sea. Satellite observations have the potential to contribute greatly to our knowledge of the present distribution of rocks and sediments on the land surface, of eolian fluxes, and of the utilization of nutrients in the photic zone. Fluxes within lakes, estuaries, seas, and the ocean are more difficult to estimate because of problems inherent in observation and measurement. In the tropics and subtropics, the major episodes of sediment transport in large bodies of water are sporadic. They are often associated with large storms, and maximum transport occurs when observation and measurement are most difficult. In polar regions, the major meltwater flux of the spring-summer transition transports sediment at a time when direct observations are difficult because of lake- and sea-ice cover. Most glacial transport occurs beneath hundreds or thousands of meters of ice, precluding direct observation.

Some of the ions apparently transported from land to sea are from salt that entered the atmosphere over the ocean and was subsequently washed out by rainfall over land. The quantity of this recycled salt must be determined and subtracted from the apparent land-to-sea flux in order to estimate accurately the net transport of material to the sea.

TABLE 1 State of Knowledge of Present Day Fluxes

Relatively well known
River fluxes — major elements, organic carbon, nutrients
Less well known
River fluxes — particulate material and its chemical composition
Storage of dissolved material in lake systems ($CaCO_3$, SiO_2, etc.)
Storage of material in endorheic regions (Asia)
Water budget of glaciers
Sources of eolian material
Chemical composition of eolian material
Not well known
Changes in dissolved or particulate fluxes with distance from source
Chemical and physical controls of dissolved and particulate fluxes
River fluxes — fate of dissolved material and trace inorganic constituents at continent-ocean boundary
Eolian fluxes
Leaching from fresh lava
Flux of volcanic ash to the atmosphere
Fluxes from volcanic and hydrothermal areas on land (water, CO_2, SO_2, etc.)
Diagenetic fluxes in terms of sediment types and accumulation rates
Hydrothermal fluxes in the deep sea
Silica budget in the ocean
Not known
River fluxes — storage of particulate materials and trace organic constituents on land, slopes, floodplains, etc., on a global scale
Sediment budget of glaciers on a global scale
Effect of dissolution of glacially produced rock flour as it is transported to the ocean
Groundwater fluxes
Fluxes from nonchannelized runoff

Rivers are the major natural transport mechanism responsible for moving detritus and dissolved solids on the land surface of the Earth. The dissolved load of rivers is dependent on the nature of the sediments and rocks underlying the drainage basin (see Meybeck, Chapter 4, this volume). The organic carbon and fixed nitrogen carried by rivers are related to the vegetation and climate. The solid load of the rivers is a function of relief, climate, and geology of the drainage basin. Variability is a characteristic of rivers; the global ratio of solid to dissolved load is about 4 to 1, but among major rivers it ranges from 80 to 0.1. The fluvial transport system has potential for great variations in response to climate change.

In most instances, measurement of fluxes associated with rivers did not begin until after human activities had modified the landscape, so that the primeval natural fluxes are not known. Even large rivers can be perturbed by large-scale agriculture, impoundment, and associated urbanization. Where these have not occurred, rivers may be in their natural state. Thus, the Amazon, Orinoco, Zaire, Yukon, and MacKenzie rivers along with many Siberian rivers may still be representative of the natural state. Most subtropical and temperate rivers have been significantly perturbed by anthropogenic activity. Indeed, human activities may have altered so many natural conditions that their effect pervades all aspects of material flux.

The alteration of sediment on the ocean floor through reaction with ocean bottom water and with pore waters results in fluxes both into and out of the sediment. The global scale of these fluxes and the time scales on which they may change are only beginning to be understood. Martin and Sayles (Chapter 10, this volume) present a review of the current state of knowledge of these important processes and associated fluxes.
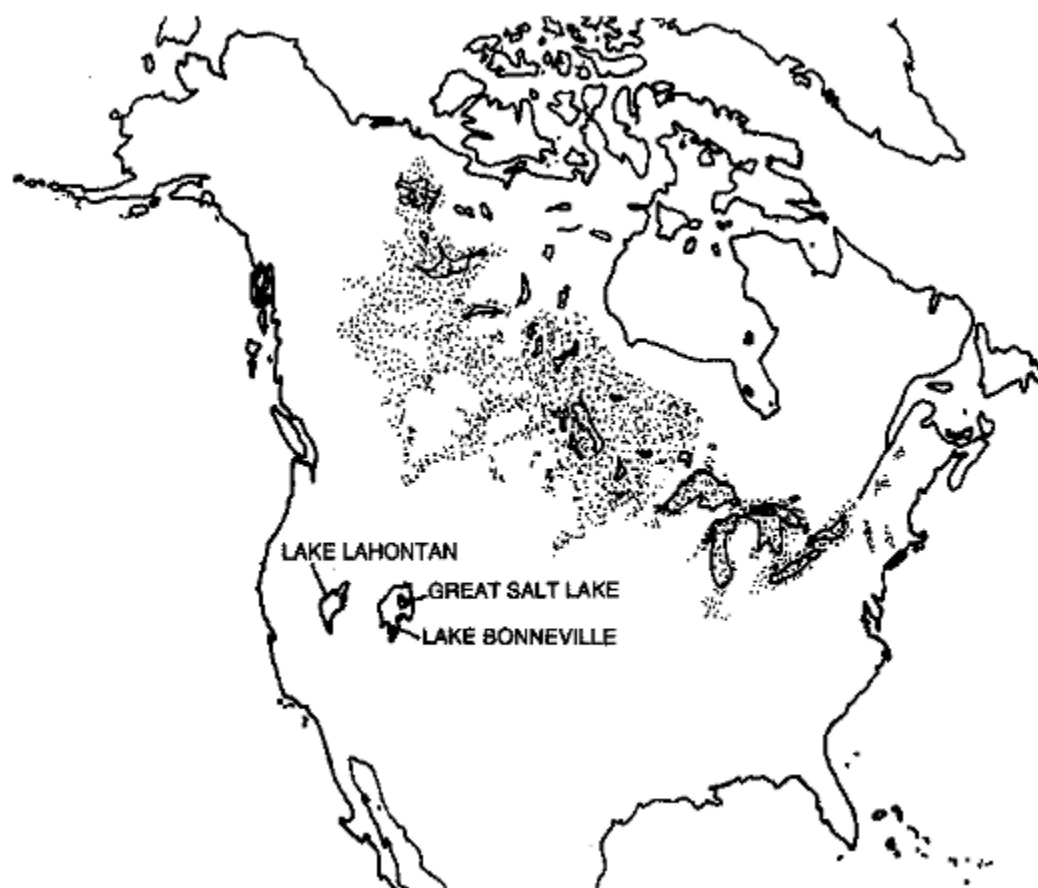
FIGURE 3 Modern lakes occupying basins excavated or dammed by drift left by the Laurentide Ice Sheet. Dots represent the presence of lacustrine sediments, indicating the extent of former glacial lakes (after Teller, 1987). Lakes Bonneville and Lahontan filled basins that presently have only interior drainage. The present Great Salt Lake is shown within the outline of Lake Bonneville.

RATES OF FLUX OF GEOLOGIC MATERIALS DURING THE MOST RECENT GLACIATION AND DEGLACIATION

The past 20,000 years have seen drastic changes in the face of the Earth. At the height of the most recent ice age, continental ice sheets similar to those of Antarctica and Greenland covered much of North America and northern Eurasia. Extensive periglacial areas were cold deserts, largely free of vegetation cover, and supplied more dust for transport by the winds than is available today. The melting continental glaciers left behind a landscape of scattered swales and depressions, many of which are filled by lakes (Figure 3). The large number of fresh water lakes in northern latitudes today is an unusual condition inherited from the erosional and depositional activity of the Pleistocene ice sheets and the effects of permafrost.

During deglaciation, between ca. 17,000 and 6000 years ago, rivers draining the glaciated regions carried the extra water and sediment supplied by the melting glaciers, as well as their regular loads (Teller, 1987). At the glacial maximum, sea level was 100 to 130 m lower than it is today; most of the transgression took place in 10,000 years, so that the sea level rise occurred at an average rate of about 1 cm/yr. Sea level, however, did not rise at a constant rate (Geophysics Study Committee, 1990). During the most rapid phases of deglaciation, sea level may have risen several meters per century, and the large volumes of fresh water entering the ocean may have affected climate and deep ocean circulation (Fairbanks, 1989). The effect of the sea-level rise has been to flood the nonglaciated continental margins, creating a fringe of estuaries and lagoons along many shores. These special shores provide a wide variety of habitats and a rich nutrient supply, and conse

quently are especially abundant in marine life. Sediments are being trapped in the estuaries and are rapidly filling them, continually changing the nature of the coastal environment.

At present, the annual global runoff from land is equivalent to a layer of water about 10 cm thick spread over the entire ocean. The incremental flux of water resulting from the melting of the ice sheets was not distributed uniformly to the world's rivers, but was concentrated in those draining eastern North America and northern Eurasia. Their flow must have increased severalfold.

The glaciated continental margins now have highly indented coastline systems of fjords, inlets, islands, shoals, and deep continental shelves. The conditions within the glaciated coastlines of the Arctic and Antarctic are highly complex and are only now beginning to be understood. Andrews and Syvitski (Chapter 7, this volume) discuss sediment fluxes along high-latitude glaciated continental margins. Sediment accumulation and oceanographic conditions within the fjords are very different from those of the open ocean and contrast with conditions on temperate and tropical continental shelves. Furthermore, there are great contrasts between different glaciologic regimes so that within these, the fluxes to the seabed vary by at least three orders of magnitude.

During the sea-level fall that accompanied the growth of Northern Hemisphere ice sheets, the continental shelves beyond the ice margins were exposed to erosion, and large masses of sediment were transported downslope to the base of the continental rise and onto the abyssal plains. On glaciated shelves, the advance of the ice onto the shelf also shifted the locus of deposition toward the continental slope. The thick sediment wedges on the continental margins have been undergoing compaction, and as the pore fluids are squeezed out, they carry a variety of solutes with them into the deep waters of the oceans (Han and Suess, 1989; Suess and Whiticar, 1989).

Kump and Alley (Chapter 3, this volume) analyze the changes in areas where different materials are exposed to weathering and changes in rates of chemical weathering processes. They conclude that in spite of these radical changes in climate and landscape, the flux of dissolved material from land to sea 18,000 years ago may have been similar to that today, although possibly with a significant increase during deglaciation. Analysis of sedimentation rates in many parts of the world suggests that the supply of material to the deep sea during the most recent glacial age was about four times the rate during the Holocene (see Hay, Chapter 1, this volume). Much of this difference is due to increased delivery of solid terrigenous sediment to the ocean, but even the rain of biogenic materials was greater during glacial times, possibly as a result of the changes in the rates of ocean mixing and nutrient resupply to the photic zone.

Subaerial exposure and subsequent flooding of the continental shelves affected the sites of $CaCO_3$ deposition and had a major effect on the global carbonate budget (Milliman, 1993). Although the data are poorer, no such glacial-interglacial variation is seen in the biogenic silica budget.

Although most of the change of sedimentary fluxes over the past 20,000 years has been attributed to the glaciation and deglaciation, it is possible that other climatic changes may be responsible. Kutzbach (1981) and Kutzbach and Guetter (1988) have shown that the precession cycle has a significant effect on tropical and subtropical climate, particularly in the northern Indian Ocean-southern Asia region. The precession of the perihelion brings the Earth closest to the Sun in different seasons. At present, the Earth is closest to the Sun in Northern Hemisphere winter. This minimizes the summer-winter seasonal contrast in the Northern Hemisphere and maximizes the seasonal contrast in the Southern Hemisphere. General circulation climate models suggest that when the perihelion occurred during Northern Hemisphere summer (9000 years ago) there was enhanced monsoon circulation over the Arabian Sea and in other parts of the world. The effects of the stronger monsoon circulation have been documented in sediments of the northern Arabian Sea by Prell *et al.* (1990).

VARIABILITY OF SURFICIAL GEOFLUXES

Superimposed on the long-term trends of deglaciation and the precessional cycle is shorter-term variability inherent in the chaotic behavior of the climate system.

Temporal Variability

Although we have a general picture of the great changes that must have taken place in the fluxes of materials on the surface of the Earth during the change from the glacial age to the present interglacial age, we know very little about the shorter-term (decade to century to millennium) changes. A number of mass transport events can best be characterized as natural cataclysms, as documented and discussed by Baker (see Chapter 6, this volume). Flood events on a scale unknown in the course of human history characterized deglaciation. Massive diversions of rivers occurred as the glaciers receded and the land rose in isostatic response to the disappearing load of ice. Although the melting of ice sheets and the isostatic response to unloading were relatively slow, continuous processes, the diversion of rivers likely was rapid, taking place in the course of days to years or decades. Monsoonal circulation was stronger in the early Holocene when precession-controlled seasonal radiation contrasts reached a maximum in the Northern Hemisphere. The enhanced monsoons caused repeated large floods in southern Asia, central Africa, and northern Australia.

Continental fluxes are mostly linked to river runoff, but the variations in runoff are poorly documented. New data sources are needed to gain insight into temporal variability. For example, it might be possible to interpret varves in tropical lakes and other environments in terms of records of hydrologic variability. Better documentation of lake-level changes should be possible. Obtaining a record of runoff in the past could be very important for differentiating the natural variability of climate from anthropogenic effects.

Against a relatively constant background of erosion, transport, and deposition, large infrequent events result in step-function changes in material fluxes. Severe storms may breach the vegetation cover and expose previously stable slopes to erosion; deposition from streams overloaded with debris during extreme flood events may cause them to alter course; windstorms during periods of drought may strip the land of its soil; earthquakes may trigger landslides and submarine slumps; volcanic activity may result in massive ashfalls and mudflows that alter the character of the landscape. Although the everyday transport of materials is a significant part of the global total in any given span of time, some of the landscape features we observe are the result of extreme, even violent, infrequent events that are very poorly documented.

Spatial Variability

On short-term time scales, fluxes are mostly driven by small areas with very high rates. Mechanical and chemical weathering, eolian transport, and even glacial erosion all demonstrate the overriding significance of small areas in influencing the global rates. Because the fluxes are so strongly dependent on changes in small areas, we expect that they have a high temporal variability that is at present, with rare exceptions, undocumented and unknown.

Mechanical weathering is most rapid in areas of high relief, resulting from active tectonic processes. In the rugged Himalaya and Alps, average rates of denudation and uplift may be about equal and on the order of 1 m per thousand years (Menard, 1961; Schaer, 1979; Dodson and McClelland Brown, 1985). In the high-relief, densely forested island terrain of southeast Asia and in many other parts of the circum-Pacific region, transport depends on breaches in the vegetation cover. Once the binding root systems are

gone, erosion of the underlying regolith can proceed unimpeded. The weathered mantle, which may have taken thousands to tens of thousands of years to form, can be eroded away in a few years.

The chemical load of rivers is very sensitive to the presence of limestones or evaporites in a drainage basin. Most of the load of nonatmospheric sulfate carried by rivers is derived from the dissolution of sulfate-rich evaporites exposed at the land surface.

Eolian transport is sensitive to both winds and source area. The Pacific Ocean east of Japan receives dust at rates 100 times higher than the average Pacific dust flux (e.g., Hovan *et al.,* 1991).

Hydrothermal solute inputs to the ocean may be highly variable in both space and time. Hydrothermal activity occurring on less than one-thousandth of the ocean floor may be responsible for 99 percent of the global flux of material exchanged between seawater and basalt (Wolery and Sleep, 1988).

Carbonate precipitation on some actively growing reefs and banks occurs at a rate 50 times that of marginal seas and 80 times that of the deep sea. Opal deposition is even more discontinuous (Lyle *et al.,* 1988).

Rapid Change and Catastrophic Events

Weathering, dissolution, and transport of solutes are ongoing processes that operate more or less continuously to denude the continents and carry material to the sea. Detrital material tends to be mobilized and transported by catastrophic events such as hurricanes and other storms, floods, landslides, and volcanic eruptions.

Very little is known about the magnitude and frequency of such episodes of rapid change. Catastrophic events can be defined as extremely rapid changes in environmental conditions; they commonly involve rapid dissipation of energy per unit area per unit time and/or a rapid rate of change of concentrations of materials or a rapid change in energy flow patterns. It is not known whether the relocation of materials on the surface of the Earth is dominated by the slower but continuous fluxes operating all of the time or by the spectacular large fluxes that operate during short-lived cataclysmic events.

Careful research and documentation might make it possible to scale rapid change and catastrophic events by order of magnitude and by frequency. What constitutes a rapid or catastrophic event with respect to sea-level change, to volcanic eruptions, to temperature change, to growth or melting of glaciers, to changes of vegetation? What is the spatial and temporal distribution of events of different orders of magnitude? How large do different kinds of events need to be to have a regional or global significance? Do rapid or catastrophic events change global fluxes? What is the qualitative influence of such events on basic processes?

Volcanic eruptions are known to be a major source of airborne dust reaching the oceans, but it is not known how large an impact can result. Occasionally (e.g., the Tambora eruption in 1815), it can exceed the annual global river input of suspended solids. The question of the impact of volcanic aerosols on climate remains unresolved. Small eruptions may have little effect, but Pleistocene deposits contain a record of volcanic eruptions far larger than any that have occurred historically (Kennett and Thunell, 1977). The injection of volcanic gases into stratosphere and troposphere may also have important effects on the environment. The 1991 eruption of Mount Pinatubo in the Philippines demonstrated that the injection of sulfur particles and sulfur dioxide, which then formed aerosol sulfuric acid in the stratosphere, may not only alter the transparency of the atmosphere, but also effect the ozone layer (Hansen, 1992; Johnston *et al.,* 1992). Some knowledge of the long-term contribution of volcanic eruptions to the global budget of sulfate and its temporal variability has become available from studies of ice cores (Legrand and Delmas, 1987; Legrand *et al.,* 1988).

Rapid weathering may also have a major impact on the delivery of solutes to the sea. The sudden exposure of evaporites, massive basalt flows, and glacial material to weathering may have a global impact. Evaporites are readily soluble, and under warm humid conditions, basalt weathers much more rapidly than many sedimentary rocks. Glaciers pulverize rock materials and greatly increase the grain surface areas that can react with surface and groundwaters (see Kump and Alley, Chapter 3, this volume). Many human activities, particularly mining and construction, promote rapid weathering. These activities bring unweathered materials to the surface; pulverize them, thereby increasing the grain surface areas and promoting reactions; and expose them to weathering by the atmosphere and pollutants. Mining activity has resulted in major increases in Na^+ and SO_4^{2-} fluxes in rivers (see Meybeck, Chapter 4, this volume).

Transport of solids is driven by catastrophic events such as hurricanes and cataclysmic floods. The late Pleistocene Missoula floods discussed by Baker (Chapter 6, this volume) are an example of flood events having a magnitude unknown in human history. Large floods were characteristic of deglaciation; what was their cumulative effect?

Massive debris flows may result from failure of saturated deposits on relatively gentle as well as steep slopes. Heavy or persistent rain, or even rapid melting of glaciers, may saturate deposits. The results are particularly disastrous when volcanic activity causes glaciers to melt, suddenly releasing great volumes of water and debris. This type of catastrophic event has occurred repeatedly on the volcanoes of the Pacific Rim (e.g., Cascade Range, Japan, and Andes) and may have a major local or regional impact. Were such events more frequent during glaciation, when many more volcanoes were glacier-covered? Detailed mapping has shown that large-scale slumping or landsliding has occurred on submarine slopes off the continents and oceanic islands. We know little about the frequency of these events or the triggering mechanisms. Do changes in sea level play a major role in controlling the frequency and magnitude of such events?

Clathrates are ices formed by low molecular weight hydrocarbons, hydrogen sulfide or other gases, and water. They form at the temperatures and pressures found in the polar regions and deep sea. Clathrates occur in the Northern Hemisphere permafrost regions and broadly in sediments of the continental slopes and rises. They may act as a seal, trapping natural gas. They may be important in slope stabilization by acting to cement the sediment in which they form. Changes in ocean temperature can cause clathrates to form more extensively or to disappear at a given water depth. Their widespread disappearance on parts of the continental slopes and polar shelves might be expected if ocean temperatures were to rise. This could lead to massive slope failures that could generate tsunamis in oceanic areas where they are presently unknown. Although the temperature of the deep sea cannot be altered significantly on time scales of less than thousands of years, the connections between marginal basins and the oceans are sensitive to sea-level fluctuations, so that conditions within marginal seas might change much more rapidly. Only 8000 years ago the Black Sea was filled with cold fresh water; now it is filled with warm salt water (Degens and Ross, 1974).

Large-scale freshwater input to the marginal seas may inhibit exchange of the surface and deep waters, and may cause episodes of anoxia. Massive floods from the Nile are thought to be the cause of periodic anoxia that affected the eastern Mediterranean in the Pleistocene and early Holocene (Cita *et al.,* 1977). The frequency of major anoxic events can be determined from study of the sediments. What other areas have been similarly affected and what are the effects on their ecosystems?

Drought can result in episodes of substantially increased dust transport. Extensive loess deposits indicate that dust deposition was a major sedimentation process during the past glacial age. Atmospheric dust transport has declined markedly since the last glacial age, but the dust bowl conditions of the U.S. Midwest in the 1930s and ongoing desertification of the Sahel demonstrate the catastrophic nature of relatively local and short-term episodes of eolian transport.

It might well be assumed that diagenetic fluxes of ions into and out of sediment in the ocean are not subject to catastrophic change, but in reality we know almost nothing about the release of pore fluids that must attend massive slope failure on the continental margins as a result of sea-level changes and earthquake activity.

Coastal pollution by tanker accidents may result in ecological catastrophes on a local or even regional scale, but natural hydrocarbon seeps also occur. Have there been catastrophic episodes of hydrocarbon release due to natural causes, such as slope failure or volcanic activity? Clathrates are known to act as a seal, trapping hydrocarbons at relatively shallow depths, so that slope failures associated with the disappearance of clathrates might cause large-scale release of methane and other hydrocarbons into the marine environment.

Little is known of the spatial and temporal variability of either oceanic or terrestrial hydrothermal activity. Do cataclysmic events occur? How valid are extrapolations of present oceanic hydrothermal fluxes into the past or future?

There is much evidence that carbonate precipitation is highly variable and very responsive to sea-level rise or fall. Could growth of carbonate banks keep up with the relatively rapid sea-level rise that might accompany disintegration of the West Antarctic Ice Sheet?

The migration and reorganization of biomes in response to deglaciation has been documented, but what were the effects of migrating biomes on soils, the organic carbon flux, and erosion?

What is the role of wetlands and mangroves in biogeochemical cycles? The areas of these environments must have changed drastically between the glacial maximum and today. Wetlands and mangrove areas must have migrated very rapidly during the deglacial rise of sea level.

What is the role of ocean processes in influencing flux rates? How frequent are abyssal storms within the deep ocean, and how much sediment is remobilized by such storms?

What are the effects of complex ocean-atmosphere interactions such as El Niño and related events on biogeochemical cycling?

Recent studies of ice cores from Greenland indicate that during deglaciation the CO_2 content of the atmosphere changed significantly on time scales of a few decades. What natural processes were involved in such rapid changes of atmospheric CO_2?

Most importantly, how has the frequency of extreme events changed with time? What are the conditions most likely to produce frequent extreme events?

Pollution is a rapid change in condition induced by human activities. It is catastrophic if the change is so rapid that the biota cannot adjust. Some natural events have exactly the same effect.

CONCLUSIONS

An immediate need, if we are to understand the operation of the Earth as a natural system and to evaluate anthropogenic impacts, is to monitor the fluxes identified in Table 1 and assess how they are changing on time scales of decades to centuries. The results of studies being conducted within the context of global change research projects, on spatial scales ranging from individual drainage basins to continents, can be used to improve the global flux picture. Specifically, the following aspects merit further consideration.

Processes in Shallow Water-Shelf Environments

In recent years, much of the focus in marine research has been on the deep sea, but in terms of biogeochemical cycling, much is happening on shelves and in shallow environments. Studies of the deep sea are vital and must continue, for these and other rationales, but additional studies of material processes in shallow waters are needed. We should, furthermore, consider the land-shelf deep sea continuum along a series of transects to understand better the fluxes over large distances in the marine realm.

Distribution of Lithologies at the Surface

Although soil maps are available for each of the continents and seafloor maps are available for each of the ocean basins, there are no continental-scale maps that show the distribution of lithologies at the Earth's surface. Surficial lithologic maps are needed to serve as a base for determining areas of different kinds of rocks exposed to weathering and erosion.

Distribution of Sources and Sinks

Prerequisites for studies of biogeochemical cycling are maps of sources and sinks of detrital and dissolved materials. These are essential to quantify global fluxes and to identify sensitive areas that are prone to rapid change. Just as topographic maps are needed for land-use planning and geologic maps are needed for resource exploration, sources and sinks maps are needed for studies of global cycles and global change.

In terms of sources, there is a need for accurate mapping to estimate the areas of different types of environment on a global scale. Accurate surficial lithological maps on a global scale will be required, with emphasis on both soluble rocks and rocks and sediments that are readily eroded physically. Special attention should be given to determining the location of rock types that are sensitive to erosion.

Global sinks maps would show the accumulation rates of different types of sediments or the rates of consumption of cycling components (e.g., CO_2).

Rates

The response times for environmental changes need to be determined. Rates of environmental change from Pleistocene to Holocene conditions are probably among the most rapid in the geologic evolution of the planet. However, it is questionable whether we know enough about more ancient geologic times to be sure that spatial and temporal climatic variability then was less than it is now.

Expanded Time Scales for Processes/Fluxes

To determine response times there is a need for additional well-dated high-resolution geologic records, especially those of short-term events. Some lakes, for example, are likely to have a sedimentary record of atmospheric fluxes as detailed as that obtained from ice cores.

To determine past flux rates we need high-resolution dating of small (1 to 5 mg) samples with a resolution of $\pm$ 30 years. The use of accelerator mass spectroscopy (AMS) determined ^{14}C is one of the most promising techniques for high-resolution dating. However, there are a variety of other dating techniques, such as tree rings, coral growth bands, varves, and layering in ice cores that can be used to achieve annual resolution.

Anthropogenic Influence

Finally, we must answer the question: When will (or when did) anthropogenic activities so perturb global fluxes that they exceed (or exceeded) the range of variability inherent in natural processes?

REFERENCES

Cita, M.B., C. Vergnaud-Grazzini, C. Robert, H. Chamley, N. Ciaranfi, and S. D'Onofrio (1977). Paleoclimatic record of a long deep sea core from the eastern Mediterranean, Quaternary Research 8 , 205-235 .

Degens, E.T., and D.A. Ross (1974). The Black Sea: Geology, Chemistry, and Biology, American Association of Petroleum Geologists Memoir 20 , Tulsa, Oklahoma, 633 pp .

Dodson, M.H., and E. McClelland Brown (1985). Isotopic and paleomagnetic evidence for rates of cooling, uplift and erosion, in The Chronology of the Geological Record, N.J. Snelling, ed., Geological Society (London) Memoir 10 , Blackwell Scientific Publications, Oxford, pp. 315-325 .

Fairbanks, R.G. (1989). A 17,000-year glacio-eustatic sea level record: Influence of glacial melting rates on the Younger Dryas event and deep-ocean circulation, Nature 342, 637-642 .

Geophysics Study Committee (1990). Sea-Level Change, R. Revelle, Panel Chairman, National Research Council, National Academy Press, Washington, D.C., 234 pp .

Han, M.W., and E. Suess (1989). Subduction-induced pore fluid venting and the formation of authigenic carbonates along the Cascadia continental margin: Implications for the global Cacycle, Palaeogeography, Palaeoclimatology, Palaeoecology 71, 97-118 .

Hansen, J., A. Lacis, R. Ruedy, and M. Sato (1992). Potential climate impact of Mount Pinatubo eruption, Geophysical Research Letters 19, 215-218 .

Hovan, S.A., D.K. Rea, and N.G. Pisias (1991). Late Pleistocene continental climate and oceanic variability recorded in northwest Pacific sediments, Paleoceanography 6, 349-370 .

Johnston, P.V., R.L. McKenzie, J.G. Keys, and W.A. Matthews (1992). Observations of depleted stratospheric NO_2 following the Pinatubo volcanic eruption, Geophysical Research Letters 19, 211-213 .

Kennett, J.P., and R.C. Thunell (1977). On explosive cenozoic volcanism and climatic implications, Science 196, 1231-1234 .

Kutzbach, J. E. (1981). The monsoon climate of the early Holocene: Climate experiment with the Earth's orbital parameters for 9000 years ago, Science 214, 59-61 .

Kutzbach, J.E., and P.J. Guetter (1988). The influence of changing orbital parameters and surface boundary conditions on climate simulation for the past 18,000 years, Journal of Atmospheric Sciences 43, 1726-1759 .

Legrand, M.R., and R.J. Delmas (1987). A 220-year continuous record of volcanic H_2SO_4 in the Antarctic Ice Sheet, Nature 327, 671-676 .

Legrand, M.R., C. Lorius, N.I. Barkov, and V.N. Petrov (1988). Vostok (Antarctica) Ice Core: Atmospheric chemistry changes over the last climatic cycle (160,000), Atmospheric Environment 22, 317-331 .

Lyle, M., D.W. Murray, B.P. Finney, J. Dymond, J.M. Robbins, and K. Brooksforce (1988). The record of Late Pleistocene biogenic sedimentation in the eastern tropical Pacific Ocean, Paleoceanography 3, 39-59 .

Menard, H.W. (1961). Some rates of regional erosion, Journal of Geology 69 , 154-161 .

Milliman, J.D. (1993). Production and accumulation of calcium carbonate in the ocean: Budget of a nonsteady state, Global Biogeochemical Cycles 7(4), 927-957 .

Prell, W.L., R.E. Marvil, and M.E. Luther (1990). Variability in upwelling fields in the northwest Indian Ocean 2. Data-model comparison at 9000 years B.P., Paleoceanography 5, 447-457 .

Schaer, J.P. (1979). Mouvements verticaux et rosion dans les Alpes, aujourd'hui et au cours du Miocene , Eclogae Geologicae Helvetiae 72, 263-270 .

Suess, E., and M.J. Whiticar (1989). Methane-derived CO_2 in pore fluids expelled from the Oregon subduction zone, Palaeogeography, Palaeoclimatology, Palaeoecology 71, 119-136 .

Teller (1987). Proglacial lakes and the southern margin of the Laurentide Ice Sheet, in North American and Adjacent Oceans During the Last Deglaciation, W.F. Ruddimann and H.E. Wright, Jr., eds., Geology of North America K-3 , Geological Society of America, Boulder, Colorado, pp. 39-69 .

Wolery, T.J., and N.H. Sleep (1988). Interactions of geochemical cycles with the mantle, in Chemical Cycles in the Evolution of the Earth, C. B. Gregor, R.M. Garrels, F.T. Mackenzie, and B.J. Maynard, eds., John Wiley & Sons, New York, pp. 77-103 .

Background

14

1

Pleistocene-Holocene Fluxes Are Not the Earth's Norm

WILLIAM W. HAY
University of Colorado

ABSTRACT

It has long been recognized that global Pleistocene-Holocene material fluxes are qualitatively distinct from those of the earlier Cenozoic and Mesozoic, but the full extent of the differences has only recently begun to emerge. Quantitative estimates of the masses of material eroded, transported, and deposited during the Pleistocene-Holocene have been difficult to obtain because of the lack of consistent information on the thicknesses and areal extent of the deposits on land and in shallow seas. Geologic maps commonly show extensive areas of Quaternary cover on older sediments, but information on the thickness of the tills, alluvium, and colluvium that make up these deposits is scattered throughout the literature and is often incomplete.

Several major changes in the erosion-sedimentation regime have affected material fluxes. These have occurred in response to alternations in the climatic regime, to related changes in the sediment transport agents, to increasing amplitude of sea-level fluctuations, and to extensive regional tectonic uplift.

The Pleistocene climatic regime results in alternations of glacial and temperate conditions at mid- and high latitudes, and arid and humid conditions at lower latitudes. Both types of change affect the rates of chemical weathering. At mid- and high latitudes the major transport agent alternates between glaciers and rivers. Glaciers are effective at removing, pulverizing, and transporting clastic sedimentary and low-grade metamorphic rocks, but less effective in attacking crystalline rocks. The glacial sediment is commonly transported uphill and deposited in such large quantities that it results in reorganization of the fluvial drainage systems. The Mississippi system of North America is an excellent example, the preglacial drainage having been truncated by two ice edge rivers, the Ohio and the Missouri. During times of deglaciation, supplies of fluvioglacial sediment often exceed the competence of the rivers, resulting in extensive alluviation. Both of these processes expose extensive areas of unweathered debris to soil-forming processes. At

lower latitudes the alternation of arid and humid climates results in alternating cycles of alluviation and incision in river valleys as well as an alternation of soil-forming processes.

The late Cenozoic-Pleistocene glaciations resulted in a series of sea-level falls of increasing amplitude. Erosion of exposed unconsolidated clastic shelf sediments and consequent isostatic compensation has resulted in large masses of sediment being off-loaded from the continental shelves onto deep-sea fans and abyssal plains by turbidity currents. Modern continental shelves with clastic sediments are adjusted to the Pleistocene low stands of sea level. The present widespread development of estuaries is a result of this condition. Interglacials are too short and the sediment supply is too small to allow shelves to build back to equilibrium grade with high sea-level stands. Although during the interglacials a few large rivers can build deltas to the shelf break and spill sediment into the deep sea, most estuaries do not fill with sediment before the next sea-level fall. In contrast, carbonate sediments become cemented by fresh water infiltration when sea level falls and, as a result, carbonate-dominated shelves and banks reflect equilibrium with high sea-level stands. Carbonate extraction from the ocean is at a maximum as shallow shelf seas flood during the late stages of deglaciation.

The largest supplies of clastic sediment come from the largest regional uplifts, the Tibetan Plateau-Himalayas and western North America. Evidence suggests that both of these regions were uplifted in the late Pliocene and Pleistocene. Their uplift may be the ultimate cause of the onset of continental glaciation and the global climatic alternations that have characterized the Earth's recent past.

Pleistocene-Holocene fluxes do not reflect the long-term state of the planet but are the result of a set of unusual conditions. It is, however, against this rapidly changing background that future global change will take place.

RECOGNITION, DEFINITION, AND LENGTH OF THE QUATERNARY AND HOLOCENE

Information on the distribution and thickness of Pleistocene and Holocene deposits is often highly inconsistent. Ordinarily, geologic maps do not show glacial deposits but do show other Quaternary sediments and volcanics, and often large areas are simply designated Quaternary alluvium. Maps of the thickness of glacial sediments have been published for a few regions, but for most areas there are not even cross sections from which thicknesses can be estimated. The areas shown as Quaternary on geologic maps, even excluding the areas covered by glacial drift, are much larger than the areas of older deposits. Gilluly (1969) reported the measured area of Quaternary sediment shown on the Geologic Map of North America (Geological Society of America, 1965) to be 2.185×10^6 km^2 and the sum of older Cenozoic sediments to be 2.075×10^6 km^2. He noted that the Geologic Map of South America (Geological Society of America, 1950) shows almost twice as large an area covered by Quaternary sediments, 4.276×10^6 km^2, and only 2.889×10^6 km^2 of Tertiary sediment.

The base of the Quaternary is taken to be the base of the Pleistocene, originally defined by Lyell (1839) as sediments characterized by fossil content containing more than 70 percent living species of mollusc. The Pleistocene later became associated with Northern Hemisphere glaciation, but because it was recognized that the beginnings of glaciation were only vaguely known, the base of the Pleistocene came to be defined by the first significant cooling of the Mediterranean, marked by the Calabrian Stage in Italy. Dispute over indications of the first cooling of the Mediterranean has led to disagreement over the criteria used to define the base of the Pleistocene in the boundary stratotype region in southern Italy. There are also difficulties in extending correlation of the base of the Pleistocene to other parts of the world. Even more serious discrepancies in the use of the term Quaternary come from those who would consider the base of the Pleistocene to be marked by the climatic change to glacial conditions in the Northern Hemisphere even though this is now thought to be between 3 and 4 million years ago (Ma). Hays and Berggren (1971), Jenkins *et al.* (1985), and Berggren *et al.* (1985) have presented useful reviews of the problems associated with the Pliocene-Pleistocene boundary.

Many of the estimates of Pleistocene sediment masses involve calculation or extrapolation of accumulation rates, so that knowledge of its duration is critically important. The age of the base of the Pleistocene was thought for many years to be about 2 Ma; this was revised to 1.8 Ma by Hays and Berggren (1971), and has more recently determined to be 1.6 Ma (Haq *et al.,* 1977). The boundary is currently thought to be just above the top of the Olduvai Normal Magnetic Polarity Event.

The criteria used to define the base of the Quaternary and the age of the base of the Quaternary are almost never given on geologic maps or in their accompanying text.

The base of the Holocene has been intended to mark the change from glacial to interglacial conditions, but this change is, of course, a more or less gradual transition. The age has usually been given as 11,000 to 10,000 yr before present (BP). Recently it has been proposed that the base of the Holocene be defined by a boundary stratotype in Sweden (Morner, 1976). The age of the base of the Holocene is now taken to be about 10,000 radiocarbon yr BP, at the end of the Younger Dryas (Harland *et al.,* 1982).

Holocene sediments are very incompletely recorded on land, generally being lumped into the general term Quaternary alluvium. The Holocene is in rare instances shown as a separate unit on specialized geological and environmental maps.

MASSES OF QUATERNARY AND HOLOCENE SEDIMENT

The masses of Quaternary material in the major depositional site categories are given in Table 1.1. The best data on Quaternary sediment masses are from the deep sea. This is in spite of the fact that the base of the Pleistocene usually lies below the depth of penetration of piston cores and is too shallow to be recovered completely intact and undisturbed even by the hydraulic piston corer developed in the later phase of the Deep Sea Drilling Project (DSDP) and used during the successor Ocean Drilling Program (ODP). The determinations of the base of the Pleistocene, usually based on the lowest occurrence of *Globorotalia truncatulinoides* or the highest occurrence of *Discoaster brouweri,* have resulted in a consistent determination of the thickness of strata that closely approximates the Quaternary as currently defined. The Gamma Ray Attenuation Porosity Evaluation (GRAPE) records permit a reasonable estimation of the porosity of Pleistocene sediments; hence the mass can be calculated with a high degree of certainty. The next best documentation of the existing sediment mass is from the areas with glacial sediment even though there are major inconsistencies in estimates of the areas covered by glaciers, the thicknesses of the glacial deposits, and the age of the older glacial deposits. The most incomplete data are for the distribution and thickness of nonglacial Quaternary deposits on the continental shelves and on land. The deposits on the shelves are often irregularly distributed and have highly variable thicknesses. I estimated the masses by making general estimates of global average thicknesses. Geologic maps of land areas often show large areas covered by Quaternary alluvium or colluvium, but the thicknesses of the deposits are almost never given. To estimate the masses of these nonglacial nonmarine sediments I resorted to projection of older rates.

TABLE 1.1 Total Mass of Quaternary Sediment

Sediment Type	Mass (10^{21} g)	
Marine		
Ocean basins		
Carbonate	4.62	
Noncarbonate	20.60	
Total	25.22	
Marginal seas		
Carbonate	0.51	
Noncarbonate	3.96	
Total	4.47	
Continental Shelves		
Carbonate	0.44	
Noncarbonate	0.15	
Total	0.59	
Total marine		
Carbonate	5.57	
Noncarbonate	24.71	
Total	30.28	
Continental	Glacial	0.94
	Clastics	9.92 to 12.20
	Other	0.43
	Total	11.29 to 13.57
Total Quaternary sediment		41.57 to 43.85

The Holocene has been extensively sampled by gravity and piston cores in the deep sea, in shallow seas, and on the continental shelves. Holocene sediments in the sea are mostly water, and there is always a question of the completeness of the record recovered. Often the surficial sediment is blown away by the pressure wave in front of the falling coring device, and the very soft sediments are easily disturbed. Compilations of the distribution of consistently collected and analyzed Holocene sediments in many parts of the deep sea and in some marginal seas have been presented by Lisitzin (1972, 1974). However, the information on marine sediments is still far from complete. Much less information is available about Holocene deposits on land. There are relatively few places on land where the base of the Holocene (i.e., the 10,000-yr BP datum) has been determined. Hence there is no global estimate of the mass of Holocene sediment.

PROCESS RATES

The traditional measure of the sedimentation process is the sedimentation rate, defined as the thickness of sedi

ment representing a given geologic interval divided by the length of the interval, expressed as a length (thickness) per unit time. The most commonly used standard is centimeters per 1000 yr (cm/kyr), but meters per million years (m/m.y.) is also often used. Sedimentation rate does not take the porosity of the sediment into account, and for young sediments, which can be up to 70 percent or more water, it can be very deceptive.

A more objective measure that can be used to compare compacted and uncompacted sediments is the accumulation rate, expressed in term of a mass per unit area per unit time (commonly g/cm²/kyr). Calculation of the accumulation rate requires that the sediment thickness be multiplied by the solidity of the sediment and by the grain density. The solidity of the sediment is one minus the porosity. The accumulation rate may be an accurate expression for the process of accumulation of modern sediments, but a problem arises in using the term in connection with older sediments. An ancient sediment accumulation rarely contains all the sediment that accumulated at a given site during the time represented by the sediment; some of the material that accumulated has been subsequently removed by erosion, dissolution, metamorphism, or subduction. The bulk of the sediment mass is simply eroded and redeposited, or recycled. Gregor (1970) suggested the term "survival rate" for the measure of mass per unit area per unit time for an ancient deposit. The term survival rate is somewhat deceptive because it is not an expression of the rate of survival of the sediment, which would more properly be a measure of the amount of sediment remaining relative to the amount originally deposited divided by the time elapsed since deposition.

Hay (1985) coined the term "apparent accumulation rate" as an alternative objective expression for the existing mass of sediment per unit area divided by the length of time it represents (= survival rate of Gregor, 1970). Rates calculated from present-day masses are always apparent accumulation rates, that is they recognize that part of the original mass of sediment deposited has been destroyed by erosion, dissolution, subduction, or metamorphism.

The term accumulation rate is often interpreted as a direct reflection of a flux rate, for example, the rain rate of pelagic sediment. Interpretation of an ancient flux rate from an apparent accumulation rate is obviously troublesome, because correction for subsequent loss from erosion and other cause must be made. Analysis of the global mass/age distribution of Phanerozoic sediment indicates that it can be generally described by a decay curve of the form

$$M_1 = Ae^{bt} \quad (1.1)$$

where M_t is the mass in existence today representing sediment of age t, A is the zero-age intercept, b is the decay constant. If t is expressed in million years, then the decay constant for all Phanerozoic sediment is about -0.002. This means, for example, that only 82 percent of the sedimentary material that accumulated 100 m.y. ago is still in existence; the half-life of Phanerozoic sediment is about 350 m.y. The sediment flux at times in the past can be estimated by multiplying the zero-age intercept by the proportional difference between the observed mass of ancient sediment and the value of the decay curve for that time (Wold and Hay, 1988, 1990; Hay and Wold, 1990). Although conversion to flux rates requires caution, it is useful to express accumulation rates in terms of flux rates so that they can be compared with modern process rates. For the Quaternary, with a mean age of 0.8 Ma, the long-term (Phanerozoic) decay constant indicates that the amount of sediment remaining should be about 99.8 percent of the amount deposited, so no correction for long-term sediment cycling is made in the figures given below.

It is likely that there is more rapid recycling on a shorter time scale that may be reflected in estimates of flux rates. Hence, in the discussion below, I distinguish three kinds of flux rates: (1) instantaneous flux rates, (2) short-term flux rates, and (3) long-term flux rates. In geology, instantaneous flux rates are measured over geologically insignificant lengths of time. Short-term flux rates are a measure over a geologically longer but internally homogeneous period of time, such as a 1000-yr episode during the deglaciation. Long-term flux rates are integrated fluxes over a longer, inhomogeneous period of geologic time, such as the Holocene, the Wisconsinan, or the Pleistocene.

LONG- AND SHORT-TERM APPARENT ACCUMULATION RATES OF QUATERNARY AND HOLOCENE SEDIMENT

Most of the information on apparent accumulation rates is from the marine realm, and most of it is for long-term rates. In a few places estimates of local short-term rates, such as those during deglaciation and during parts of the Holocene have become available.

Deep-Sea Sediments

The deep sea contains more than half of the total Quaternary sediment mass. The flux rates of sediment to the deep sea, based largely on the study of DSDP cores by Sloan (1985), are summarized in Table 1.2; the apparent accumulation rate in the ocean averages about 5 g/cm²/kyr.

The area of continental rise deposits is that given by Sloan (1985) and includes the major deep sea fans. The area of high productivity is after Berner (1982) and includes 23.5 ∞ 10⁶ km² of the Pacific, 19 ∞ 10⁶ km² of the Southern Ocean, and 1.5 ∞ 10⁶ km² of margin high productivity

areas in the Atlantic and Indian oceans. The total of 323 x 10^6 km^2 includes the Pacific, Atlantic (and Caribbean), Indian, and Arctic Ocean basins. It does not include areas less than 200 m deep (mostly shelves) or the marginal seas discussed below.

TABLE 1.2 Quaternary Apparent Accumulation Rates and Sediment Masses in the Ocean

	Continental Rises	High Productivity	Ocean Basins	Total
Area (10^6 km^2)	19	44	260	323
Approximate accumulation rate (g/cm^2/kyr)	5.85	9.45	4.05	4.88
Total mass (10^{21})	1.78	6.65	16.79	25.22

TABLE 1.3 Cenozoic Deep-Sea Apparent Accumulation Rates and Carbonate/Noncarbonate Proportions (in part modified after Sloan, 1985)

Age Unit	Apparent Accumulation Rates (g/cm^2/yr)			
	Total	Noncarbonate	Carbonate	Percentage Carbonate
Quaternary	4.89	3.99	0.90	18.4
Pliocene	3.03	2.19	0.88	28.6
Late Miocene	1.73	0.99	0.73	42.2
Mid Miocene	1.71	1.01	0.70	40.9
Early Miocene	1.56	0.88	0.67	42.9
Late Oligocene	1.38	0.56	0.82	59.4
Early Oligocene	1.03	0.51	0.52	50.5
Late Eocene	1.50	1.07	0.43	28.7
Middle Eocene	1.73	1.08	0.65	37.6
Early Eocene	1.49	0.98	0.51	34.2
Late Paleocene	1.38	0.58	0.66	47.8
Early Paleocene	0.64	0.32	0.32	50.0

Table 1.3 shows apparent accumulation rates and the proportions of carbonate for sediments in the ocean basins through the Cenozoic, taken from Sloan (1985). The apparent accumulation rate of Quaternary sediments is 54 percent higher than the rate for the Pliocene, and almost three times Miocene rates. Further, carbonate is only 18.4 percent of the total Quaternary in the ocean basins, whereas it is typically 40 to 50 percent of the Miocene and earlier sediments.

There has been no compilation of Holocene apparent accumulation rates for sediments in the ocean as a whole, but Lisitzin (1972, 1974) has presented maps that allow rates for large areas of the major ocean basins to be estimated, and a global deep sea average to be calculated, as shown in Table 1.4.

Holocene sediment accumulation rates in the Atlantic Ocean are about three times the rate in the Pacific and Indian oceans. The global Holocene accumulation rate in the ocean is about one-fifth the Quaternary average for the ocean. Sediment supply to the deep sea is clearly in response to the glacial-interglacial changes in sea level. During sea-level low stands, material is delivered directly to the deep sea, whereas during sea-level high stands it is retained on the continental shelves and the supply to the deep sea is much reduced.

Damuth (1977) presented maps of sedimentation rates for Holocene and late Pleistocene sediments in the equatorial Atlantic. Average Holocene apparent accumulation rates for different regions can be calculated from the data presented on the maps, as shown in Table 1.5. The solidity of the Holocene sediment is assumed to be 30 percent.

The accumulation rates calculated from Damuth's data show that the continental rises receive almost twice as much sediment as the deep seafloor above 5-km depth,

which in turn receives about twice as much sediment as the deep seafloor below 5 km. From the proportional areas of rise, basin <5 km and basin >5 km, the average Holocene accumulation rate in the equatorial Atlantic can be calculated to be 2.07 g/cm^2/kyr, not very different from the average Holocene accumulation rate for the entire Atlantic determined from analysis of Lisitzin's (1972, 1974) maps. The higher value for the equatorial Atlantic is expected because this area receives sediment from the Amazon.

TABLE 1.4 Holocene Sediment Apparent Accumulation Rates and Masses in the Oceans(after Lisitzin, 1972, 1974)

	Atlantic	Pacific	Indian	Total
Area (10^6 km^2)	82.8	176.0	74.2	333.0
Approximate accumulation rate (g/cm^2/kyr)	1.71	0.50	0.66	0.84
Total mass (10^{21} g)	0.0156	0.0089	0.0054	0.0098

TABLE 1.5 Holocene Apparent Accumulation Rates for Sediment in the Equatorial Atlantic Ocean (after Damuth, 1977)

	Continental Rises	Basins <5 km	Basins >5 km
Average sedimentation rate (cm/kyr)	5.5	3.0	1.5
Approximate accumulation rate (g/cm^2/kyr)	4.37	2.39	1.19

Damuth also presented maps showing sedimentation rates during the last glacial (Wisconsinan) and the last interglacial (Sangamon) for the equatorial Atlantic. From these maps it can be estimated that during the glacial, average sediment accumulation rates were 2.75 times higher than the Holocene, and during the last interglacial the average rate was 0.77 that of the Holocene. On the Amazon Cone, Wisconsinan rates were 4.18 times the Holocene rate.

Marginal Sea Sediments

The shallow marginal seas occupying the sites of the Northern Hemisphere ice caps—the Baltic Sea, Barents Sea, and Hudson Bay—have almost no Pleistocene sediment but do contain a thin veneer of Holocene sediment. According to Dietrich and Koester (1974), Holocene sediments in the Baltic average about 0.22 m in thickness; if a solidity of 30 percent is assumed, this indicates an accumulation rate of only 1.75 g/cm^2/kyr.

Some other marginal seas outside the glaciated areas but with extensive areas shallower than 200 m, such as the Persian Gulf, were exposed to erosion during the Pleistocene sea-level low stands. During much of the Pleistocene they were sites of erosion rather than sedimentation, and they have negligible amounts of Quaternary sediment. Kassler (1973) reported that the major Pleistocene unit in the Persian Gulf region is a limestone (Kargh Limestone) with thicknesses varying from 5 to 30 m. If an average thickness of 15 m and a solidity of 50 percent are assumed, the Quaternary average apparent accumulation rate is only 1.24 g/cm^2/kyr. The average of late Holocene sedimentation rates given by Melguen (1973) indicates an accumulation rate of 48.9 g/cm^2/kyr; projected over 10,000 yr this would give an average Holocene thickness of 6.15 m. This is of the same order of magnitude as the Pleistocene sediment, which should represent a much longer time. Clearly, little of the sediment deposited in the Persian Gulf during sea-level high stands has survived the erosional forces operating during sea-level low stands. Although the Persian Gulf produces a large quantity of carbonate sediment, some of the Holocene accumulation within the Gulf is detritus from the small rivers entering the Gulf from Iran; the high late Holocene accumulation rate may reflect the high carbonate production plus an unusually large detrital input in response to increasing aridity of the region.

In terms of the Mesozoic and Cenozoic, the Gulf of Mexico is the best known of the deeper marginal seas because of the detailed atlas prepared for the Ocean Margin Drilling Program (Buffler *et al.,* 1984). The maps and drill hole data have been analyzed, and by estimating solidity from the compaction curve of Baldwin and Butler (1985), the mass of Quaternary sediment has been compiled by Shaw (1988, 1989). The total mass of "glacial age" (<<3 Ma) sediment in the northern and western Gulf of Mexico is 2.07 x 10^{21} g, of which 1.87 x 10^{21} g is Quaternary. This accounts for about 80 percent of the total Quaternary sediment in the Gulf of Mexico so that the total Quaternary sediment mass of the entire Gulf of Mexico must be about 2.34 x 10^{21} g or equal to 10 percent of all the Quaternary sediment in the ocean basins proper. The average accumulation rate for the Quaternary is 88.3 g/cm^2/kyr, two orders of magnitude higher than oceanic rates. Although there is no figure for the mass of Holocene sediment in the Gulf of Mexico, participants in DSDP Leg 96 evaluated the difference between Holocene and glacial Pleistocene accumulation rates on the Mississippi Cone. There, glacial accumulation rates have been determined by Wetzel and Kohl (1986) to range from 842 to 1572 g/cm^2/kyr (1000 to 2000 times oceanic rates), but

Holocene rates are only 1.5 to 12.8 g/cm^2/kyr. Very high sediment accumulation rates have also been cited by Perlmutter (1985) for an episode of rapid deglaciation just prior to the Holocene. He estimated that during a 3000-yr interval the suspended load of the Mississippi may have been an order of magnitude larger than it is today. If the Mississippi's load under natural conditions (Late Holocene, prior to arrival of European settlers) was 400 x 10^{14} g/yr (R.H. Meade, U.S. Geological Survey, personal communication), it alone would supply sediment at the rate of 26.0 g/cm^2/kyr to the entire area of the Gulf of Mexico.

The average thickness of Quaternary sediment in 28 DSDP and ODP holes drilled in the Mediterranean is 182 m (Cita *et al.,* 1978; Kastens *et al.,* 1987), and the estimated solidity is 52 percent; the long-term apparent accumulation rate is 15.67 g/cm^2/kyr. Holocene rates are more difficult to estimate because the base of the Holocene is reported in a less consistent manner. Judging from the descriptions of cores with well-preserved stratigraphy discussed by Thunell *et al.* (1977), the average thickness of Holocene sediment in the basins is about 0.5 m; if a solidity of 30 percent is assumed, this implies an apparent accumulation rate of 3.98 g/cm^2/kyr. In the Mediterranean, as in the major ocean basins, the Holocene accumulation rate is about one-quarter the Quaternary average.

Investigations by the DSDP permit comparison of Pleistocene, glacial, Holocene, and late Holocene apparent accumulation rates in the Black Sea basin. The Quaternary has been penetrated at three sites (Hsü, 1978a,b; Ross, 1978; Stoffers *et al.,* 1978). Two of the DSDP sites were at widely separated locations in the deep basin floor; they have thicknesses of 620 and 640 m, respectively. Although the exact ages of different layers are somewhat uncertain (Degens *et al.,* 1978; Hsü, 1978a,b; Stoffers *et al.,* 1978). Degens and Ross (1974) and Degens *et al.* (1978) have calculated detailed sedimentation rates at several intervals during the Quaternary based on the varved sediments. A summary of the Leg 42 and earlier results, recalculated as accumulation rates obtained by assuming 30 percent solidity for the Holocene and late Pleistocene sediments and a solidity of 50 percent for the Quaternary as a whole, is presented in Table 1.6. Again, as in the deep sea, Holocene rates are about one-fifth of the Quaternary average.

Four DSDP sites in the Red Sea, one of which did not completely penetrate the Pleistocene, can be used to compute an average thickness of 112 m for the Quaternary (Stoffers and Ross, 1974) and an estimated solidity of 49 percent. The Holocene sediment averages about 1.81-m thickness, and should have a solidity of about 30 percent. In this case the long-term average accumulation rates for the Pleistocene and the Holocene are 9.09 g/cm^2/kyr and 14.39 g/cm^2/kyr, respectively. The Red Sea is one of the rare places where the Holocene accumulation rate is higher than the Quaternary average.

The average thickness of Quaternary sediments in the Bering Sea is 207 m, the estimated solidity is 53 percent, and the average apparent accumulation rate is 18.17 g/cm^2/kyr. Lisitzin (1972, 1974) presented maps of the Holocene accumulation rates in the Bering Sea. The average rate for the Holocene determined from measurement of his maps is 10.1 g/cm^2/kyr, about half the Quaternary average. This may be the result of continuing supply from rivers that were unable to transport the loads during deglaciation.

There are no data that would permit an estimate of the average thickness of Quaternary sediments in the Sea of Okhotsk, but Lisitzin has presented a map of the mean thickness of Holocene sediments. The average thickness of the Holocene sediments is 2.22 m; if a solidity of 30 percent is assumed, this implies an average accumulation rate of 17.66 g/cm^2/kyr, similar to the Quaternary rate for the Bering Sea.

The data and estimates for marginal seas are summarized in Table 1.7. Clearly, the dominant control on sedimentation in marginal seas, as in the deep sea, is sea-level rise and fall. Typically this results in Holocene rates that are 20 to 25 percent the Quaternary average, but in marginal seas in the polar regions the difference is much less. The Red Sea apparently has received more sediment during the Holocene than the Quaternary average.

During glacials, the lowered sea level exposes the shelves, and most sediments are delivered directly to the deep sea. During the high sea-level stands of the interglacials, most sediments are retained on the shelves and in shallow areas. However, each successive sea-level fall seems to have resulted in the sediments of the previous interglacial being eroded and deposited in the deep sea.

TABLE 1.6 Sediment Accumulation Rates in the Black Sea Basin (after Degens and Ross, 1974; Degens et al., 1978).

	0 to 1 kyr BP	1 to 5 kyr BP	Holocene	Deglaciation	Quaternary
Average sedimentation rate (cm/kyr)	30	10	12	1000	40
Approximate accumulation rate (g/cm^2/kyr)	23.85	7.95	9.54	795	53

TABLE 1.7 Quaternary and Holocene Sediment Fluxes in Marginal Seas

Marginal Sea	Average Accumulation Rate (g/cm^2/kyr)	
	Quaternary	Holocene
Gulf of Mexico	88.3	30 ?
Mediterranean	15.67	3.98
North Sea	14.78	?
Red Sea	9.09	14.39
Black Sea	65.74	9.54
Bering Sea	18.17	10.10
Sea of Okhotsk	?	17.66

Continental Shelves

The late Cenozoic-Pleistocene glaciations resulted in a series of sea-level falls with amplitudes up to 130 m or more. The unconsolidated clastic shelf sediments become exposed to erosion, and they are off-loaded from the continental shelves onto deep-sea fans and abyssal plains by turbidity currents, largely through submarine canyons. As the sediment load is removed, isostatic compensation raises the shelf and causes further erosion. Hay and Southam (1977) suggested that the shelf break of the present detrital sediment-dominated shelves represents a glacial equilibrium. At the low stands of sea level it would have been at a depth of about 50 m rather than 200 m. One can assume that before the Pleistocene sea-level fluctuations, the detrital sediment dominated shelves were at an average depth of 50 m. If a sea-level fall of 130 m and a sediment solidity of 65 percent are assumed, a wedge of sediment having a thickness of almost 600 m at the shelf break must be eroded to bring the position of the shelf break back to a depth of 50 m. Hay and Southam (1977) estimated that 5.10×10^{21} g of detrital sediment might have been off-loaded from the shelves into the deep sea by this process in response to the Pleistocene sea-level falls. The pattern of the falls would be important to the delivery of sediment to the deep sea. If one of the early falls was very large, most of the sediment transfer from shelf to deep sea would have taken place at that time. The data presently available do not permit the relative effect of the different sea-level falls to be assessed.

Modern continental shelves with clastic sediments are adjusted to the Pleistocene low stands of sea level. The interglacials are too short and the sediment supply is too small to allow shelves to build back to equilibrium grade with high sea-level stands. The present widespread development of estuaries (drowned rivermouths) is a result of this condition. Although during the interglacials a few large rivers can build deltas to the shelf break and spill sediment into the deep sea, most estuaries do not fill with sediment before the next sea-level fall.

In contrast to detrital sediment, carbonate sediments become cemented by fresh water infiltration when sea level falls; as a result, carbonate-dominated shelves and banks reflect equilibrium with high sea-level stands. During glacial low stands of sea level, carbonate removal from the ocean is carried out mostly by the carbonate-secreting plankton, chiefly planktonic foraminifers and coccolithophores. As sea level rises, reef growth and extraction by shallow water organisms return to play a major role. Carbonate extraction from the ocean is at a maximum as shallow shelf seas flood during the late stages of deglaciation. Milliman (1974) estimated the average Holocene sedimentation rate on carbonate-dominated shelves and banks to be 40 cm/kyr; this corresponds to an accumulation rate of 31.80 g/cm^2/kyr. However, high rates of carbonate accumulation cannot be sustained unless sea level continues to rise. After sea level stabilizes a balance among carbonate production, sedimentation, and loss to the deep sea must be reached. Much of the aragonite secreted by algae and other organisms on carbonate banks today is exported to the surrounding deep-sea areas during storms. Hay and Southam (1977) suggested that the present carbonate flux onto shelves and banks is at least equal to the supply from rivers and might exceed the river supply by a factor of three.

In the estimates presented in Table 1.8, I have assumed an average Holocene sedimentation rate of 100 cm/kyr for detrital sediment, a solidity of 33 percent, and a carbonate

TABLE 1.8 Quaternary and Holocene Sediment Fluxes on Continental Shelves

	Accumulation Rates (g/cm^2//kyr)				
		Quaternary		Holocene	
	Area (10^6 km^2)	Total	Carbonate	Total	Carbonate
Detrial shelves	15.7	0.55	0.14	8.74	2.19
Carbonate shelves	10.3	4.53	4.08	31.80	28.62

content of 25 percent. For carbonate shelves the sedimentation rate has been assumed to be 40 cm/kyr, the solidity 30 percent, and the carbonate content 90 percent.

Glacial Sediments on Land

To estimate the masses of glacial sediments on land (moraines, ground moraine, and associated glaciofluvial and glaciolacustrine deposits), I measured the areas of the peripheral parts of the glaciated regions, where the glacial sediments accumulated, shown on the Quaternary geologic maps of the continents in Gerasimov (1964). These areas were multiplied by the estimated average thickness of 20 m, an assumed solidity of 80 percent, and a solid grain density of 2.65 g/cm^3. Because the same thickness and solidity were assumed everywhere, the Quaternary average apparent accumulation rate works out to be 2.65 $g/cm^2/kyr$ everywhere. Apportionment of the glacial sediment masses to the different glaciations is at best a guess, but probably about 80 percent of the deposits preserved today are referred to as the last glaciation although some of the material must be reworked from older glacial deposits. Assuming that 80 percent of the mass was deposited in 80,000 yr gives an accumulation rate for the last glacial of 33.92 $g/cm^2/kyr$.

Nonglacial Continental Sediments

Nonglacial continental sediment is the least certain of all the sediment masses because geologic maps poorly represent the actual distribution of Quaternary sediments (Choubert and Faure-Muret, 1976). The extent to which Quaternary sediments are shown varies greatly from map to map. Although the largest volumes are likely to be in active orogenic areas, where large thicknesses of Quaternary sediments may accumulate in intermontane basins and in smaller structures, the largest areas of Quaternary sediments shown on the maps are in regions with flat-lying strata. Even where the extent of Quaternary deposits is accurately depicted on maps there is generally little information on the thickness of the deposits. This is especially true in Asia, Africa, Australia, and South America, where nonglacial Quaternary sediments are widespread.

Because the data cannot be read directly from maps, I made two projections from Pliocene and Neogene data: first, it was assumed that the accumulation of nonglacial sediments on the continents is simply a continuation of Pliocene rates; second, it was assumed that on a global scale, all rates of sediment flux have increased in the Quaternary and that the fluxes of continental clastic sediment have increased proportionally to other flux increases. The second assumption appears to be plausible because Ronov *et al.* (1986) have noted that throughout the Phanerozoic an increase in one sediment reservoir almost always corresponds to increases in other sediment reservoirs. They referred to this phenomenon as a major law of sediment cycling. However, not all of the increases in Pleistocene flux rates are well known. The best known increase is the rate of accumulation of material in the deep sea. The data indicate that during the Pliocene and Pleistocene sediment accumulation in the ocean basins reflected a supply greater than that persisting through the earlier Cenozoic. According to Sloan (1985; see also Table 1.3), Quaternary apparent accumulation rates in the deep sea were 54 percent higher than they were in the Pliocene. However, Hay and Southam (1977) had noted that about 5.10 x 10^{21} g of the sediment in the deep sea should be material off-loaded from the shelves in response to the approximately 130-m sea-level changes of the late Pleistocene. This off-loaded material forms about 20 percent of the total of Quaternary sediment in the ocean basins, and taking this into account lowers the projected accumulation rate increase from 1.54 to 1.23 times the Pliocene rate. According to Khain *et al.* (1979), the average thickness of Pliocene sediments on the continents on a global scale is 256 m. Because only 5 percent of their Pliocene sediment inventory for the continents is marine, we can assume that the average thickness of nonmarine Pliocene sediments is probably close to 256 m. If a solidity of 70 percent and the duration of the Pliocene of 3.5 m.y. are assumed, the apparent accumulation rate would be 13.57 $g/cm^2/kyr$. If a Pleistocene acceleration of 1.23 is assumed, the apparent accumulation rate might be 16.69 $g/cm^2/kyr$, but this would be the case only if the area over which the Quaternary sediments were deposited had not increased.

DISCUSSION

The mass of Quaternary sediment is significantly larger than would be expected from knowledge of the masses of sediment representing older stratigraphic entities. The apparent increased mass could be the result of (1) erosion and recycling of young sediment; (2) the effect of ice-age climate and erosion; (3) general increases in erosion rates as a result of tectonic activity; or (4) a combination of all of these factors.

However, it is apparent from the determinations of Holocene accumulation rates that the global Holocene rate is only a fraction of the Quaternary average. Within the Quaternary there seems to be as much variability between rates as there has been at different times during the Phanerozoic (Hay and Wold, 1986; Hay *et al.,* 1987).

Sediment Cycling

Gilluly (1969) first clearly stated the idea that the sediments observed today are largely derived by cannibaliza

tion of older sedimentary rocks. The idea was developed by Garrels and Mackenzie (1971a,b), who suggested that post-Devonian sediment might have been recycled more rapidly than Devonian and older sediments. The notion of the possibility of differential cycling rates for younger and older sediments was further explored by Mackenzie and Pigott (1981). Wold *et al.* (1987) suggested that the observed mass/age distribution of sediments is a reflection of a slow rate of recycling for older (pre-Cretaceous) sediments and a rapid rate of recycling for Cretaceous and younger sediments. They emphasized that young, unconsolidated sediments are in greater jeopardy with respect to erosion than are older, more indurated and more deeply buried sedimentary rocks. Clearly, the increased mass of sediment being deposited in the Quaternary suggests that cycling rates have increased. However, the differences between Holocene and average Quaternary rates suggest that global rates of erosion and sedimentation may vary considerably on time scales of tens to hundreds of thousands of years.

The Effect of Glacial-Interglacial Alternations

The Pleistocene climatic regime results in alternations of glacial and temperate conditions at mid- and high latitudes, and arid and humid conditions at lower latitudes. Both types of change affect the rates of chemical weathering directly through temperature and soil moisture content, and indirectly through the changes in density and type of plant cover. At mid- and high latitudes the major transport agent alternates between glaciers and rivers. Glaciers are effective at removing, pulverizing, and transporting clastic sedimentary and low-grade metamorphic rocks, but less effective in attacking crystalline rocks. The glacial sediment may be transported uphill and deposited in such large quantities that it results in reorganization of the fluvial drainage systems. The Mississippi River system of North America is an excellent example of glacial reorganization. The preglacial drainage of the interior of North America was probably largely through the St. Lawrence into the North Atlantic (Hay *et al.,* 1989), with the Mackenzie River, Mississippi River, and a river through Hudson Strait draining smaller areas. The Cenozoic drainage system was buried by the glaciers that deposited an average of 20 m of drift over the old topography. The drainage outside the glaciated area was truncated by ice edge rivers. In many places, the courses of the Ohio and the Missouri Rivers mark the outline of glacial advances. During times of deglaciation, supplies of fluvioglacial sediment often exceeded the competence of the rivers, resulting in extensive alluviation. Both of these processes exposed extensive areas of unweathered debris to soil-forming processes. At lower latitudes the alternation of arid and humid climates results in alternating cycles of alluviation and incision in river valleys as well as an alternation of soil-forming processes.

Despite the obvious changes in the glaciated area and its periphery, it is not yet clear whether continental glaciation increases or decreases the long-term erosion rate on a global scale. The motion in an ice cap is mostly above the base, so that its ability to erode the rock on which it rests is questionable. Flint (1971) argued that the evidence suggests that the Laurentian ice cap, and probably its counterparts in Europe and Asia, was ineffective in eroding the Canadian Shield. White (1972), noting that the sites of the centers of the Laurentian and Scandinavian ice caps are now marked by shallow seas, suggested that they had removed large masses of sedimentary rock from the Canadian and Fennoscandian shields. Gravenor (1975) and Sugden (1976) countered that there was no evidence for the removal of large amounts of sediment from the sites of these ice caps, but Bell and Laine (1985) have estimated that 1.81×10^6 km^3 of terrigenous sediment derived from the Laurentian ice cap was deposited in the ocean, 1.01×10^6 km^3 in the North Atlantic Basin, and 0.82×10^6 km^3 in the Gulf of Mexico. Shaw (1988, 1989) contended that most of the sediment in the Gulf of Mexico considered by Bell and Laine to be derived from the Laurentide region is derived from erosion of the Cretaceous deposits of the Great Plains. If continental glaciers are effective erosional agents, most of the sedimentary material on the Laurentian and Fennoscandian shields would have been eroded by the first significant ice cap, in the early Pleistocene.

Increased Tectonic Activity

The idea that the large mass of young sediment is the result of increased tectonic activity dominated geological thinking throughout the first half of this century (Stille, 1936). More recently it has been thought that the large masses of Pliocene (and presumably Quaternary) sediment might merely be the expression of the greater degree of preservation of younger sediments. However, it is now clear that the excess mass of Quaternary sediment over that projected from Miocene rates is very large. A number of studies have suggested that uplift of the Himalayas and Tibet (Hsü, 1978c; Zeitler *et al.,* 1982) and western North America (Gable and Hatton, 1983; Shaw, 1988, 1989) has occurred mostly during the Pliocene and Quaternary. On a global scale the supply of sediment to the oceans increased markedly in the Pliocene, before the development of the large Northern Hemisphere ice caps.

There may be a direct link between increased tectonic activity and initiation of the Northern Hemisphere glaciations. Ruddiman *et al.* (1986) have suggested that the uplift of the Tibet-Himalayan region and western North

America may have caused reorganization of the atmospheric circulation, resulting in conditions favoring the growth of the Northern Hemisphere continental ice caps.

CONCLUSION

It seems likely that the global increase in sediment mass deposited during the Pliocene and Pleistocene does reflect a real increase of tectonic activity, and that this has climatic consequences that further enhance erosion. In any case, it is now evident that Pleistocene-Holocene fluxes do not reflect the long-term state of the planet but are the result of a set of unusual conditions. It is within this rapidly changing natural system that future anthropogenic global change will take place.

ACKNOWLEDGMENTS

REFERENCES

Baldwin, B., and C.D. Butler (1985). Compaction curves, American Association of Petroleum Geologists Bulletin 69, 622-626 .

Bell, M., and E.P. Laine (1985). Erosion of the Laurentide region of North America by glacial and glaciofluvial processes, Quaternary Research 23, 154-174 .

Berggren, W.A., D.V. Kent, and J.A. van Couvering (1985). The Neogene: Part 2, Neogene geochronology and chronostratigraphy, in The Chronology of the Geological Record, N.J. Snelling, ed., Geological Society (London) Memoir 10 , Blackwell Scientific Publications, Oxford, pp. 211-250 .

Berner, R.A. (1982). Burial organic carbon and pyrite sulfur in the modern ocean: Its geochemical and environmental significance, American Journal of Science 282, 451-473 .

Buffler, R.T., S.D. Locker, W.R. Bryant, S.A. Hall, and R.H. Pilger, Jr. (1984). Ocean Margin Drilling Program: Gulf of Mexico Atlas, OMDP Regional Atlas Series 6, Marine Science International, Woods Hole, Mass., 36 pp .

Choubert, G., and A. Faure-Muret, eds. (1976). Geological World Atlas, UNESCO, Paris, 17 sheets .

Cita, M.B., W.B.F. Ryan, and R.B. Kidd (1978). Sedimentation rates in Neogene deep-sea sediments from the Mediterranean and geodynamic implications of their changes, in Initial Reports of the Deep-Sea Drilling Project 42, part 1, K.J. Hsü, L. Montadert, et al., eds., U.S. Government Printing Office, Washington, D.C., pp. 991-1002 .

Damuth, J.E. (1977). Late Quaternary sedimentation in the western equatorial Atlantic, Geological Society of America Bulletin 88, 695-710 .

Degens, E.T., and D.A. Ross (1974). The Black Sea: Geology, Chemistry and Biology, Memoir 20 , American Association of Petroleum Geologists, Tulsa, Okla., 633 pp .

Degens, E.T., P. Stoffers, S. Golubic, and M.D. Dickman (1978). Varve chronology: Estimated rates of sedimentation in the Black Sea deep basin, in Initial Reports of the Deep Sea Drilling Project 42, part 2, D.A. Ross, Y.P. Neprochnov, et al., eds., U.S. Government Printing Office, Washington, D.C., pp. 499-508 .

Dietrich, G., and R. Koester (1974). Geschichte der Ostsee, in Merreskunde der Ostsee, L. Magaard and G. Reinheimer, eds., Springer-Verlag, Berlin, pp. 5-10 .

Flint, R.F. (1971). Glacial and Quaternary Geology, John Wiley & Sons, New York, 892 pp .

Gable, D.J., and T. Hatton (1983). Maps of vertical crustal movements in the conterminous United States over the last 10 million years, U.S. Geological Survey Miscellaneous Investigations Series Map 1-1315 .

Garrels, R.M., and F.T. Mackenzie (1971a). Gregor's denudation of the continents, Nature 231, 382-383 .

Garrels, R.M., and F.T. Mackenzie (1971b). Evolution of Sedimentary Rocks, Norton, New York, 397 pp .

Geological Society of America (1950). Geologic Map of South America, Geological Society of America, New York, N.Y.

Geological Society of America (1965). Geologic Map of North America, Geological Society of America, Boulder, Colo.

Gerasimov, I.P. (1964). Fiziko-Geograficheskii Atlas Mira, Akademiya Nauk SSSR i Glavnoe Upravlenie Geodezii i Kartografii GGK SSSR, Moscow, 298 pp .

Gilluly, J. (1969). Geological perspectives and the completeness of the geologic record, Geological Society of America Bulletin 80, 2303-2312 .

Gravenor, C.P. (1975). Erosion by continental ice sheets, American Journal of Science 275, 594-604 .

Gregor, C.B. (1970). Denudation of the continents, Nature 228, 273-275 .

Haq, B.U., W.A. Berggren, and J.A. Van Couvering (1977). Corrected age of the Pliocene/Pleistocene boundary, Nature 269, 483-488 .

Harland, W.B., A.V. Cox, P.G. Llewellyn, C.A.G. Pickton, A. G. Smith, and R. Walters (1982). A Geologic Time Scale, Cambridge University Press, Cambridge, 128 pp .

Hay, W.W. (1985). Potential errors in estimates of carbonate rock accumulating through geologic time, in The Carbon Cycle and Atmospheric CO_2: Natural Variations, Archaean to Present, E.T. Sundquist and W.S. Broecker, eds., Geophysical Monograph 32 , American Geophysical Union, Washington, D.C., pp. 573-583 .

Hay, W.W., and J.R. Southam (1977). Modulation of marine sedimentation by the continental shelves: in The Fate of Fossil Fuel CO_2 in the Oceans, N.R. Anderson and A. Malahoff, eds., Marine Science Series 6, Plenum Press, New York, pp. 569-604 .

Hay, W.W., and C.N. Wold (1986). A 150 m.y. cycle in erosion and sedimentation rates, Geological Society of America Abstracts with Programs 18, 632 .

Hay, W.W., and C.N. Wold (1990). Relation of selected mineral deposits to the massage distribution of Phanerozoic sediments, Geologische Rundschau 79, 495-512 .

Hay, W.W., M.J. Rosol, J.L. Sloan, II, and D.E. Jory (1987). Plate tectonic control of global patterns of detrital and carbonate sedimentation, in Carbonate-Clastic Transitions, L.J. Doyle and H.H. Roberts, eds., Developments in Sedimentology, v. 42 , Elsevier, Amsterdam, pp. 1-34 .

Hay, W.W., R. DeConto, M. Leslie, and C.A. Shaw (1989). The St. Lawrence River: A major influence on the North Atlantic during the Cenozoic, Terra Abstracts 1, 438 .

Hays, J.D., and W.A. Berggren (1971). Quaternary boundaries and correlations, in The Micropaleontology of Oceans, B.M. Funnell and W.R. Riedel, eds., Cambridge University Press, Cambridge, pp. 669-691 .

Hsü, K.J. (1978a). Correlation of Black Sea sequences, in Initial Reports of the Deep Sea Drilling Project 42, part 2, D.A. Ross, Y.P. Neprochnov, et al., eds., U.S. Government Printing Office, Washington, D.C., pp. 489-497 .

Hsü, K.J. (1978b). Stratigraphy of the lacustrine sedimentation in the Black Sea, in Initial Reports of the Deep Sea Drilling Project 42, part 2, D.A. Ross, Y.P. Neprochnov, et al., eds., U.S. Government Printing Office, Washington, D.C., pp. 509-524 .

Hsü, J. (1978c). On the paleobotanical evidence for continental drift and Himalayan uplift, Paleobotany 25, 131-142 .

Jenkins, D.G., D.Q. Bowen, C.G. Adams, N.J. Schackleton, and S.C. Brassell (1985). The Neogene: Part 1, in The Chronology of the Geological Record, N.J. Snelling, ed., Geological Society (London) Memoir 10 , Blackwell Scientific Publications, Oxford, pp. 199-210, 251-260 .

Kassler, P. (1973). The structural and geomorphic evolution of the Persian Gulf, in The Persian Gulf: Holocene Carbonate Sedimentation and Diagenesis in a Shallow Epicontinental Sea, B.H. Purser, ed., Springer-Verlag, Berlin, pp. 11-32 .

Kastens, K.A., J. Mascle, C. Auroux, et al., ed., (1987). Initial Reports of the Deep Sea Drilling Project 107, Part A, Initial Report, Tyrrhenian Sea, U.S. Government Printing Office, Washington, D.C., 1013 pp .

Khain, V.Y., A.B. Ronov, and A.N. Balukhovskiy (1979). Neogene lithologic associations of the world, Sovetskaya Geologiya (International Geology Rev. 1981(4) , 426-454).

Lisitzin, A.P. (1972). Sedimentation in the World Ocean, Special Publication 17, Society of Economic Paleontologists and Mineralogists, 219 pp .

Lisitzin, A.P. (1974). Osadkoobrazovanie v Okeanach, Izdatelstvo Nauka, Moscow, 438 pp .

Lyell, C. (1839). Nouveaux Elements de Geologie, Pitois-Levrault et Cie., Paris, 648 pp .

Mackenzie, F.T., and J.D. Pigott (1981). Tectonic controls of Phanerozoic sedimentary rock cycling, Journal of the Geological Society of London 138, 183-196 .

Melguen, M. (1973). Correspondence analysis for recognition of facies in homogeneous sediments off an Iranian river mouth, in The Persian Gulf: Holocene Carbonate Sedimentation and Diagenesis in a Shallow Epicontinental Sea, B.H. Purser, ed., Springer-Verlag, Berlin, pp. 99-114 .

Milliman, J.D. (1974). Marine Carbonates, Springer-Verlag, Heidelberg, 375 pp .

Morner, N.-A. (1976). The Pleistocene/Holocene boundary proposed boundary stratotype in Gothenburg, Sweden, Boreas 5, 193-275 .

Perlmutter, M.A. (1985). Deep water clastic reservoirs in the Gulf of Mexico: A depositional model, Geo-Marine Letters 5 , 105-112 .

Ronov, A., V. Khain, and A.N. Balukhovsky (1986). Quantitative distribution of sediments in oceans, Litol. Polezn. Iskop. 2, 3-16 .

Ross, D.A. (1978). Summary of results of Black Sea drilling, in Initial Reports of the Deep Sea Drilling Project 42, part 2, D. A. Ross, Y.P. Neprochnov, et al., eds., U.S. Government Printing Office, Washington, D.C. , pp. 1149-1178 .

Ruddiman, B., M. Raymo, and A. McIntyre (1986). Matuyama 41,000 year cycles: North Atlantic ocean and northern hemisphere ice sheets, Earth and Planetary Science Letters 80 , 117-129 .

Shaw, C.A. (1988). Balanced paleogeographic reconstructions of the northwestern Gulf of Mexico margin and its western-central North American source area since 65 Ma, U.S. Geological Survey Open-File Report 88-683, 227 pp .

Shaw, C.A. (1989). Mass-Balanced Paleogeographic Modeling: Examples from Western North Atlantic Ocean and Gulf of Mexico, Ph.D. thesis, University of Colorado, Boulder, 381 pp .

Sloan, J.L., II (1985). Cenozoic Organic Carbon Deposition in the Deep-Sea, Cooperative Thesis 89 , National Center for Atmospheric Research, Boulder, Colo., 197 pp .

Stille, H. (1936). The present tectonic state of the Earth, American Association of Petroleum Geologists Bulletin 20 , 849-880 .

Stoffers, P., and D.A. Ross (1974). Sedimentary history of the Red Sea, in Initial Reports of the Deep Sea Drilling Project 23 , R.B. Whitmarsh, O.E. Weser, D.A. Ross, et al., eds., U.S. Government Printing Office, Washington, D.C., pp. 849-865 .

Stoffers, P., E.T. Degens, and E.S. Trimonis (1978). Stratigraphy and suggested ages of Black Sea sediments cored during Leg 42B, in Initial Reports of the Deep Sea Drilling Project 42, part 2, D.A. Ross, Y.P. Neprochnov, et al., eds., U.S. Government Printing Office, Washington, D.C., pp. 483-487 .

Sugden, D.E. (1976). A case against deep erosion of shields by ice-sheets, Geology 4 , 580-582 .

Thunell, R.C., D.F. Williams, and J.P. Kennett (1977). Late Quaternary paleoclimatology, stratigraphy and sapropel history in eastern Mediterranean deep-sea sediments, Marine Micropaleontology 2, 371-388 .

Wetzel, A., and B. Kohl (1986). Accumulation rates of Mississippian sediments cored during Deep Sea Drilling Project Leg 96, in Initial Reports of the Deep Sea Drilling Project 96 , A. H. Bouma, J.M. Coleman, A.W. Meyer, et al., eds., U.S. Government Printing Office, Washington, pp. 595-600 .

White, W.A. (1972). Deep erosion by continental ice-sheet, Geological Society of America Bulletin 83, 1037-1056 .

Wold, C.N., and W.W. Hay (1988). Estimating ancient sediment masses and flux rates, Geological Society of America Abstracts with Programs 20, A78 .

Wold, C.N., and W.W. Hay (1990). Estimating ancient sediment fluxes, American Journal of Science 290, 1069-1089 .

Wold, C.N., W.W. Hay, and K.M. Wilson (1987). Reconstructed mass-age distributions of young sediment through the Phanerozoic, Geological Society of America Abstracts with Programs 19, 895 .

Zeitler, P.K., R.A.K. Tahirkheli, C.W. Naeser, and N.M. Johnson (1982). Unroofing history of a suture zone in the Himalaya of Pakistan by means of fission-track annealing ages, Earth and Planetary Science Letters 57, 227-240 .

2

Surficial Weathering Fluxes and Their Geochemical Controls

ABRAHAM LERMAN
Northwestern University

ABSTRACT

Surficial fluxes of materials from chemical weathering of the bedrock and soils are controlled by the following factors: volume flows and residence times of water on the continents; areal exposure of major rock types; rates of dissolution of minerals reacting with surface water and groundwater solutions; neutralization of acidity brought in part by atmospheric precipitation and in part produced within the weathering zone of the rock; and such major climate-controlled factors as temperature, and carbon fixation by plants and its storage in soils. Variations in some of these factors on the Earth's surface in recent time provide bracketing values for the environmental changes that were occurring between the time of the latest glaciation maximum (18,000 yr ago) and the beginning of the time of anthropogenic effects. The weathering fluxes based on field-analytical observations and experimentally determined dissolution rates of major silicate and carbonate minerals are analyzed for their mutual consistency. Neutralization of acidity by weathering reactions and subsequent increases in the alkalinity of waters reflect the geochemical reactivity of different rock types. The alkalinity-pH relationships of waters reacting with different rock types indicate that the system is exposed to CO_2 pressures from the level of the present atmosphere to levels more than 10 times higher. The formation of new minerals in soils as a by-product of weathering of the primary source rocks provides a temporary storage reservoir that modifies the surficial runoff fluxes in response to environmental changes, of magnitudes comparable to those that occurred in postglacial time. The role of weathering reactions as geoflux buffers is compatible with the rates of soil formation and the rates of chemical denudation on global, continental, and regional scales.

INTRODUCTION

The surficial geofluxes, as understood in this volume, are the fluxes of solid, gaseous, and dissolved materials occurring at the Earth's surface. This chapter deals specifically with the geofluxes associated with *chemical weathering* (or *weathering,* for short) — an assemblage of processes that are related to biogeochemical reactions between waters and minerals or biogenic solids in the surficial sections of the continental crust. Some, and sometimes practically all, of the products of weathering are transported by running surface water and groundwater, which amounts to a release of the crustal materials to the surficial environment, and their subsequent transport on the continents and off the continents to the oceans.

In this volume, various aspects of material transport on global or continental scales have been addressed for the dissolved and suspended materials in rivers (Meybeck, Chapter 4; Milliman and Syvitski, Chapter 5); for sediment transport, crustal denudation, and river flows in Glacial times (Andrews and Syvitski, Chapter 7; Kump and Alley, Chapter 3; Baker, Chapter 6); for eolian transport (Rea *et al.,* Chapter 8); and for the chemical, biogenic, and detrital material fluxes in the oceans (Dymond and Lyle, Chapter 9; Hay, Chapter 1; Martin and Sayles, Chapter 10; see also Schneider and Kellogg, 1973; Milliman, 1993). In view of the importance of continental waters to the weathering geofluxes, the present chapter addresses the following aspects of the weathering releases:

- the residence times of surficial water flows on the continents;
- the main mechanisms of chemical weathering of surficial crustal rocks and soils;
- the dependence of weathering processes on the major environmental changes, comparable to those that occurred since the latest glaciation peak, 18,000 yr ago;
- the magnitudes of variation in the weathering geofluxes that are controlled by water-rock chemical interactions and water flow; and
- the resistance to change displayed by the surficial geofluxes when the surficial environment is exposed to major environmental perturbations.

Water flow is the main agent of material transport from the continents to the oceans and it accounts for the major fraction of the masses of solid and dissolved materials transported from the continents to the oceans: about 90 ± 5 percent of the global material flux from land to the oceans is due to water runoff from the continental surface, and the remaining 10 ± 5 percent of the flux are carried by winds (Garrels and Mackenzie, 1971; Goldberg, 1971; Lerman, 1979; Drever, 1988; Meybeck, Chapter 4, this volume; Milliman and Syvistski, Chapter 5, this volume; Rea *et al.,* Chapter 8, this volume).

Water as a transport agent of continental materials is unique in its continuous movement in a cycle from the oceans to the atmosphere and land, with two-way precipitation and evaporation flows, its occurrence on the Earth's surface as a liquid, gas, and solid; and its ability to react chemically with minerals and biogenic materials, dissolving or altering them in the process. The dual characteristic of water as a substance interacting chemically with the crustal solids and as transport agent carrying dissolved and solid materials is its most important feature in the context of the surficial geofluxes. The flows of ions and electrons occurring in chemical reactions between water and solids underlie such macroscopic processes as dissolution and precipitation, oxidation and reduction, ion exchange, recrystallization of minerals, and the entire complex of biological primary production and respiration.

Ideally one would like to be able to estimate the magnitudes of the surficial geofluxes under different environmental conditions for the past, present, and future by relying on conceptual and mathematical models of the surficial weathering and transport processes. For example, an adequate model for estimation of the weathering geofluxes should ideally be based on fundamental knowledge of such processes as the mechanical disaggregation of rocks by moving ice sheets, mineral dissolution and precipitation rates under different temperatures, chemical composition of flowing waters as controlled by inorganic chemical reactions and biological processes, and the principles of fluid transport by water and wind. Such straightforward estimates, however, derived from "bottom-up" models based on fundamental data and leading to reliable conclusions on regional, continental, or global scales have been achieved more often as exceptions rather than as rules. The complexity of the surficial environment and changes occurring within it on different physical and time scales make many of the estimates based on fundamental principles useful only as orientational values.

On a time scale of some 16,000 yr, from the peak of the last glaciation about 18,000 yr ago to early human times that preceded the spreading of agriculture and the later industrial activity, a number of major environmental changes were likely to affect the surficial releases by the weathering geofluxes. These changes included the reduction of the ice-sheet cover of the continents in the Northern Hemisphere (Kump and Alley, Chapter 3, this volume), the rise of global sea level by some 80 to 120 m; inundation of the continental shelves; an increase in the continental drainage area; changes in the areal exposure of crystalline and carbonate rocks (Meybeck, 1984); possible changes in the volumes of water discharge from land to the oceans; broad

changes in the zonation of the global climate, temperature, and distribution of the vegetation types (NGS, 1988); and likely changes in the storage patterns of the organic material in soils.

The broad global and continental-scale changes in the environment, as listed in the preceding paragraph, remain distinct from the shorter-term events that may have pronounced effects on the physical environment and the major material transport paths. Catastrophic events, such as volcanic eruptions, earthquakes, or floods, may profoundly change the physical environment on a more or less great regional scale, affecting in the process the weathering releases through changes in the water drainage pattern, type of rock exposure, or vegetation cover. The entire scope of anthropogenic activities includes a long and continuously growing list of environmental perturbations that may affect to a variable degree the background surficial weathering and transport, on scales from global to regional. Such a list may begin with the possible global climate change due to anthropogenic increases in the atmospheric greenhouse gases and the anticipated changes in temperature and continental water discharge; continue to the anthropogenic accumulation on land and in waters of reduced metals (iron, copper, zinc, and others), chemically reactive calcium-silicate phases in constructional cements, and by-products of the mining and organic chemical industries; and go on to the chemical changes due to fertilizers in soils, and a changing residence time of organic carbon on land due to reduction of the forest-covered area of the continents.

The physical environment of the surficial weathering releases that is considered in this chapter is shown schematically in Figure 2.1. Water evaporating from the ocean surface precipitates as snow and rain; meltwater and net atmospheric precipitation (precipitation less evaporation) flow over the land surface, penetrate underground, reside for variable lengths of time in lakes, and continue to the oceans. Chemical interactions between water and mineral or biogenic solids result in net releases to, and transport by, water flow.
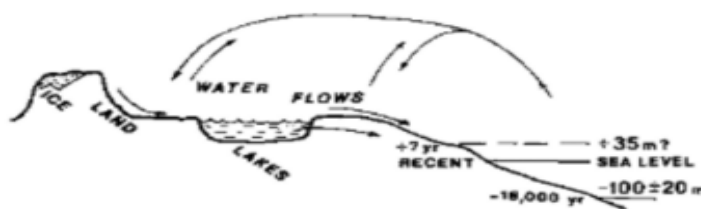
FIGURE 2.1 Continental waters and domains of surficial weathering fluxes.

GLOBAL AND ZONAL WATER FLOWS

Surficial Flows and Storage in Lakes

The volume flow or discharge of water from land to the oceans varies greatly over the globe. To allow for differences between water discharge from land areas of different sizes, a more meaningful measure of volume flow is the specific discharge or discharge per unit area q:

$$q = \frac{Q}{A} \quad (km/yr) \qquad (2.1)$$

where Q is water discharge (km^3/yr) and A is the surface area (km^2) of a drainage basin as measured on a map.

Specific water discharge values for 5°-wide latitudinal zones of the globe have been compiled for water flows from the continents to the oceans, as well as to the internal drainage basins, by Baumgartner and Reichel (1975). Specific discharge is taken equal to the difference between the annual amounts of atmospheric precipitation and evaporation, and as such it includes both the surficial runoff and the groundwater flow. The values of specific discharge are representative of the water volumes flowing to the oceans from each latitudinal zone if the volume storage on the surface and underground remains constant. An increase in the annual amount of net precipitation (i.e., precipitation less evapotranspiration from land) may be expected to be initially distributed in some greater storage of water on the land surface and underground, ultimately finding its way in the flow to the oceans. A large uncertainty associated with estimates of the length of time it would take for the surface runoff to respond to a major change in the amount of water input to land from the atmosphere is related to the knowledge of the volumes and residence times of surficial water and groundwater.

The value of the surficial global water discharge to the oceans is 3.74×10^4 km ^{3}/yr, excluding the discharge from Greenland and Antarctic, and the global drainage area for discharge to the oceans is nearly 1×10^8 km^2 (Baumgartner and Reichel, 1975; Meybeck, 1984; Table 2.1). The volume of global continental ice and snow, excluding the Antarctic and Greenland, is about 122,000 km^3 (Barry, 1985). Faster melting of the continental snow and ice sheets at a rate of 1 percent per year would initially increase the discharge from land by up to 3 percent. Increased storage capacity of the meltwater in big periglacial lakes, such as the big lakes occurring on the margins of the Canadian shield and the older lakes (Baker, Chapter 6, this volume), might reduce this estimate of an initial increase in global discharge. Ultimately, however, continuous melting would add more water to the continental surface and likely

exceed its storage capacity for making new lakes. The present-day continental ice and snow volume, 122,000 km^3, is almost equal to the global volume of freshwater lakes, 125,000 km^3 (Table 2.1).

The estimate of the freshwater lake volume (Table 2.1) excludes such big bodies of brackish or saline waters as the Caspian Sea, Aral Sea, Great Salt Lake, and other saline lakes. There are relatively few large-volume lakes in the world, with water volumes greater than 1000 km^3—10 or 11—and even fewer (3) with volumes greater than 10,000 km^3. The 10 largest lakes account for about 61 percent of the total freshwater lake volume, and lakes of volume greater than 1 km^3 account for 67 percent of the total (Lerman and Hull, 1987). It is difficult to decide where a line should be drawn defining a lake of "a minimum size." A conventional practice of classifying lakes by their surface areas rather than volume does not give the measure needed for the water retention times on land. An arbitrary cutoff volume of about 1 km^3 was adopted here for lakes, and the plot in Figure 2.2 of the water residence times for a sample of such lakes indicates a modal class of residence times between about 3 and 10 yr, with a mean of about 5.5 yr. The geographic distribution of the lakes, particularly of the bigger ones, is very uneven: most of the biggest lakes of known water residence time occur in the Northern Hemisphere, such as the Laurentian Great Lakes discharging to the North Atlantic and Lake Baikal discharging via the Angara River to the Arctic Ocean.

TABLE 2.1 Water Residence Times on Land and Background Data

Parameter	Value	References and Comments
Global water discharge to Oceans (Q_T)	3.74 X 10^4 km^3/yr	Baumgartner and Reichel (1975) Meybeck (1984)
Continental drainage area for discharge to oceans (A_T)	9.9913 X 10^7 km^2	Baumgartner and Reichel (1975)| Meybeck (1984)
Continental ice and snow cover (without Greenland and Antarctic)	1.22 X 10^5 km^3	Barry (1985)
Freshwater lakes		Herdendorf (1982) and additional References in Lerman and Hull (1987)
Volume (V_L)	1.25 X 10^5 km^3	
Surface area (A_L)	8.55 X 10^5 km^2	
Drainage basin area (A_{DB})	=2.5 X A_L km^2	
Water residence times		This chapter
Freshwater lakes (t_L)	= 5.5 yr	
Rivers without major lakes in their basins (t_r)	0.65 to 6.5 yr	
Global average for discharge to oceans (t)	0.3 to 3 yr	
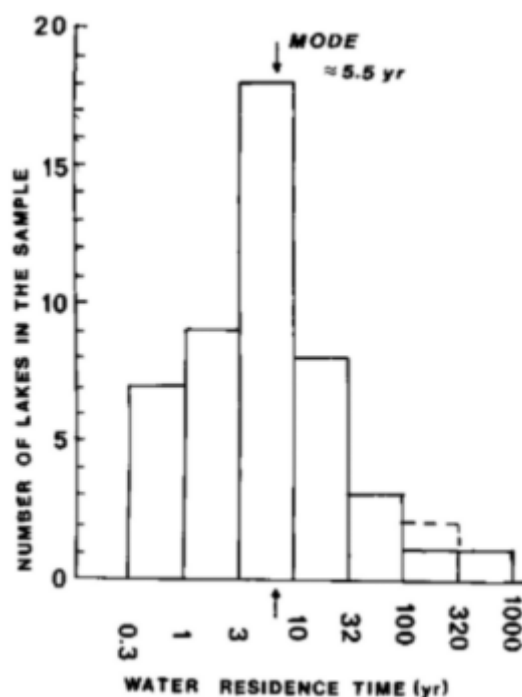
FIGURE 2.2 Residence times of water in lakes of volume >1 km^3. Residence time equals volume/outflow. From data tabulated in Lerman and Hull (1987).

Residence Times of Zonal Water Discharge

The residence time of water on the continents may be expected to vary greatly, from the short flow times for water in river channels to the much longer times for waters in deeper aquifers. For big rivers, the residence times of waters in the main river channel are relatively short, if estimated as times of flow, at velocities of 10° cm/s, over distances of 10^3 km—less than one year. For the latitudinal zonal runoff from the continents, the water residence time is numerically equal to the volume pore space of the surface rocks through which it flows, divided by the volume discharge. The net thickness of the porous layer for surface flow may be bracketed between 10 cm and 1 m, corresponding to a two- to fivefold variation in thickness of a rock or soil layer, of porosity 50 to 20 percent. Then the mean residence time of water, computed as shown below, is bracketed by a factor of 10 (Eq. 2.2): This cumulative distribution of the zonal water residence times is shown in Figure 2.3. The median residence time is about 3 yr at the long end and about 0.3 yr at the short end of the estimates. In arriving at these estimates, it should be borne in mind that small values of specific discharge q that are characteristic of dry or cold high latitudes, produce longer residence times, accounting for the conclusion from Figure 2.3 that 50 percent of the surface discharge may have residence times longer than 3 yr.

$$\bar{t} = \frac{0.1}{q} \text{ to } \frac{1}{q} \text{ (yr).} \qquad (2.2)$$
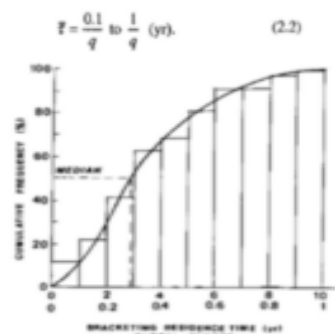
FIGURE 2.3 Residence times of water on the continents with respect to discharge to the oceans. Water runoff (discharge per unit area, q) data for 5°-wide latitudinal zones, from 80° N to 80° S (Baumgartner and Reichel, 1975), and Eq. (2.2). Assumed net thickness of the discharge conducting layer, 10 to 100 cm, results in a tenfold range of residence time values on the abscissa.

Residence Times on a Global Scale

Global discharge to the ocean includes the rivers that drain the major lakes and lake systems, as well as river and land-surface flows that do not pass through big lakes in their drainage basins. Estimates of the two kinds of discharge may be arrived at as follows.

As shown schematically in Figure 2.4, the total water discharge to the oceans Q_T is the sum of a discharge from the lakes (Q_L) and discharge from rivers without lakes (Q_r):

$$Q_T = Q_L + Q_r \text{ (km}^3/\text{hr)} \qquad (2.3)$$

A fraction of the total flow passing through lakes is a ratio of the global freshwater lake volume V_L and the mean residence time $<St>_L$ (data in Table 2.1):

$$Q_L = \frac{V_L}{\tau_L} = \frac{125,000}{5.5} = 2.27 \times 10^4 \text{ km}^3/\text{yr.} \qquad (2.4)$$

The straight river discharge, from Eq. (2.3), is therefore

$$Q_r = Q_T - Q_L = (3.74 \times 10^4) - (2.27 \times 10^4) \qquad (2.5)$$
$$= 1.5 \times 10^4 \text{ km}^3/\text{yr.}$$
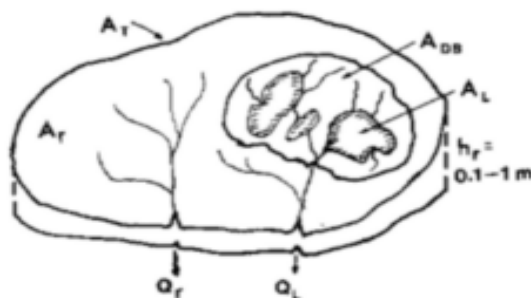
FIGURE 2.4 Global land drainage area for discharge to the oceans (A_T), surface area of freshwater lakes (A_L) and their drainage basins (A_{DB}), and the remaining area for rivers without major lakes in their drainage basins (A_r). A surface layer of rock and soil for conductance of the discharge has a net thickness $[h_r] = h$, or bulk thickness times porosity.

The residence time of the river discharge portion Q_r is where, as shown in Figure 2.4, h_r is the net thickness of a layer through which water flows (h_r = 10 to 100 cm) and A_r is the drainage area of the rivers without lakes. This drainage area is the difference between the global total drainage area A_T and the sum of the global lake surface area A_L and the area of the lake drainage basins A_{DB} (Table 2.1):

$$\tau_r = \frac{A_r h_r}{Q_r} \quad (yr),\qquad (2.6)$$

$$A_r = A_T - (A_L + A_{DB}) \qquad (2.7)$$
$$= 9.991 \times 10^7 - [8.55 \times 10^5 (1 + 2.5)]$$
$$\approx 9.7 \times 10^7 \ km^2.$$

The total area of the lake surface and drainage basin is small relative to the land area, and the factor of 2.5 assumed for the drainage basin to lake surface area does not significantly affect the estimate. From the preceding values, an estimate of the residence time of straight river flow from the continents to the oceans is, from Eq. (2.6),
t_r = 0.65 to 6.5 yr.

This estimate for the residence time of the direct runoff is comparable to the estimate of the mean water residence time in lakes, the lower and upper bounds reflecting the factor of 10 in the assumed range of the effective thickness of the water-conducting surficial layer h_r.

Summary of Water Flows and Residence Times

Mean residence times of water on the land surface, partitioned into a river flow component passing through lakes and a component running off directly to the oceans are of the same order of magnitude: a mean of 5.5 yr for the lake outflow and 6.5 yr for an upper-end estimate of direct runoff. The mean residence time for lake-draining rivers does not well represent the very wide range of lake residence times that extends up to several centuries and their geographically uneven occurrence.

If the water residence time t estimates are taken at their face value, the response times would be short (years to decades) for changes in the chemical characteristics of surface flows—changes in inputs from chemical weathering or other sources. A measure of t is a characteristic time of the system response to changes in the chemical inputs.

WEATHERING FLUX

A Conceptual Mode

Water flowing over the land surface and within a shallow conductive layer of some thickness within the rocks and soils reacts with minerals, producing some dissolution that results in a net transport of dissolved materials. Figure 2.5 illustrates schematically the direction of the surficial water discharge as it passes through a porous layer of some net thickness h_r, assumed to be bracketed between the values of 10 cm and 1 m. A material balance equation for the process depicted in Figure 2.5 should take into account the various processes that either add or remove solutes in the runoff. Such processes include inputs of dissolved materials from dissolution of bedrock and soil minerals; inputs from atmospheric precipitation; and either storage of dissolved materials in, or their removal from, the pools of exchangeable cations in secondary minerals in soils or the biomass (Drever, 1988, p. 224; Wright, 1988). The transport balance equation for net weathering as shown in Figure 2.5 may be written in the following form:

[Transport in solution] =

[bedrock and soil mineral dissolution] ±

[leaching from, or storage in, secondary minerals] ±

[input from, or storage in, vegetation] +

[input from atmospheric precipitation].

Soil is a product of chemical alteration of the bedrock and organic matter accumulation from vegetation, and it contains some of the primary minerals of the bedrock, some newly formed secondary minerals (such as clays), and organic matter (humus) (Sposito, 1985). Thus the entry in
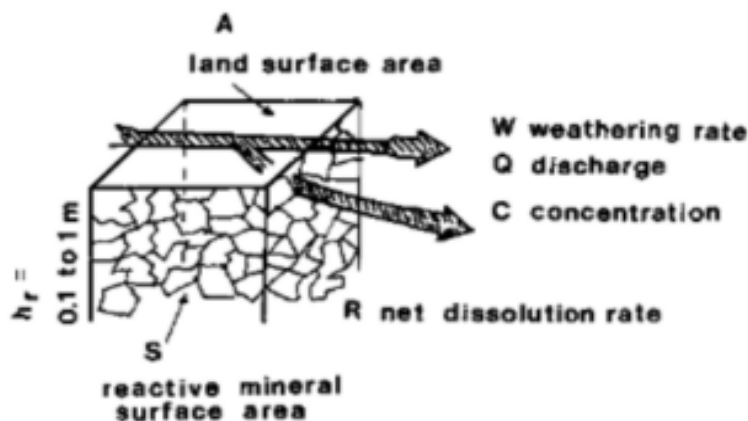
FIGURE 2.5 Water flow through a porous surface layer of bulk thickness h and net thickness h_r = h, as in Figure 2.4. A is the horizontal projection or map area; S is the surface area of minerals in contact with water flow within the layer h.

the balance equation labeled bedrock and/or soil mineral dissolution represents total possible input from dissolution processes. If the pool of secondary minerals in soils and the mass of vegetation are constant—that is, the rate of soil growth is balanced by its erosion rate and the vegetation growth is balanced by its decay—then the flux of dissolved material in solution is equal to the rate of its supply from mineral dissolution. The question of a constant mass of secondary minerals in soils and of vegetation deserves further notice.

Experimental work and field studies demonstrate that addition of acid waters to rocks and soils generally results in greater weathering (Likens *et al.,* 1977; Cronan, 1985; Folster, 1985; Wright, 1988; Probst *et al.,* 1990, 1992). The same authors have also recorded that, on geologically short time scales of months to a few years, higher water acidity variably results in an increased uptake of cations by vegetation and increased leaching from the so-called "cation pool of soil." The exchangeable cations in soils, however, represent only a very limited pool relative to the bedrock that is available to dissolution and release to the weathering flux: it has been estimated that at the observed rates of cation dissolution from soils, the entire cation-exchange pool would be exhausted in about 50 to 100 yr if there were no replenishment from the bedrock dissolution (Schnoor and Stumm, 1986). Therefore it is important to emphasize that prehuman background weathering fluxes are effectively those of the rock mineral dissolution rather than a transient perturbation of the pool of exchangeable cations in the secondary minerals of soils.

Weathering Flux Equations

Mass and Linear Weathering Rates Based on the conclusions of the preceding section, the flux of dissolved materials in global runoff is treated as a measure of bedrock and soil weathering. The rate of weathering is usually expressed as mass loss per unit area of the geographic rock surface per unit of time:

$$W = Cq = \frac{RS}{A}, \qquad (2.8)$$

where W is the net weathering rate (mol or g/cm^2/s), C is concentration in solution (mol/cm^3), q is specific discharge defined in Eq. (2.1) (cm/s), R is a mineral dissolution rate (mol/cm^2/s), A is a horizontal or map surface area (cm^2), and S is the reactive surface area of the rock in contact with water, as shown in Figure 2.5 (cm^2). The mass weathering rate W can be converted to a linear rate W_h (cm/s) that represents a vertical recession of a solid surface due to dissolution:

$$W_h = \frac{W}{(1 - \phi)\rho}, \qquad (2.9)$$

where ρ is the mineral density (mol/cm^3) and is the rock porosity (0 - < 1). For a solid of zero porosity and uniform density, the linear dissolution rate is the quotient W/ρ. The preceding relationships for the rate of weathering are simolifications that do not reflect the detailed nature of the various mechanisms of mineral-water interactions (Murphy *et al.,* 1989).

Rates of weathering of different rocks and soils, and continental units are summarized in Table 2.2. These rates have generally been estimated in the literature sources by using procedures similar to the computational method of Eq. (2.8): the rates are based on the analytically determined concentrations of dissolved constituents in surficial and shallow-ground runoff, and water discharge data summed for the drainage areas of regions, continents, and the globe.

Weathering rates $W,$ computed as a product of concentration of dissolved constituents in river water and river discharge, produce near-linear plots in graphs of log W as a function of log q for sets of rivers draining geologically diverse terrains (Berner and Berner, 1987; Meybeck, Chapter 4, this volume). The log-log plots of W against q also indicate considerable variability in river-water concentrations of solutes that reflects differences in lithology and hydrology of the drainage basins. An approximately linear relationship between log W and log q is a feature that holds for the river basins where concentration and discharge values presumably reflect averages over periods of years. On a shorter time scale, however, concentrations of land-derived materials in rivers may depend pronouncedly on seasonal water discharge.

Surface Areas: Reactive Rock (S) and Land Surface (A) The ratio of the reactive surface area of mineral grains exposed to water below a unit of land surface area, as shown in Figure 2.5, appears as a quotient S/A in the weathering rate Eq. (2.8). The reactive surface area of minerals is not necessarily equal to the physical surface area of the grains, as commonly determined by the gas adsorption method. White and Peterson (1986) concluded that the reactive surface areas of minerals, computed from laboratory dissolution experiments, may be smaller that the physical grain areas by a factor of as much as 100. A simple estimate of a representative range of values for the area ratio S/A may be obtained as follows. The physical surface areas of common types of sediments are in the range of 1 to 20 m^2/g (10^4 to 10^5 cm^2/g). The column of a rock or sediment through which discharge is conducted (Figure 2.5), may be characterized by some thickness $h,$ effective porosity and mineral density ρ. The mass of

such a column may be estimated by using representative values of

TABLE 2.2 Chemical Weathering Rates (W) for Different Rock and Soil Types, from Different Areas (see also Figure 2.7)

Weathering	Weathering Rate Mass/Area/Time (W)	Length/Time (W_h)	References and Comments
Global mean	33 to 40 g/m^2/yr	14 ± 1 mm/ka (ka = 1000 yr)	Meybeck (1988), mass rate converted to Linear rate for bulk density, r » 2.5 to 2.7 g/cm^3
Continental averages			Garrels and Mackenzie (1971)
Africa	24 g/m^2/yr		
Asia	32 g/m^2/yr		
Australia	2 g/m^2/yr		
Europe	42 g/m^2/yr		
North America	33 g/m^2/yr		
South America	28 g/m^2/yr		
Shields and sediments		5 to 30 mm/ka	Stallard (1988)
Silicate rocks		80 mm/ka	Stallard (1988), Andean drainage
Carbonates and shales		200 mm/ka	Stallard (1988), Andean drainage
Evaporites		700 mm/ka	Stallard (1988), Andean drainage
Volcanics	18 g/m^2/yr	7 mm/ka	Drever (1988), andesitic terrain in Absaroka Mts., Wyoming
Sandy-silty soils	0.05 to 0.27 eq/m^2/yr	7 to 40 mm/ka	Cronan (1985)
Small stream watersheds and catchment areas	0.024 to 0.20 eq/m^2/yr	4 to 30 mm/ka	Fölster (1985), data compiled for areas in United States, Norway, Sweden, England, and Germany
Various soils			
Loess soils	0.04 to 0.10 eq/m^2/yr	6 to 15 mm/ka	Fölster (1985)
Soils in lake drainage basins	0.06 eq/m^2/yr	9 mm/ka	Wright (1988), literature data for Adirondack Mts., New York, and
Deglaciated terrains	0.93 eq/m^2/yr	140 mm/ka	Cascade Mts., Oregon

NOTE: Conversion of the weathering rates in units of g/m^2/yr to units of vertical recession of the land surface, in millimeters per 1000 yr (mm/ka), was done by dividing the mass rate by a rock density value of about 2.5 g/cm^3; see Eq. (2.9).
The rates in eq/m^2/yr are often based on concentrations of four cations (Ca^{2+}, Mg^{2+}, Na$^+$, and K$^+$) in runoff. To convert to millimeters/year, the values in eq/m^2/yr are multiplied by averaging factors of 1.5 mol/eq and molar density of minerals (100 cm^3/mol), the latter based on round-figure values of about 250 g/mol for feldspars and a density of 2.5 g/cm^3. Such W_h estimates are good to a factor of about two.

$$h_s = h(1 - \phi) = 10 \text{ to } 100 \text{ cm, and } \rho \approx 2.5 \text{ g/cm}^3$$

and a mass of

$$Ah_s\rho = 1 \times \binom{10}{100} \times 2.5 = 25 \text{ to } 250 \text{ g.}$$

The area ratio within such a material column is, approximately,

$$\frac{S}{A} = \left(\frac{10^4}{10^5}\right) \times \left(\frac{25}{250}\right) \approx 2.5 \times 10^{6\pm1}.$$

From the preceding estimates of the surface area in a 0.1- to 1-m-thick layer, the ratio of S to unit map-surface area A is

$$\frac{S}{A} = 10^5 \text{ to } 10^7. \qquad (2.10)$$

A more accurate computational estimate of the rock surface area S can be made if the particle-size and shape distributions for the surface rock layer are known. In Figure 2.6 are shown the particle-size distributions of a granite in Wisconsin and of a residual soil. The weathered rock is, as expected, characterized by larger particle sizes than the overlying soil, and the size distribution for the rock is pronouncedly skewed toward larger particles. The particle-size spectral distributions in Figure 2.6 indicate

that the smaller particles in soils may become more abundant at the expense of the larger particles in the parent rock.
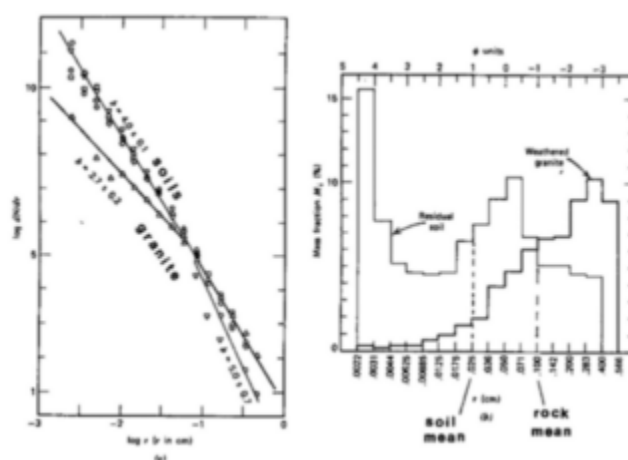
FIGURE 2.6 Particle-size distributions for a Wisconsin granite, its residual soil, and residual soils on other crystalline rocks. Right: frequency histogram for granite and soil; left: particle-size spectra for the granite and residual soils. From Lerman (1979) with permission of John Wiley & Sons, New York.

The total surface area of particles in a sediment column of unit cross-sectional area and height h can be written as

$$s = (1 - \phi)h \int_{r_1}^{r_2} s(e)f(r)dr, \qquad (2.11)$$

where is the sediment layer porosity, h is the bulk thickness (i.e., solid particles and pore space) per unit area of the layer, $s(r)$ is the surface area of a particle of a characteristic linear dimension r, $f(r)$ is the number of particles with size between r and $r + dr$ occurring in a unit volume of the sediment layer (particle-size distribution is $dN = f(r)\, dr$, where N is a number of particles per unit volume), and r_1 and r_2 are the lower and upper size limits of the particle sample.

For spherical particles of a mean radius r, the ratio of the areas S/A is

$$\frac{S}{A} = 4\pi r^2 Nh. \qquad (2.12)$$

The number of spherical particles of radius r in a unit volume of solid, $1-$, is

$$N \approx \frac{1 - \phi}{4\pi r^3 / 3}, \qquad (2.13)$$

which gives, in combination with Eq. (2.12),

$$\frac{S}{A} = \frac{3h_s}{r}. \qquad (2.14)$$

The mean particle sizes for a weathered rock and a residual soil on it may be taken from the data in Figure 2.6: (rock) $r \approx 0.1$ cm, (soil) $r \approx 0.025$ cm.

By using the preceding estimates, the surface area quotient *S/A* can be computed as

$$\frac{S}{A} = \frac{3 \times (10 \text{ to } 100 \text{ cm})}{(0.1 \text{ to } 0.025 \text{ cm})} = 10^3 \begin{bmatrix} \times 10 \\ +10 \end{bmatrix}. \qquad (2.15)$$

The latter estimate of the area ratio *S/A* is lower than the estimate in Eq. (2.10), emphasizing the uncertainties involved in the estimates of two fundamental parameters: the thickness of the rock-soil layer conducting most of the surficial water flow and the surface area of the reactive solid fraction.

Mineral Dissolution Rates (R)

Terminology For a discussion of weathering processes in mineral-water systems, a brief clarification of some of the concepts and terms is given:

- Dissolution is a process of transfer of mass from a solid to the aqueous phase. A rate of dissolution is measured in units of mass per unit of surface area of a dissolving mineral per unit of time, commonly in units of $mol/cm^2/s$.
- Solubility of a solid phase is a measure of the mass that can be dissolved in an aqueous solution at an equilibrium with the solid. Units of solubility are those of concentration—mol/cm^3, for consistency with the units of the dissolution rate.
- Leaching is a broader term, frequently used in soil science and environmental engineering literature, and it denotes transfer of some of the components of the solid to solution. Thus, leaching may indicate a net result of such combinations of processes as ion exchange, dissolution, and precipitation; recrystallization of a solid and release of some of its minor constituents; or a preferential dissolution of some of the solid components that is also referred to as incongruent dissolution.

Dissolution Rates of Silicate and Carbonate Minerals As a generalization, highly soluble minerals are often also characterized by relatively faster dissolution in water. This observation has historically lead to a not-always-valid conclusion that the rate of dissolution of a solid is directly related to "its distance from saturation" or to the difference between instantaneous concentration in solution and concentration at saturation. In such a mode, dissolution is initially relatively fast, but it slows down as an equilibrium or saturation is approached.

The common evaporite minerals halite (NaCl), gypsum ($CaSO_4$-$2H_2O$), and anhydrite ($CaSO_4$) dissolve faster than carbonates and silicates in pure water (Van Name, 1929); and the surficial environment, evaporite deposits containing these minerals also weather faster than rocks made of silicates and carbonates (Garrels and Mackenzie, 1971, with references to earlier observations; Colman and Dethier, 1986; Stallard, 1988, 1989). The rates of dissolution of a number of silicate minerals are listed in Table 2.3. Additional information on dissolution rates of these and other silicate minerals can be found in the publications referenced in the table.

A somewhat striking characteristic of the dissolution rates of the common silicates, even for a small sample of minerals listed in Table 2.3, is a variation by a factor of up to 10^5 in the rates from one mineral to another, quartz

TABLE 2.3 Dissolution Rates R Silicate Minerals.

Mineral	Formula	Log *R* (mol $SiO_2/cm^2/s$)	*n* for Acid Range	*n* for Alkaline Range	Reference
			Dependence of *R* on $[H^+]^n$		
Albite	$NaAlsi_3O_8$	-15.8 to -14.3	0.5	-0.3	Chou and Wollast (1985)
Anorthite	$CaAl_2Si_2O_6$	-15.5 to -13	1.0	-0.3	Brady and Walther (1989) with additional references
Chrysotile	$Mg_3Si_2O_5(OH)_4$	-16.0 to -15.5	—	-0.3	Bales and Morgan (1985)
Diopside	$CaMgSi_2O_6$	-14.5 to -12	0.5	—	Schott *et al.* (1981)
Forsterite	Mg_2SiO_4	-13.8 to -12	0.5	-0.3	Blum and Lasaga (1988)
Quartz	SiO_2	-16.3 to -14.5	~0	-0.3	Brady and Walther (1989)
Nepheline	$NaAlSiO_4$	-12.5 to -10.5	1.0	-0.3	Tole *et al.* (1986)

NOTE: Lower values of *R* apply to the near-neutral pH range from about 5.5 to 7.5. Rates increase as the pH becomes lower or higher than near-neutral (see Figure 2.7).

having reportedly the lowest rates at 25°C. The band of dissolution rates of silicates is plotted in Figure 2.7.
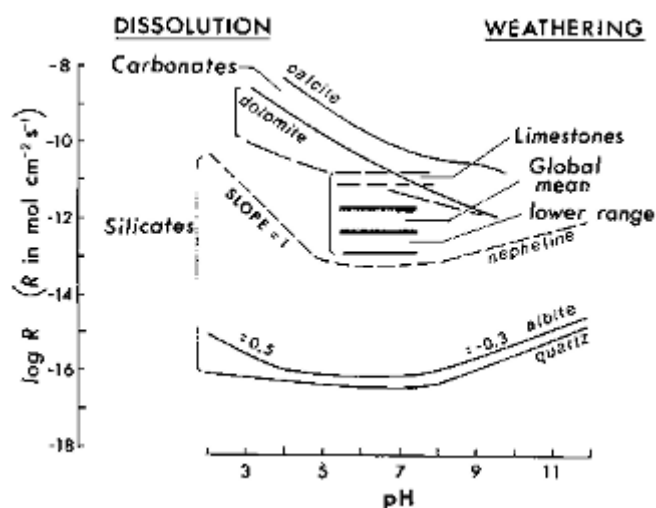
FIGURE 2.7 Dissolution rates of silicates and carbonates as a function of pH. Band bracketing dissolution rates for silicates are from data in Table 2.3. For carbonates, data of Plummer et al. (1978) are used for calcite, and of Chou et al. (1989) for calcite and dolomite. Chemical weathering rates shown for comparison with the experimental values are from Table 2.2. Adopted from Lerman (1979).

For carbonates, the experimentally determined rates of dissolution for calcite and dolomite (Plummer *et al.,* 1978; Chou *et al.,* 1989), shown in Figure 2.7, are significantly higher than those for silicates; this feature finds its reflection in the weathering rates of carbonate rocks, which are generally higher than those of crystalline silicate rocks.

HYDROGEN-ION AND TEMPERATURE DEPENDENCE OF DISSOLUTION RATES

The pH and Natural Acidity

The rate of dissolution of a mineral is generally some function of the environmental conditions, such as the composition of the aqueous solution and temperature. The H^+ concentration (a characteristic of the aqueous solution composition) and the temperature are two of the environmental variables addressed in this section.

The silicate and carbonate mineral dissolution rates are plotted in Figure 2.7 as bands bracketing the higher and lower values of the dissolution rates of the individual minerals. For the silicates it should be noted that in acidic solutions of pH $\leq$ 5.5, the dissolution rates increase in proportion to a power of the hydrogen-ion concentration as $[H^+]^{0.5}$ to $[H^+]^{1.0}$. The solution pH at which an increase in the dissolution rate begins has been reported to vary from mineral to mineral, occurring between a pH of about 5.5 and lower.

In the near-neutral pH range from approximately 5.5 to 7.5 or 8, the dissolution rates are about constant near the low end of each range shown in Table 2.3. In alkaline solutions, above pH 7.5 to 8, the dissolution rates increase in proportion to $[H^+]^{-0.3}$. Theoretical interpretations of the dependence of silicate dissolution rates on a power of $[H^+]$ have been advanced through the mechanisms of surface reactions and transition-state theory (Wollast and Chou, 1988; Schott and Petit, 1987).

Carbon dioxide is the main atmospheric gas that determines the background acidity of atmospheric precipitation and fresh waters exposed to the atmosphere. Variations in the reported CO_2 content of the atmosphere during the past 18,000 yr indicate an increase from about 180 parts per million by volume (ppmv) or a PCO_2 of 1.8 x 10^{-4} atm, through the preindustrial-age value of about 280 ppmv, to the present concentration of 345 ppmv (Barnola *et al.,* 1987; Siegenthaler and Oeschger, 1987). Such variations in the carbon dioxide partial pressures could have had only very minor effects on the pH of pure rainwater, which indicates a decrease of about 0.14 pH unit:

PCO_2 = 1.8 x 10^{-4} atm: pH = 5.73 (5°C) and 5.79 (25°C),

PCO_2 = 3.4 x 10^{-4} atm: pH = 5.59 (5°C) and 5.65 (25°C).

For ocean water, in anticipation of a continued anthropogenic CO_2 increase in the atmosphere, Whitfield (1974) estimated that a rise from 313 to 453 ppmv would lower the pH of surface ocean water by about 0.08 pH unit, from 8.24 to 8.16.

Additional sources of background natural acidity in atmospheric precipitation are the oxidation products of reduced nitrogen and sulfur emissions, which yield H_2SO_4 and HNO_3, and some HCl emissions from active volcanoes. On the land surface, the primary sources of acidity are the oxidation of pyrite (FeS_2) to produce sulfuric acid; the release of organic acids by living plants and humus; and the oxidation of organic matter, which mostly contributes CO_2 to groundwaters. The importance of the latter process to weathering releases is discussed later.

For purposes of visualization in Figure 2.7, where an increase in the silicate dissolution rate is shown to begin at pH $\approx$ 5.5, a decrease in the pH of a solution by 1 pH unit may result in a three- to tenfold increase in the dissolution rate.

Temperature Effects on Dissolution Rates

The warming trend since the glaciation peak about 18,000 yr ago translates into a rise in mean global temperature from about 10 to 16°C at present (Lorius *et al.,* 1985; Jouzel *et al.,* 1987). Considerably greater variations in temperature char

acterize the Northern Hemisphere at present. Any direct effects of temperature on the dissolution rates of silicate minerals in the bedrock and soils may overlap the effects of increased biological productivity and carbon fixation by plants, with an attendant increase in bacterial activity in soils that may be a significant contributor to weathering. An increase in the rate of net primary production of land plants by a factor of 4 to 5 occurs for a move from cold regions (0 to 5°C, carbon fixation rate 500 to 750 $g/m^2/yr$) to the humid tropics (about 25°C, 2000 to 2700 $g/m^2/yr$) (Lieth, 1975). An increase in bacterial activity from colder to warmer latitudes is also indicated by the lower humus content in tropical soils because of its faster decomposition than in temperate and northern latitudes (Post *et al.,* 1982). Coincidentally with the north to south increase in plant productivity by a factor of 4 to 5, an increase by a similar factor in the dissolved SiO_2 of rivers from the tundra to the humid tropics has been reported by Meybeck (Chapter 4, this volume); from about 3 to 15 mg/liter. A similar increase may be anticipated in an inorganic silicate-water system due to a temperature rise from 5 to 25°C, as shown below.

The dependence of the rate of a dissolution reaction on temperature is an Arrhenius-type equation where the subscript 0 denotes a reference temperature and reaction rate, R is the dissolution rate ($mol/cm^2/s$), T is temperature (kelvin), R is the gas constant, R = 8.314 ∞ 10^{-3} kJ/mol/°C, and ΔE is an activation-energy parameter for the reaction (kJ/mol). The values of ΔE for commonly occurring silicate minerals, in the pH range from about 4 to 8, vary from 38 kJ/mol for diopside (Table 2.3) to 72 kJ/ mol for quartz (Rimstidt and Barnes, 1980; Schott and Petit, 1987; Brady, 1991). By taking a mean of this range, with the temperature increasing from 5 to 25°C, the dissolution rate increase can be computed as

$$\log \frac{R}{R_0} = \frac{\Delta E}{2.3R}\left(\frac{1}{T_0} - \frac{1}{T}\right), \qquad (2.16)$$

$$\log \frac{R}{R_0} = \frac{55 \pm 15}{2.3 \times 0.0083}\left(\frac{1}{278} - \frac{1}{298}\right) \text{ and} \qquad (2.17)$$

$$\frac{R}{R_0} \approx 5.5 \pm 2.5.$$

As pointed out previously, an increase in the silicate dissolution rate by a factor of about 5 due to a temperature increase from the tundra to the tropics coincides with an increased rate of carbon fixation by plants. It must also be viewed in light of the experimental results on the dissolution of silicate and other types of minerals by soil bacteria (Eckhardt, 1985; Berthelin, 1988), where bacterially induced rates of dissolution were reported as up to 100 times faster than in the absence of bacteria.

WEATHERING AND DISSOLUTION

The estimates of mean weathering rates for the continental surface are plotted for comparison with the experimental dissolution rates for silicates and carbonates in Figure 2.7. The surface area for global discharge is given in Table 2.1. The global estimates and estimates for the major continental drainage systems fall within a bracketing range of about a factor of 10 of each other. The global mean, as may be expected, falls between the slower-weathering silicate rocks and the faster-weathering limestones.

The differences between the weathering rates based on field-analytical data and the experimentally determined dissolution rates of the individual minerals (Tables 2.2 and 2.3; Figure 2.7) are, in many cases, difficult to explain (Deike, 1989). For example, Paces (1985) and Velbel (1985) concluded that field dissolution rates, based on the best reasonable estimates of the mineral surface areas, are much slower than the rates indicated by laboratory results.

The weathering rates of sandy-silty soils, volcanic rocks and crystalline silicate rock terrains (Table 2.2) are in the range of about 18 to 200 $g/m^2/yr$. The dissolution rates of common silicate minerals given in Table 2.3 are much lower, 10 to 10^{-5} $g/m^2/yr$. For dissolved SiO_2 in rivers, taken as a measure of the weathering rate of crystalline bedrock, the computed weathering rate W is also considerably higher than the experimentally determined dissolution rates R of the common silicate minerals:

$$W/R \approx 10 \text{ to } 10,000.$$

The big differences between the weathering and dissolution rates may be reconciled by the surface-area ratio factor, *S/A,* of comparable magnitude, as discussed earlier. However, any such agreement between the weathering rates may fortuitously overlap the effects of other biogeochemical factors in the weathering process.

For the global flux of calcium in rivers, the following fractions have been attributed to different rock types (Wollast and Chou, 1988, based on data in Wollast and Mackenzie, 1983):

from carbonate weathering: 68 percent

from silicate weathering: 12 percent

from evaporites: 14 percent

from sulfide oxidation: 6 percent.

In the preceding balance of calcium sources in weathering, about 80 percent should be accounted for by weathering of carbonate and silicate rocks. The outcrop area of carbonate rocks on continents at present time is about 16 percent of the total area (Meybeck, Chapter 4, this volume). The weathering rate W for calcium in carbonate and silicate rocks can be written as a weighted sum of weathering rates (compare Eq. 2.8):

$$W = \frac{1}{A_T}(R_1 A_1 + R_2 A_2)\frac{S}{A} = (R_c x_c + R_s x_s)\frac{S}{A}, \quad (2.18)$$

where the subscripts c and s denote carbonates and silicates, respectively, and x is the fraction of the total drainage area due to each rock type. Further refinement, such as inclusion of the individual dissolution rates of limestones, dolostones, and different types of silicate rocks, is not justified for this simple computation.

By using the ranges of carbonate and silicate dissolution rates from Figure 2.7, and the preceding estimates of the carbonate outcrop area and the percentage contributions of rock types, the weathering rate W is

$$W = \left[\begin{pmatrix} 10^{-9} \\ 10^{-11} \end{pmatrix} \times 0.16 + \begin{pmatrix} 10^{-11} \\ 10^{-16} \end{pmatrix} \times 0.84\right]\frac{S}{A} \quad (2.19)$$

$$= \left[\begin{pmatrix} 10^{-10} \\ 10^{-12} \end{pmatrix} + \begin{pmatrix} 10^{-11} \\ 10^{-16} \end{pmatrix}\right] \times \begin{pmatrix} 10^3 \\ 10^2 \end{pmatrix}.$$

An upper bound of the weathering rate W from the preceding equation is 10^{-7}, a value much greater than the mean chemical denudation rate of about 10^{-12} mol/cm^2/s, shown in Figure 2.7 and Table 2.2.

In this computation, the same value of the S/A ratio was arbitrarily taken for the carbonate and silicate rocks. A more careful inspection of the numerical terms in the computation of W would show that the first term of the sum representing carbonate dissolution is the main contributor to the high value of W, which is further magnified by the surface-area ratio term $S/A >> 1$. This contribution would have been reduced if the S/A value for rocks were small; for example, surface dissolution without water penetrating the rock is an approximation to dissolution of dense limestone or marble surfaces exposed to rain or running water (Reddy, 1988). However, theoretical and empirical estimates of the rock surface areas (S), the ratio S/A, and the volume of water flow through the rocks are such that regional or global estimates of the chemical denudation rates based on them have large margins of uncertainty.

NEUTRALIZATION OF ACIDITY BY WEATHERING RELEASES

Background — Alkalinity [Alk], Acidity [Acy], CO2, and pH

Observations of weathering in small drainage basins of streams and lakes exposed to acid rain, and experimental results from acid water leaching of soils in lysimeters show that variable, yet significant fractions of imported acidity, measured as [H$^+$, are neutralized by reactions of water with minerals (Likens *et al.,* 1977; Henriksen, 1980; Wright, 1983, 1988; Folster, 1985; Paces, 1985; Colman and Dethier, 1986; Schnoor and Stumm, 1986; Berner and Berner, 1987; Drever, 1988; Norton *et al.,* 1989; Velbel and Romero, 1989). These conclusions corroborate the older and broader ideas that crustal weathering is a chemical acid-base titration on a planetary scale (Sillen, 1961, p. 551; Stumm and Morgan, 1981; Holland, 1984).

Acidic streams and acidic lakes exist because neutralization reactions in some areas are not fast enough. Whenever waters react with carbonate and/or silicate rocks, consumption of the hydrogen ions from solution is balanced by releases of chemically equivalent amounts of other metal cations. The released cations may be transported away by flow or they may in part be stored in secondary minerals and vegetation of the drainage area, as discussed in an earlier section. More generally, H$^+$-sensitive reactions are those that produce changes in the *alkalinity* of the solution (function [Alk] defined below), and they result in concentration increases for cations derived from the reacting minerals.

One of the simpler definitions is that alkalinity is the acid neutralization capacity of a solution. A more specific definition is that alkalinity is the difference between the concentrations of the H$^+$-independent cations and anions in solution. Extensive textbook-level discussions of alkalinity of natural waters are given by Stumm and Morgan (1981) and Drever (1988). The main ions in natural waters that are H$^+$ dependent include the anions bicarbonate, carbonate, and hydroxyl. In certain continental waters, phosphate ions may also contribute to the alkalinity. In acidic waters, the positively charged aluminum hydroxide aqueous complexes add to the balance along with the hydrogen ion. Anions of organic acids may also be important in waters enriched in dissolved organic carbon.

In a simplified general case, alkalinity is the difference between the following anion and cation concentrations, given in equivalents per liter:

$$[\text{Alk}] = \left[\text{HCO}_3^-\right] + 2\left[\text{HCO}_3^{2-}\right] + [\text{OH}] - \left[\text{H}^+\right], \quad (2.20)$$

The preceding form of alkalinity, which is based on the carbonate, hydroxyl, and hydrogen ions, is also known as the carbonate alkalinity.

In acidic solutions, where concentrations of the bicarbonate, carbonate, and hydroxyl ions are negligibly low, the hydrogen ion is dominant and the values of [Alk] become negative. Thus for acidic solutions, the negative alkalinity is defined as acidity [Acy]:

-[Alk] = [Acy]. (2.21)

TABLE 2.4 Parameters Used in Computation of Alkalinity [Alk] (for more complete definitions of alkalinity, see text)

Definition of alkalinity

$$[Alk] = [HCO_3^-] + 2[HCO_3^{2-}] + [OH] - [H^+]$$

$$[Alk] = \frac{PCO_2 K_H}{\alpha_0}(\alpha_1 + \alpha_2) + [OH] - [H^+];$$

$$[Acy] = -[Alk]$$

Total dissolved inorganic carbon

$$[C_T] = [H_2CO_3^0] + [CO_3^{2-}]$$

$$[C_T] = \frac{PCO_2 K_H}{\alpha_0}$$

Definitions of constants at 25°C

$$K_H = 0.034 \frac{mol}{1 \cdot atm}; \quad K_1 = \frac{[H^+][HCO_3^-]}{[H_2CO_3^0]} = 10^{-6.3};$$

$$K_2 = \frac{[H^+][HCO_3^{2-}]}{[HCO_3^-]} = 10^{-10.25}$$

Definition of parameters α

$$\alpha_0 = \frac{1}{\left(1 + \frac{K_1}{[H^+]} + \frac{K_1 K_2}{[H^+]}\right)}; \quad \alpha_1 = \frac{1}{\left(\frac{[H^+]}{K_1} + 1 + \frac{K_2}{[H^+]}\right)};$$

$$\alpha_2 = \frac{1}{\left(\frac{[H^+]^2}{K_1 K_2} + \frac{[H^+]}{K_2} + 1\right)}$$

Note: Small brackets [ ] denote concentration in moles per liter.
SOURCE: Stumm and Morgan (1981).

It should be noted that in the presence of other positively charged species, such as aluminum hydroxide complexes, the acidity would be greater than the hydrogen-ion concentration alone. The acidity values [Acy] are generally greater than indicated by the pH measurements in many natural acidic waters and human-produced discharges.

Alkalinity, as defined in Eq. (2.20), is a function of two variables: the pH and the total dissolved inorganic carbon in solution. Table 2.4 lists explicit equations for alkalinity and the auxiliary parameters defining it in terms of the hydrogen-ion concentration, and either total dissolved inorganic carbon (C_T) or the CO_2 pressure at equilibrium with the solution (PCO_2).

During weathering, as hydrogen ions are consumed by reactions with minerals and cations are released into a solution open to the atmosphere, the alkalinity increases, and its increase is reflected in the higher concentrations of dissolved inorganic carbon (CO_2, HCO_3^-, and CO_3^{2-}). For a given partial pressure of CO_2 at equilibrium with a solution, a higher pH corresponds to higher [Alk] values. This relationship holds for continental waters exposed to atmospheric CO_2, as was documented for freshwater and saline lakes (Lerman and Stumm, 1989). A similar relationship between alkalinity and pH is shown in Figure 2.8.

For natural freshwaters approximated by dilute aqueous solutions, the two curves of [Alk] versus pH in Figure 2.8 represent present atmospheric CO_2 and a partial pressure 10 times higher, approximating the values in soils near the plant-root zone. Waters remaining in contact with the bedrock longer and, possibly, developing higher levels of
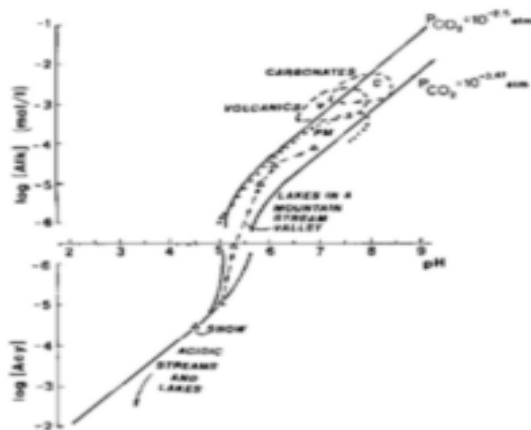
FIGURE 2.8 Alkalinity [Alk] and acidity [Acy] of waters open to an external CO_2. NOTE: vertical scale near [Alk] = 0 interrupted for values between 10^{-6} and -10^{-6} moles/liter to allow for the logarithmic [Alk] scale. [Alk] values in this range are ≈0. —•— sequence of Alpine-valley lakes (Schnoor and Stumm, 1986). Acidic rivers and lakes (Berner and Berner, 1987; Norton *et al.,* 1989). PM, V, C are rivers from plutonic and metamorphic, volcanic, and carbonate terrains (Meybeck, 1984).

biological productivity show a progressive increase in [Alk] and pH values: a sequence of small Alpine lakes represents a progression from acidic waters of the source stream emerging from a snow field through several lakes of lengthening water residence time, each occurring downstream of the preceding (Schnoor and Stumm, 1986). Concentrations of inorganic solutes in water emerging from snow fields and glaciers are generally very low (Raiswell, 1984).

On a physically larger scale, streams flowing through crystalline rock terrains have as a whole lower alkalinity and pH values than rivers draining volcanic rocks. Waters in carbonate drainage basins show the highest [Alk] and pH values of the three classes (Figure 2.8).

In acidic waters, up to a pH of about 5.5, that have not (or not yet) become neutralized by chemical weathering reactions, for all practical purposes an increase in dissolved CO_2 does not affect the [Alk] or [Acy] value of the solution. In less acidic and near-neutral waters, at $pH \geq 5.5$, smaller changes in dissolved CO_2 may more significantly affect the [Alk] and pH values of the solution. The range of dissolved CO_2 values in rivers and freshwater lakes varies from some degree of undersaturation with atmospheric carbon dioxide to values higher than the saturation by a factor of about 3, corresponding to an equilibrium PCO_2 = 1000 ppmv (Kempe, 1988). The higher PCO_2 values in such rivers, computed from the carbonate- and hydrogen-ion equilibria, are associated with supersaturation of river waters with respect to calcite ($CaCO_3$), a phenomenon variably controlled by primary productivity or discharge of carbon dioxide-supersaturated waters from the subsurface (Holland, 1978, pp. 105-107; Kempe, 1988).

SUMMARIZING DISCUSSION

The weathering releases of dissolved materials from bedrock and soil to continental waters, viewed as a process of acid neutralization and mineral dissolution, are the basis of any conceptual model that ties the surficial transport fluxes into one interactive system. An increase in input of acidity to the bedrock should, in a steady state system, result in faster dissolution rates and greater amounts of solutes transported in flow. Because the residence time of surface runoff from the continents is short, months to years, the effects of higher dissolution rates might be expected to show in the runoff on time scales comparable to those of the runoff residence times. Although historical data on dissolved loads of streams and rivers in preindustrial times are difficult to come by, some modern analogues to the magnitudes of past changes in weathering are provided by chemical surveys of lakes over the past 40 to 60 yr.

Data on the pH of freshwater lakes on the Scandinavian shield, going back to late 1930s, indicate a continuous decrease in the lake water pH by about 1 pH unit in 25 yr. This suggests, as pointed out in an earlier section, that the rates of water-rock neutralization reactions do not always keep pace with an environmental change. Another set of historical records going back to the 1920s is the result of surveys of lake-water chemistry in a population of 145 lakes in Wisconsin and a number of lakes in the Adirondack Mountains of New York (Kramer *et al.,* 1986): during the 50- to 60-yr period since the 1920s and 1930s, there have been very small changes in the mean values of alkalinity in the two regions. In the Wisconsin lakes, [Alk] has increased by about 0.04×10^{-3} eq/liter; in the Adirondack Mountains the change was a decrease by 0.04×10^{-3} to 0.07×10^{-3} eq/liter. These numbers, compared to the [Alk] values of $>10^{-4}$ eq/liter shown in Figure 2.8, indicate a very small change over a half a century of accelerating acid-producing emissions.

Another longer-term effect may reflect the stabilizing capacity of the rock-soil-water system that tends to keep the weathering release rates nearly constant on time scales of 10^3 to 10^4 yr. The rates of soil formation on time scales of 10^3 to 10^6 yr, summarized by Brunsden (1979), range from 60 to 450 mm/1000 yr for soils in subtropical regions. Slower rates of formation characterize ferralites (15 to 45 mm/1000 yr) and duricrusts on granite (9 mm/1000 yr). These rates overlap the rates of chemical weathering given in Table 2.2. Thus, on time scales of 10^3 to 10^4 yr, changes in the rates of dissolution of the bedrock, which might have been caused by combinations of environmental and biological factors, could be in part taken up in a faster development of the residual soil profiles rather than only in higher solute concentrations in runoff.

One of the major trends of industrial times is an increase in the acidity of atmospheric precipitation caused by emissions of nitrogen and sulfur oxides from burning of fossil fuels. However, an additional component of potential acidity resides in the living and dead organic carbon on land. On a global scale, from tropical to cold climatic zones, carbon density in soils increases by a factor of about three, as shown in Figure 2.9. This trend runs opposite to the declines in net primary productivity and standing crop of the plant mass, from the tropics to the tundra, over a temperature range from about 25 to 5°C (Lieth, 1975; Post *et al.,* 1982). The opposite trends of carbon storage in soils and in the living phytomass are shown in Figure 2.9 by the curve labeled carbon density ratio. The soil/biomass carbon ratio is generally higher in colder climates than in warmer. This trend also accounts for the longer residence times of carbon in colder soils, where net primary productivity is lower than in the tropics. The soil carbon is a potential source of additional acidity, both organic and inorganic, that in a warmer climate of the future may promote a faster development of the regolith and contribute to a greater dissolved load in riverine flow.
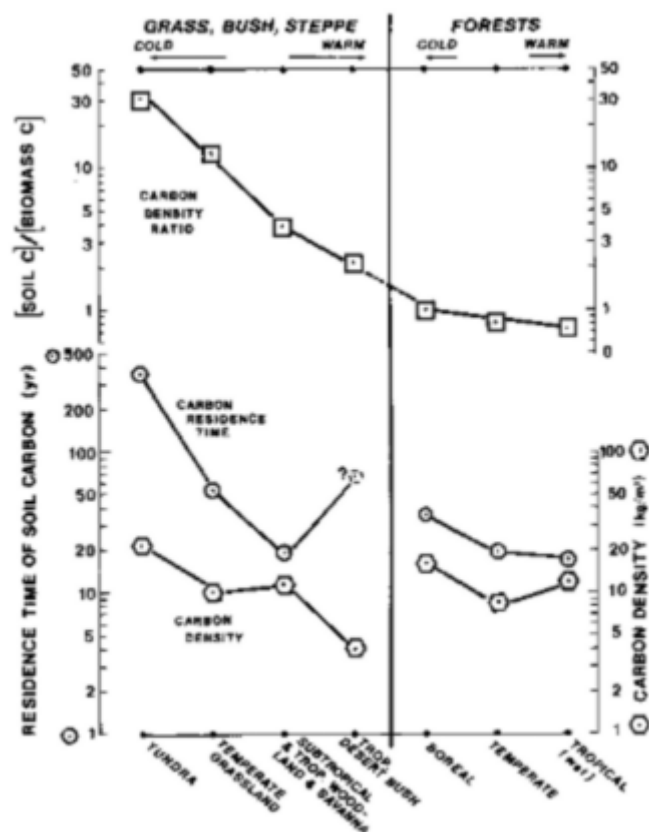
FIGURE 2.9 Condition of constant alkalinity as controlled by changes in PCO_2 and pH, *left ordinate* (Eq. (2.25) and Table 2.4). Range of PCO_2 for surficial waters and soil groundwaters, *right ordinate.*

In judging by the acidity or alkalinity values of surface land waters at the present time, newly formed acidity may be effectively neutralized in carbonate-mineral terrains, but it may persist for longer periods in waters that are in contact with crystalline silicate rocks.

ACKNOWLEDGMENTS

REFERENCES

Bales, R.C., and J.J. Morgan (1985). Dissolution kinetics of chrysotile at pH 7 to 10, Geochimica et Cosmochimica Acta 49, 2281-2288 .

Barnola, J.M., D. Raynaud, Y.S. Korotkevich, and C. Lorius (1987). Vostok ice core provides 160,000-year record of atmosphere CO_2 , Nature 329, 408-414 .

Barry, R.G. (1985). Snow cover, sea ice, and permafrost, in Glaciers, Ice Sheets and Sea Level: Effect of a CO_2-Induced Climatic Change, Committee on Glaciology, National Academy Press, Washington, D.C., pp. 241-247 .

Baumgartner, A., and E. Reichel (1975). The World Water Balance, Elsevier, Amsterdam, 179 pp .

Berner, E.K., and R.A. Berner (1987). The Global Water Cycle: Geochemistry and Environment, Prentice-Hall, Englewood Cliffs, N.J.

Berthelin, J. (1988). Microbial weathering processes in natural environments, in Physical and Chemical Weathering in Geochemical Cycles, A. Lerman and M. Meybeck, eds., Kluwer Academic, Dordrecht, pp. 33-60 .

Blum, A., and A. Lasaga (1988). Role of surface speciation in the low-temperature dissolution of minerals, Nature 331, 431-433 .

Brady, P.V. (1991). The effect of silicate weathering on global temperature and atmospheric CO_2 , Journal of Geophysical Research 96, 18101-18106 .

Brady, P.V., and J.V. Walther (1989). Controls of silicate dissolution rates in neutral and basic pH solutions at 25°C. Geochimica et Cosmochimica Acta 53, 821-832 .

Brunsden, D. (1979). Weathering, in Process in Geomorphology, C. Embleton and J. Thornes, eds., Annold, pp. 73-129 .

Chou, L., and R. Wollast (1985). Steady-state kinetics and dissolution mechanisms of albite, American Journal of Science 285, 963-993 .

Chou, L.R.M. Garrels, and R. Wollast (1989). Comparative study of the kinetics and mechanisms of dissolution of carbonate minerals, Chemical Geology.

Colman, S.M., and D.P. Dethier, eds. (1986). Rates of Chemical Weathering of Rocks and Minerals, Academic Press, New York.

Cronan, C.S. (1985). Chemical weathering and solution chemistry in acid forest soils: Differential influence of soil type, biotic processes, and H^+ , in The Chemistry of Weathering, J.I. Drever, ed., D. Reidel, Dordrecht, pp. 175-196 .

Deike, R.G. (1989). Dolomite dissolution rates and possible Holocene dedolomitization of waterbearing units in Edwards Aquifer, south-central Texas, 28th International Geological Congress, Abstracts 1, 323.

Drever, J.I. (1988). The Geochemistry of Natural Waters, Prentice-Hall, Englewood Cliffs, N.J.

Eckhardt, F.E.W. (1985). Solubilization, transport, and deposition of mineral cations by microorganisms—efficient rock weathering agents, in The Chemistry of Weathering, J.I. Drever, ed., D. Reidel, Dordrecht, pp. 161-174 .

Fölster, H. (1985). Proton consumption rates in Holocene and present-day weathering of acid forest soils, in The Chemistry of Weathering, J. I. Drever, ed., D. Reidel, Dordrecht, pp. 197-210 .

Garrels, R.M., and F.T. MacKenzie (1971). Evolution of Sedimentary Rocks, W.W. Norton & Co., New York.

Goldberg, E.D. (1971). Atmospheric dust, the sedimentary cycle and man, Geophysics 1, 117-132 .

Henriksen, A. (1980). Acidification of fresh waters — A large scale titration, in Ecological Impact of Acid Precipitation, D. Drablos and A. Tollan, eds., SNSF Project, Oslo-As, pp. 68-74 .

Herdendorf, C.E. (1982). Large lakes of the world, Journal of Great Lakes Research 8(3), 379-412 .

Holland, H.D. (1978). The Chemistry of the Atmosphere and Oceans, John Wiley & Sons, New York.

Holland, H.D. (1984). The Chemical Evolution of the Atmosphere and Oceans, Princeton University Press, Princeton, N.J.

Jouzel, J., C. Lorius, J.R. Petit, and others (1987). Vostok ice core: A continuous isotope temperature record over the last climatic cycle (160,000 years), Nature 329, 403-408 .

Kempe, S. (1988). Freshwater carbon and the weathering cycle, in Physical and Chemical Weathering in Geochemical Cycles, A. Lerman and M. Meybeck, eds., Kluwer Academic Publishers, Dordrecht, pp. 197-224 .

Kramer, J.R., A.W. Andren, R.A. Smith, A.H. Johnson, R.B. Alexander, and G. Oehlert (1986). Streams and lakes, in Acid Deposition: Long-Term Trends, National Academy Press, Washington, D.C., pp. 231-299 .

Lerman, A. (1979). Geochemical Processes — Water and Sediment Environment, John Wiley & Sons, New York.

Lerman, A., and A.B. Hull (1987). Background aspects of lake restoration: Water balance, heavy metal content, phosphorus homeostasis, Schweiz Zeitschrift Hydrology 49, 148-169 .

Lerman, A., and W. Stumm (1989). CO_2 storage and alkalinity trends in lakes, Water Research 23(2), 139-146 .

Lieth, H. (1975). Modeling the primary productivity of the world, in Primary Productivity of the Biosphere, H. Lieth and R.H. Whittaker, eds., Springer, New York, pp. 237-263 .

Likens, G.E., F.H. Bormann, R.S. Pierce, J.S. Eaton, and N.M. Johnson (1977). Biogeochemistry of a Forested Ecosystem, Springer-Verlag, New York, 146 pp .

Lorius, C.,J. Jouzel, C. Ritz, L. Merlivat, N.I. Barkov, Y.S. Korotkevich, and V.M. Kotlyakov (1985). A 150,000-year climatic record from Antarctic ice, Nature 316, 591-596 .

Meybeck, M. (1984). Les fleuves et le cycle geochimique des Elements, These d'etat (no. 84-35), Ecole Normal Superieure, Laboratoire de Geologie, Universite Pierre et Marie Curie, Paris, France.

Murphy, W.M., E.H. Oeklers, and P.C. Lichtner (1989). Surface reaction versus diffusion control of mineral dissolution and growth rates in geochemical processes, Chemical Geology 78, 357-380 .

National Geographic Society (1988). Vegetation cover of the world 18,000 b.p., on the map Endangered Earth, National Geographic Society, Washington, D.C.

Norton, S.A., F.H. Howd, C.V. Guidotti, T.A. Haines, and R.B. Davis (1989). Influence of Conway Granite (Triassic?) in New Hampshire on biogeochemical response to acidic precipitation, 28th International Geological Congress, Abstracts 2, 524.

Paces, T. (1985). Sources of acidification in Central Europe estimated from elemental budgets in small basins, Nature 315, 31-36 .

Plummer, L.N., T.M.L. Wigley, and D.L. Parkhurst (1978). The kinetics of calcite dissolution in CO_2-water systems at 5° to 60°C and 0.0 to 1.0 atm CO_2 , American Journal of Science 278, 179-216 .

Post, W.M., W.R. Emmanuel, P.J. Zinke, and A.G. Stangenberger (1982). Soil carbon pools and world life zones, Nature 298, 156-159 .

Probst A., E. Dambrine, D. Viville, and B. Fritz (1990). Influence of acid atmospheric inputs on surface water chemistry and mineral fluxes in a declining spruce stand within a small granitic catchment (Vosages Massif, France), Journal of Hydrology 116, 101-124 .

Probst A., D. Viville, B. Fritz, B. Ambroise, and E. Dambrine (1992). Hydrochemical budgets of a small forested granitic catchment exposed to acid deposition: The Strengbach catchment case study (Vosages Massif, France), Water, Air and Soil Pollution 62, 337-347 .

Raiswell, R. (1984). Chemical models of solute acquisition in glacial meltwaters, Journal of Glaciology 30, 49-57 .

Reddy, M.M. (1988). Acid rain damage to carbonate stone: A quantitative assessment based on the aqueous geochemistry of rainfall runoff from stone, Earth Surface Processes and Landforms 13, 335-354 .

Rimstdt, J.D., and H.L. Barnes (1980). The kinetics of silica-water reactions, Geochimica et Cosmochimica Acta 44, 1683-1700 .

Schneider, S. H., and W.W. Kellogg (1973). The chemical basis for climate change, in Chemistry of the Lower Atmosphere, S. I. Rasool, ed., Plenum, New York, pp. 203-249 .

Schnoor, J.L., and W. Stumm (1986). The role of chemical weathering in the neutralization of acidic deposition, Schweiz Annals of Hydrology 48, 171-195 .

Schott, J., and R.A. Berner (1985). Dissolution mechanisms of pyroxenes and olivines during weathering, in The Chemistry of Weathering, J.I. Drever, ed., D. Reidel, Dordrecht, pp. 35-54 .

Schott, J., and J.C. Petit (1987). New evidence for the mechanism of dissolution of silicate minerals, in Aquatic Surface Chemistry, W. Stumm, ed., John Wiley & Sons, New York, pp. 293-315 .

Schott, J., R.A. Berner, and E.L. Sjoeberg (1981). Mechanism of pyroxene and amphibole weathering—I. Experimental studies of iron-free minerals, Geochimica et Cosmochimica Acta 45, 2123-2135 .

Siegenthaler, U., and H. Oeschger (1987). Biospheric CO_2 emissions during the past 200 years reconstructed by deconvolution of ice core data, Tellus 39B, 140-154 .

Sillen, L.G. (1961). The physical chemistry of sea water, in Oceanography, M. Sears, ed., American Association for the Advancement of Science, Washington, D.C., Pub. No. 67, pp. 549-581 .

Sposito, G. (1985). Chemical models of weathering in soils, in The Chemistry of Weathering, J.I. Drever, ed., D. Reidel, Dordrecht, pp. 1-18 .

Stallard, R.F. (1988). Weathering and erosion in the humid tropics, in Physical and Chemical Weathering in Geochemical Cycles, A. Lerman and M. Meybeck, eds., Kluwer Academic, Dordrecht, pp. 225-246 .

Stallard, R.F. (1989). Weathering processes and chemical composition of tropical rivers from diverse tectonic settings , 28th International Geological Congress, Abstracts 3, 169.

Stumm, W., and J.J. Morgan (1981). Aquatic Chemistry, John Wiley & Sons, New York.

Tole, M.P., A.C. Lasaga, C. Pantano, and W.B. White (1986). Factors controlling the kinetics of nepheline dissolution, Geochimica et Cosmochimica Acta 50, 379-392 .

Van Name, R.G. (1929). The velocity of dissolving of crystals in liquids, in International Critical Tables 5 , McGraw-Hill, New York, pp. 55-60

Velbel, M.A. (1985). Geochemical mass balance and weathering rates in forested watersheds of the southern Blue Ridge, American Journal of Science 285, 904-930 .

Velbel, M.A., and N.L. Romero (1989). Amphibolite weathering and cation budgets in southern Blue Ridge and Colorado Front Range, USA, 28th International Geological Congress, Abstracts 3, 291.

White, A.F., and M.L. Peterson (1986). Role of reactive-surface-area characterization in geochemical kinetic models, in Geochemical Processes at Mineral Surfaces, J.A. Davis and K.F. Hays, eds., American Chemical Society Symposium Series 323, pp. 461-477 .

Whitfield, M. (1974). Accumulation of fossil CO_2 in the atmosphere and the sea, Nature 247, 523-525 .

Wollast, R., and L. Chou (1988). Rate control of weathering of silicate minerals at room temperature and pressure, in Physical and Chemical Weathering in Geochemical Cycles, A. Lerman and M. Meybeck, eds., Kluwer Academic, Dordrecht, pp. 11-32 .

Wollast, R., and F.T. Mackenzie (1983). The global cycle of silica, in Silicon Geochemistry and Biogeochemistry, S.R. Aston, ed., Academic Press, New York, pp. 39-76 .

Wright, R.F. (1983). Acidification of freshwaters in Europe, Water Quality Bulletin 8, 137-142 .

Wright, R.F. (1988). Influence of acid rain on weathering rates, in Physical and Chemical Weathering in Geochemical Cycles, A. Lerman and M. Meybeck, eds., Kluwer Academic, Dordrecht, pp. 181-196 .

3

Global Chemical Weathering on Glacial Time Scales

LEE R. KUMP AND RICHARD B. ALLEY
Pennsylvania State University

INTRODUCTION

Scoured valleys, jagged peaks, expansive moraines, and thick deposits of till bear firm testament to the erosive power of glaciers. The effects of glaciers on chemical denudation rates are less visible. The products of chemical weathering are either dissolved solutes, which are efficiently transported to the sea, or clays, which thicken the soil mantle or are transported away by streams.

Intuition gives little extra information on changes in chemical weathering on glacial time scales. A number of environmental variables influence chemical weathering rates globally. Many of these are studied in the laboratory: temperature, chemistry of the dissolving fluid, surface area, fluid transport rates. However, many others are peculiar to the natural setting. In calculating global chemical weathering rates one typically measures the composition and discharge of the world's major rivers (Meybeck, Chapter 4, this volume). Each of these rivers represents a mixture of contributions from different lithologies and climatic and tectonic regimes. The flux of dissolved material from a given river then depends on the geographical distribution of lithologies relative to climate patterns, rates of tectonic activity (uplift), vegetational zonations, and heterogeneities in the intensity of physical weathering processes that produce reactive materials. Thus, to scale up from laboratory measurements to calculations of global weathering rates requires much additional information on environmental conditions (Lerman, Chapter 2, this volume).

It is only after we have determined how these factors have varied that we will be able to make an estimate of the changes in global chemical weathering rates on glacial time scales. Our initial interpretations may be wrong. For example, cooler temperatures and the coverage by glaciers of a large portion of the land surface might suggest that chemical weathering rates were lower during glaciations (e.g., Broecker, 1983). However, other factors may have more than compensated for these changes: the production of fine, easily weathered material by glaciers and the increase in land area due to eustatic sea-level fall.

This chapter is a summary of what is presently known about variations in chemical weathering variables on glacial time scales, with a focus on the time period from 18 ka (1000 yr before present) to today. We begin with a discussion of climate change, in terms of both global and regional changes in temperature, precipitation, evaporation, and runoff. Both empirical data and modeling studies are considered. Next we assess the areal changes in rock exposure due to coverage by glaciers, sea-level fall, and the geographic distribution of rock types. The production and transport of fine-grained material by glaciers is then considered as an important variable in global weathering, followed by an assessment of the role of subglacial chemical weathering in the global scheme.

Because these factors are changing simultaneously on glacial time scales, it is important that we consider their combined effects on chemical weathering. This we do in the next section by speculating on weathering feedbacks with vegetation, the transport of fine-grained material across climatic zones, the coverage of key rock types by glaciers, and the effect of latitudinally specific land area changes. We then close with a summary and a discussion of the implications of these effects for glacial/interglacial changes in oceanic and atmospheric chemistry, and climate. Uncertainties in our knowledge of many important parameters are sufficiently large that we can draw few firm conclusions, but we hope to have identified important areas for further research.

FACTORS THAT INFLUENCE GLOBAL CHEMICAL WEATHERING

Climate

A large body of observational and model evidence is available on differences between the climate of the Wisconsinan glacial maximum of about 18 ka and the modern climate. Convergence of results from different techniques allows some comparisons to be made with confidence (e.g., CLIMAP, 1976; Manabe and Broccoli, 1985; Kutzbach and Guetter, 1986; Rind, 1987; COHMAP, 1988). Globally, these include (where trends are known more accurately than absolute changes) the following:

- the ice-age world was a few degrees colder than today. Ice-age cooling was smallest in the tropics ($\approx$ to 5°C), increased to the poles ($\approx$ 5 to 10°C) and was quite large on the midlatitude ice sheets (tens of degrees Celsius);
- lower ice-age temperatures reduced both precipitation and evaporation below modern values (by about 10 percent); and
- any changes in globally averaged soil moisture were smaller than the uncertainties in our knowledge.

Regionally, during the ice age (Figure 3.1),

- soil moisture was significantly less than today in a large area of Eurasia south and east of the Fennoscandian ice sheet, and in a smaller area of North American south of the Laurentide ice sheet. These drier areas probably developed because of the combined effects of anticyclonic circulation over the ice sheets and of the ice sheets acting as cold traps for water vapor and reducing precipitation nearby;
- the southwestern United States was significantly wetter than today, probably owing to a southward shift in storm tracks caused by the topography of the Laurentide ice sheet;
- other regional changes occurred: soil moisture was probably reduced in equatorial regions, causing reduction in extent of ice-age tropical rain forests, but increased in some areas at higher southern latitudes; and
- precipitation over ice sheets was reduced substantially compared to modern precipitation in the previously glaciated regions.

The evolution from ice-age to modern climates was not monotonic (Figure 3.2). In particular, a peak in Northern Hemisphere summer insolation around 9 ka caused strengthened monsoonal circulation and large soil-moisture increases compared to today and to the glacial maximum across the northern monsoon belt (primarily Africa and Asia), with decreased monsoonal circulation and soil moisture over smaller areas of land in the Southern Hemisphere (Kutzbach and Guetter, 1986; COHMAP, 1988).

SOIL MOISTURE CHANGES
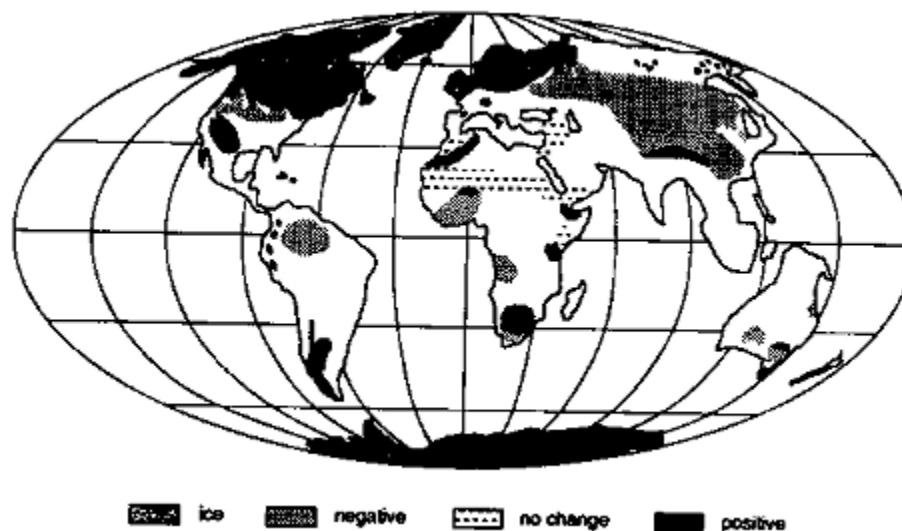
FIGURE 3.1 Changes in soil moisture, 18 ka relative to today. Areas marked "positive" were wetter 18 ka than today. Maximum extent of glacier ice during the last glacial episode is also shown (Kutzbach and Guetter, 1988; COHMAP, 1988; ice extent from Broecker, 1983).
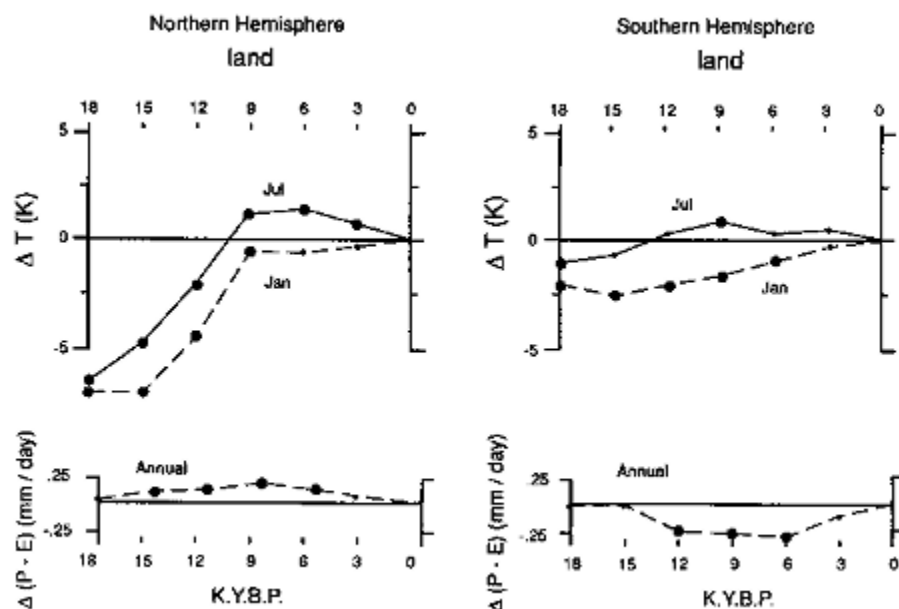
FIGURE 3.2 Seasonal temperature and mean-annual net precipitation [Δ(P-E)] changes in the (a) Northern and (b) Southern Hemispheres, calculated by a general circulation/climate model, for the period 18 ka to present [abscissa in thousands of years before present (K.Y.B.P. = ka); from Kutzbach and Guetter, 1988].

Erosional Area

Glacial Coverage At the height of the last glaciation, vast areas of North American and Europe were covered with thick sheets of glacier ice (Figure 3.1). In addition, expanded mountain glaciers at this time covered smaller areas of Eurasia, North America, South America, Africa, and New Zealand. In sum, about 30 percent of the present land area was glaciated 18 ka (Flint, 1971).

Most of the areas covered were poleward of 40°N, with most of the rest being poleward of 40°S. Mountain glaciers expanded at all latitudes, especially in North America, South America, and Africa, and despite limited areal extent might have been important in affecting global chemical weathering rates.

FIGURE 3.3 Areas of subaerial shelf exposure at 18 ka (by assuming a 130-m sea-level lowstand).

Shelf Exposure As the Wisconsinan ice sheets grew, sea level fell, progressively exposing more and more of the continental shelf region (Figure 3.3), which then became subject to glaciation at high latitudes and chemical weathering processes at lower latitudes. At full exposure, the continental shelves represent about 13 percent of the total land area of the planet; the majority of this was exposed at the glacial maximum. Interestingly, this "new land" would have appeared preferentially in the tropics; approximately 40 percent of the total shelf area falls between 20° north and south of the equator (Figure 3.4).

Some of the more important shelf emergences include the Amazon and southeastern South American shelves, the perimeter of the Gulf of Mexico, and a large area of southwestern Asia and Oceania. Today, land areas adjacent to

these shelves experience intense chemical weathering; such weathering may have occurred on the expanded land areas at the last glacial maximum. If so, then global chemical weathering rates actually could have been higher during the glacial period, although one must consider climate change as well.
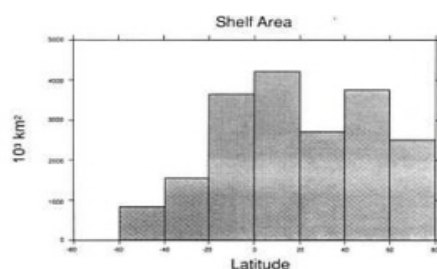
FIGURE 3.4 Shelf area as a function of latitude (South Pole is -90°; Rand McNally, 1977).

Rock Types Exposed

A quick glance at a geological map confirms that the distributions of rock types exposed on the surface of the Earth is nonuniform. Nevertheless, these heterogeneities are typically ignored in models of geochemical cycles (e.g., Berner *et al.,* 1983). In considering chemical weathering changes on glacial time scales, however, it is of interest to determine the changes in the areal distribution of rock types that occurred as a result of coverage by glaciers and the relationship of these changes to climate change.

The most important rock types in terms of their contributions to the global chemical weathering flux are limestones and rocks containing silicate minerals (shales and igneous and metamorphic rocks). Limestones are important because they dissolve easily during attack by groundwater; the streams with the highest dissolved loads (excluding those weathering evaporites subject to intense evaporation) are those passing through carbonate terrains (Gibbs, 1970; Holland, 1978; Berner and Berner, 1987). Silicate rocks are important because during their weathering (Eq. 3.1) CO_2, undergoes net consumption:

Weathering reactions (on land)

$$CaSiO_3 + 2\,CO_2 + 3\,H_2O \leftrightarrow Ca^{2+} + 2\,HCO_3^- + H_4SiO_4 \quad (3.1)$$

$$CaCO_3 + CO_2 + H_2O \leftrightarrow Ca^{2+} + 2\,HCO_3^- \quad (3.2)$$

Precipitation reactions (in ocean)

$$Ca^+ + 2\,HCO_3^- \leftrightarrow CaCO_3 + CO_2 + H_2O \quad (3.3)$$

$$H_4SiO_4 \leftrightarrow SiO_2 + 2\,H_2O \quad (3.4)$$
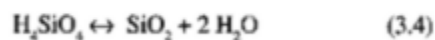
Net CO_2 consumption (Eq. 3.1 + Eq. 3.3 + Eq. 3.4)

$$CaSiO_3 + CO_2 \leftrightarrow CaCO_3 + SiO_2. \quad (3.5)$$

Although CO_2 is consumed during carbonate weathering (Eq. 3.2), there is no net consumption on the time scale that the oceanic $CaCO_3$ budget is achieved (thousands of years; Broecker and Peng, 1987). The ocean is saturated with respect to $CaCO_3$, so the products of carbonate weathering precipitate on reaching the sea (Eq. 3.3).

The present distribution of limestone is shown in Figure 3.5 (after Snead, 1980). This common rock type appears on all continents. There is a general lack of exposure of carbonates at high northern latitudes: thus, their

FIGURE 3.5 Major limestone exposures of the world (Snead, 1980).

outcrop areas were not significantly affected by the last glaciation. The glaciation of Europe is probably most significant, because chemical denudation there is most influenced by carbonate weathering. Yet even on this continent, most of the exposures are equatorward of the furthest extent of ice during the last glaciation. We must also consider the increase in limestone exposures due to sea-level fall; much of the increase in land area at low latitudes is the result of the exposure of carbonate platforms (Florida, Yucatan, Bahamas, northwest Australian shelf, Oceania). The presence of Pleistocene sinkholes and other karst features attests to the extensive dissolution of these limestones and the deep groundwater circulation during glaciation (e.g., Bloom, 1978, p. 146).
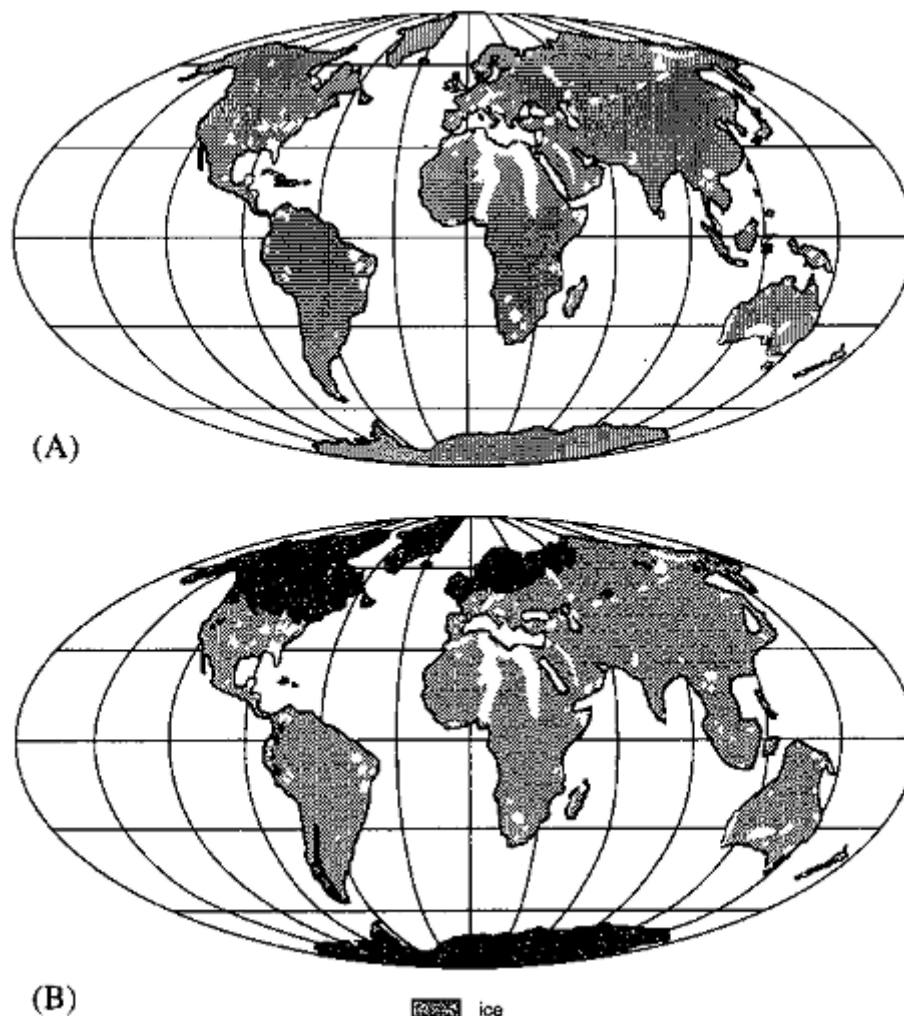
FIGURE 3.6 Noncarbonate exposures of the world (see Figure 3.5): (A) today and (B) at 18 ka.

In contrast to its effect on carbonate exposure, glaciation caused a significant reduction in the area of exposure of silicate rocks (Figure 3.6). (All nonlimestone exposures are considered as "silicate" rocks.) The expansive shield region of North America was completely covered, as were the exposures in Scandinavia and Great Britain. Although one may thus conclude that the potential for CO_2 consumption was reduced by glaciation, an accurate assessment of the overall effect depends on the corresponding change in climate on regional scales. We will consider this coupled change below.

Glacier Weathering and Erosion Processes

Temperature and Water Production Glaciers and ice sheets are among the most complex and variable systems on Earth. The most important factor controlling processes at glacier beds is temperature. A glacier frozen to a rigid bed does little or no geomorphic work (e.g., Gellatly *et al.,* 1988); it halts the action of subaerial weathering processes and reduces erosion rates essentially to zero. Onset of basal melting facilitates glacial erosion, at typical rates of 1 mm/yr (Boulton, 1979) and extreme rates as high as 10 mm/day for short periods over restricted areas (Humphrey, 1986).

The controls on basal temperature are not simple. Temperate glaciers (those entirely at the pressure melting point) commonly form in regions of high snowfall with mean annual temperatures near or even above freezing (Porter, 1977), especially in maritime climates. Farther inland, glacier existence usually requires mean annual air temperatures and near-surface ice temperatures below freezing over at least part of the glacier (the accumulation zone). Heat then is supplied to the glacier bed by geothermal flow and by viscous dissipation ("friction") of ice flow. Heat is removed by upward conduction through the ice to its cold surface; the rate of conduction is affected by vertical and lateral ice flow. The balance of these processes determines the basal temperature (see review in Paterson, 1981, Ch. 10).

Consider first the central region of a large ice sheet, such as the Laurentide, Fennoscandian, or the modern Antarctic and Greenland ice sheets. Near the center, flow velocities are low and viscous dissipation is small compared to geothermal heating. When the ice sheet is sufficiently large and thick (more than a few hundred kilometers in diameter, >1000 m thick) to affect atmospheric circulation significantly, surface temperature and accumulation will decrease with increasing ice-sheet elevation. Surface air temperature will decrease approximately at the atmospheric lapse rate (=1° C/100 m). Precipitation usually will be limited by the ability of the cold air to transport water vapor onto the ice sheet; in modern East Antarctica, accumulation varies exponentially with temperature (Robin, 1977).

In the absence of ice flow, the insulating ability of ice would cause the difference between bed and surface temperatures to increase by about 2° C/100 m of ice thickness, whereas surface temperatures cool only about 1° C/100 m; the result would be rapid bed warming with increase of ice thickness and thawed beds beneath all but the thinnest glaciers. However, flow processes cause surface ice to move down into an ice sheet in accumulation areas. (Ice spreads and thins under the gravitational stresses caused by its weight and surface slope; new snowfall balances this thinning in a steady ice sheet and exceeds it in a growing ice sheet.) This ice motion advects the surface cold downward and chills the bed.

This vertical advection effect scales approximately with $(b/h)^{1/2}$, where b is accumulation rate and h is ice thickness (Robin, 1955). A thin, high-accumulation ice sheet has a cold bed in the central regions, but its behavior becomes more like that of a stagnant ice layer as the ice thickness increases and the accumulation rate drops. For likely conditions in the center of a continental ice sheet initiated in a subfreezing climate, the bed will remain frozen until the ice thickness exceeds = 3000 m.

The 3500-m-thick East Antarctic ice sheet is underlain by a wet bed in places (Oswald and Robin, 1973) but almost as great a thickness of ice in Greenland shows widespread freezing to its bed (Radok *et al.,* 1982; Robin, 1983). The bed of the West Antarctic ice sheet is largely thawed; however, it occurs in a recently active tectonic region, which probably has high geothermal flux (Alley and Bentley, 1988), and rests on low bedrock (typically 500 to 2000 m below sea level; Drewry, 1983), allowing thick ice to have a low, warm surface. By simple analogy and by physical reasoning, it is likely that the Laurentide and Fennoscandian ice sheets were frozen to their beds in central regions until their sizes increased close to their maximum values (Hooke, 1977; Sugden, 1977).

If basal melting occurs beneath the central part of an ice sheet, it will be slow. A typical geothermal flux will melt about 5 mm/yr of ice in the absence of heat conduction into the ice; beneath cold ice, a melt rate <<1 mm/yr will be more typical.

An ice sheet thins away from its center, which from the discussion above would tend to cool the bed, and colder ice formed at higher elevation is transported to lower regions with higher surface temperatures by ice flow, also cooling the bed. However, flow velocities and viscous dissipation increase outward, tending to warm the bed. Local details of bed topography, geothermal flux, accumulation rate, and other factors are likely to be more important in controlling basal temperature than any "typical" variation along flow, although zones of net basal freeze-on of meltwater (e.g., Byrd Station in West Antarctica; Gow *et al.,* 1979) or frozen bed will occur downstream of thawed regions in many cases.

At some point near the ice-sheet margin, flow tends to funnel into fast-moving, often relatively thin ice streams or outlet glaciers. These channelized flows may occur between regions of bare rock outcrop, but often occur between thin ice ridges nourished by local accumulation but not by flow from upstream. Viscous dissipation in ice streams is strong, typically melting O(10 to 100 mm/yr) [O(x) signifies "of the order of magnitude of x"]; interstream ridges are likely to be frozen to their beds. This situation can give rise to selective linear erosion, with the ice stream carving a channel between ridges experiencing little or no erosion (Sugden, 1978).

Surface melting on ice sheets is limited to warm areas at lower elevations and latitudes. Following the onset of melting, meltwater initially drains into surface snow and refreezes. Sufficient melting will cause surface runoff. Such runoff can drain to the bed if the ice is sufficiently thin, warm, and crevassed. At present, surface melting is common and supplies water to the bed on many mountain glaciers, but this is restricted to a relatively narrow band around the coast of Greenland and is almost absent in Antarctica. Where surface melting occurs it generally dominates the glacier water budget; rates of O(1 m/yr) are common.

Glacial-geologic evidence from the Laurentide and Fennoscandian ice sheets indicates the presence of frozen beds, wet beds, and surficial meltwater at various times (e.g., Sugden and John, 1976); however, most of the data reflect processes near the ice margin during retreat. A likely history is that large areas of the Wisconsinan midlatitude ice sheets were frozen to their beds during growth. The bed probably thawed in central regions during the glacial maximum. Thawed beds existed beneath channelized ice flows across large areas of the southern margins and smaller areas of the northern margins, but frozen beds occurred between these channelized flows. Surficial meltwater reached the bed in large quantities in marginal areas, especially on the southern margin during ice-sheet retreat. (For a similar but more exhaustive review of much of this material, the interested reader is referred to Hooke, 1977; Sugden, 1977; and Hughes, 1981).

Carbon Dioxide in Glacial Meltwater The amount of CO_2 available in ice for chemical weathering can be estimated reasonably well and is not large (e.g., Stauffer and Berner, 1978; Neftel *et al.,* 1982; Oeschger and Stauffer, 1986). During the transformation of snow to ice without melting, the ice traps about 10 percent air by volume with the prevailing atmospheric CO_2 concentration. This is retained in the air bubbles as CO_2 (or in some form such that CO_2 gas is recovered if the ice is crushed under vacuum), for a total of about 10^{-6} mole CO_2/kg ice (CO_2:H_2O molar ratio = 2×10^{-8}, within a factor of two to three depending on atmospheric CO_2 partial pressure, atmospheric pressure when air was trapped, and other variables). By comparison, rainwater in equilibrium with the atmosphere has a CO_2 concentration an order of magnitude or more higher than this. Refrozen surficial meltwater in glaciers falls between the ordinary ice and rainwater CO_2 concentrations.

When ice is melted beneath a glacier, water production rates are low, flow velocities are slow, and flow paths to the ice front typically are long; thus, it is likely that chemical weathering continues to completion and consumes the CO_2 in the meltwater. Wet-based glaciers are reasonably efficient at eroding unconsolidated sediment in some areas and depositing it elsewhere (see below), so it is unlikely that organic-rich soils will remain in contact with a glacier and supply abundant CO_2 to meltwaters over any significant time.

Under certain circumstances, surficial meltwater can remain in contact with both rock debris and atmospheric CO_2. For example, compressive stresses near ice fronts may cause folding or thrusting of basal debris to the ablating ice surface. Under such open-system conditions, meltwater can obtain CO_2 from the air as it is consumed in weathering; total CO_2 consumption then can exceed initial CO_2 content of the water (Raiswell, 1984). This process continues beyond the glacial margin in proglacial streams and differs from nonglacial streams only in that (1) glacial streams often transport material with more total area of fresh, unweathered mineral surface than similar nonglacial streams (see below); but (2) glacial streams generally lack CO_2 input from organic-rich soils and thus have much lower CO_2 concentrations than equivalent nonglacial streams.

Observations bearing directly on glacial chemical weathering are relatively scarce. Edmond (1973) and Hurd (1977) showed that Antarctic glaciers contribute very little to the dissolved silica in ocean waters adjacent to the Antarctic. Mountain glaciers are observed to have two meltwater systems: one with slow drainage and limited CO_2 in which chemical weathering proceeds to equilibrium and solute concentrations are relatively high, and one with rapid, channelized drainage of surficial water in which solute concentrations are low, whether that drainage occurs on, in, or under the glacier (Collins, 1979; Raiswell, 1984). Proglacial mixing of these waters allows the CO_2-bearing surficial meltwaters to weather silt supplied by the basal waters, but the extent to which equilibrium is reached and further CO_2 is taken from the air is not known well. Ford (1971) found that glacial meltwater above tree line in limestone regions of the Canadian Rockies was saturated with respect to $CaCO_3$ at only 50 to 90 mg/liter, compared to groundwater saturation at 100 to 265 mg/liter below tree line and creek and lake saturation at 100 to 140 mg/liter below tree line.

Glaciated basins in high mountains in maritime climates have high denudation rates (= 1 mm/yr) and chemical weathering is faster than the global average, but runoff is very high (4 m/yr is typical; Corbel, 1959; Reynolds and Johnson, 1972). No data are available on how much of that chemical weathering is associated with soil processes in unglaciated parts of the basins; the work of Ford (1971) suggests that much of it may be. In addition, glaciers in such maritime climates often have abundant englacial and supraglacial debris from rockfalls along with abundant meltwater; thus they are poor analogues for all except the narrow margin of a continental ice sheet.

Based on this discussion, chemical weathering in contact with continental ice sheets can be summarized as follows:

- large areas of ice sheets are frozen to their beds and slow or stop chemical weathering, especially during ice-sheet growth;
- central ice-sheet regions with thawed beds produce <O(1 mm/yr) basal meltwater, with CO_2 available for weathering equivalent to that in <O(0.1 mm/yr) rainwater, and this CO_2 generally is consumed in rock weathering;
- fast-moving marginal regions produce O(10 to 100 mm/yr) basal meltwater over perhaps 10 percent of the ice

sheet, with CO_2 equivalent to O(1 to 10 mm/yr) rainwater over this area, and this CO_2 also is consumed in rock weathering;

- ablation zones along ice-sheet margins may produce O(1 m/yr) surficial meltwater with CO_2 concentration between that of ice and rainwater, and more atmospheric CO_2 is available to this open system; however, high flow velocities and scarcity of supraglacial debris generally prevent rapid chemical weathering; and
- glacial meltwater generally does not gain significant CO_2 from soil processes, whereas soil processes in unglaciated regions often increase CO_2 by an order of magnitude or more from rainwater values (Cawley *et al.,* 1969). (In this respect, it is worth noting that much of the glacial discharge from the southern margins of the Laurentide and Fennoscandian ice sheets drained into climatically dry regions caused by the ice sheets, where soil processes producing CO_2 may have been slowed compared to more humid regions.)

Taken together, these points suggest that continental ice sheets reduce chemical weathering significantly—probably by one or more orders of magnitude—compared to preglacial or postglacial rates in the glaciated regions. However, some marginal regions of continental ice sheets occupy areas that are marine during interglaciations, so local increases of chemical weathering can accompany glaciation.

Erosion Rates Although it seems likely that ice-sheet glaciation reduces chemical weathering in the glaciated region, there is no general agreement on the effect on physical weathering and erosion rates. This question is of interest because fresh, reactive mineral surfaces produced subglacially possibly undergo enhanced chemical weathering beyond glacier margins.

Subglacial erosion rates span the entire range of terrestrial values, as noted above. Glacier erosion involves three major processes: plucking, abrasion, and subglacial fluvial action (e.g., Sugden and John, 1976, part III). Plucking is the glacial removal of clasts from the bed. Plucking is most effective where freeze-thaw processes cause ice to attach to previously jointed rock on the downstream sides of bumps in the bed, so that the ice motion pulls blocks free. Neither freezing-on nor preexisting bumps are absolutely necessary for plucking, but glacial stresses are sufficiently small that preexisting jointing or unconsolidated sediments are necessary for plucking. However, a glacier may contribute to the formation of joints through freeze-thaw processes, fluctuating water pressures, or erosion causing formation of unloading joints (sheeting).

Abrasion is the process by which glacially transported clasts scratch and gouge other clasts or subglacial bedrock, wearing away contact points and typically forming silt-sized particles. In the classical theory of abrasion (Hallet, 1979, 1981), the rate of abrasion of bedrock caused by a clast in basal ice increases with the clast velocity over the bed and the clast force on the bed. The clast force assumes that value needed to shove the clast upward into the softer, plastically deforming ice at the rate at which surrounding ice in contact with the bedrock is melted away or strained downward. Observations also show that clast-clast interactions in deforming subglacial till (see below) cause rapid abrasion and silt generation (Boulton *et al.,* 1974), and that abrasion of bedrock occurs beneath deforming till (MacClintock and Dreimanis, 1964). Abrasion requires a source of clasts (from plucking, supraglacial sources, or reworking of preexisting unconsolidated sediments) because the abrading clasts are themselves abraded and must be replaced.

Erosion by subglacial streams is similar to that by proglacial streams. It is limited primarily to marginal regions where abundant channelized surficial meltwater reaches the bed, but it can be quite active there (e.g., Sugden and John, 1976, Ch. 15).

Glacial shear stresses can deform unconsolidated subglacial sediments. Such sediments may be created by other subglacial processes of erosion, or the glacier may advance over preglacial or proglacial sediments. Subglacial deformation of unconsolidated sediments can be a very efficient mechanism of erosion/transport (Boulton, 1979; Alley *et al.,* 1989), moving far more material than other subglacial processes of erosion. Glaciers thus erode unconsolidated materials more efficiently than they erode bedrock.

Direct glacial deposits (tills) contain all grain sizes but exhibit modal peaks in the silt range (abrasion) and in the pebble-cobble range (plucking). Glaciofluvial deposits are sorted according to fluvial processes.

Much debate has centered on the depth of erosion achieved by the Pleistocene ice sheets of northern midlatitudes, especially the Laurentide ice sheet (e.g., White, 1972; Gravenor, 1975; Sugden, 1978; Bell and Laine, 1985). Estimates vary by an order of magnitude.

Based on the volume of sediments on land and in marine basins around the Laurentide region, Bell and Laine (1985) estimated denudation of at least 120 m (and perhaps as much as 200 m) over the past 3 million years (m.y.) during which major Northern Hemisphere continental glaciation occurred. Glacial sediments on land account for only one-fifteenth of the total. They further estimated that fluvial processes in the absence of glaciation would have produced little more than 10 percent of this sediment. Based on these estimates, the glacial erosion rate over the entire Laurentide region and the entire 3 m.y. is only about 0.05 mm/yr. However, glaciers were absent for some periods, and were frozen to their beds or depositing rather than eroding in some areas when present.

If we speculate that wet-based glaciation occupied only one-quarter of the Laurentide region for one-quarter of the glacial period (possible but unproven numbers), then the wet-based erosion rate was about 1 mm/yr, similar to mountain-glacier rates (Boulton, 1979).

It must be noted, however, that some geological observations on land are not consistent with 120 to 200 m of glacial erosion in North America over the past 3 m.y., but seem to indicate only glacial stripping of regolith with little bedrock erosion (e.g., Gravenor, 1975; Sugden, 1978). If so, then glacial denudation rates are similar to interglacial rates, but glacial rates are controlled by physical processes whereas chemical weathering is more important during interglacials.

Analogy to the modern Antarctic ice sheet is not very helpful. Documented sedimentation of material transported by the ice sheet is quite slow, indicating slow subglacial erosion. However, data from the best-studied drainage basin of West Antarctica suggest a subglacial erosion rate of $O(0.1$ to 1 mm/yr$)$, with deposition localized at the grounding line beneath several hundred meters of floating ice shelf (Alley *et al.,* 1989). The generality of this result is unknown.

To summarize, then,

- ice in wet-based accumulation zones of glaciers and ice sheets erodes and transports unconsolidated materials efficiently; the cumulative effect of midlatitude ice sheets in eroding bedrock remains uncertain;
- sediments of demonstrable glacial origin from the Laurentide ice sheet indicate denudation rates similar to subaerial values in the region today; and
- an order of magnitude more sediments than those of demonstrable glacial origin may have been produced by the Laurentide ice sheet and deposited in marine environments.

COUPLED CHANGES

From glacial times until the present, virtually all of the important factors in global chemical weathering experienced significant changes. The planet warmed, the glaciers receded and exposed new materials to weathering, the continental shelves flooded, and precipitation and runoff fields experienced significant perturbations. The net effect of all of these changes on the global rate of chemical denudation is difficult to assess. In this section we will examine some of the coupled changes that occurred, glacial to recent, and finally make an assessment of their net effect.

The Climate/Rock Type Connection

The highest chemical weathering rates on the present Earth occur in regions of high rainfall, high relief, and with limestone and evaporite (e.g., the Yangtze and Brahmaputra rivers) or recent volcanic lithologies (Berner and Berner, 1987). These regions do not occur at high northern latitudes today (or in the recent geologic past) so they did not experience direct glacial coverage during the Wisconsin glaciation. In fact, few of these regions of high chemical denudation fell in zones of decreased soil moisture 18 ka (compare Figures 3.1 and 3.5). Thus there is no clear reason to suspect that glacial, global chemical weathering rates were reduced relative to today, on this basis.

In terms of a climate feedback, silicate weathering is paramount, for as shown above, it is during the weathering of this rock type that net CO_2 consumption occurs (averaged over thousands of years). Walker *et al.* (1981) and Berner *et al.* (1983) have argued that the balance of CO_2 consumption during silicate weathering and production during volcanism regulates atmospheric CO_2 concentrations, and thus climate, on time scales longer than a few thousand years. This time scale represents the residence time of atmospheric CO_2 with respect to recycling by the carbonate-silicate geochemical cycle (about 3000 yr). Of course, on these short time scales one must consider ocean/atmosphere exchange to be fast, so that perturbations in weathering and volcanism on thousand-year time scales are damped. However, the residence time of the entire ocean/atmosphere carbon reservoir with respect to the geochemical cycle is on the order of 100,000 yr, so we must consider changes in this cycle as potential climate modifiers on glacial time scales.

Where is CO_2 being consumed today? For a region to qualify as a significant CO_2 sink it should be dominated by silicate exposures and be in a region of high runoff and high physical erosion. By excluding those regions of Figure 3.6 that (1) lie in areas where runoff averages less than 500 mm/yr and (2) are in areas undergoing >100 tons/km^2 of physical erosion per year, a map of CO_2 sinks is produced (Figure 3.7).

Rapid consumption of CO_2 occurs over a relatively restricted part of the land surface. The more important regions include the southeastern United States, the Andes, and southeast Asia. Regions typically assumed to be areas of high chemical weathering (e.g., Amazonia) do not appear, for they have developed thick soil mantles, and chemical weathering rates are actually low.

Of these areas, none fall within a region of higher soil moisture at 18 ka (Figure 3.1), and some probably experienced drier conditions (especially those in southeast Asia and South America). This would suggest that perhaps CO_2 consumption rates were somewhat diminished by glacial climates, a negative feedback.

Forest Coverage and Weathering

The presence of forests on land enhances chemical weathering rates by their effect on the soil environment (e.g.,

Knoll and James, 1987). Root respiration produces CO_2 in the soil and, aided by bacterial decomposition of forest litter, generates CO_2 pressures that are 10 to 100 times the atmospheric value (Cawley *et al.,* 1969; Holland *et al.,* 1986). In addition, roots aid in the physical breakdown of the bedrock. Organic acid production in forest soils also increases the solubility of minerals. These effects would be diminished if the areal extent of forests were diminished.

FIGURE 3.7 Modern CO_2 sinks defined as regions of "silicate" exposure (Figure 3.6) that have high physical erosion rates (Snead, 1980; Broecker, 1983) and high runoff (UNESCO, 1978).

A marked effect of glaciation on forests is the loss of the temperate deciduous and evergreen forests (e.g., Broecker, 1983). These forests today cover a large fraction of North America, Europe, and Asia (Figure 3.8A); during glacial maximum they were largely removed, either from being overrun by glaciers or from increased aridity (Figure 3.8B).

The areal extent during glacial time of the tropical rainforests of South America and Africa was also reduced due to aridity. This reduction was partially offset by the expansion of tropical forests, especially in Oceania, into shelf regions that became exposed as sea level fell.

In total, it seems that the biological enhancement of chemical weathering rates was significantly reduced during glacial times due to restriction of the areas of temperate and tropical forests. However, these areas were largely replaced by grasslands; the enhancement factor of this ecosystem type should be less, but relative enhancements are poorly known. The implied reduction of chemical weathering rates should, over thousands of years, have tended to increase atmospheric CO_2 concentrations due to (1) decrease in the carbonate ion concentration of the ocean, caused by the decrease in the rate of supply of alkalinity from weathering, and thus an increase in the equilibrium pCO_2 (e.g., Broecker and Peng, 1987); and (2) an excess of CO_2 production by volcanism over consumption by silicate weathering (e.g., Volk, 1987). This feedback is negative; it would tend to counter the climate perturbations producing glacial conditions.

Climate and Glacial Sediment Supply

Wet-based continental ice sheets probably suppress chemical weathering but speed physical erosion, as discussed above. Some results of the growth and decay of a large ice sheet include

- removal of regolith from central regions, leaving fresh bedrock exposed or covered by a thin layer of glacial sediments;
- ice-contact deposition of thick sequences of glacially transported sediment in marginal regions, often on top of older regolith, these glacially transported sediments contain much fresh mineral surface area formed by abrasion/comminution and may be deposited in seas, lakes, or on land; some of the terrestrial deposits are flooded by subsequent sea-level rise;
- fluvial transport of glacially eroded and comminuted sediment into lakes and seas, although typically with significant aggradation of river channels and thus sediment storage [the common occurrence of glacial-age fluvial terraces along modern streams shows that such storage still is occurring (Schumm and Brakenridge, 1987)]; and
- eolian transport of glaciogenic silt off outwash plains to be deposited as loess in adjacent regions, especially if dry or seasonally dry climates suppress vegetation on outwash and allow desiccation and easier wind erosion (Pye, 1984).

The net result is to increase the chemical reactivity of mineral surfaces in all glacially affected areas. Weathered regolith is thinned or removed beneath the center of the ice sheet to expose fresh bedrock, and comminuted regolith and bedrock are deposited over weathered regolith beneath and beyond the ice margins. Comprehensive data are not available on increases in mineral reactivity from ice-sheet glaciation, but such increases are likely to be significant.
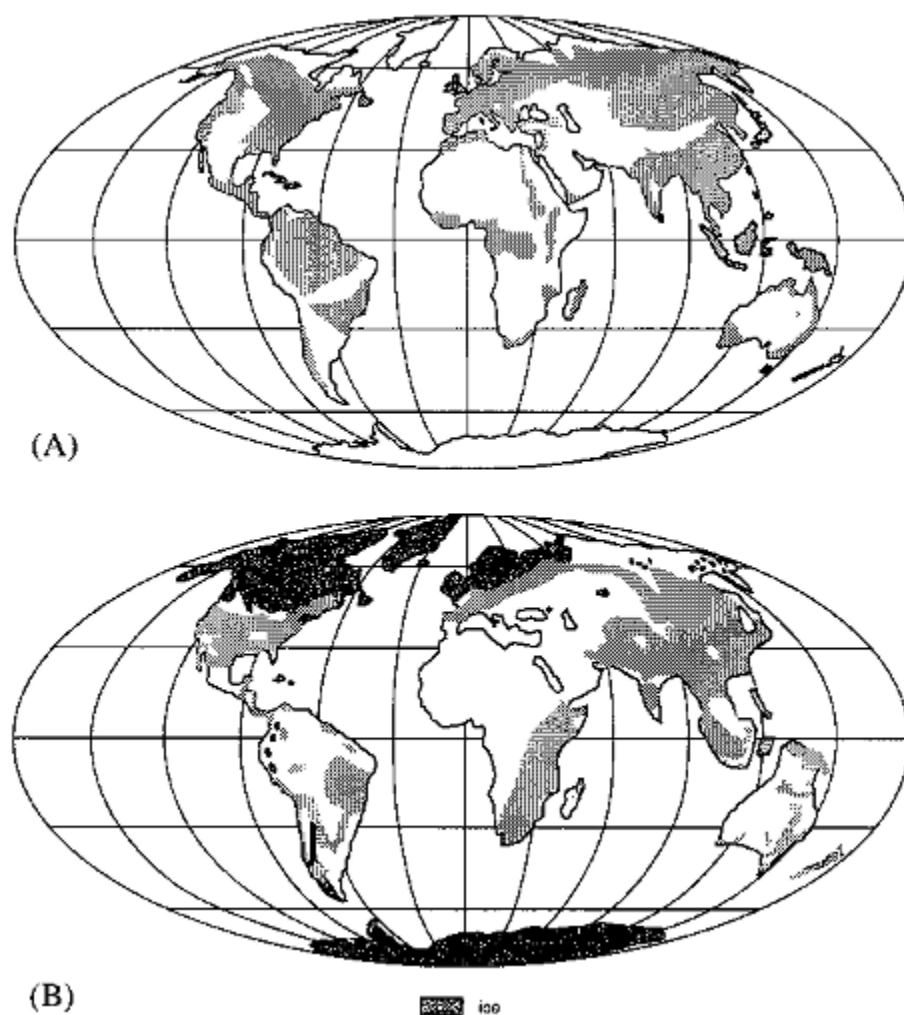
FIGURE 3.8 (A) Regions of present-day forest (Snead, 1980). (B) Extent of forests at 18 ka (National Geographic Society, 1988).

It is of further interest that some glacial-maximum sediment discharge occurred into regions of low soil moisture caused by ice-sheet effects on climate (e.g., COHMAP, 1988), encouraging eolian erosion of outwash plains and loess deposition; source areas not receiving glacial sediments in glacially desiccated climatic regions of Asia may have experienced eolian erosion contributing to downwind loess deposition as well (Pye, 1984). Loess deposits are shown in Figure 3.9, modified from Pye (1984); especially in North America, a little loess extends north of the glacial limit.

These loess deposits typically contain silt-sized, subangular clasts, and are porous, permeable, and relatively unweathered when formed. Subsequent to formation, most have experienced increases in soil moisture and, by inference, in rates of chemical weathering. Some deposits fall within the belt of enhanced monsoonal circulation that peaked around 9 to 12 ka, and these deposits experienced strongly increased soil moisture during that time (compare Figures 3.1 and 3.9; COHMAP, 1988). Loess deposits north of this enhanced monsoonal belt experienced more seasonal climates following deglaciation, with hot, dry summers peaking around 9 to 6 ka. Some loess areas have higher soil moisture today than at any other time since the previous interglaciation, but almost all areas experienced soil-moisture levels higher than those prevailing during loess deposition at some time following deposition (e.g., Kutzbach, 1987; Webb *et al.,* 1987; COHMAP, 1988). The pattern of loess deposition during glacial periods followed by enhanced chemical weathering and soil development on loess has been repeated numerous times, and probably for every Pliocene-Pleistocene Northern Hemisphere glaciation (Fink and Kukla, 1977). The quantitative significance of this pattern for geochemical fluxes is not well constrained, but merits further study.

FIGURE 3.9 Loess deposits (after Pye. 1984) and regions with greater soil moisture at 9 ka (based on COHMAP, 1988).

IMPLICATIONS FOR OCEANIC AND ATMOSPHERIC CHEMISTRY AND CLIMATE

To summarize the interpretations given above of the changes in the global environment for chemical weathering 18 ka relative to today, we find that there was

- no significant, global average change in soil moisture;
- a small decrease in the global area, but a significant increase in the tropical area, of subaerial exposure;
- a decrease in the forested area;
- an increase in carbonate exposures, especially at low latitudes; and
- a decrease in silicate exposures at high northern latitudes.

To do a convincing job of weighing these factors and determining a net change in the global chemical weathering rate, one would want to make a geographically based geochemical-cycling/climate calculation. In lieu of this, we can merely speculate that these changes in the global chemical weathering rate were roughly compensatory and thus that globally averaged chemical weathering rates during glacial times were similar to those during interglaciations (with large error bars).

The change between 18 ka and today was nonlinear, and some factors that are similar today to their glacial conditions experienced significant perturbations during deglaciation. These probably include

- an increase in the reactivity of the weathering surface, due to the exposure of "fresh" surfaces (scraped free of regolith or covered with comminuted material) and loess as the glaciers retreated, over about 25 percent of the modern land surface;
- a peak in the chemical weathering rate of this material in the 0° to 30° N latitude band, at about 12 to 9 ka, when soil moisture values peaked; after this time, weathering rates probably decreased as the fresh surface became covered with a weathered soil; and
- peaks in chemical weathering of this material corresponding to increasing soil moisture in other bands.

If indeed these perturbations were globally significant, they should have left a record in terms of changes in oceanic or atmospheric chemistry, or in climate. Perhaps the most sensitive indicator of change in the rate of chemical denudation of the continents is the level of the calcium compensation depth (CCD) in the ocean. The depth of this horizon, which separates the region of carbonate sediment accumulation from the deeper region of net carbonate dissolution, is determined by the requirement of carbonate balance of the ocean (Broecker and Peng, 1982; Bender, 1984). For example, an increase in the rate of bicarbonate (and alkalinity) input to the ocean from weathering should cause a depression of the CCD (and an increase in the carbonate ion concentration of the ocean), to ensure that the burial rate of $CaCO_3$ increases and the balance of input and output is thus achieved.

Broecker and Peng (1987) have assessed the sedimentary evidence (Berger, 1970; Peterson and Prell, 1985) for changes in the CCD over the period of interest (Figure 3.10) and have concluded that

- there was no significant difference between glacial and interglacial times in the carbonate ion content of the ocean or the depth of the CCD; and
- there was, however, a several-thousand-year perturbation in these oceanic variables centered on 9 ka, coincident with deglaciation.

The first of these conclusions is consistent with our suggestion that chemical weathering rates were similar during

glacial and interglacial times. Broecker and Peng (1987) suggest a change in the rate of nutrient recycling in the ocean to explain the perturbation in the CCD at the close of glacial time. They, and Broecker (1983), do acknowledge that little is known of the potentially important effect of glacial/interglacial changes in continental weathering rates on the carbonate budget of the ocean. We do not propose, based on what we have presented, that such changes are primarily responsible for the CCD perturbation, but they are consistent with it. As our knowledge of oceanic changes in the rate of Quaternary carbonate accumulation improves, perhaps the need will arise to invoke changes in global chemical weathering rates to explain these observations.
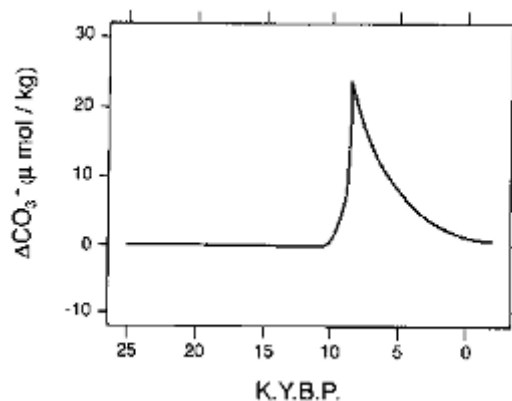
FIGURE 3.10 Perturbation in the carbonate ion concentration of the ocean during the past deglaciation (Broecker and Peng, 1987).

Finally, we have found that there is reason to believe that the rate of CO_2 consumption during silicate weathering varies on glacial time scales, due both to the direct effects of glacial coverage and erosion, and to the indirect effect of glaciation on climate. In our search for positive and negative feedbacks in glacial climate regulation we must consider this important, apparently negative, and thus stabilizing feedback (Marshall *et al.,* 1988). Too often we think of such geological processes as only acting on million-year time scales or longer; as demonstrated here, changes in chemical weathering rates can affect climate change on 1000 to 100,000 yr periods as well.

ACKNOWLEDGMENTS

REFERENCES

Alley, R.B., and C.R. Bentley (1988). Ice-core analysis on the Siple Coast of West Antarctica, Annals of Glaciology 11, 1-7 .

Alley, R.B., D.D. Blankenship, S.T. Rooney, and C.R. Bentley (1989). Sedimentation beneath ice shelves — The view from ice stream B, Marine Geology 85(2/4), 101-120 .

Bell, M., and E.P. Laine (1985). Erosion of the Laurentide region of North America by glacial and glaciofluvial processes, Quaternary Research 23, 154-174 .

Bender, M.L. (1984). On the relationship between ocean chemistry and atmospheric pCO2 during the Cenozoic, in Climate Processes and Climate Sensitivity, J.E. Hansen and T. Takahashi, eds., Monograph Series 29, American Geophysical Union, Washington, D.C., pp. 352-359 .

Berger, W.H. (1970). Deep-sea carbonate and the deglaciation spike in pteropods and foraminifera, Nature 269, 301-303 .

Berner, E.A., and R.A. Berner (1987). The Global Water Cycle: Geochemistry and Environment, Prentice-Hall, Englewood Cliffs, N.J., 397 pp .

Berner, R.A., A.C. Lasaga, and R.M. Garrels (1983). The carbonate-silicate geochemical cycle and its effect on atmospheric carbon dioxide over the past 100 million years, American Journal of Science 283, 641-683 .

Bloom, A.L. (1978). Geomorphology: A Systematic Analysis of Late Cenozoic Landforms, Prentice-Hall, Englewood Cliffs, N.J., 510 pp .

Boulton, G.S. (1979). Processes of glacier erosion on different substrata, Journal of Glaciology 23(89), 15-38 (including discussion).

Boulton, G.S., D.L. Dent, and E.M. Morris (1974). Subglacial shearing and crushing, and the role of water pressures in tills from south-east Iceland, Geografisica Annaler 56A(3-4), 135-145 .

Broecker, W.S. (1983). The ocean, Scientific American 249, 146-161 .

Broecker, W.S., and T.-H. Peng (1982). Tracers in the Sea, Eldigio Press, New York, 690 pp .

Broecker, W.S., and T.-H. Peng (1987). The role of CaCO3 compensation in the glacial to interglacial atmospheric CO2 change, Global Biogeochemical Cycles 1, 15-29 .

Cawley, J.L., R.C. Burruss, and H.D. Holland (1969). Chemical weathering in central Iceland: An analog of pre-Silurian weathering, Science 165, 391-392 .

CLIMAP (1976). The surface of the ice-age Earth, Science 191, 1131-1136 .

COHMAP (1988). Climatic changes of the last 18,000 years: Observations and model simulations, Science 241, 1043-1052 .

Collins, D.N. (1979). Quantitative determination of the subglacial hydrology of two Alpine glaciers, Journal of Glaciology 23(89), 347-362 .

Corbel, J. (1959). Vitesse de l'erosion, Zeitschrift fir Geomorphologie 3, 1-28 .

Drewry, D.J. (ed.) (1983). Antarctica: Glaciological and Geophysical Folio, Scott Polar Research Institute, University of Cambridge.

Edmond, J.M. (1973). The silica budget of the Antarctic circumpolar current, Nature 241, 391-393 .

Fink, J., and G.J. Kukla (1977). Pleistocene climates in central Europe: At least 17 interglacials after the Olduvai event, Quaternary Research 7(3), 363-371 .

Flint, R.F. (1971). Glacial and Quaternary Geology, John Wiley & Sons, New York, 892 pp .

Ford, D.C. (1971). Characteristics of limestone solution in the southern Rocky Mountains and Selkirk Mountains, Alberta and British Columbia, Canadian Journal of Earth Sciences 8, 585-609 .

Gellatly, A.F., J.E. Gordon, W.B. Whalley, and J.D. Hansom (1988). Thermal regime and geomorphology of plateau ice caps in northern Norway: Observations and implications, Geology 16(11), 983-986 .

Gibbs, R.J. (1970). Mechanisms controlling world water chemistry, Science 170, 1088-1090 .

Gow, A.J., S. Epstein, and W. Sheehy (1979). On the origin of stratified debris in ice cores from the bottom of the Antarctic ice sheet, Journal of Glaciology 23(89), 185-192 .

Gravenor, C.P. (1975). Erosion by continental ice sheets, American Journal of Science 275, 594-604 .

Hallet, B. (1979). A theoretical model of glacial abrasion, Journal of Glaciology 23(89), 39-50 .

Hallet, B. (1981). Glacial abrasion and sliding: Their dependence on the debris concentration in basal ice, Annals of Glaciology 2, 23-28 .

Holland, H.D. (1978). The Chemistry of the Atmosphere and Oceans, John Wiley & Sons, New York, 351 pp .

Holland, H.D., B. Lazar, and M. McCaffrey (1986). Evolution of atmosphere and oceans, Nature 320, 27-33 .

Hooke, R. LeB. (1977). Basal temperatures in polar ice sheets: A qualitative review, Quaternary Research 7(1), 1-13 .

Hughes, T.J. (1981). Numerical reconstruction of paleo-ice sheets, in The Last Great Ice Sheets, G.H. Denton and T.J. Hughes, eds., John Wiley & Sons, New York, pp. 221-261 .

Humphrey, N. (1986). Suspended-sediment discharge from Variegated Glacier during pre-surge and surge phases of motion, abstract presented to Chapman Conference on Fast Glacier Flow, Whistler Village, British Columbia, Canada, May 4-8.

Hurd, D.C. (1977). The effect of glacial weathering on the silica budget of Antarctic waters, Geochimica et Cosmochimica Acta 41, 1213-1222 .

Knoll, M.A., and W.C. James (1987). Effect of the advent and diversification of vascular land plants on mineral weathering through geologic time, Geology 15, 1099-1102 .

Kutzbach, J.E. (1987). Model simulations of the climatic patterns during the deglaciation of North America, in North America and Adjacent Oceans During the Last Deglaciation, W.F. Ruddiman and H.E. Wright, Jr., eds., vol. K-3 , The Geology of North America, The Geological Society of America, Boulder, Colorado, pp. 425-446 .

Kutzbach, J.E., and P.J. Guetter (1986). The influence of changing orbital parameters and surface boundary conditions on climate simulations for the past 18,000 years, Journal of the Atmospheric Sciences 43, 1726-1759 .

MacClintock, P., and A. Dreimanis (1964). Reorientation of till fabric by overriding glacier in the St. Lawrence Valley, American Journal of Science 262, 133-142 .

Manabe, S., and A.J. Broccoli (1985). The influence of continental ice sheets on the climate of an ice age, Journal of Geophysical Research 90(D1), 2167-2190 .

Marshall, H.G., J.C.G. Walker, and W.R. Kuhn (1988). Long-term climate change and the geochemical cycle of carbon, Journal of Geophysical Research 93, 791-802 .

National Geographic Society (1988). Endangered Earth (map), National Geographic 174(6) .

Neftel, A., H. Oeschger, J. Schwander, B. Stauffer, and R. Zumbrunn (1982). Ice core sample measurements give atmospheric CO_2 content during the last 40,000 yr, Nature 295, 220-223 .

Oeschger, H., and B. Stauffer (1986). Review of the history of atmospheric CO_2 recorded in ice cores, in The Changing Carbon Cycle: A Global Analysis, J.R. Trabalka and D.E. Reichle, eds., Springer-Verlag, New York, pp. 89-108 .

Oswald, G.K.A., and G. de Q. Robin (1973). Lakes beneath the Antarctic ice sheet, Nature 245, 251-254 .

Paterson, W.S.B. (1981). The Physics of Glaciers, 2nd ed., Pergamon Press, Oxford, 380 pp .

Peterson, L.C., and W.L. Prell (1985). Carbonate preservation and rates of climatic change: An 800 kyr record from the Indian Ocean, in The Carbon Cycle and Atmospheric CO_2: Natural Variations Archean to Present, E.T. Sundquist and W. S. Broecker, eds., American Geophysical Union, Washington, D.C., pp. 251-269 .

Porter, S.C. (1977). Present and past glaciation threshold in the Cascade Range, Washington, U.S.A.: Topographic and climatic controls, and paleoclimatic implications, Journal of Glaciology 18(78), 101-116 .

Pye, K. (1984). Loess, Progress in Physical Geography 8, 176-217 .

Radok, V., R.G. Barry, D. Jenssen, R.A. Keen, G.N. Kiladis, and B. McInnes (1982). Climatic and Physical Characteristics of the Greenland Ice Sheet, Cooperative Institute for Research in Environmental Sciences (CIRES), University of Colorado, Boulder, 193 pp .

Raiswell, R. (1984). Chemical models of solute acquisition in glacial meltwaters, Journal of Glaciology 30(104), 49-57 .

Rand McNally (1977). The Atlas of the Oceans, Rand McNally and Co., Chicago, 208 pp .

Reynolds, R.C., and N.M. Johnson (1972). Chemical weathering in the temperate glacial environment of the northern Cascade Mountains, Geochimica et Cosmochimica Acta 36, 537-554 .

Rind, D. (1987). Components of the ice age circulation, Journal of Geophysical Research 92(D4), 4241-4281 .

Robin, G. de Q. (1955). Ice movement and temperature distribution in glaciers and ice sheets, Journal of Glaciology 2(18), 523-532 .

Robin, G. de Q. (1977). Ice cores and climatic change, Philosophical Transactions of the Royal Society of London Series B 280, 143-168 .

Robin, G. de Q. (1983). General glaciology, in The Climatic Record in Polar Ice Sheets, G. de Q. Robin, ed., Cambridge University Press, pp. 94-97 .

Schumm, S., and G.R. Brakenridge (1987). River responses, in North America and Adjacent Oceans During the Last Deglaciation, W.F. Ruddiman and H.E. Wright, Jr., eds., vol. K-3 , The Geology of North America, The Geological Society of America, Boulder, Colorado, pp. 221-240 .

Snead, R.E. (1980). World Atlas of Geomorphic Features, Krieger, New York, 301 pp .

Stauffer, B., and W. Berner (1978). CO_2 in natural ice, Journal of Glaciology 21(85), 291-299 (with discussion, p. 300).

Sugden, D.E. (1977). Reconstruction of the morphology, dynamics and thermal characteristics of the Laurentide Ice Sheet at its maximum, Arctic and Alpine Research 9, 21-47 .

Sugden, D.E. (1978). Glacial erosion by the Laurentide ice sheet, Journal of Glaciology 20(83), 367-391 .

Sugden, D.E., and B.S. John (1976). Glaciers and Landscape: A Geomorphological Approach, John Wiley & Sons, New York, 376 pp .

UNESCO (1978). World Water Balances and Water Resources of the Earth, UNESCO Press, Paris.

Volk, T. (1987). Feedbacks between weathering and atmospheric CO_2 over the last 100 million years, American Journal of Science 287, 763-779 .

Walker, J.C.G., P.B. Hays, and J.F. Kasting (1981). A negative feedback mechanism for the long-term stabilization of Earth's surface temperature, Journal of Geophysical Research 86, 9776-9782 .

Webb, T., III, P.J. Bartlein, and J.E. Kutzbach (1987). Climatic change in eastern North America during the past 18,000 years: Comparisons of pollen data with model results, in North America and Adjacent Oceans During the Last Deglaciation, W.F. Ruddiman and H.E. Wright, Jr. , eds., Vol. K-3 , The Geology of North America, The Geological Society of America, Boulder, Colorado, pp. 447-462 .

White, W.A. (1972). Deep erosion by continental ice sheets, Geological Society of America Bulletin 83, 1037-1056 .

4

Origin and Variable Composition of Present Day Riverborne Material

MICHEL MEYBECK
Universite de Paris VI

ABSTRACT

Rivers are a major pathway in the global geochemical cycles of elements. However, little consideration has been given so far to the geographic distribution of their loads and contents because most scientists use only global figures. Actually, river chemistry is highly variable. Ionic contents are highly dependent on the lithology of the basin area; total organic carbon (TOC) and nitrogen are closely related to climate and vegetation; and total suspended solids (TSS) level and composition are linked to relief and climate. Finally, oceanic aerosols may greatly contribute to the dissolved load of surface waters. Because of these different sources, the chemical composition of water from small watersheds is extremely variable: about 15 chemical types have been reported, and most elements vary by two to four orders of magnitude. However, these ranges are only from one to three orders of magnitude for major rivers ($>100,000$ km^2). When global budgets are considered, crystalline rocks contribute to only a minor proportion of dissolved inputs to oceans. Carbonate rocks (16.3 percent of the continental surfaces) and evaporites (1.3 percent) are by far the major sources, together with soil and atmospheric CO_2, and oceanic aerosols.

The geographic origin of river load results from the combined influences of lithology, relief, and climate. Dissolved silica originates mainly from the humid tropics, as does total organic carbon derived from soil erosion; ions are relatively more abundant in the temperate regions due to their higher proportions of limestone; TSS originates from mountainous and dry regions found in the temperate zone, and the Huang He river alone accounts for more than 6 percent of the total river load. If the solid transport rate per unit area (T_s) is globally four times the dissolved transport rate (T_d), the ratio T_s/T_d actually varies from 80 to 0.1 for major rivers, and for 40 percent of the world rivers T_s/T_d is $\ll 1$. Global averages of river loads are therefore of little use in understanding the present-day pattern of element circulation and distribution, and should be considered carefully when used in geological models.

INTRODUCTION

When referring to riverine material, many sedimentologists, geochemists, and even hydrobiologists consider global or continental averages. This tendency is now reinforced by the increasing use of present-day global river inputs to oceans to model past geochemical cycles (Berner *et al.,* 1983; Wilkinson and Walker, 1989). Actually, global averages mask the extended chemical diversity of river water and particulates as well as the wide range of river transport rates.

The purpose of this chapter is (1) to assess the variability of river chemistry, (2) to review the main environmental factors that control these variations, and (3) to estimate the contributions to the global river loads from various geographic, geologic, and climatic environments. Because of the amount of information available, the focus is put on major elements, nutrients, and organic carbon. The anthropogenic influence is not considered here, [i.e., river data have been screened so that most polluted rivers have been discarded and only predamming data on total suspended solids (TSS) have been retained]. Extended compilations of river chemistry started in the 1960s (Durum *et al.,* 1960; Livingstone, 1963; Turekian, 1969). More recent basic data have already been published or previously referenced (Meybeck, 1979, 1982, 1983, 1986, 1987, 1988; Kempe, 1982; SCOPE CARBON, 1982, 1983, 1985, 1987). In addition to these, some regional studies on river water chemistry in unpolluted or less polluted environments have been used: the Mackenzie river watershed (Reeder *et al.,* 1972), Japan rivers in 1943 to 1957 (Kobayashi, 1960), Thailand rivers in 1956/1957 (Kobayashi, 1959), and the entire Amazon River basin (Stallard, 1980).

ENVIRONMENTAL FACTORS CONTROLLING CHEMISTRY OF WATER AND SUSPENDED MATTER

River water chemistry is controlled by many environmental factors, most of them known for a long time (Erikson, 1960; Gorham, 1961; Drever, 1982; Stallard and Edmond, 1981, 1983, 1987; Meybeck, 1984, 1986; Berner and Berner, 1987). They can be presented in three major groups: sources (lithosphere, atmosphere, biosphere), sinks (vegetation uptake, settling), and rate-controlling factors (temperature, water circulation). In addition, the river basin size plays a major part through the integration of diverse environments.

Lithology is a key factor for most major dissolved elements (Si, Ca, Mg, Na, Cl, S, C). Carefully selected, pristine monolithologic watersheds are characterized by distinctly different water quality compositions (Table 4.1A),

TABLE 4.1 Variability of Dissolved Major Elements in Pristine Stream Waters Draining Various Rock Types

	Elec. cond.	pH	TZ+	SiO$_2$	Ca^{2+}	Mg^{2+}	Na$^+$	K$^+$	Cl	SO$_4$	HCO$_3$
A. Most common rock types											
Granite[a]	35	6.6	166	150	39	31	88	8	0	31	128
Gneiss[a]	35	6.6	207	130	60	57	80	10	0	56	135
Volcanic rocks[a]	50	7.2	435	200	154	161	105	14	0	10	425
Sandstone[a]	60	6.8	223	150	88	63	51	21	0	95	125
Shale[a]	—	—	770	150	404	240	105	20	20	143	580
Carbonate rock[a]	400	7.9	3,247	100	2,560	640	34	13	0	85	3,195
Evaporitic deposits[b]	1,700	8.0	18,000	125	3,060	1,440	13,500	90	13,500	2,340	2,160
Evaporitic deposits[c]	—	—	20,000	110	12,400	7,000	600	40	600	15,000	4,400
B. Influence of water-rock interaction on water chemistry											
U.S. rivers[d]			2,800	232	1,600	700	430	70	300	650	1,800
U.S. groundwaters[e]			4,914	282	2,500	950	1,400	64	450	700	3,700

Note: TZ+ is the sum of the cations µeq/l) SiO$_2$ in µmole/l; ions in µeq/l.

[a] Averages from survey of 250 pristine streams in France (Meybeck, 1986) and from 75 sites worldwide, both corrected for oceanic Cylic salts (Meybeck, 1987).

[b] Mostly rock salt, 13 watersheds (Meybeck, 1987).

[c] Mostly gypsum and anhydrite, 6 French streams (Meybeck, 1986).

[d] Discharge-weighted average for the Mississippi, Columbia, and Colorado rivers; references in Meybeck (1979).

[e] Median distributution from Davis (1964), potable groundwaters.

directly related to the mineralogy of surficial rocks exposed to weathering. Stallard (1988) has defined the sequence of mineral stability in tropical soils (from the more stable to the less stable): quartz > K-feldspar, micas >> Na-feldspar > Ca-feldspar, amphiboles > pyroxene, chlorite > dolomite > calcite > gypsum, anhydrite >> halite. Water chemistry results from the combination of this weathering order and the relative abundance of the minerals. Meybeck (1987) has ordered the chemical weathering of common rock types found in France on the basis of total cations (TZ^+) observed in pristine streams (in order of increasing weathering): granite, gneiss, micaschist << gabbro, sandstone << volcanic rocks (basalts mainly) << shales << serpentine, marble, amphibolite <<< carbonate rocks <<< gypsum << rock salt. The influence of lithology on TSS level and chemical composition is much less known. In regions where high mechanical erosion occurs, thus exceeding chemical erosion, river particulates are a mixture of rock debris and poorly weathered soil particles and closely reflect the chemical composition of parent rock (Table 4.2A). The following scale of rock sensitivity to mechanical erosion is tentative (in order of increasing erosion): pure limestones << granite and gneiss << micaschists << consolidated volcanic rocks << shales <<< volcanic ash, sands, glacial deposits << clays << loess. Based mainly on major rivers, it remains to be tested on small monolithologic watersheds.

Atmospheric aerosols may greatly affect the chemistry of surface waters (Gorham, 1961; Sugawara *et al.,* 1982), particularly where waters drain crystalline rocks and near the ocean coastline. Ocean aerosols are the major source of major elements (Na^+, Cl^-, Mg^{2+}, SO_4^{2-}) in atmospheric precipitation and can be traced as far as 2000 km inland, as in Central Amazonia where they still contribute to an important part of the so-called Black Waters, the less mineralized world waters (Stallard, 1980; Stallard and Edmond, 1981, 1983). Near the ocean, relatively high ionic contents may result from atmospheric inputs as in pristine streams draining sand deposits in the extended Landes pine forest in southwestern France (Figure 4.1). From the coastline to 20 km inland, stream waters are rich in NaCl, and all major ions (Ca^{2+}, Mg^{2+}, Na^+, K^+, Cl^-, SO_4^{2-}) show a steep exponential decrease. From 20 to 100 km, Na^+ and Cl^- still decrease at a lower rate, whereas Ca^{2+}, Mg^{2+}, SO_4^{2-}, and K^+ show a marked increase. This last feature is intriguing and could be due to the influence of continental aerosols partly produced by the pine forest itself. From 0 to 100 km, the atmospheric inputs far exceed the weathering products of these quartz and feldspar sands.

Evapotranspiration of water within river basins leads to the concentration of solute by a factor equal to the rain/ runoff ratio. In the previous example of Landes streams (Figure 4.1), the NaCl pattern mimics the Cl^- double exponential decrease observed in rainfall with a stream/rain concentration factor of 3:1 similar to the rain/runoff ratio. In New Zealand, the stream/rain ratio for Cl^- is (47.5 mg/l)/ (3.9 mg/l), close to the rain/runoff ratio of 10 (Claridge, 1973). Where waters are concentrated through evapotranspiration, the $CaCO_3$ saturation limit may be reached; and only the Ca^{2+}—SO_4^{2-} or Na^+—Cl^- are left in these saline rivers (TZ^+ > 10 meq/l), which are generally not perennial.

Rainfall pattern is a major factor in mechanical erosion and TSS transport. Where annual rainfall is distributed during a few rainstorm events (arid regions) or during a short intense rainy period (wet subtropics), the TSS levels found in rivers are the highest, as in the southwestern United States or in monsoonal southeastern Asia.

TABLE 4.2 Chemical Composition of River Suspended Matter (wt.%)[a]

	IL (1000°C)									
	SiO_2	Al_2O_3	Fe_2O_3	MnO	MgO	CaO	Na_2O	K_2O	TiO_2	
A. Influence of lithology										
Migmatite	81.5	9.22	1.82	0.03	0.51	trace	0.96	2.82	0.55	2.09
Basalt	62.2	14.8	7.53	0.17	2.87	4.97	3.01	2.34	1.96	0.0
Limestone	45.2	6.67	2.49	0.04	1.42	24.9	0.35	1.07	0.34	17.8
B. Influence of climate and geology[b]										
Tropical and arid zone	56.5	21.5	8.8	0.11	1.6	1.05	0.69	2.19	1.2	
Cold and temperate zone	60.6	14.2	6.65	0.14	2.1	4.4	1.1	2.75	0.8	
Huang He	57.8	15.1	4.57	0.10	2.17	8.4	1.2	(2.5)	0.66	

Note: The ignition loss (IL) accounts for CO_2 from particulate organic carbon and carbonate minerals.

[a] A Monolithologic French Streams, average altitude of watersheds is 1000 m.

[b] Average values based on about 10 major rivers each (Meybeck, 1988).
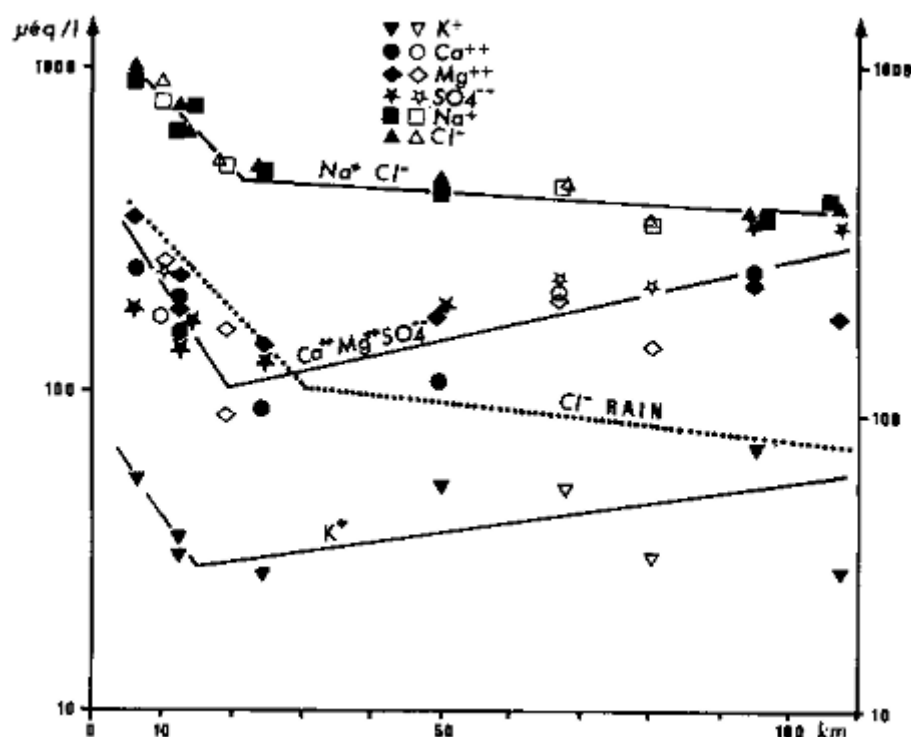
FIGURE 4.1 Evolution of stream water chemistry in the Landes forest (southwest France) as a function of the average distance of the watersheds from the ocean. The ocean and continental (forest origin?) aerosols that mask the chemical weathering of quartz and feldspars sands are evident from the exponential decrease of Na^+ and Cl^-.

Temperature influence on weathering is best evidenced for silica and for total cations (TZ^+) originating from crystalline rocks (Figure 4.2). This positive relation is probably due to the combined influence of feldspars dissolution kinetics and of higher bacterial activity in soil of the tropical belt. For carbonate rocks, an inverse relationship between temperature, Ca^{2+} and HCO_3^- has been observed (Harman *et al.,* 1975).

Contact between water and rock (water residence time, nature or contact) is an important factor. As a result, phreatic groundwaters are usually one to three times more mineralized than surface waters depending on the element considered (Table 4.1B).

Geomorphologic features control both TSS and dissolved organic carbon (DOC). In similar climatic types with identical dominant vegetation, those river basins with a greater proportion of wetlands (peat bogs, swamps, etc.) have much higher DOC levels. In the well-drained Mamai basin, New Zealand, the average DOC is 4.5 mg/l compared to 43.5 mg/l for the proximate Larry basin draining a peat bog (Moore, 1987). Although much less documented, the geomorphologic influence on nitrogen and phosphorous levels and transport rates by rivers is likely. Relief pattern, particularly the slope distribution, is a key factor in mechanical erosion: all mountain ranges are drained by rivers with high TSS levels (Milliman and Meade, 1983).

Vegetation influence on river chemistry is still poorly known, except for the well-known nutrient increase in waters after a forest fire. Concerning TSS, the vegetal cover is one of the four major controlling factors in mechanical erosion, along with bedrock, slopes, and rainfall pattern: unprotected bare soils are sensitive to rainsplash impact, and developed root system lower mass wasting and subsequent erosion.

Past geological history in a river basin is seldom considered although post glacial features may affect chemical and physical weathering in many ways. Glacial deposits in those mountain previously glaciated (Alps, Rockies, Himalayas) are still an important source, if not the major one, of river particulates. The Quaternary eolian loess deposits are a peculiar case: they form the major TSS source of the Huang He River, the most turbid river (TSS average > 20 g/l, about 6 percent of the present global TSS input to oceans). Past geological events may also limit chemical weathering: (1) when former glacial abrasion has left only bare rock, as in Canadian and Scandinavian Shields, the chemical weathering is limited; (2) in lowland regions exposed to erosion for millions of years, as is common in Africa, the resulting soil layer extends over meters or more and is highly depleted in soluble elements and the subsequent chemical erosion is limited. When these important soil layers have developed, the river TSS is generally low and enriched in the less soluble elements (Al, Fe, Ti, Mn), whereas Ca, Mg, and Na are strongly depleted; Si and K are generally similar to parent rock. The average TSS composition of active mountain ranges is close to the average shale (Table 4.2B). The Huang He TSS has a loess composition.
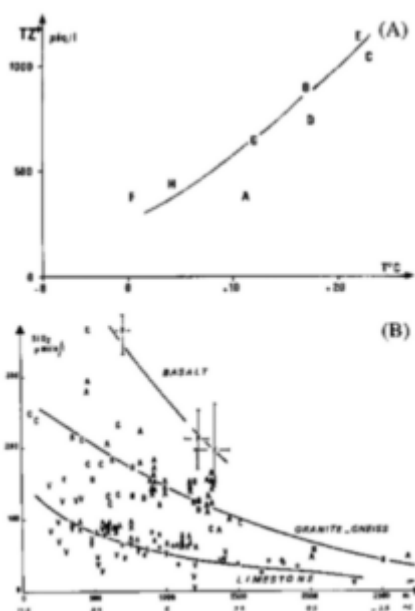
FIGURE 4.2 Influence of temperature on stream and river chemistry (monolithologic basins). (A) Total cations (TZ^+) in volcanic basins. Columbia River tributaries. A (Santos, 1965); Kenyan rivers, B; Java rivers, C (Kobayashi *et al.*, 1974); La Reunion rivers, D; Uganda rivers, E (Viner, 1975); Icelandic rivers, F; Japan rivers, G (Kobayashi, 1960); French Streams, H (Meybeck, 1986). (B) Dissolved silica in French monolithologic streams at various altitudes (Meybeck, 1986). Three sets of watersheds: basalts, gneiss and granite, limestone.

Lake retention of calcite, nutrients (organic C, N, P, Si), and of TSS may greatly affect river chemistry. In many hard-water lakes, calcite precipitates during the planktonic production period, when pH increases. In such systems, 25 to 40 percent of Ca^{2+} and HCO_3 may be retained. The biological uptake of nutrients decrease NO_3^-, PO_4^{3-}, and dissolved SiO_2 at lake outlets. In alpine French lakes, 40 to 80 percent of dissolved silica inputs are stored in lake sediments. The settling rate of TSS in lakes commonly varies between 90 and 99 percent, and only the finest and most organic particles may escape the trap.

Tectonic and volcanic controls on river chemistry and transport rates are multiple. Active volcanism, an event barely studied, is probably important on a long-term scale as a primary source of ions (Ca^{2+}, Na^+, SO_4^{2-}, F^-, Cl^-, NH_4^+, etc.) and of TSS, which do not originate from the recycling of sedimentary material, the major source of river material. Uplift rates are probably a key factor in long-term river transport, as Stallard (1988) described for the humid tropics: in the South American Shield (uplift rates of 10 to 20 mm/1000 yr) and in tectonically active environments such as Taiwan (rates of 10^3 to 10^4 mm/1000 yr), the erosion rates are of the same order of magnitude or slightly lower than the uplift rates. Other environmental factors rarely encountered may also influence river chemistry, for example, hydrothermal springs.

Globally, the control of water chemistry—mainly by thermodynamic equilibrium at the mineral scale (Garrels and Christ, 1965)—is much more complex than sometimes indicated (Gibbs, 1970) when streams and rivers are considered. Total suspended solids are also regulated by numerous factors that prevent any simple correlation between TSS levels or TSS transport rate (Ts, in $t/km^2/yr$) with runoff, temperature, relief, etc. (Walling and Kleo, 1979; Walling and Webb, 1983). A multiple regression approach is needed, as proposed by Janssen and Painter (1974), under the condition that river basin size is taken into consideration, because the amount of particulate matter transported downstream by a river is only a small part, the sediment delivery ratio, of the material produced by upland erosion (Walling and Kleo, 1979).

DISTRIBUTION OF RIVER WATER QUALITY

The distribution of ions, silica, organic carbon, and TSS in world river systems depends on the relative importance of the environmental factors mentioned and on the basin size. Because of the great diversity of environments, particularly of surface rock types, found on the scale of streams and small rivers (area << 1000 km^2), their water chemistry can vary considerably: from two (DOC and SiO_2) to four (Na^+ and H^+) orders of magnitude, depending on the element considered. In major rivers (area > 10^5 or 10^6 km^2), the effect of extreme environments, such as evaporite outcrops, loess deposits, or peat bogs, is highly diluted by the influence of more common environments such as crystalline rock outcrops and well-drained systems. In these major systems, the water quality is more unified and ranges of concentrations are one order of magnitude less than for small streams. This evolution is illustrated on Figure 4.3 for dispersion of major cation sum (TZ^+) as a function of basin size.

In given river systems, the statistical distributions of ions and silica clearly reflect the prevailing regional conditions and the occurrence of some rare environments. Five regional distributions have been set up for medium-sized

rivers, for the arctic and subarctic Mackenzie river watershed (data from Reeder *et al.,* 1972), for the Lower and Central Amazon basin (Stallard, 1980), for the Andean tributaries of the Amazon (Stallard, 1980), and for the rivers of Japan and Thailand (Kobayashi, 1959, 1960). A global distribution is also considered based on 50 major world rivers (distribution weighted by water discharge, data from Meybeck, 1979). Three distributions for small streams are given: (1) a set of 250 monolithologic pristine French Streams located 20 to 600 km from the coastline (Meybeck, 1986); (2) a set of 75 monolithologic streams (Miscellaneous Streams) from various literature sources (chosen to be representative of global rock types) and grossly corrected for oceanic aerosol influence; (3) a set of pristine streams, the Temperate Stream Model, derived from set 1 after systematic correction of atmospheric inputs and selected as representative of the global distribution of rock types (Meybeck, 1987). The distribution of some ions and silica is given for these small, medium, and large rivers on Figure 4.4 and Table 4.3.
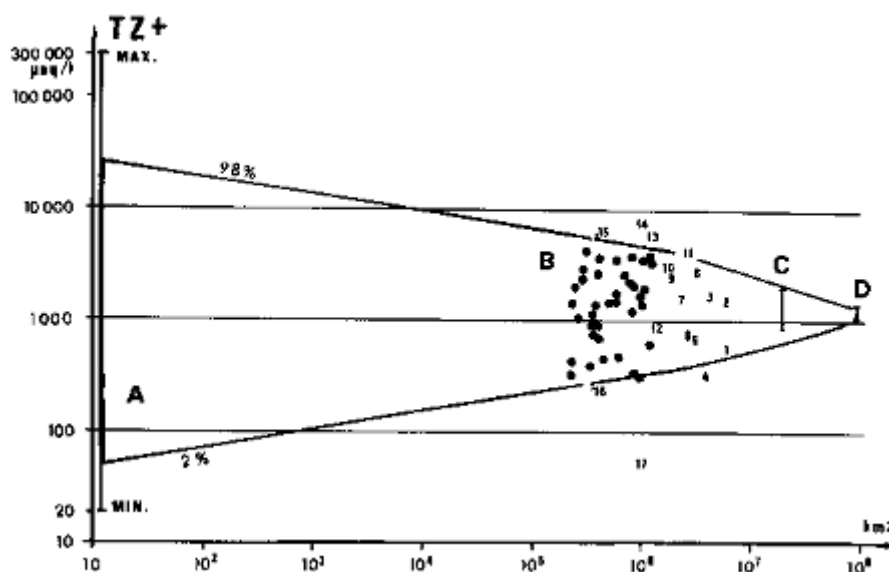
FIGURE 4.3 Range of total cations (TZ^+) in streams and rivers as a function of basin size. (A) Distribution observed for small monolithologic watersheds from France and other regions, worldwide (Meybeck, 1986, 1987). (B) Distribution for major world rivers (Meybeck, 1979); 1 = Amazon, 2 = Ob + Yenissei, 3 = Lena + Kolyma + Indigirka, 4 = Zaire, 5 = Amur, 6 = Parana, 7 = White Nile, 8 = Mississippi, 9 = Chiang Jiang, 10 = Mackenzie, 11 = Volga, 12 = Zambezi, 13 = Murray, 14 = Texas, 15 = rivers in Spain and Portugal, 16 = North West Territories, 17 = Rio Negro (Brazil). (C) Range for the global watersheds of the four oceans. (D) World mean.

The K^+ distribution (Figure 4.4A) can be considered as unimodal and log-normal. Potassium originates mainly from a few aluminosilicate minerals that weather at comparable rates. For the Temperate Stream Modal, K^+ is much lower, due to an overcorrection of atmospheric inputs. Other distributions are similar, median values are within a factor of two and distributions are parallel, except for Thailand rivers for unknown reasons. The sample of major rivers is similar to the French Streams and Miscellaneous Streams, which indicates that the data used are still largely unaffected by pollution.

The dissolved silica pattern (Figure 4.4B) is similar to that of K^+, which confirms a common origin. A major discrepancy is noted for the Mackenzie tributaries for which the SiO_2 level is about half that in other regions and has a significant drop in the lower decile value. This is most probably due to the SiO_2 uptake in numerous lakes of this basin, whereas K^+ is not used by freshwater plants. As a result, the K^-/SiO_2 ratio of medians is 0.36 in the Mackenzie, compared to 0.04 to 0.07 for other pristine waters (Meybeck, 1987).

Bicarbonate distribution (Figure 4.4C) is usually bimodal. The first mode corresponds to the soil and atmospheric CO_2 used in the weathering of noncarbonate rock (Garrels and Mackenzie, 1971), the second to the weathering of carbonate rocks, in which only 50 percent originate from calcite or dolomite. Concentrations related to the second mode are generally 5 to 10 times greater than those of the first one. In large basins where carbonate rocks are absent, as in Central and Lower Amazonia, the distribution is unimodal. In sedimentary regions, the HCO_3^- distribution shows an upper limit near 6 meq/l that corresponds to the $CaCO_3$ saturation.

Sodium distribution (Figure 4.4D) is also complex, due to a triple source: weathering of aluminosilicate mineral, weathering of rock salt, and inputs of oceanic aerosols. The Central and Lower Amazon tributaries have an unimodal Na^+ distribution reflecting the first source only. The influence of oceanic aerosols is well illustrated by Japanese rivers; the minimum Na^+ values are much higher than those of the Amazon tributaries. Rock salt dissolution leads to the very high values, from 0.5 to 10 meq/l, noted for the Mackenzie tributaries, Andean rivers, French Streams, and Miscellaneous Streams.

The percentiles values of distributions are presented on Table 4.3A for small streams (French streams and literature

survey) and for the major rivers (discharge weighted distribution). If the 98 percent/2 percent ratio is taken as an index of the natural variability of water chemistry, the most variable elements in small streams are (in order of decreasing variability):
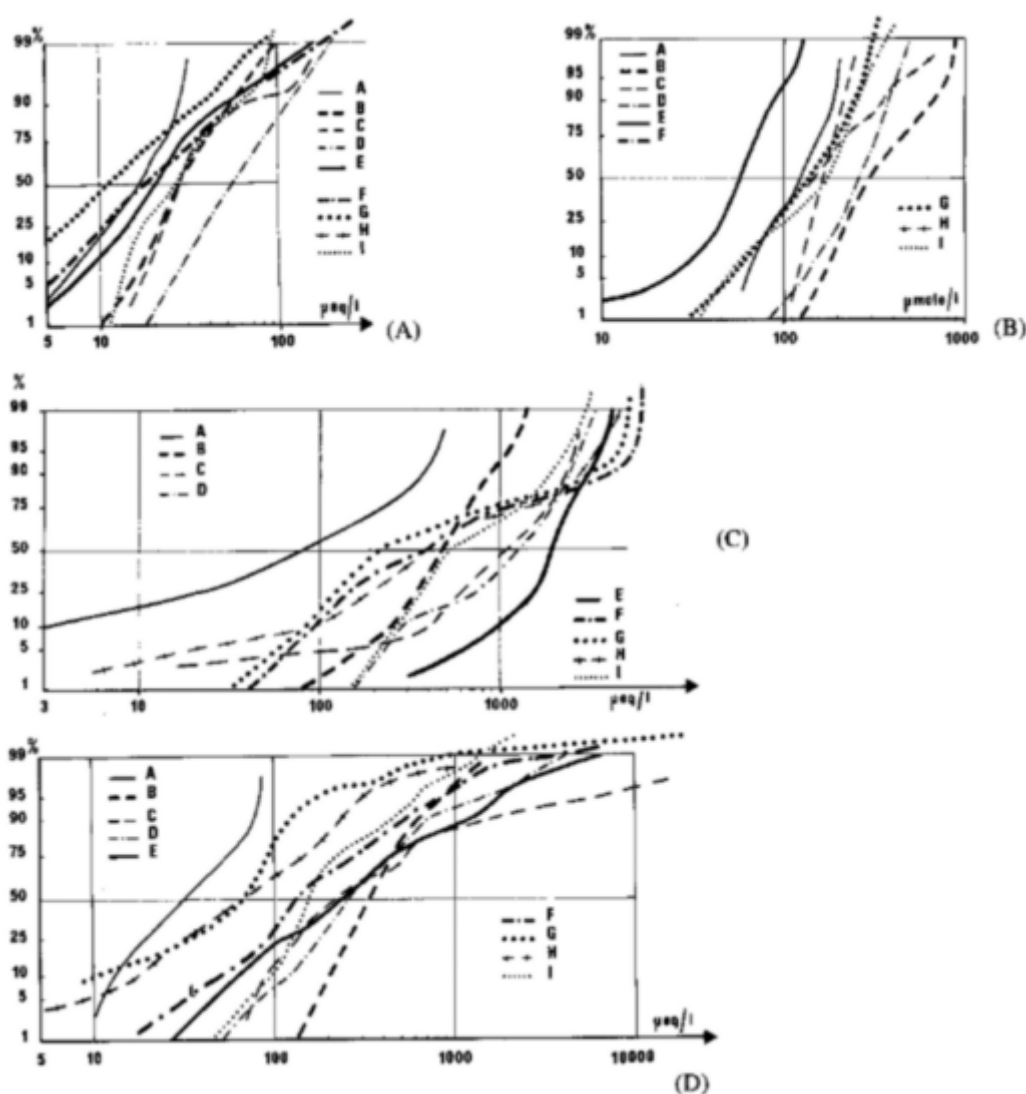
FIGURE 4.4 Cumulative distributions of major dissolved elements [(A) potassium, (B) silica, (C) bicarbonate, and (D) sodium] in rivers from selected regions: Central and Lower Amazon, A ($n = 40$. data from Stallard, 1980); Japan, B ($n = 225$, from Kobayashi, 1959); Andean tributaries of the Amazon, C ($n = 42$, from Stallard, 1980); Thailand, D ($n = 31$, from Kobayashi, 1960); Mackenzie, E ($n = 100$. from Reeder *et al*., 1972); monolithologic French Streams, F ($n = 250$, from Meybeck, 1986); Temperate Stream Model, G (Meybeck, 1987); monolithologic Miscellaneous Streams, H ($n = 75$, from various sources); major world rivers, I ($n = 60$, from Meybeck, 1979).

$$H^+ = HCO_3^- > TSS > Cl^- = Na^+ = SO_4^{2-} > Ca^{2+} > Mg^{2+} \gg SiO_2 = DOC > K^+.$$
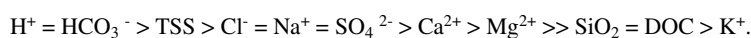
For major rivers, this order is somewhat different:

$$TSS > Cl^- > Ca^{2+} = SO_4^{2-} > Na^+ = HCO_3 = Mg^{2+} > PO_4^{3-} = NH_4^+ > SiO_2 > NO_3^-.$$
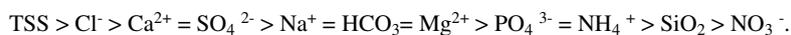
The great variability of H^+ and HCO_3^- in streams is due to the occurrence of the acidic Black Waters of the Amazon and Orinoco basins (Stallard, 1980, 1988). In major rivers,

the pH is commonly between 6.5 and 8.2. The TSS distribution presented in Table 4.3B is tentative because it is highly dependent on the sediment delivery ratio (SDR). Because SDR is a function of basin size, the TSS distribution is presented for three classes of basin area. Median TSS value and TSS range are both greatly reduced in major rivers.

TABLE 4.3 Statistical Distributions of Dissolved Concentrations, TSS, and of Rates of Total Dissolved Transport (Td) and Particulate Transport (Ts)

	M[a]	1%	10%	25%	50%	75%	90%	99%
A. Distribution of selected major ions (µeq/l)								
Small streams[b]								
K^+		3.3	7	11	19	30	60	170
Na^+		<3	19	32	70	140	220	[3]800
Ca^{2+}		10	40	100	210	800	2,100	5,500
Major rivers[c]								
K^+	33	12	15	19	27	40	65	100
Na^+	225	50	95	125	160	250	520	1,600
Ca^{2+}	670	90	160	250	400	900	1,500	2,700
B. Transport rates of major rivers (t/km^2/yr)[d]								
T_d	40	<2	6.0	14	27	45	64	160
Ts	175	3.2	6.4	10	45	100	500	1,900
T_d/Ts	4.4	<0.1	0.3	0.5	1.3	4	8	50
C. Total suspended solids (TTS) (g/l)								
Streams[e]			40		700		6,000	
Medium-sized rivers[f]			70		600		4,500	
Major rivers[g]								
M = 415			40		180		1,000	

[a] M is equal to discharge weighted natural content (DWNC, Meybeck and Helmer, 1989)

[b] Based on a set of 75 Monolithologic basins, chosen to be representative of global lithology distribution, corrected fromocean atmospheric inputs.

[c] Based on a set of 60 major rivers (Meybeck, 1979), distribution weighted by water discharges.

[d] Same source as footnotes c (Meybeck, 1976, 1979), distribution weighted by drainage area. *Ts* values prior to river damming.

[e] Area from 10 to 103 km^2., [f] area from 104 to 106 km^2., [g] area from 10^4 to 10^6 km^2. From a set of 128 world rivers (Fournier, 1969).

The chemistry of streams and small rivers in very different environments is highly variable (Stallard, 1980; Meybeck, 1986) and more than 15 different water types and subtypes have been observed (Ca^{2+}— HCO_3^-, Ca^{2+}—SO_4^{2-}, Mg^{2+}—HCO_3^-, Mg^{2+}—SO_4^{2-}, Na^+—HCO_3^-, Na^+ —SO_4^{2-}, Na^+—Cl^-, etc.).

The chemical types of major river waters are much less variable than for small basins. When the water discharge to oceans is taken into account, the Ca^{2+}—HCO_3^- type of water is largely dominant, about 97.3 percent (46.7 percent for the $Ca^{2+} > Mg^{2+} > Na^+ > K^+$ and $HCO_3^- > SO_4^{2-} > Cl^-$ subtypes; 33.1 percent for the $Ca^{2+} > Na^+ > Mg^{2+} > K^+$ and $HCO_3^- > Cl^- > SO_4^2$ subtypes; and 17.5 percent for other Ca^{2+}—HCO_3^- subtypes). Other major types are Ca^{2+}—SO_4^{2-}, about 1 percent, and Na^+—HCO_3^-, about 1.4 percent.

CONTROL AND DISTRIBUTION OF RIVERINE TRANSPORT RATES

Transport rates (t/km^2/yr) of individual elements i (T_{di}), of total dissolved solids (T_d, sum of major ions and dissolved silica rates), and of total suspended solids (T_s) are the products of discharge-weighted by annual mean concentrations C_d (mg/l), by annual river runoff q (mm/yr or l/s/km^2). Some major ions show an inverse correlation between C_{di} and q: $C_{di} = aq^b$ with $-1 \ll b \ll 0$. Most other water quality descriptors either are not directly correlated with q or present a positive correlation. Therefore, in a given homogeneous environment, where q is the only variable, all of the transport rates of any riverine material would be positively correlated with q. If the region is heterogeneous, the environmental factors (lithology, tem

parature, morphology, etc.) will scatter the T_{di} or T_s versus q relationships. Two examples of such scattering are presented in Figure 4.5 for the calcium transport rate ($T_d Ca^{2+}$) in major rivers, still controlled by the lithological nature of the watersheds, and for the dissolved silica transport rate ($T_d SiO_2$), still influenced by annual air temperature.

The plot of T_d versus T_s plot for major rivers is highly scattered, but when the biggest rivers are considered, the correlation is positive (Figure 4.6) and quite different from the one observed by Judson and Ritter (1964) for U.S. rivers. Maximum T_d and T_s are both observed for high mountain watersheds in humid climate due to high runoff, steep slopes, and occurrence of sedimentary rocks. Minimum T_d is noted in arid lowlands and in crystalline shields; minimum T_s is also noted in shields or in very flat sedimentary lowlands. When the T_s/T_d ratio is plotted against average runoff q (Figure 4.6B), the figure is much more complex than the inverse trends described by Langbein and Dawdy (1964) and Leopold *et al.* (1964) due to a major control by basin morphology. For specific elements, relationships may also be drawn between dissolved and particulate transport. Although this data base is much less documented than total transport rates, the correlation T_{di} versus T_{si} is also positive, except for organic carbon.

Global statistics of T_d, T_s, and T_s/Td for 60 major world rivers are presented in Table 4.3C. As ionic concentrations were weighted by river discharge (Table 4.3A), the transport rates presented here are weighted by the river drainage area. The total river sample corresponds to 45 to 65 percent of the nonglaciated continental exorheic area (99.9×10^6 km^2) and of the river water discharged to the oceans (37,400 km^3/yr; Baumgartner and Reichel, 1975). Because of the skewed distributions of T_s, the dissolved transport predominates in more than 40 percent of the exorheic area, whereas the global T_s/T_d ratio is about 4.

GLOBAL ORIGINS OF RIVERBORNE MATERIAL

An important part of the continental area (148.9×10^6 km^2) is not drained by rivers to the oceans: (1) 22.3 percent is drained toward the interior of continents, as the Caspian Sea of Lake Chad, which corresponds to a water discharge of 2000 km^3/yr (which ultimately evaporates)
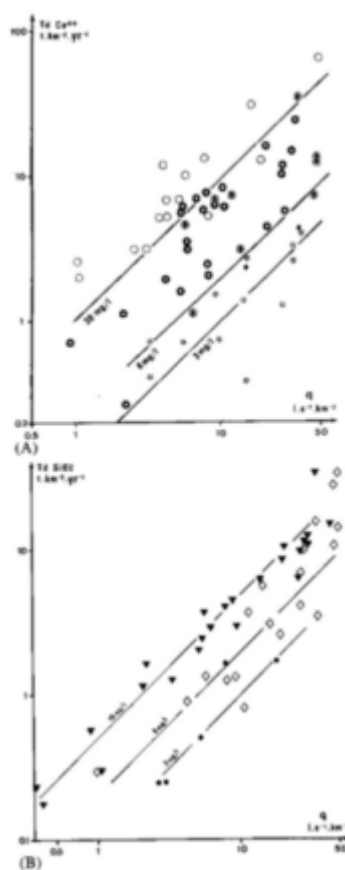
FIGURE 4.5 Evolution of annual dissolved transport rates of calcium and silica (T_d in t/km^2/yr) as a function of annual runoff (q in l/s/km^2) for major rivers. (A) Calcium transport is influenced by the watershed lithology (★ granite and gneiss basins: `; volcanic; ○ sedimentary). (B) Silica transport is influenced by average basin temperature (• cold regions; à temperate; ▼ tropical).

and (2) 10.5 percent is covered by ice caps, mostly Antarctica, which discharge about 2300 km^3/yr of ice to oceans (Baumgartner and Reichel, 1975).

What is the influence of environmental factors on riverine transport on a global scale? This question was raised a long time ago for dissolved materials. Erikson (1960) and Garrels and Mackenzie (1971) tried to estimate the relative contributions of atmospheric inputs and of the weathering of major rock types. The question was readdressed by Meybeck (1987) through consideration of the chemical composition of waters from small monolithologic watersheds and of the relative abundance of a dozen rock types at the continental surface. Atmospheric inputs were also reassessed (Meybeck, 1983). The breakdown of major ions, Sr^{2+}, and dissolved silica by rock weathering and atmospheric inputs is given in Table 4.4A. The influence of rare evaporitic outcrops (about 1.2 percent of the Earth's surface) on Ca^{2+}, Na^+, SO_4^{2-}, Cl^-, and Sr^{2+}
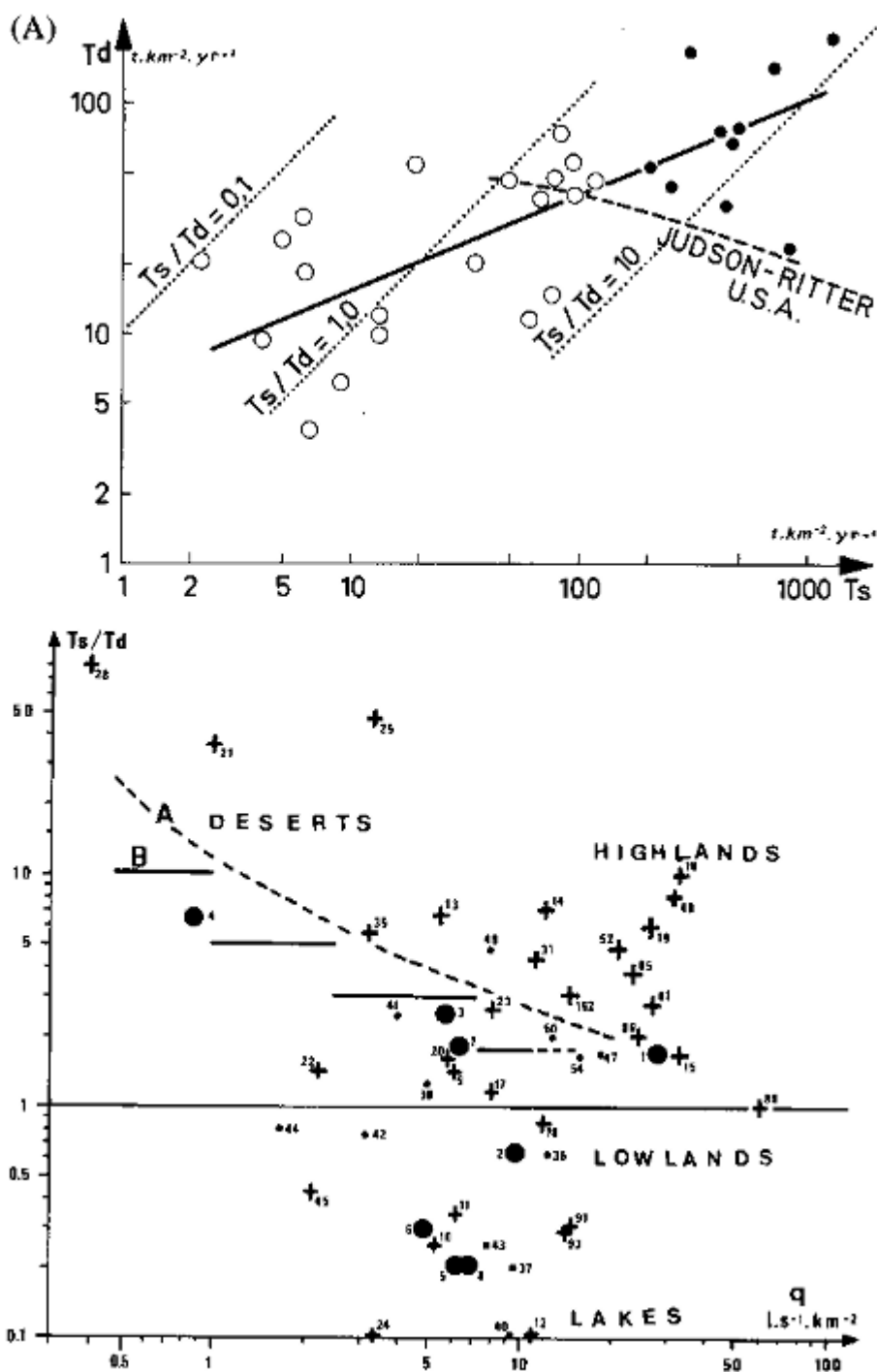
FIGURE 4.6 Global evolution of total dissolved (T_d) and particulate (T_s) transport rates of worldwide rivers. (A) Influence of basin relief on Td versus Ts relationship (• mountainous watersheds, ◯ others), compared to the Judson and Ritter (1964) variations for U.S. rivers. (B) Influence of basin morphology on the T_s/T_d ration versus runoff q compared to relationships from (A) Langbein and Dawdy (1964) and (B) Leopold et al. (1964). (• river basin > 2.4 x 10^6 km^2; + river basins from 0.5 x 10^6 km^2 to 2.4 x 10^6 km^2; ◯ other rivers).

budgets is evident. Although 62 percent of Ca^{2+} originate from carbonate rock weathering, 67 percent of HCO_3^- originates from soil and atmospheric CO_2.

TABLE 4.4 Origins of Global Riverborne Material (Exorheic Drainage)

A. Lithological Origins of Dissolved Matter (percent of total natural inputs)[a]

Rock Type	Area	SiO_2	Ca^{2+}	Na^+	Sr^{2+}	Cl^-	SO_4^{2-}	HCO_3^-
Atmospheric CO_2	—	—	—	—	—	—	—	67.2
Plutonic, metamorphic, and volcanic	33.5	36.1	6.3	12.9	14.3	0.0	8.7	0.0
Sandstones and shales	48.9	51.6	21.9	20.1	39.3	3.9	38.0	2.4
Carbonate rocks	16.3	11.3	62.0	2.5	18.6	0.0	8.2	28.9
Evaporites	1.3	0.6	9.4	35.5	27.8	49.2	40.2	1.5
Oceanic aerosols	—	0.0	0.4	29.0	29.0	46.9	4.9	—

B. Geographic Origins of Riverborne Material (percent of total input to oceans)[b]

Rock Type	Area	SiO_2	Ca^{2+}	Na^+	Sr^{2+}	Cl^-	SO_4^{2-}	HCO_3^-
Cold regions	23.4	14.7	5.4	15.5	17.5	2.7		
Temperate	22.4	27.5	19.9	39.9	28.5	56.5		
Tropical	37.0	57.2	73.6	41.8	52.0	34.2		
Arid	17.2	0.65	1.0	2.8	1.3	6.6		

[a] Meybeck (1987, 1988). Marble is included in carbonate rocks; area refers to the percentage of surficial rocks.

[b] Meybeck (1979, 1988). Total organic carbon (TOC) budget has been reviewed. The Huang He River is in the temperate Regions.

[c] Smis suspended matter.

The breakdown of river transport by geographic origins (Meybeck, 1979, 1982, 1988) is based on a typology of transport rates for a dozen morphoclimatic environments from tundra to mountainous wet tropics, defined by their average temperature (cold, temperate, desertic, tropical) and by their average runoff (five classes of runoff). It has been postulated that in these budgets, lithology is of secondary influence compared to runoff at scales on which these environments have been defined (10^6 to 10^7 km^2). The relative importance of the four main climatic environments is presented in Table 4.4B. Because of its major contribution to the water budget, the tropical zone is the major source of silica and organic carbon. Given their relative area and water discharge, temperate regions contribute 60 percent more than tropical regions to the ionic budget: the hypothesis of equal distribution of rock types in morphoclimatic environments is effectively limited; most limestone outcrops are in temperate regions (Balazs, 1977).

In considering the global TSS budget to the oceans, Milliman and Meade (1983) found that Southeast Asia alone (from the Huang He to the Indus, 12×10^6 km^2, islands included) is responsible for 35 percent of the global sediment discharge. Here, all major factors of high erosion rates (sedimentary rocks, volcanic ash in Indonesia, loess deposits in China, steep relief in Himalaya, monsoon climate) are combined with high sediment delivery ratio (steep slopes until river mouths in many cases). This rate (450 t/km^2/yr) is twice that observed for the combined temperate and tropical zones (230 t/km^2/yr).

When comparing the global riverine transport of major elements in dissolved and particulate states, the ratio of dissolved materials to total transport is highly variable, from 99 to 0.1 percent and the typical ranges are shown below:

90%	50%	10%	1%
Cl S, Na, C, Ca	Ng, N, K	P, Si, Mn	Ti, Fe, Al

Actually, these numbers may vary by nearly one order of magnitude, depending mainly on the amount of TSS. For example, the ratio of dissolved silica to total silica transport varies from 0.3 percent for regions of high mechanical erosion to 40 percent for lowlands.

CONCLUSIONS

The use of present-day river transport data for past geological times, particularly in ocean and climate modeling, should be undertaken cautiously. The following considerations need to be addressed:

- the area contributing effectively to the ocean budget (i.e., the nonglaciated nondesertic exorheic area) should be known accurately;
- the postglacial Quaternary period is peculiar and characterized by high sediment sources (fluvioglacial deposits, loess) and sinks (millions of lakes, floodplains) and moderate weathering rates;
- water runoff and detailed lithology distribution (limestone and evaporites) are two essential factors in river transport that can never be well known for the past; and
- the great variability of transport rates in today's rivers suggests that past global inputs to oceans of dissolved and particulate matter may well have varied by one order of magnitude within geologic evolution.
- the great variability of transport rates in today's rivers suggests that past global inputs to oceans of dissolved and particulate matter may well have varied by one order of magnitude within geologic evolution.

Human influence is now an important one (Meybeck and Helmer, 1989). In this chapter, it has been avoided as much as possible in order to understand natural processes. The river particulate loads measured these past 30 years may not reflect natural processes, even in regions less affected by agriculture: (1) the proportions of accelerated erosion and accelerated storage are unknown, and (2) the storage-transport processes now observed may not reflect those occurring at short, medium, and long geological scales (Meade, 1988).

For the dissolved elements, man is already a very effective geologic agent who increases sources (e.g., through mining, deforestation, atmospheric fixation of N) and sometimes sinks (e.g., reservoir building, eutrophication), thus already modifying major global cycles (Na, Cl, S, N, P, F, etc). Deciphering natural processes in the actual cycles will be increasingly more difficult.

ACKNOWLEDGMENTS

REFERENCES

Balazs, D. (1977). The geographical distribution of karst areas, Proceedings of the 7th International Congress on Speleology, Sheffield, 13-15 .

Baumgartner, A., and E. Reichel (1975). The World Water Balance, Elsevier, New York, 179 pp .

Berner, E.A., and R.A. Berner (1987). The Global Water Cycle, Geochemistry, and Environment, Prentice-Hall, Englewood Cliffs, N.J., 397 pp .

Berner, R.A., A.C. Lasaga, and R.M. Garrels (1983). The carbonate, silicate geochemical cycle and its effect on atmospheric carbon dioxide over the past million years, American Journal of Science 283, 641-683 .

Claridge, G.G.C. (1973). Studies on element balances in a small catchment at Taita, N.Z., in Studies and Reports in Hydrology 12 , Unesco Press, Paris, pp. 3245-3262 .

Davis, S.N. (1964). Silica in streams and groundwaters, American Journal of Science 262, 870-891 .

Drever, J.I. (1982). The Geochemistry of Natural Waters, Prentice-Hall, Englewood Cliffs, N.J., 388 pp .

Durum, W.H., G. Heidel, and L.J. Tison (1960). Worldwide runoff of dissolved solids, International Association of Hydrological Science 51, 618-628 .

Erikson, E. (1960). The yearly circulation of chloride and sulfur in nature: Meteorological, geochemical and pedological implications, Tellus 12, 63-109 .

Fournier, F. (1969). Transports solides effectues par les coursd'eau, International Association of Hydrological Science Bulletin 14(3), 7-49 .

Garrels, R.M., and C.L. Christ (1965). Solutions, Minerals, and Equilibria, Freeman Cooper, San Francisco, 450 pp .

Garrels, R.M., and F.T. Mackenzie (1971). Evolution of Sedimentary Rocks, W.W. Norton, New York, 397 pp .

Gibbs, R.J. (1970). Mechanism controlling world water chemistry, Science 170, 1088-1090 .

Gorham, E. (1961). Factors influencing the supply of major ions to inland waters with special reference to the atmosphere, Geological Society of America Bulletin 72, 795-840 .

Harman, R.S., W.B. White, J.J. Drake, and J.W. Hess (1975). Regional hydrochemistry of North American carbonate terrains, Water Resources Research 11(6), 963-967 .

Jansen, J.M.L., and R.B. Painter (1974). Predicting sediment yield from climate and topography, Journal of Hydrology 21, 371-380 .

Judson, S., and D.F. Ritter (1964). Rates of regional denudation in the United States, Journal of Geophysical Research 69(16), 3395-3401 .

Kempe, S. (1982). Long-term record of CO_2 pressure fluctuations in fresh water, Mitt. Geol. Paläont. Institut Hamburg 52, 91-332 .

Kobayashi, J. (1959). Chemical investigation on river waters of Southeastern Asiatic countries, Bericht Ohara Institut für Lanwirtschaft Biologie II(2), 167-223 .

Kobayashi, J. (1960). A chemical study of the average quality and characteristics of river water of Japan, Bericht Ohara Institut für Lanwirtschaft Biologie III(3), 313-357 .

Kobayashi, J., et al. (1974). Chemical Properties of River Waters in the Southeastern Asian Countries, Report to the Ministry of Education, 30 pp .

Langbein, W.B., and D.R. Dawdy (1964). Occurrence of dissolved solids in the surface waters in the United States, U.S. Geological Survey Professional Paper 501D, D115-D117 .

Leopold, L.B., M.G. Wolman, and J.P. Miller (1964). Fluvial Processes in Geomorphology, Freeman, San Francisco, 522 pp .

Livingstone, D.A. (1963). Chemical composition of rivers and lakes, U.S. Geological Survey Professional Paper 440G, G1-G64 .

Meade, R.H. (1988). Movement and storage of sediments in river systems, in Physical and Chemical Weathering in Geochemical Cycles, A. Lerman and M. Meybeck, eds., Kluwer, Dordrecht, pp. 165-179 .

Meybeck, M. (1979). Concentration des eaux fluviales en elements majeurs et apports en solution aux oceans, Rev. Geo. Dyn. Géogr. Phys. 21(3), 215-246 .

Meybeck, M. (1982). Carbon, nitrogen and phosphorus transport by world rivers, American Journal of Science 282, 401-450 .

Meybeck, M. (1983). Atmospheric inputs and river transport of dissolved substances, in Symposium on "Dissolved Loads of Rivers," International Association of Hydrological Science Publication 141, 173-192 .

Meybeck, M. (1984). Variabilité géographique de la composition chimique naturelle des eaux courantes, Verh. Int. Verein. Limnol. 22, 1766-1774 .

Meybeck, M. (1986). Composition chimique naturelle des ruisseaux non pollués en France, Sci. Geol. Bull. Strasbourg 39, 3-77 .

Meybeck, M. (1987). Global chemical weathering of surficial rocks estimated from river dissolved loads, American Journal of Science 287, 401-428 .

Meybeck, M. (1988). How to establish and use world budgets of river material, in Physical and Chemical Weathering in Geochemical Cycles, A. Lerman and M. Meybeck, eds., Kluwer, Dordrecht, pp. 247-272 .

Meybeck, M., and R. Helmer (1989). The quality of rivers: From pristine stage to global pollution, Palaeogeography, Palaeoclimatology, Palaeoecology 75, 283-309 .

Milliman, J.D., and R.H. Meade (1983). World-wide delivery of river sediment to the oceans, Journal of Geology 91, 1-21 .

Moore, T.M. (1987). Dissolved organic carbon in forested and cutover drainage basins, Westland, N.Z., International Association of Hydrological Science 167, 481-487 .

Reeder, S.W., B. Hitchon, and A.A. Levinson (1972). Hydrogeochemistry of the surface waters of the Mackenzie river drainage basin, Canada, I. Factors controlling inorganic composition, Geochimica et Cosmochimica Acta 36, 825-865 .

Santos, J.F. (1965). Quality of surface waters in the Lower Columbia river basin, U.S. Geological Survey Water Supply Paper 1784, 78 pp .

SCOPE Carbon Unit (1982, 1983, 1985, 1987). Transport of carbon and minerals in major world rivers, Mitt. Geol. Paläont. Institut Hamburg 52, 55, 58, 64 .

Stallard, R.F. (1980). Major Element Geochemistry in the Amazon River System , Ph.D. thesis, Woods Hole Oceanographic Institution, WHOI-80-29, 362 pp .

Stallard, R.F. (1988). Weathering and erosion in the humid tropics, in Physical and Chemical Weathering in Geochemical Cycles, A. Lerman and M. Meybeck, eds., Kluwer, Dordrecht, pp. 225-246 .

Stallard, R.F., and J.M. Edmond (1981). Geochemistry of the Amazon I. Precipitation chemistry and the marine contribution to the dissolved load at the time of peak discharge, Journal of Geophysical Research 86, 9844-9858 .

Stallard, R.F., and J.M. Edmond (1983). Geochemistry of the Amazon II, The influence of the geology and weathering environment on the dissolved load, Journal of Geophysical Research 88, 9671-9688 .

Stallard, R.F., and J.M. Edmond (1987). Geochemistry of the Amazon III, Weathering chemistry and limits to dissolved inputs, Journal of Geophysical Research 92, 8293-8302 .

Sugawara, K.T. Yoshihara, K. Yanagi, and M. Ambe (1982). A new chemical approach to the study of waters of Mt. Fuji environs, Archiv. Hydrobiol. 94, 269-285 .

Turekian, K.K. (1969). Oceans, streams, and atmosphere, in Handbook of Geochemistry, K.H. Wedepohl, ed., Springer-Verlag, Berlin, pp. 297-323 .

Viner, A.B. (1975). The supply of minerals to tropical rivers and lakes (Uganda), in Coupling of Land and Water Systems, A. D. Hasler, ed., Springer, New York, pp. 227-261 .

Walling, D.E., and A.H.A. Kleo (1979). Sediment yields of rivers in areas of low precipitation, International Association of Hydrological Science Publication 128, 479-493 .

Walling, D.E., and B.W. Webb (1983). The dissolved load of rivers: A global overview, International Association of Hydrological Science Publication 141, 3-20 .

Wilkinson, B.H., and J.C.G. Walker (1989). Phanerozoic cycling of sedimentary carbonates, American Journal of Science 289, 525-548 .

5

Geomorphic/Tectonic Control of Sediment Discharge to the Ocean: The Importance of Small Mountainous Rivers

JOHN D. MILLIMAN
Virginia Institute of Marine Studies
JAMES P. M. SYVITSKI
Bedford Institute of Oceanography

ABSTRACT

Analysis of data from 280 rivers discharging to the ocean indicates that sediment loads/ yields are log-linear function of basin area and maximum elevation of the river basin. Other factors controlling sediment discharge (e.g., climate, runoff) appear to have secondary importance. A notable exception is the influence of human activity, climate, and geology on the rivers draining southern Asia and Oceania. Sediment fluxes from small mountainous rivers, many of which discharge directly onto active margins (e.g., western South and North America a most high-standing oceanic islands), have been greatly underestimated in previous global sediment budgets, perhaps by as much as a factor of three. In contrast, sediment fluxes to the ocean from large rivers (nearly all of which discharge onto passive margins or marginal seas) have been overestimated, as some of the sediment load is subaerially sequestered in subsiding deltas. Before the proliferation of dam construction in the latter half of this century, rivers probably discharged about 20 billion tons of sediment annually to the ocean. Prior to widespread farming and deforestation (beginning 2000-2500 yr ago), however, sediment discharge probably was less than half the present level. Sediments discharged by small mountainous rivers are more likely to escape to the deep sea during high stands of sea level by virtue of a greater impact of episodic events (i.e., flash floods and earthquakes) on small drainage basins and because of the narrow shelves associated with active margins. The resulting delta/fan deposits can be distinctly different than the sedimentary deposits derived from larger rivers that discharge onto passive margins.

INTRODUCTION

Estimating the flux and fate of fluvial sediments discharged to the ocean has proved to be difficult, as rivers for which we have at least some data account for only about two-thirds of the land area draining into the ocean. Small rivers (drainage basins $<<10,000$ km^2) drain only about 20% of the land area, but they number in the many thousands (Figure 5.1) and, as will be seen in this paper, collectively they may contribute much more sediment than previously estimated. Previous attempts (e.g., Holeman, 1968; Milliman and Meade, 1983) assumed that global sediment flux could be calculated by extrapolating the yield of large and medium-sized rivers over large regions. By failing to take into account adequately smaller rivers, however, this assumption led to mistaken conclusions regarding seaward flux of fluvial sediment.

To predict the sediment load of a small river, we need to understand the interaction of numerous factors, including climate, precipitation (both average and peak), discharge (volume and velocity), basin geology, human impact, and the size of the drainage basin. Many workers have tried relating sediment load (or yield-load normalized for basin area) to net and/or gross precipitation, with varying results (see review by Walling and Webb, 1983). For small basins in the western United States, Langbein and Schumm (1958) showed that yields are high with low precipitation (where vegetation is too sparse to retard the erosive capacity of heavy rain and runoff), decrease in areas of medium precipitation, and then increase with higher levels of precipitation. A better relationship was seen between the annual variability of rainfall and sediment transport (Douglas, 1967), with basin relief also having an effect (Fournier, 1960). Other workers, however, have noted a variety of sediment transport trends relative to precipitation (e.g., Ahnert, 1970), leading Walling and Webb (1983, p. 84) to conclude that, "Current evidence concerning the relationship between climate and sediment yield emphasizes that no simple relationship exists."

In this paper we explore fluvial sediment discharge with respect to basin area and basin elevation. Both of these factors have been analyzed previously, but separately. For example, Ruxton and McDougall (1967) found that denudation rates in the Hydrographers Range (Papua New Guinea) are directly related to local relief. Pinet and Souriau (1988) found that the solid load of a river correlated well with mean basin elevation but not with environmental factors (such as rainfall). Potter (1978), Inman and Nordstrom (1971), and Audley-Charles *et al.* (1977, 1979) showed that large rivers (and their deltas) drain orogenic belts, but mostly discharge into intracratonic basins and trailing edge margins (see Dickinson, 1988, for a detailed review). These latter papers seem to have been overlooked by most geologists and oceanographers.

An inverse relationship between sediment yield and drainage basin area also has been noted (e.g., Schumm and Hadley, 1961), and Wilson (1973) suggested that sediment yield depends mainly on land use and basin area (not precipitation). Milliman and Meade (1983) reported that sediment yield increases by about seven-fold for every order of magnitude decrease in drainage basin area, but this correlation considered only rivers with sediment loads >15 million tons (mt)/yr, thereby excluding rivers with smaller sediment loads.
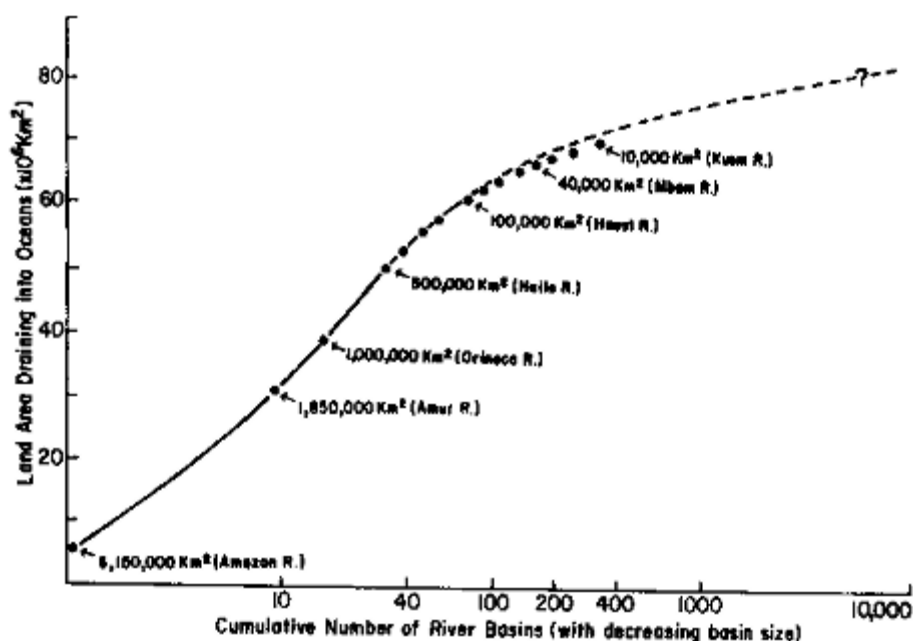
FIGURE 5.1 Cumulative drainage basin area of the world's 400 largest rivers with decreasing basin size. Data from Unesco (1978), this paper, and various IAHS publications. The largest river basin (Amazon) accounts for about 6 x 10^6 km^2 of the 90 x 10^6 km^2 land area (estimated by Milliman and Meade, 1983) draining into the oceans; the next nine largest rivers drain an additional 32 x 10^6 km^2 of land. (Numbers by the dots indicate the drainage basin area for that particular river.) The remaining 20 x 10^6 km^2 of the land surface are probably drained more than 10,000 small rivers.

RIVER DATA

We began by assuming that the topographic/tectonic character of a river basin plays the major role in determining its sediment load/yield, and that sediment yield was partly determined by basin area. Rather than using mean basin elevation as the topographic parameter, we used maximum headwater elevation, because in many rivers much of the sediment load comes from mountains where the river originates. The Amazon is a widely cited example, in which >80% of the sediment load is derived from the Andes, which constitute only about 10% of the river basin area (Gibbs, 1965; Meade *et al.,* 1985). Also, maximum elevations can be estimated quickly from a topographic map. Ahnert (1970) pointed out the strong correlation between local relief and denudation (see review by Summerfield, 1991), but such a calculation becomes difficult when dealing with the number and diversity of rivers cited here.

We subdivided river basins into five categories based on the maximum elevation within the hinterland: high mountain (headwaters at elevations >3000 m), mountain (1000-3000 m), highland (500-1000 m), lowland (100-500 m) and coastal plain (<<100 m). Based on a preliminary analysis of the yields, mountainous rivers, comprising the largest data set, were subdivided into three categories: Asia and Oceania (generally with very high sediment loads/yields); the high Arctic and non-alpine Europe (with low sediment loads/yields); and the rest of the world (i.e., North and South America, Africa, the Alps, and Asia Minor, Australia, etc.) Clearly this classification is not without problems. For example, in terms of relief, a small island with elevations of 800-900 m probably should be considered mountainous, not upland. Still, as seen in the following analysis, our elevation-based classification seems valid.

Geomorphologists and hydrologists often use the terms "yield," "sediment yield," or "specific yield" to compare sediment loads between disparate river basins by normalizing sediment load relative to size of the river basin ($t/km^2/yr$). Waythomas and Williams (1988) argue, however, that statistically the comparison of yield versus basin area can give spurious results, since area is common to both axes; they propose the comparison of sediment load and basin area instead. In this paper, data are presented in terms of both yield and load.

Our data base consists of the loads and yields for 280 rivers (Table 1, Milliman and Syvitski, 1992). Collectively these rivers account for $>62 \times 10^6 \ km^2$, or about two-thirds of the land surface draining into the ocean (Milliman and Meade, 1983). Basin sizes range from <200 km^2 to >6,000,000 km^2, and loads vary from <0.02 to >1000 mt/yr. Where discharge values are available, we have converted them to runoff (discharge/basin area). The data come from many sources and from a wide variety of techniques, and therefore the quality is variable. Moreover, many of the data are recycled: for example, some of the data used by Lisitzin (1972) are from Strakov (1961), some of which came from Lopatin (1950) and early IAHS/Unesco compilations.

Modern river sediment loads seldom represent natural loads. Sediment discharge changes as erosion levels change or sediment is stored (i.e., river diversion projects). With the exception of Arctic rivers, where human civilization has had minimal impact, most rivers reflect the results of human activity on the erosional capacity of the rivers, both through deforestation and poor soil conservation (see Milliman *et al.,* 1987) and urbanization (Meade, 1982). In contrast, the increased diversion and damming of many rivers has decreased sediment discharge dramatically. The Nile and Colorado deliver no sediment to the ocean, and many other rivers, such as the Mississippi, Zambesi, and Indus, have experienced markedly decreased sediment discharges in recent years. Sediment loads of other rivers have decreased because of other human activities; for example, present-day bed loads of some northeast Italian rivers are 1.5 to 20 times lower than they were in the early 1950s because of legal and illegal riverbed dredging (Idrosser, 1983; I.N. McCave written communication, 1991). Often these human impacts work in conflicting ways: dams on the Ganges have decreased sediment discharge, whereas increased erosion in the mountains of Nepal (from deforestation) has increased the load of the confluent Brahmaputra (Hossain, 1991). In this paper we cite sediment loads of rivers prior to river diversion (at least, where data are available). However, the values given in this paper still reflect increased soil erosion and thus probably are higher than they would be in natural conditions.

RESULTS

Plots of runoff versus basin area, load versus runoff, and load/yield versus basin area (Figure 5.2) show a variety of trends. Runoff decreases with increased basin area (Figure 5.2a), probably because larger river basins tend to include a greater proportion of "lowland," with reduced precipitation and increased evapotranspiration (D. Walling, written communication, 1991). Also, our data for smaller rivers are biased toward rivers with high runoff, as small rivers with low runoff are seldom gauged. With respect to sediment load versus runoff, we find the same random relationship noted by Walling and Webb (1985) for load versus precipitation (Figure 5.2b). In contrast, load/yield vary directly/indirectly with basin area, although the scatter is considerable (Figure 5.2c, d).

When we divide the rivers into the seven topographic categories, a number of trends show much better correlation.
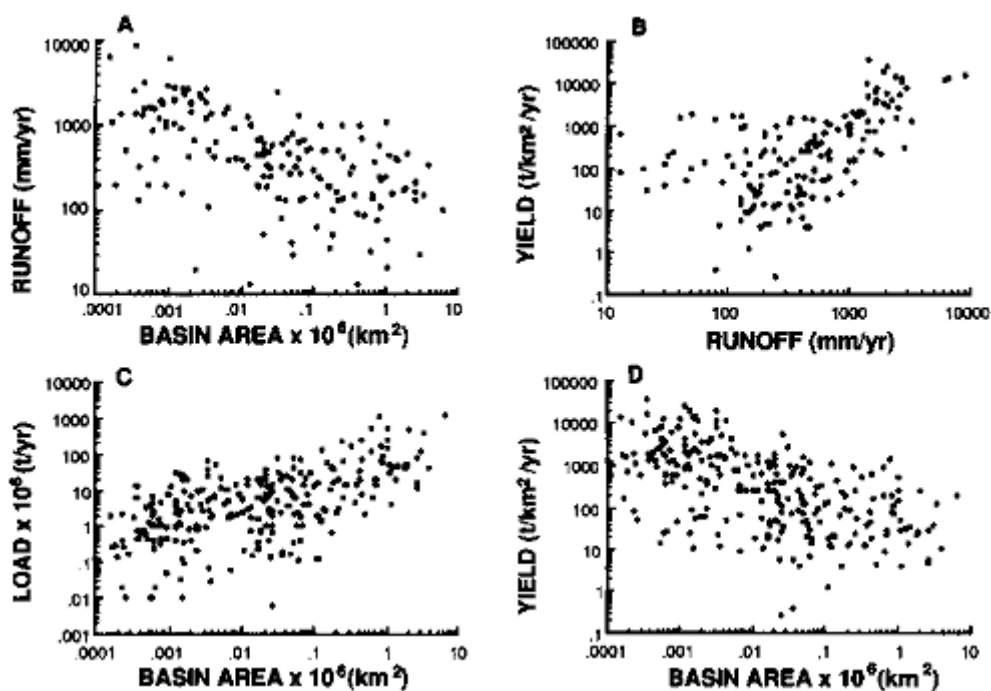
FIGURE 5.2 Runoff versus basin area (A); sediment yield Vs runoff (B); and load (C); and yield (D) versus basin area for the rivers listed in Table 2 (Milliman and Syvitski, 1992). Note the generally inverse relationship between runoff and yield with basin area the strongly positive correlation between load and basin area, and the great amount of scatter for yield versus runoff.

For example, the orographic control of precipitation can be seen from the fact that higher elevation rivers have greater maximum values of runoff versus basin area (Figure 5.3). The greater scatter of runoff with decreasing basin size reflects the influence of local climate (i.e., precipitation versus evaporation) in small basins. While the trends of sediment load/yield versus runoff vary with topography (Figure 5.4), the correlation coefficients (r^2) between load/yield and runoff within any topographic category are not meaningful (Table 2, Milliman and Syvitski, 1992).

Log-linear trends within our seven topographic categories were determined from best-fit regression analysis. In accordance with the well-accepted method for not allowing spurious data to influence the slope of the regression, points that fell more than one standard deviation from the determinant (y axis as load or yield) were plotted but not considered in determining the variance accounted for by the best-fit curve (Table 2, Milliman and Syvitski, 1992). Our philosophy was simple: we could not be sure of what errors were hidden within sediment load data, we assumed little error in the x-axis (drainage basin area), and we wished to discount as few data points as possible.

In Table 2 (Milliman and Syvitski, 1992), <10% of the rivers were discounted on the basis of having either load or yield values more than 1 standard deviation from the mean. In fact, deviations from the predicted norm often reflect either unique fluvial/drainage basin conditions or possible erroneous data bases; various examples are discussed below.

For load/yield versus basin area, the correlations with the various topographic categories are generally good, ranging from 0.70 to 0.82 (load versus area) and 0.62 to 0.89 (yield versus area) (Figures 5.5 and 5.6; see Table 2, Milliman and Syvitski, 1992). The relatively poor correlation coefficients ($r^2 = 0.81$ for load, but 0.32 for yield) for coastal plain rivers, however, suggest that basin area plays little or no role in determining sediment discharge from these low-lying rivers.

Mountainous rivers have greater loads and yields than do upland rivers, which in turn have greater loads and yields that lowland rivers (Figures 5.5 and 5.6), although there is some overlap in values. For example, mountainous rivers with basin areas of about 10,000 km² have sediment yields between 140 and 1700 t/km²/yr (e.g., Negro, Porong), whereas yields for similar-sized upland rivers are 60-250 (e.g., Sabin, Tone), and lowland rivers 20-60 (e.g., Cape Fear River). With the exception of two rivers (Waiapu and Niger), no upland, lowland or coastal plain river has a sediment load >20 mt, even though more than 25 upland and lowland rivers have drainage basin areas >100,000 km². In contrast, nearly 60 mountainous rivers have loads ≥20 mt (Table 1, Milliman and Syvitski, 1992). Mountainous rivers draining South Asia and Oceania

have much greater yields (2-3 fold) than rivers draining other mountainous areas of the world, and an order of magnitude greater than rivers draining high-Arctic and European mountains (Figure 5.5).

The trend of increasing sediment yield with decreasing size of mountainous rivers becomes less pronounced in river basins less than about 4000 km^2 in area, as seen by the relative number of rivers that fall >1 standard deviation from the mean (Table 1, Milliman and Syvitski, 1992). Some very small rivers in New Zealand and Taiwan, for example, have yields much lower than expected, while others have much higher yields; together they account for one-third of the deviating rivers designated in Table 1 (Milliman and Syvitski, 1992). Slaymaker (1987) noted a decreased sediment yield in rivers <1000 km in western Canada. This variance of sediment yield in very small river basins probably reflects the dominance of single types of geology or microclimate in small basins, whereas larger river basins are modulated by a greater range of conditions.

With the exception of the high Arctic, latitude does not appear important. Equatorial rivers (e.g., the Tana in Kenya) do not have significantly higher yields than rivers of similar size in higher latitudes e.g., the Susitna in Alaska). High-Arctic mountainous rivers whose headwaters rise in the Arctic (e.g., Colville, Babbage), however, have much lower yields than Arctic rivers whose headwaters are in lower latitudes (e.g., Copper, Yukon, MacKenzie). The reason is not clear, but it may be related to lower levels of precipitation and shorter periods during which the rivers can transport sediment (Milliman and Syvitski, unpublished data).

DISCHARGE OF SEDIMENT BY WORLD RIVERS

North America

Most rivers draining eastern North America are upland, lowland, or coastal plain rivers, with correspondingly low sediment loads. Much of the sediment leaving the contiguous United States and Canada comes from three large rivers—the Mississippi, MacKenzie, and Colorado (now dammed)—and smaller west coast rivers (e.g., Eel, Columbia, Fraser), most of which drain mountains. Large discharges of sediment also come from rivers draining western Canada and Alaska; the Susitna, Cooper, and Stekine rivers, for example, collectively drain an area <<4% that of the Mississippi, but discharge nearly a third as much sediment (Table 1, Milliman and Syvitski, 1992); the many other rivers along this coast also must contribute large amounts of sediment: the average thickness of Holocene sediment on the southeast Alaskan shelf is 55 m (Molnia *et al.,* 1978) and fjords into which many of these rivers discharge have Quaternary sediment thicknesses >500 m (Syvitski *et al.,* 1987).

South America

Eastern South America is drained by four major rivers (Magdalena, Orinoco, Amazon, Parana) all having their headwaters in the Andes Mountains. Collectively they drain more than half the continent (10 of 17 million km^2). In contrast, rivers draining the western Andes are less known, but collectively their sediment discharge may be of the same magnitude as the larger rivers draining eastward
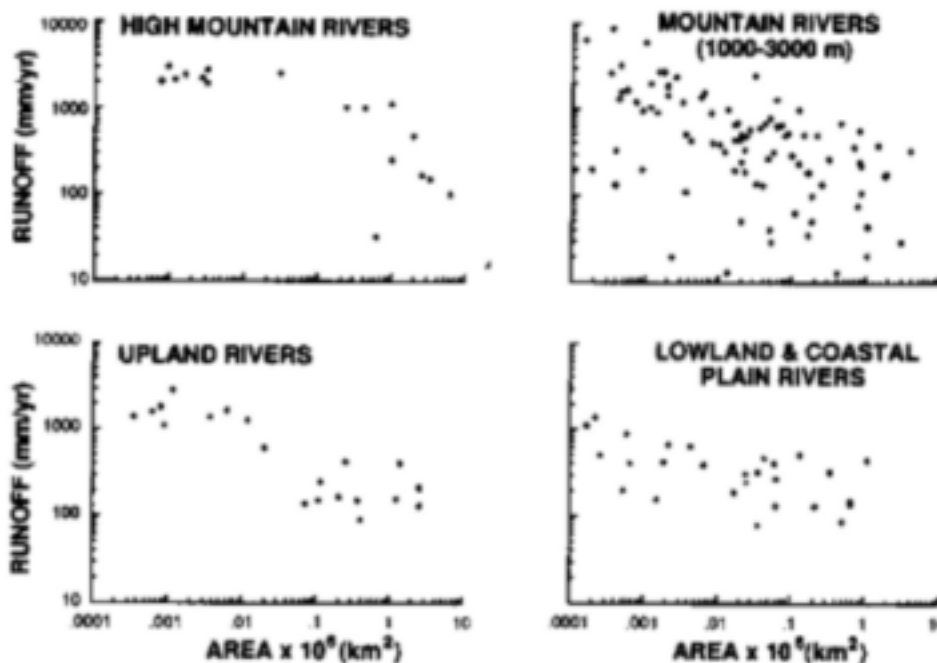
FIGURE 5.3 Variation of runoff versus basin area for rivers within four topographic categories. Note the decreasing maximum runoff values with increased river basin area and with lower elevations.

(smaller area but higher yields). If the average river draining the western sides of the mountains is 15,000 km^2, then the average sediment yield would be about 1200 t/km^2/yr (Figure 5.6c), equaling a sediment discharge of 2.4 bt/yr (1200 multiplied by an area of 2 x 10^6 km^2). This calculated sediment flux may be unrealistically high, as the arid parts of the western slope may contribute little sediment to the sea; nevertheless, the total sediment discharge from western South American rivers probably is much higher than the 168 mt estimated by Milliman and Meade (1983). At present we can cite only one west coast river, the Chira (Peru), and the data represent only two years of measurement, for one of which, however, the load was 75 mt (yield 3700 t/km^2, Burz, 1977).
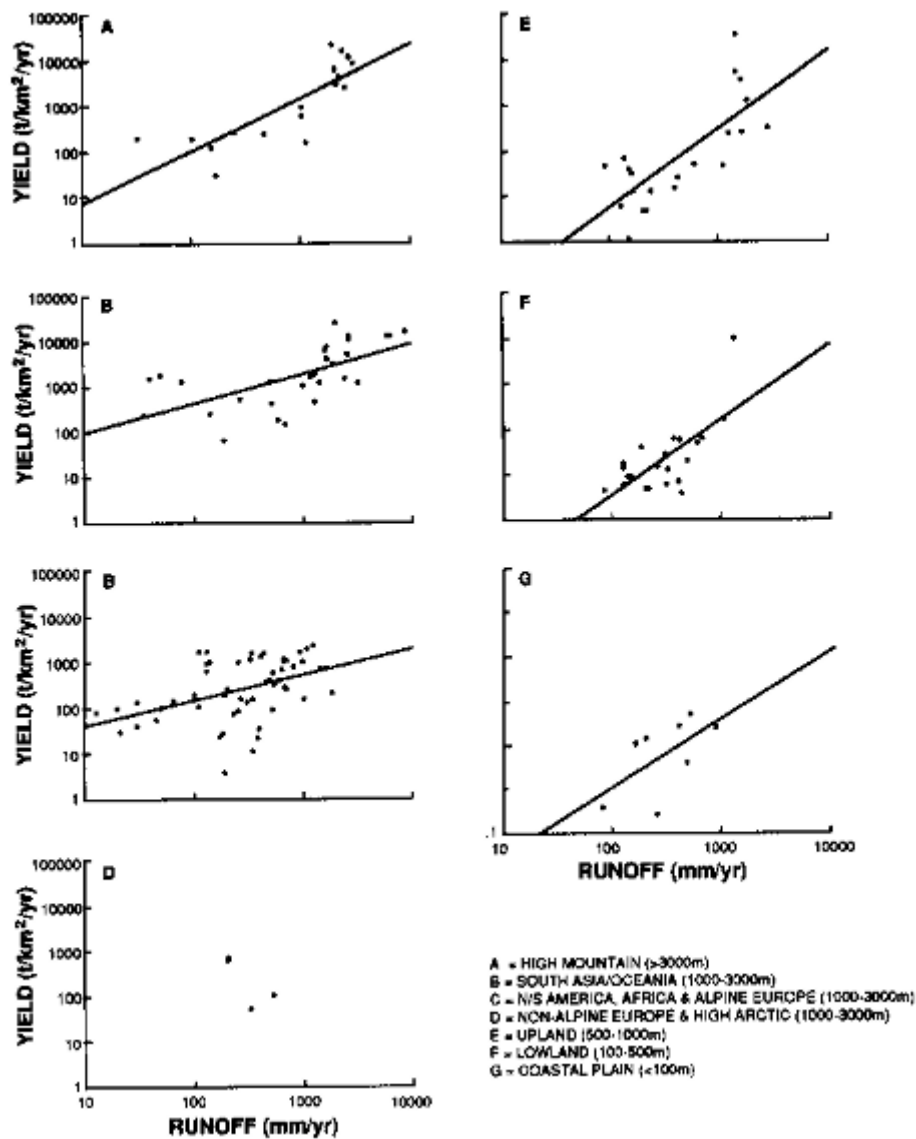
FIGURE 5.4 Relation of sediment yield and runoff for the seven topographic categories of river basins listed in Table 1 (Milliman and Syvitski, 1992). The equations for the slope plus the correlation coefficients are given in Table 2 (Milliman and Syvitski, 1992). In nearly all instances, the correlation coefficients are poor and the deviations from the trend are numerous.

Europe

Europe is generally regarded as having the lowest sediment flux to the sea (e.g., Holeman, 1968; Milliman and Meade, 1983). However, the Alps (a collision orogen) are a major sediment source, and the short rivers draining south into the Mediterranean have high to very high yields, generally 500 to >1000 t/km^2/yr (Table 2, Milliman and Syvitski, 1992). For example, the little known Semani River (Albania) has more than twice the annual discharge (22 mt) of the collective sediment discharges of the well-known north-flowing rivers Garonne, Loire, Seine, Rhine, Weser, Elbe, Oder, and Vistula, most of which drain upland or lowland terrain. Many rivers draining north from

the Alps are tributaries to the Danube, the largest river in Europe. The Rhine is the only large alpine river that drains north to the sea, but most of its sediment load is trapped in Lake Constance; upstream of Lake Constance, the river has a sediment yield consistent with other alpine rivers, but downstream of the lake, its yield is similar to a lowland/coastal plain river (Holeman, 1968).
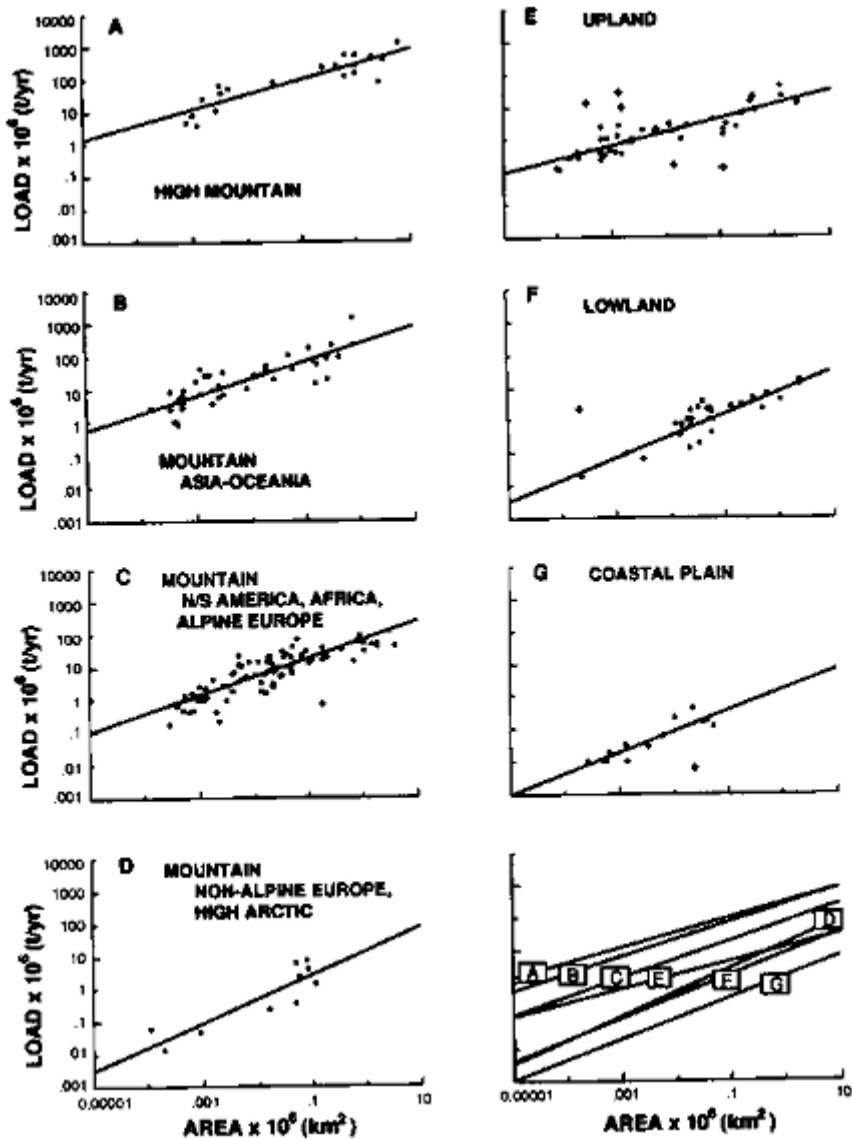
FIGURE 5.5 Variation of sediment load with basin area for the seven topographic categories of river basins listed in Table 1 (Milliman and Syvitski, 1992). For all river types the correlation is strong (r^2 ranging from 0.70 to 0.82). Note that only 13 rivers deviate by more than one standard deviation from the computed means.

USSR and Asia Minor

The large rivers of the former Soviet Union draining north to the Arctic Sea (Ob, Lena, and Yenesi) are generally considered to have anomalously low sediment yields (see Milliman and Meade, 1983). However, their sediment yields and those of other Russian rivers correlate well with other upland and lowland rivers throughout the world (Figure 5.6; Table 1, Milliman and Syvitski, 1992). Russian and Ukrainian rivers draining south into the Black Sea are considered lowland rivers, with correspondingly low sediment loads.

Although poorly documented in western literature, the rivers draining the Caucasus Mountains and the Anatolian and Taurus mountains in Turkey have high sediment yields, which is to be expected from rivers draining the same collision orogen as the Alps. Before dam construction in the 1950s, the three largest Turkish rivers emptying into the Black Sea discharged an estimated 50 mt of sediment annually (Hay, 1987). Collectively, in fact, the rivers draining northern Turkey and the western Caucasus Mountains may contribute more sediment to the Black Sea than the Danube and southwestern Russian and Ukranian rivers.

FIGURE 5.6 Variation of sediment yield with basin area for the seven topographic categories of river basins listed in Table 1 (Milliman and Syvitski, 1992). For all river types, except lowland and coastal plain rivers, the correlation is strong (r^2 ranging from 0.70 to 0.89).

Africa

Rivers draining Africa discharge a disproportionately small amount of sediment to the sea, although the discharge calculated by Milliman and Meade (1983) is probably low (Walling, 1985). At first it seems incongruous that Africa, one of the highest-standing continents (in terms of average elevation), has a low sediment flux. Only when viewed in terms of drainage basin morphology does the discharge pattern make sense; some large rivers with low loads (e.g., Senegal, Niger) are nonmountainous, and many small rivers in western Africa are lowland rivers, with correspondingly low sediment loads/yields. The major sediment discharge comes from rivers draining the rift mountains in eastern Africa (Nile, Zambesi, Limpopo, Rifiji) or rivers draining the mountains in Morocco, Algeria, and Tunisia (e.g., Mouloura, Sebou, Cheliff). The loads and yields of these rivers compare well with other mountainous rivers of similar size. The lack of rainfall throughout most of central Africa contributes to the low discharge rates (Walling, 1985).

Asia and Oceania

With notable exceptions of the loess-imparted Yellow River basin, the high sediment yield in Asia is restricted to rivers draining the Himalayan Mountains in southern Asia. These loads and yields are substantially higher than all other mountainous rivers of the world (save Oceania). Rivers draining eastern Asia have normal (Korea) or low (Japan) sediment loads relative to other mountainous rivers; dams in Japan may be important in these values. The

Chao Phya has a much smaller load (11 mt) and yield (68 t/km^2/yr) than other south Asian rivers of similar size; one wonders if the river basin has anomalous erosion patterns or if the data are erroneous.

Milliman and Meade (1983) used data from Taiwan and New Zealand to suggest that rivers draining the high-standing islands between Australia and Asia have unusually high sediment yields. Assuming a sediment yield of 1000 t/km^2/yr, they calculated that these high-standing islands may account for 20% of the global sediment flux to the oceans. In fact, new data from New Guinea, the Philippines, Java, New Zealand, and Taiwan (Table 1, Milliman and Syvitski, 1992) suggest average yields closer to 3000.

Australia

While Australia is nearly as large in area (2.2 x 10^6 km^2) as the islands in Oceania, the continent is generally low standing. Only rivers draining mountainous areas in the north (e.g., Ord) and east (e.g., Murray) appear to have high loads. The fact that much of Australia has an arid climate accentuates the low discharge from rivers, although the yields from the Ord, Murray, and Burdekin compare favorably with other rivers of similar size (Table 1, Milliman and Syvitski, 1992).

IMPLICATIONS

Factors Controlling Sediment Discharge

The data presented in Tables 1 and 2 (Milliman and Syvitski, 1992) and Figures 5.5 and 5.6 clearly show the importance of basin size and topography in terms of sediment discharge. Because sediment yields are strongly dependent upon the size of the drainage basin, they cannot be portrayed accurately on a map; global displays of sediment yields (e.g., Milliman and Meade, 1983; Walling, 1987) essentially reflect topography (as well as basin size)—high yields equate to mountainous areas, low yields to lowlands.

While many of our data need to be re-evaluated and updated, we suggest that topography and basin area have order-of-magnitude control over sediment discharge of most rivers. In contrast, average net precipitation and runoff generally affect sediment discharge to a lesser extent. For example, the Orange, Sous, and Isser rivers, which drain arid basins, have similar or slightly lower sediment yields than mountainous rivers with moderate rainfall, whereas rivers draining areas with very heavy precipitation (e.g., Solo, Purari, Cooper) have slightly higher yields (see Table 1, Milliman and Syvitski, 1992).

The role of sediment erodability (mainly a function of geology, vegetation cover, and human activity) clearly cannot be discounted. High erosion rates throughout much of southern Asia partly reflect poor soil conservation, the result of deforestation and over-farming. Milliman *et al.* (1987) concluded that the Huanghe's sediment load was an order of magnitude lower before humans began farming the loess hills of northern China. (Saunders and Young [1983] suggested that moderate land use can increase sediment yield by a factor of 2-3, while intensive land use can increase it an order of magnitude.) In contrast, the anomalously low sediment yields of northern European and English rivers at least partly reflect river channel management (see Petts *et al.,* 1989) combined with extensive vegetation cover and relatively low soil erodibility (D. Walling, 1991 written communication). The Oder, for example, has the lowest yield (1.2) of any river cited in this paper.

We should emphasize that elevation or relief is, in some ways at least, only a surrogate variable for tectonism. This paper and others (e.g., Hay *et al.,* 1989) that have emphasized the correlation between topography and sediment yield, relief or elevation is used because it is easily expressed numerically and therefore can be manipulated as a statistical variable. However, the strong correlation between sediment and topographic relief may not indicate that the second is the cause of the first, but rather that both are caused by another factor less susceptible to numerical description—namely, tectonism. It is probably the entire tectonic milieu of fractured and brecciated rocks, oversteepened slopes, seismic and volcanic activity, rather than simple elevation/relief, that promotes the large sediment yields from active orogenic belts.

What Is the Sediment Flux to the Sea?

This question really has two parts: how much sediment is carried by rivers, and how much escapes the present-day land/estuarine environment? The answer to both is more or less the same—we don't know. The sediment discharged, however, may be more than previously estimated. Milliman and Meade (1983) calculated an annual global discharge of 13.5 bt by extrapolating average sediment yields for documented rivers over large regions with similar topography. However, since the data used by Milliman and Meade came mostly from large rivers, the yields were necessarily lower than if they also had included smaller rivers. In addition, constrained by the lack of data, Milliman and Meade conservatively estimated the yields for mountainous coastal rivers to be 1000 t/km^2/yr. The new data presented in this paper suggest that the yields for rivers draining Oceania are probably ≥3000/km^2/yr, meaning that the high-standing islands of Oceania (approximate area of 3 x 10^6 km^2) may be closer to 9 bt than the 3 bt estimated

by Milliman and Meade. Similar percentage increases might hold for southeastern Alaska, western South America, the southern Alps-Caucasus orogen, and NW Africa (e.g., Walling, 1985).

There is another way to calculate the flux: The rivers (listed in Table 1, Milliman and Syvitski, 1992) are greater than 10,000 km^2 in drainage basin area, and collectively they discharge (before dam construction) slightly more than 8 bt of sediment annually. River basins <<10,000 km^2 account for slightly >20% of the total drainage area to the ocean (20 x 10^6 km^2; Figure 5.1). Assuming that the mean drainage basin area of these rivers is 1000 km^2, an additional 20,000 rivers would be required to account for the entire 20 x 10^6 km^2. If we assume that 10% of these rivers (i.e., 2000) are mountainous and that of these half drain high mountains and or Asia/Oceania and the other half drain mountains exclusive of the Arctic and non-alpine European, the combined loads of these rivers would be (8 mt/river/yr x 1000 rivers) + (1.5 mt/river/yr x 1000 rivers) (see Figure 5.5), or a total of 9.5 bt/yr. This number is surprisingly close to our estimate for the rivers (mostly small) draining Oceania, but since it does not include southern Asia or western North and South America, our calculation may be too conservative. Although the yields for similar-sized upland and lowland rivers are significantly lower (900 and 90 t/km^2/yr, respectively), there are more of them, and the combined small upland and lowland rivers might contribute another 1-2 bt annually. Adding undocumented rivers larger than 10,000 km^2 probably would add another 1-2 bt. The combined total suspended discharge conservatively might be 20 bt.

A regional example of the influence of small mountainous rivers in sediment discharge can be seen in southern Europe. Milliman and Meade (1983) pointed out that the rivers draining south from the Alps have much higher yields than those rivers draining northern Europe. Assuming a yield of 120 t/km^2/yr and a combined drainage of 0.55 x 10^6 km^2, Milliman and Meade calculated that the southern rivers discharge 66 mt/yr to the Mediterranean Sea. In fact, the sediment loads of southern alpine rivers are much greater: the 24 mountainous rivers listed in Table 1 (Milliman and Syvitski, 1992) drain only 0.22 x 10^6 km^2, but collectively they discharge more than 140 mt of sediment annually. If the values are similar for the remainder of the combined drainage area, total sediment discharge would be 350 mt/yr, five times the value calculated by Milliman and Meade.

Unfortunately, calculating world-wide discharge is more complicated, because not all sediment carried by large rivers reaches the sea: some is stored along the lower reaches of rivers and adjoining deltas. If subsidence rates in the Bengal Delta are 1-2 cm/yr (cf. Milliman *et al.,* 1987; J.R. Curray, oral communication, 1991), for example, 40-80% of the sediment load carried by the Ganges/ Brahmaputra may be sequestered in the subaerial portion of the delta, perhaps explaining the relative lack of Holocene sediment accumulating on the adjacent shelf (Kuehl *et al.,* 1989) and the lack of net progradation of the delta front (Alam, 1987). As a result, it is entirely possible that the present sediment discharge of large rivers has been overestimated.

Because rivers are being dammed at an increasing rate, many of the numbers given in this paper are probably out of date. Pearce (1991) states that 13% of all fluvial discharge is presently dammed. Ironically, with their high sediment yields and therefore (at least relatively) high sediment loads, Asian rivers can fill their dammed reservoirs quickly thereby shortening the lives of these dams more quickly than calculated by the engineers who designed them. But since pre-dam sediment loads for most rivers were artificially high due to human activities in the drainage basins, dam construction, for example on the southeastern US rivers, probably has offset anthropogenically enhanced erosion, and post-dam discharges may not be too different from those prior to European colonization (Meade and Parker, 1985).

Even if the present global flux of river sediment could be calculated, the significance of such a number to either future or past river discharge is questionable. Mid-twentieth century river discharge (to the sea) may have been about 20 bt/yr, nearly half of this amount coming from oceania and another third from southern Asia. But because sediment loads may have increased by a factor of 2-10 since humans began farming (see Saunders and Young, 1983; Berner and Berner, 1987), the annual sediment discharge 2000-2500 yr ago may have been considerably 8810 bt. Extensive human influence in Oceania and southern Asia suggests that sediment loads in this area are disproportionately elevated.

Active Versus Passive Margin Rivers

All rivers with large sediment loads originate in mountains. Most large rivers discharge to the sea along passive continental margins, and they act as point-sources for sediment influx; as a result, large deltas (e.g., Mississippi, Nile, Amazon, Ganges, Indus, Yangtze) form on passive margins or in marginal seas (Audley-Charles *et al.,* 1977; Inman and Nordstrom, 1971; Potter, 1978).

In contrast, rivers that drain mountainous islands and the active edges of continental margins (e.g., western North and South America) or collision margins (southern Europe, southern Asia) are generally much smaller, but collectively they may transport similar amounts of sediment

as do passive margin rivers. In most instances, however, classic deltas do not form, although coalescing deltaic/fan deposits may form along the outer continental margins (e.g., Thornberg *et al.,* 1990). Because these small rivers empty onto active margins, the deposits may be subducted, such that the sedimentary sequences are neither thick nor old. The sedimentary sequences also should experience an accelerated thermal history, thus complicating petroleum maturation.

These calculated trends still may underestimate the relative importance of small rivers in terms of sediment delivery to the sea: smaller rivers often have no estuaries, are more susceptible to periodic floods and (because of their steeper gradients and proximity to source material) have larger contributions from bedload material, which seldom is included in the sediment load values reported in the literature (e.g., Syvitski and Farrow, 1983). In addition, along active margins earthquakes and volcanic eruptions can result in mudslides and floods that can increase the sediment loads of adjacent rivers. In the four months following the eruption of Mount St. Helens (Washington State), for example, the sediment load of the Cowlitz River (a tributary of the Columbia) was 140 mt, compared to normal annual load for the Columbia of 10 mt (Hubbell *et al.,* 1983); for the few years after the eruption, the Columbia River discharged an estimated 35 mt/yr (Meade and Parker, 1985).

Smaller mountainous rivers are therefore more likely to discharge larger percentages of their sediment loads directly to the sea than do larger rivers. Moreover, the sediment is more likely to escape the narrow shelves to deeper basins during both high and low stands of sea level.

The Santa Clara River (southern California) serves as an example of both the episodicity and shelf-escape possible with small rivers. During 18 yr of monitoring, more than half the total sediment transported by the Santa Clara was carried in three floods, lasting a total of seven days (Milliman, 1991, after Meade, 1992). Following a major flood in 1969, Drake *et al.* (1972) traced the fate of the discharged sediment as it entered the Santa Barbara Basin and ultimately was dispersed there by a series of slumps and turbidity currents.

If sediment discharged from small mountainous rivers can by-pass active margins during high stands of sea level, then standard models of sequence stratigraphy, which have been so successful in determining the position of eustatic sea level in older sedimentary deposits (e.g., Haq *et al.,* 1987), may have less application off active margins. On the other hand, active margin deposits appear to be far less common in the geological record, probably because many of them are subducted back into the arc/orogens that border the active margins (von Huene and Scholl, 1991).

ACKNOWLEDGMENTS

REFERENCES

Ahnert, F. (1970). Functional relationships between denudation, relief, and uplift in large mid-latitude drainage basins, American Journal of Science 268, 243-263 .

Alam, M. (1987). Bangladesh, in The Encyclopedia of World Regional Geology II, R.W. Fairbridge, ed., van Nostrand Reinhold, Stroudsburg, Pa.

Audley-Charles, M.G., J.R. Curray, and G. Evans (1977). Location of major deltas , Geology 5, 341-344 .

Audley-Charles, M.G., J.R. Curray, and G. Evans (1979). Significance and origin of big rivers: A discussion, Journal of Geology 87, 122-123 .

Berner, E.K., and R.A. Berner (1987). The Global Water Cycle: Geochemistry and Environment, Prentice-Hall, Englewood Cliffs, N. J., 397 pp .

Burz, J. (1977). Suspended-load discharge in the semiarid region of northern Peru, International Association of Hydrological Sciences, Publication 122, 269-277 .

Dickinson, W.R. (1988). Provenance and sediment dispersal in relation to paleotectonics and paleogeography of sedimentary basins, in New Perspectives in Basin Analysis, K.L. Kleinspehn and C. Paola, eds., Springer-Verlag, New York, pp. 3-25 .

Douglas, I. (1967). Man, vegetation, and the sediment yield of rivers, Nature 215, 925-928 .

Drake, D.E., R.L. Kolpack, and P.J. Fischer (1972). Sediment transport on the Santa Barbara-Oxnard shelf, Santa Barbara Channel, California, in Shelf Sediment Transport: Process and Pattern, D.J.P. Swift, D.B. Duane , and O.H. Pilkey, eds., Dowden, Hutchinson and Ross, Stroudsburg, Pa., pp. 207-331 .

Fournier, F. (1960). Climat et Erosion, Presses Universitaires de France, Paris, 201 pp .

Gibbs, R.J. (1965). The geochemistry of the Amazon River system: Part I. The factors that control the salinity and the composition and concentration of the suspended solids, Geological Society of America Bulletin 78, 1203-1232 .

Haq, B.U., J. Hardenbol, and P. Vail (1987). Chronology of fluctuating sea levels since the Triassic, Science 235, 1156-1167 .

Hay, B.J. (1987). Particle flux in the western Black Sea in the present and over the last 5000 years: Temporal variability, source and transport mechanisms, unpublished Ph.D. thesis, WHOI-MIT, Cambridge, MA., 201 pp .

Hay, W.W., C.A. Shaw, C.A., and C.N. Wold (1989). Balanced paleogeographic maps: Geologische Rundshau 78, 207-242 .

Holeman, J.N. (1968). Sediment yield of major rivers of the world, Water Resources Research 4, 737-747 .

Hossain, M.M. (1991). Total sediment load in the lower Ganges and Jumuna, Bangladesh University of Engineering and Technology, 15 pp .

Hubbell, D.M., J.M. Laenen, and S.W. McKenzie (1983). Characteristics of Columbia River sediment following the eruption of Mount St. Helens on May 18, 1980, U.S. Geological Survey Circular 850-J, 21 pp .

Idroser (1983). Piano progettuale per la difesa della costa adriatica Emiliano-Romagnola: Vol. IV. Il transport solido fluviale nei bacini tributari dell'adriatico, Bologna, 429 pp .

Inman, D.L., and C.E. Nordstrom (1971). On the tectonic and morphologic classification of coasts, Journal of Geology 79, 1-21 .

Kuehl, S.A., T.M. Hariu, and W.S. Moore (1989). Shelf sedimentation off the Ganges-Brahmaputra river system: Evidence for sediment bypassing to the Bengal fan, Geology 17, 1132-1135 .

Langbein, W.B., and S.A. Schumm (1958). Yield of sediment in relation to mean annual precipitation, Transactions, American Geophysical Union 39, 1076-1084 .

Lisitzin, A.P. (1972). Sedimentation in the World Ocean, Special Publication 17, Society of Economic Paleontologists and Mineralogists, Tulsa, Okla.

Lopatin, G.W. (1950). Erozia y stok nanosov: Priroda no. 7.

Meade, R.H. (1982). Sources, sinks, and storage of river sediment in the Atlantic drainage of the United States, Journal of Geology 90, 235-252 .

Meade, R.H. (1992). River-sediment inputs to major deltas, in Rising Sea Level and Subsiding Coasts, J.D. Milliman, ed., Wiley, New York.

Meade, R.H., T. Dunne, J.E. Richey, U. de M. Cents, and E. Salati (1985). Storage and remobilization of suspended sediment in the lower Amazon River of Brazil, Science 228, 488-490 .

Meade, R.H., C.F. Nordin, Jr., W.F. Curtis, F.M. Rodigues, C. M. do Vale, and J.M. Edmond (1979). Sediment loads in the Amazon River, Nature 278, 161-163 .

Milliman, J.D., and R.H. Meade (1983). World-wide delivery of river sediment to the oceans, Journal of Geology 91, 1-21 .

Milliman, J.D., Y.S. Qin, M.E. Ren, and Y. Saito (1987). Man's influence on the erosion and transport of sediment by Asian rivers: The Yellow River (Huanghe) example, Journal of Geology 95, 751-762 .

Molnia, B.F., P.R. Carlson, and W.P. Levy (1978). Holocene sediment volume and modern sediment yield, northeast Gulf of Alaska (abs), American Association of Petroleum Geologists Bulletin 62, 545 .

Pearce, F. (1991). A dammed fine mess, New Scientist (May 4), 36-39 .

Petts, G.E., H. Møller, and A.L. Roux, eds. (1989). Historical Changes of Large Alluvial Rivers: Western Europe, Wiley, Chichester, 365 pp .

Pinet, P., and M. Souriau (1988). Continental erosion and large-scale relief, Tectonics 7, 563-582 .

Potter, P.E. (1978). Significance and origin of big rivers, Journal of Geology 86, 13-33 .

Ruxton, R.P., and I. McDougall (1967). Denudation rates in northeast Papua from potassium-argon dating of lavas, American Journal of Science 265, 545-561 .

Saunders, I., and A. Young (1983). Rates of surface processes on slopes, slope retreat, and denudation, Earth Surficial Processes and Landforms 8, 473-501 .

Schumm, S.A., and R.F. Hadley (1961). Progress in the application of landform analysis in studies of semiarid erosion, U.S. Geological Survey Circular 437, 14 pp .

Slaymaker, O. (1987). Sediment and solute yields in British Columbia and Yukon: Their geomorphic significance reexamined, in International Geomorphology 1986, Part I, V. Gardiner et al., eds., Wiley, Chichester, pp. 925-945 .

Strakhov, N.M. (1961). Onekotroykh zakonomermostiakh denudatsii i perenosa osadochnogo materiala na ploshchadyakh gymidnykh klimatov, in Sovremennye osadki moei i oceanov, N.M. Strakov, P.L. Bezrykov, and V.S. Yablokov, eds., Izdatelstovo Akademia Nauk SSSR, Moscow, pp. 5-27 .

Summerfield, M.A. (1991). Global Geomorphology, Longman Scientific and Technical, Essex (England), 537 pp .

Syvitski, J.P.M., and G.E. Farrow (1983). Structures and processes in bayhead deltas: Knight and Butte Inlets, British Columbia, Sedimentary Geology 36, 217-244 .

Syvitski, J.P.M., D.C. Burrell, and J. Skei (1987). Fjords: Processes and Products, Springer-Verlag, New York, 379 pp .

Thornberg, T.M., L.D. Kulm, and D.M. Hussong (1990). Submarine fan development in the southern Chile Trench: A dynamic interplay of tectonics and sedimentation, Geological Society of America Bulletin 102, 1658-1680 .

UNESCO (1978). World register of rivers discharging into the oceans, unpublished manuscript.

von Huene, R., and D.W. Scholl (1991). Observations at convergent margins concerning sediment subduction, subduction erosion, and the growth of continental crust, Reviews of Geophysics 29, 279-316 .

Walling, D.E. (1985). The sediment yields of African rivers, International Association of Hydrological Sciences, Publication 144, 265-283 .

Walling, D.E. (1987). Rainfall, runoff, and erosion of the land: A global view, in Energetics of Physical Environment, K.J. Gregory, ed., Wiley, London, pp. 89-117 .

Walling, D.E., and B.W. Webb (1983). Patterns of sediment yield, in Background to Palaeohydrology, K.J. Gregory, ed., Wiley, Chichester, pp. 69-100 .

Waythomas, C.F., and G.P. Williams (1988). Sediment yield and spurious correlation — Toward a better portrayal of the annual suspended-sediment load of rivers, Geomorphology 1 , 309-316 .

Wilson, L. (1973). Variations in mean annual sediment yield as a function of mean annual precipitation, American Journal of Science 273 , 335-349 .

6

Glacial to Modern Changes in Global River Fluxes

VICTOR R. BAKER
University of Arizona

ABSTRACT

Continental records of fluvial paleohydrology indicate major changes in global fluxes of water and sediment since the last full-glacial maximum. Spectacular cataclysmic floods occurred during deglaciation of the temperate zone, while more equatorial areas had reduced average streamflow at full glaciation, about 18,000 yr ago (18 ka). Southern Asia, central Africa, and northern Australia experienced enhanced monsoonal activity and large floods in the earliest Holocene. Relatively small-scale cyclic fluctuations of fluvial activity characterized the Holocene of the temperate zone. New research methods, such as the study of flood slackwater deposits and paleostage indicators, offer the potential for very accurate paleoflow reconstructions. A global program of fluvial paleohydrology could be combined with ongoing work in paleoclimatology to greatly improve the understanding of possible future changes in the Earth system.

INTRODUCTION

Rivers form the dynamic link that operates on the Earth's land surface between the oceanic storage and the atmospheric transfer of global water. Along with a flux of water from the hydrosphere, rivers transfer a flux of sediment that modifies the lithosphere. Chemical components of the other great global environmental cycles move with these two great river fluxes of water and sediment.

This chapter discusses ancient aspects of change in river fluxes of water and sediment. In adopting a paleohydrological approach to rivers, emphasis is placed on the time since the last glaciation. There are several important reasons for this approach. (1) River fluctuations in this period encompass the range of fluvial adjustment to Quaternary climatic change for which the future will be an extension. (2) Examples of cataclysmic change during this period illustrate the extremes of what is possible in river systems. (3) Very detailed late Quaternary records of fluvial hydrological change are preserved in certain ideal settings. (4) Records of late Quaternary paleohydrology can be compared to other very detailed Quaternary paleoclimatological data and to model simulations of the atmospheric-hydrologic system.

FLUVIAL PALEOHYDROLOGICAL PRINCIPLES

Records of fluvial changes since the last glaciation have been most extensively studied by the analysis of sediments in terraces, floodplains, and valley fills. Where possible, such studies are combined with the results of recent advances in understanding the relationship of channel morphology to climatic and hydrological controls (Schumm and Brakenridge, 1987). However, preserved paleochannels are limited to certain special alluvial settings such as those studied on the riverine plain of eastern Australia (Schumm, 1968), the north Polish plain (Kozarski and Rotnicki, 1977), and the Gulf Coastal Plain of the United States (Baker and Penteado-Orellana, 1977). Paleochannel preservation tends to be best for meandering river environments and poorer for environments characterized by braided or straight channels. Most often the sediments must be analyzed without the morphological clues. Pitty (1971, p. 16) aptly summarizes the situation: "Lending confidence to the geomorphologist during his hypothetical leaps between form and process is the flimsy safety net provided by the study of sediments."

Regime Changes and Sediment Transport Mechanics

Two broad classes of paleoflow estimation derive from the two classical divisions of fluvial hydraulics (Leliavsky, 1955): regime theory and sediment transport mechanics. The regime approach to fluvial paleohydrology involves the use of various empirical relationships that relate the driving variables of (1) relatively high-probability flow discharge and (2) sediment characteristics to various dependent variables, including paleochannel dimensions, river patterns, and gradients. The relationships apply only to alluvial rivers with beds and banks composed of the same types of sediment as in transport by the channel-forming flows. Paleohydrological work in this area was pioneered by Dury (1954, 1965) and by Schumm (1965, 1968).

Because of the interplay of sediment and water discharge in fluvial response, alluvial rivers may display a degree of complex response to changes in their drainage basins (Schumm, 1977). Lag times also occur between causative agents and responses. For example, the effect of glaciation on sediment yields continues as long as the unstable drift in proglacial or postglacial environments remains easily accessible to fluvial erosion and transport (Church and Ryder, 1972). The high sediment yields associated with glacier-related deposits may persist with long lag times from the emplacing processes. Church and Slaymaker (1989) show that Holocene sediment yields in British Columbia are dominated by these effects, and the influence of relict glacial sediments continues to the present day.

Most of the equations used in alluvial regime paleohydrology are listed by Williams (1984). The approach is subject to many limitations and provides relatively low accuracy of paleoflow retrodiction (Ethridge and Schumm, 1978; Rotniki, 1983; Dury, 1985). However, in a semiquantitative sense, the regime approach combined with detailed studies of floodplain sedimentology can show the pattern of fluvial responses to changing environmental conditions (Baker and Penteado-Orellana, 1977).

A variety of procedures from sediment transport theory have been used to relate sediment characteristics to shear stress, flow velocity, or stream power. Combined with information on paleochannel dimensions, these procedures can yield paleoflow estimates (Baker, 1974; Costa, 1983; Williams, 1983). Unfortunately, numerous problems may contribute to a relatively low accuracy level for these procedures (Church, 1978; Maizels, 1983).

Despite the problems with both the regime theory and the sediment transport mechanical approaches to fluvial paleohydrology, these methods have the most universal range of applicability with regard to ancient river deposits. Most of the literature on late Quaternary fluvial change is based on the study of alluvial valleys interpreted by classical stratigraphy combined with some regime or sediment transport theoretical analysis.

SWD-PSI Analysis

A relatively new development in Quaternary paleohydrology is the recognition that certain stable-boundary fluvial reaches may, under ideal circumstances, preserve remarkably complete and accurate records of river flood stages. This technique was used for cataclysmic Pleistocene glacial floods (Baker, 1973; Patton *et al.,* 1979) and found also to apply to arid-region Holocene floods (Baker *et al.,* 1979, 1983; Kochel and Baker, 1982). Paleodischarges are calculated using hydraulic flow models (O'Connor and Webb, 1988) that relate slackwater deposits and paleostage indicators (SWD-PSI) to paleowater-surface profiles. Modern SWD-PSI paleoflood hydrology results in remarkably complete catalogues of the number, timing, and magnitudes of the largest floods occurring over periods of centuries or millennia (Baker, 1987a). The data can be used directly in magnitude-frequency analysis (Stedinger and Baker, 1987; Baker, 1989), understanding regional patterns (Enzel *et al.,* 1993) or in interpreting the effects of environmental change on flood time series (Baker, 1987b; Jarrett, 1991).

Although most SWD-PSI paleoflood hydrology studies have been done on relatively small rivers, the methodology is not limited in scale. If appropriate study reaches can be found, then large rivers can also be analyzed. Chatters and Hoover (1986) used the methodology to analyze a 1800-yr record of late Holocene floods on the Columbia

River. The paleofloods of the Huang He (Yellow River) in China were studied by Shi Fucheng *et al.* (1987). The Narmada River in central India, which has historical floods as great as 60,000 m3/s, displays exceptional slackwater depositional sites in its middle reaches (Baker, 1988a; Kale *et al.,* 1992). Excellent sites for SWD-PSI paleoflood analysis have recently been discovered on the Colorado River in Arizona (Ely *et al.,* 1992).

The SWD-PSI paleoflood studies require certain ideal combinations of conditions that allow rivers to chronicle their own cataclysms (Baker and Pickup, 1987). The method has been found to be especially applicable in arid, tropical, and savanna environments of relatively high flow variability. Because these environments have generally proven difficult to characterize with other fluvial paleohydrological tools, SWD-PSI paleoflood hydrology seems to have a high potential for increasing our understanding of flow changes in the global context (Figure 6.1). Some localities where excellent paleoflood records have recently been discovered include the following: northern Australia (Gillieson *et al.,* 1991; Patton *et al.,* 1993; Wohl, 1992a), South Africa (Smith, 1991, 1992), China (Ding Xianrong and Yan Yuanling, written communication, 1992), India (Vishwas Kael, written communication, 1993), Israel (Wohl *et al.,* in press), Greece (Lewing *et al.,* 1991), and Spain (G. Benito, written communication, 1993).

FLUVIAL CATACLYSMIC PROCESSES

The emphasis in global change studies by many of the emerging scientific initiatives has been on progressively acting processes. Atmospheric increases in various trace gases, tropical deforestation, and water pollution all proceed progressively. Moreover, responses to change are generally considered in terms of mean variables. The predictions of general circulation models, for example, are expressed in terms of changes in mean values for temperature and precipitation.

The geological record has taught us, however, that the Earth also displays cataclysmic processes that lead to immense short-term responses. For river flows, our knowledge of cataclysmic processes is limited, and that limited knowledge has sometimes led to limited appreciation of these phenomena by modern geomorphologists (Baker, 1988b). Modern measurements of cataclysmic floods are inadequate because of the very small chance of cataclysm occurrence at a specific observational site and because of physical problems in actually measuring a powerful cataclysmic process.

In nearly all the hydrological literature on extreme floods, such events are not treated directly. Rather, extrapolations are made according to statistical assumptions about an observational record of small flows, or a computer simulation is performed according to an ideal contemplation of flood behavior. The scientific inadequacy of such procedures, which were developed for purposes of engineering design, is only now becoming clear to the hydrological community (Klemes, 1986, 1987, 1989).

In relation to fluxes of water and sediment associated with rivers, if we are to understand changes, we must not limit that understanding to adjustments of mean conditions. It is also critical to understand variances in the extreme events that dictate local, intense fluxes. Are there global patterns of these extremes through time and space? In a general sense, most floods are the products of global climatic systems (Hayden, 1988). Moreover, extreme floods seem to result from important anomalous patterns of atmospheric circulation, including persistence of pattern, rare configurations, and unusual combinations or locations of circulation types (Hirschboeck, 1987, 1991). Even rather small-scale climatic changes, if persistent, can produce rather dramatic responses in flood magnitudes and frequencies, as demonstrated for the upper Mississippi River (Knox, 1984, 1993). To improve understanding of cataclysmic floods one must expand the horizons of time and space, reconstructing ancient flood occurrences on a global scale.

A possible example of global adjustment to extreme river flux changes is provided by the long-recognized Younger Dryas cooling of northwestern Europe that took place approximately 11 to 10 ka. This change seems to have been
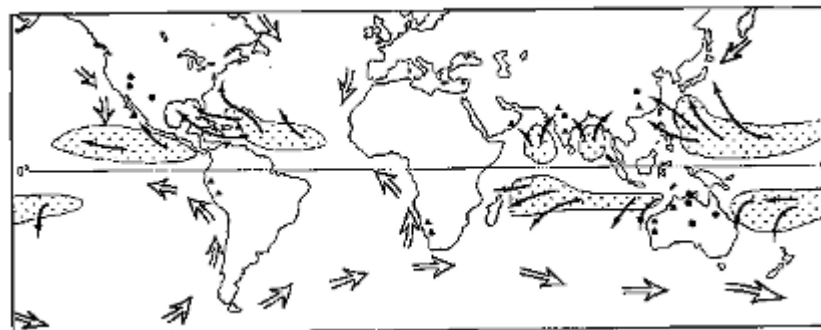
FIGURE 6.1 Relationship of SWD-PSI paleoflood hydrological investigation sites to sources of tropical storms (dot pattern), typical tropical storm tracks (small arrows), and major cold-water ocean currents (large arrows). Locations of recently completed SWD-PSI studies are indicated by large dots. Locations of potential study sites with appropriate geomorphological settings are indicated by triangles. From Baker (1988a).

abruptly imposed on the long-term deglacial warming trend. Broecker *et al.* (1988) attribute the Younger Dryas intense reversal of that trend to a sharp drop in sea surface temperature as North American meltwater was diverted from the Mississippi River to the St. Lawrence. Shaw (1989) posed the more provocative hypothesis that immense volumes of subglacially stored water may suddenly be released in floods exceeding 10^6 m³/s around the margins of the Laurentide Ice Sheet. Such floods would have immense consequences in rapid sea-level rise and the climatic effects of a cold meltwater lid on warmer ocean water. Considerable skepticism remains (Mueller and Pair, 1992), however, especially concerning the drumlin topography ascribed to cataclysmic flood origin (Shaw *et al.,* 1989).

A complex system of proglacial lakes developed during deglaciation along the southern margin of the Laurentide Ice Sheet in North America. As reviewed by Teller (1987, 1990), much of the proglacial discharge passed through the Mississippi River to the Gulf of Mexico until about 11 ka. Then the immense Lake Agassiz Basin was integrated into the St. Lawrence drainage to the Atlantic Ocean. At about 10 ka the Lake Agassiz discharge briefly returned to the Mississippi system. There still remains some controversy as to the correlations between land meltwater shifts and the paleoceanographic interpretation of marine sediments. Moreover, the mechanism of climatic cooling induced by the meltwater influx to the Atlantic remains a problem. However, the clear evidence of drastic changes in river fluxes and associated oceanic influences points to an important need to understand rapid changes in river processes.

The usual model of proglacial drainage is one in which outwash streams gradually aggrade their beds, producing a wedge of sediment thickening toward the glacial front. The meltwater from the late Pleistocene Laurentide Ice Sheet initially produced such a pattern. However, after the ice sheet has retreated behind either major morainal fea
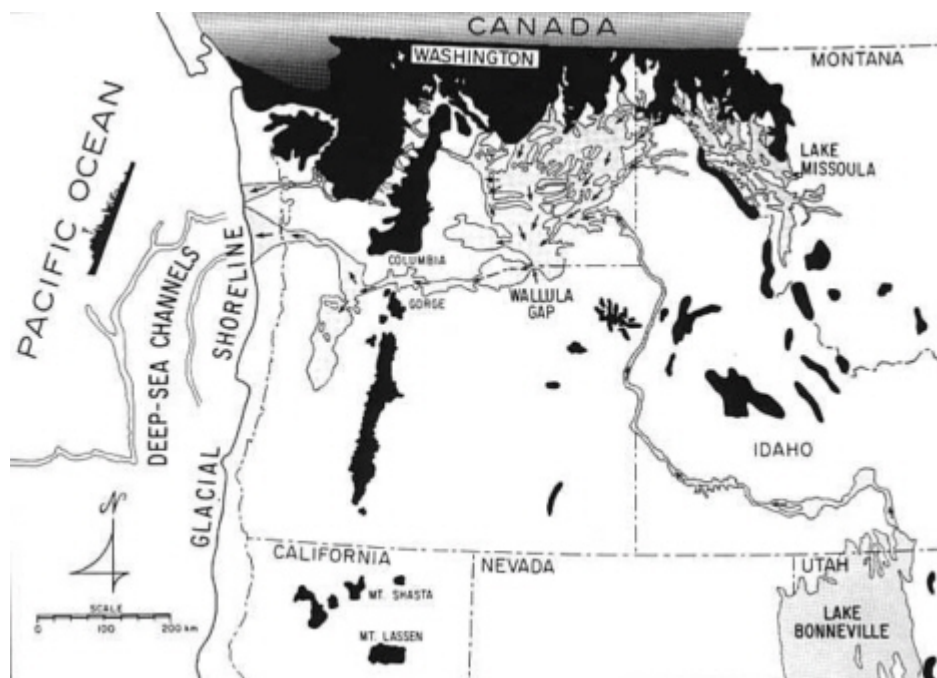
FIGURE 6.2 Map showing regions of the northwestern United States affected by cataclysmic flooding in the late Pleistocene (arrows) in relation to glacial Lake Missoula and Lake Bonneville. Areas of glaciation are indicated in black. From Baker et al. (1987).

tures or landform divides, meltwater became mainly ponded as proglacial lakes. As lake levels rose, the water was released as glacial-lake outburst floods (Kehew, 1982; Kehew and Lord, 1986, 1987; Lord and Kehew, 1987). These floods eroded enormous volumes of sediment when they carved various glacial-lake spillways. The floods were rapidly conveyed to the ocean, particularly through the Mississippi River system to the Gulf of Mexico. Grosswald (1980) envisioned a somewhat similar set of circumstances for a late Pleistocene ice sheet of of northern Eurasia, which dammed north-flowing rivers in a radical pattern from Yenisei in the east (Siberia) to the Polish rivers in the west. A proglacial system of lakes and spillways involved water transfers to the Aral, Caspian, Black, and Mediterranian Seas. Velichko *et al.* (1984) reconstructed more limited extents to late Pleistocene Eurasian glaciers and ice-dammed lakes.

Studies of the great late-glacial floods provide knowledge of possible extreme effects of short-term changes in river fluxes. In addition to the Laurentide Ice Sheet floods, glacial cataclysmic floods have recently been recognized for the Fennoscandian Ice Sheet in Swedish Lapland (Elfstrom, 1987). Rudoy (1988, 1990) and Ruday and Baker (1993) document cataclysmic late Pleistocene flood features, including huge gravel bars and giant current ripples, for glacial floods in the Altay Mountain region of south-central Siberia. However, to date the best studied cataclysmic flood features are those in the northwestern United States associated with the Cordilleran Ice Sheet and with Pleistocene Lake Bonneville (Figure 6.2). The Bonneville flood occurred about 14.5 ka (Currey, 1990), releasing a peak flow of about 9×10^5 m^3/s (Jarrett and Malde, 1987; O'Connor, 1993). This compares to the largest known recent flood, the 3.85×10^5 m^3/s discharged by the Amazon River in 1953 (Oltman, 1968). Lake Bonneville released 4700 km^3 stored volume, sustaining flow for perhaps six weeks (Malde, 1968).

The cataclysmic outbursts of glacial Lake Missoula (Figure 6.2) occurred repeatedly during two late-glacial phases: (1) approximately 35 to 40 ka (Baker *et al.,* 1991), and (2) approximately 12 to 17 ka (Baker and Bunker, 1985). The relative number, timing, and sizes of individual floods in these phases remain controversial (Baker and Bunker, 1985; Waitt, 1985; Smith, 1993). However, it is clear that the largest discharges were among the greatest known freshwater flows on the planet (O'Connor and Baker, 1992). Baker (1973) originally estimated the peak flow at approximately 2.1×10^7 m^3/s. However, the released discharge peak to the Pacific Ocean was probably about 1.0×10^7 m^3/s because of downstream hydraulic ponding (O'Connor and Baker, 1992; Baker *et al.,* 1993). Total water released from glacial Lake Missoula was on the order of 2000 km^3, allowing large flows to persist from a few days to a week (Baker, 1973; Clarke *et al.,* 1984; Craig, 1987).

TABLE 6.1 Flow Dynamics of Some Major River Floods (Baker and Costa, 1987; Baker et al., 1993).

Flood	Age	Peak Discharge (m^3/s)	Power/Unit Area (W/m^2)
Altay	Late Pleistocene	1.8×10^7	1,000,000
Missoula	12-17 ka	1×10^7	300,000
Bonneville	14.5 ka	9×10^5	75,000
Amazon	Modern	3×10^5	12
Mississippi	Modern	3×10^4	12

The influence of various late-glacial cataclysmic floods on sediment fluxes remains largely underappreciated. Griggs *et al.* (1970) noted the influence of the Missoula floods in transporting sediment to the abyssal seafloor off the mouth of the Columbia River. However, few other studies have considered this mechanism of sediment transport for sporadic and rapid transfers of sediment through fluvial systems.

Some measure of sediment transport capacity for cataclysmic floods can be estimated by using Bagnold's (1966) concept of stream power. The rate of energy dissipation ω, or power, per unit area of streambed *m* can be expressed as

$$\omega = \frac{\gamma QS}{W} = \tau \bar{V} \qquad (6.1)$$

where W is bed width, Q is discharge, S is energy slope, g is the specific weight of the transporting fluid, V^* is the mean flow velocity, and t is the bed shear stress. For short time periods cataclysmic floods generated tremendous fluxes. The peak Lake Missoula flows were an order of magnitude larger than the average total global discharge of all rivers to the ocean, approximately 1×10^6 m^3/s estimated by Milliman and Meade (1983). Moreover, at least the potential sediment loads, expressed in terms of stream power, were also immense (Table 6.1).

REGIONAL PATTERNS

Global fluvial paleohydrology is a subject in its scientific infancy. Under the auspices of the International Union of Quaternary Research (INQUA) Holocene Commission, a working group on Global Paleohydrology was organized in 1987. On August 7, 1991, the INQUA Council initiated a new Commission on Global Continental Paleohydrology (GLOCOPH) led by Professor Leszek Starkel. The emphasis of this new commission will be to study changes in water fluxes and storages over the past 20,000 yr (Starkel,

1993). The program will include (1) the compilation of computer data bases on individual elements of the hydrological cycle; (2) the establishment of interrelationships, including storages, transfers, and energetics, among elements of the hydrological cycle; and (3) the comparison of paleodata to simulations with a Global Hydrological Model (GHM). There is at present no functioning GHM, but several modeling groups are working on the goal of achieving one. A GLOCOPH data base was established at the Geodata Institute, University of Southampton, directed by Professor K.J. Gregory.

This chapter can only highlight selected aspects of global fluvial paleohydrology, because the whole subject will be expanding greatly over the next several years.

Europe and North America

Considerable fluvial paleohydrological work was performed from 1977 to 1988 under the auspices of the International Geological Correlation Programme (IGCP) Project 158 "Paleohydrology of the Temperate Zone During the Last 15,000 Years." Subproject A under the leadership of Laszek Starkel organized 17 national efforts in the reconstruction of fluvial changes between 35 and 70°N latitude, concentrating on 20 major river valleys. Researchers employed the traditional methodologies of floodplain studies and regime-based paleoflow estimates (Starkel and Thornes, 1981). Most of the project studies were in Europe, with some related work in North America.

As summarized in various IGCP Project 158 volumes (Gregory, 1983; Korzarski, 1983; Gregory *et al.,* 1987; Starkel *et al.,* 1991), there is a general pattern of late-glacial to modern fluvial changes. Glaciofluvial and post-glacial rivers were dominated by bed load transport until about 10 ka. A shift then occurred to meandering rivers dominated by suspended load. In Poland the change from braiding to large-scale meandering occurred at 13 to 12 ka, and from large to small paleomeanders at approximately 10 ka (Korzarski and Rotnicki, 1977). Smaller fluctuations in the Holocene reflect the influence of forest vegetation until about 5 to 4 ka, when anthropogenic influences began to increasingly influence fluvial systems.

One of the most interesting results of IGCP Project 158 was the recognition of synchroneity in episodes of Holocene fluvial activity. These episodes are well documented in central Europe (Korzarski, 1983; Starkel, 1983) and the north-central United States (Brakenridge, 1980, 1981; Knox, 1983, 1985). The episodes may be of variable duration and magnitude, and their characteristics may be out of phase from region to region even though they are responding to the same large-scale dynamics of the global atmosphere-ocean system. Although the alluvial phases do not correlate precisely in time between sites, there is a
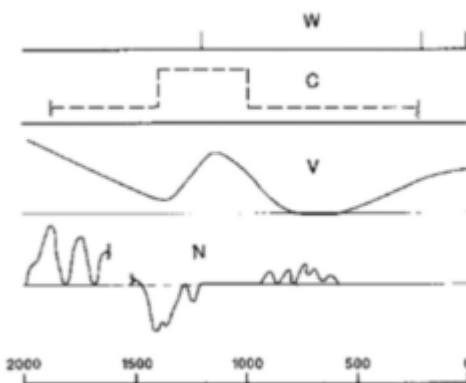
FIGURE 6.3 Correlation of flood activity on major northern hemisphere rivers. Data are plotted for ages (years A.D.). Bars in the W Sequence show ages of major alluvial discontinuities in the United States associated with flooding episodes (Knox, 1983). Heights of the dashed lines in C illustrate relative levels of flood frequency on the Columbia River, Washington (Chatters and Hoover, 1986). Similarly, curve V shows interpreted levels of fluvial activity in the upper Vistula River basin of Poland (Starkel, 1983). The lower curve N shows Nile River activity in terms of the cumulative sum of discharge departures from the average divided by average discharge (Riehl and Meitin, 1979). Where this curve is increasing with time (from right to left), discharge is above the long-term average; where the curve is decreasing with time, discharge is below the long-term average.
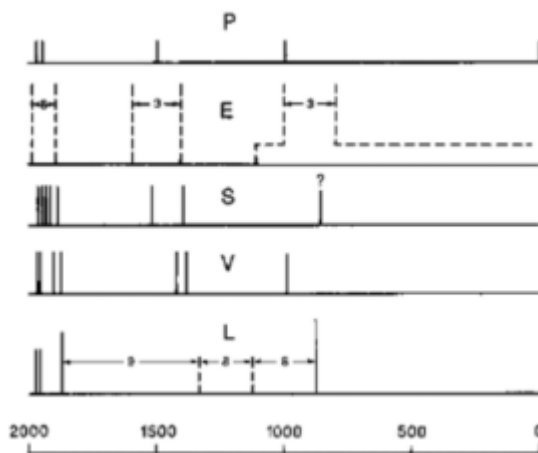
FIGURE 6.4 Exceptionally large paleofloods on rivers in the south-western United States plotted against age (years A.D.). Vertical bars show flood ages on the Pecos River, P, from Kochel and Baker (1982); the upper Salt River, S, from Partridge and Baker (1987); and the Verde River, V, from Ely and Baker (1985). Concentrations of large floods, indicated by the numbers, are shown for the Escalante River, E, from Webb (1985); and the lower Salt River, L, from Fuller (1987).

consistent overall pattern: (1) 1000- to 2000-yr aggradational episodes coinciding with phases of lower flood frequency, and (2) 300- to 500-yr phases of higher flood frequency involving river entrenchment or avulsion. The overall period of 2000 to 2500 yr coincides with other detailed proxy records of Holocene climate such as Denton and Karlen's (1973) analysis of mountain glaciation and the oxygen isotope variations in the Camp Century, Greenland, ice core (Dansgaard *et al.,* 1986).

Paleoflood hydrological investigations are just beginning to provide a perspective on extreme river flows over the past 2000 yr (Figure 6.3). The most interesting patterns are appearing in the southwestern United States, where approximate 1000- and 500-yr periods are observed (Figure 6.4). A recent compilation of SWD-PSI studies (Ely *et al.,* in press) has established the regional coherence of these patterns of flooding.

South America

Baker (1983) suggested that the effects of Quaternary climatic change on South American rivers might be used as a surrogate to explore potential effects of man-induced environmental change in the region. During the last full glacial, most of South America north of the Tropic of Capricorn was dominated by climates drier than present (Tricart, 1985). The Amazon Basin rivers have a remarkable diversity of patterns, reflecting the influence of Andean source region and the relative abilities of lowland rivers to rework relict alluvium deposited during the drier full-glacial periods (Baker, 1978). Although little fluvial paleohydrological work has been done in the region, the global importance of Amazon and Orinoco Basin hydrology would seem to warrant further attention.

Central-western South America is strongly influenced by the El Niño-Southern Oscillation (ENSO) phenomenon. This coupled oceanic-atmospheric oscillation is associated with anomalous periods of flood and drought in diverse parts of the Earth (Yarnal, 1985). The ENSO is of considerable interest for understanding the clusterings of floods and droughts observed in paleohydrological records. Preliminary work from northern Australia suggests that patterns of tropical storm activity and related floods may reflect ENSO variations (Wohl, 1988). Western South America would appear to be very important for establishing the pulse of ENSO variation from studies of Holocene flood sediments (Wells, 1987).

Africa, Australia, Southern Asia

Fluvial responses in much of equatorial Africa, northern Australia, and southern Asia are dominated by the annual monsoonal weather cycle (Figure 6.5). Monsoons are extremely complex meteorological phenomena characterized by dramatic variability from year to year, as documented by the historical record (Mooley and Parthasarathy, 1984). Both droughts and wet anomalies occur in runs, suggesting clumping or persistence of wet and dry anomaly values (Kutzbach, 1986).
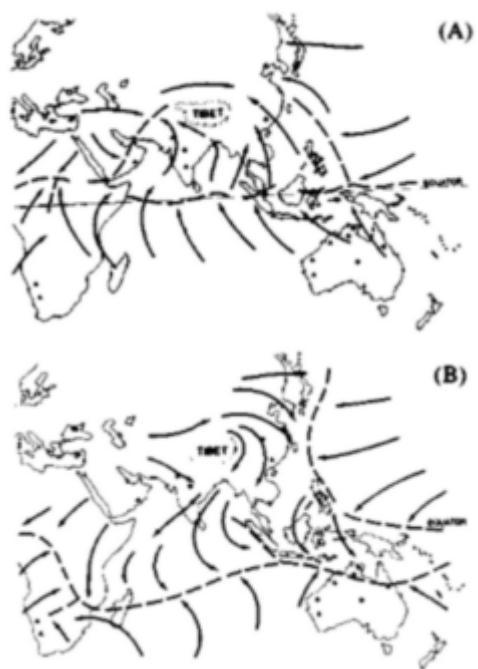
FIGURE 6.5 Maps showing wind patterns (arrows) and convergence zones (dashed lines) at 70 mbar (about 3000 m) for Eastern Hemisphere monsoons. Data from Nieuwolt (1977). (A) Pattern for the Asian summer monsoon (June to September). (B) Pattern for the Asian winter monsoon and northern Australia summer monsoon (December to March). Active (dot) and potential (triangle) SWD-PSI paleoflood investigation sites should document variations in monsoonal activity through the Holocene.

Paleohydrological data from tropical Africa indicate relatively dry conditions, reduced annual discharge in the Nile, Niger, and Senegal rivers, but with high flood peaks between 17 and 25 ka (Williams, 1985). The latest Pleistocene and early Holocene is a markedly wetter period (COHMAP, 1988). Exceptionally high Nile floods occurred around 12 to 11 ka, and fluctuations in flow levels occurred later into the Holocene, but at reduced levels from the late-glacial extremes.
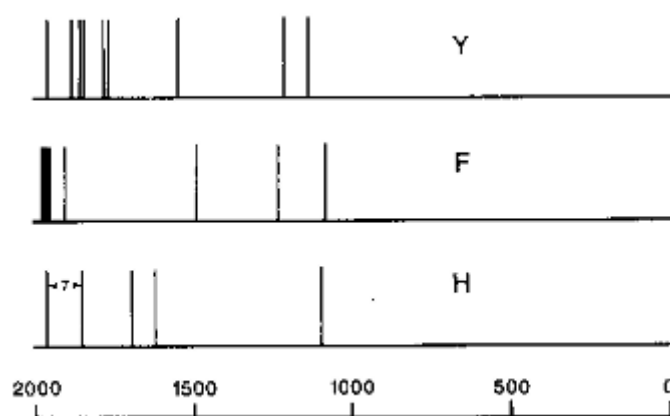
FIGURE 6.6 Exceptionally large paleofloods on rivers in Asia and Australia plotted against age (years A.D.). Vertical bars show flood ages for the Chang Jiang (Yangtze River), Y, in China (Luo Cheng-Zheng, 1987); the Finke River, F, in central Australia (Pickup et al., 1988); and the Herbert River, H, in northeastern Australia (Wohl, 1988, 1992b). The number 7 refers to the number of exceptional floods in the indicated time interval.

Northern Australia shows a generally similar pattern to that in Africa. During full-glacial time, about 18 ka, monsoonal activity seems to have been weaker than at present (COHMAP, 1988). Drier, windier conditions prevailed until a period of enhanced monsoonal activity in the latest Pleistocene and early Holocene (COHMAP, 1988). Recent paleoflood work in central and northern Australia (Figure 6.6) is just beginning to reveal the occurrences of late Holocene floods. The clustering of large floods in recent years has been attributed to the influence of global warming on the generation of storm systems responsible for the floods (Pickup *et al.,* 1988).

The northwestern Deccan upland region of India has an excellent fluvial record of long-term variations in monsoonal hydrology (Rajaguru and Kale, 1985). Between about 17 to 10 ka the aggrading rivers in this area changed from coarse bed load streams to suspended load streams. Kale and Rajaguru (1987) attribute reduced streamflow in this period to weakened monsoonal activity, as also shown in Prell's (1984) paleoceanographic work from the Indian Ocean. A period of markedly increased runoff marks the early Holocene, resulting in regional incision of rivers (Kale and Rajaguru, 1985). This energetic early Holocene fluvial activity persisted until approximately 4.5 ka, at which time a phase of overbank sedimentation generated a lower terrace inset in relation to the extensive late Pleistocene aggradational fill. After approximately 3 ka the scale of fluvial change lessened with streams characterized by general incision and minor phases of deposition.

FUTURE WORK

Ultimately fluvial paleohydrological data will be compared to model simulations of hydrological change. This general approach is illustrated by COHMAP (Cooperative Holocene Mapping Project), which compared a global assay of well-dated paleoclimatic data to general-circulation model (GCM) simulations of climatic change (COHMAP, 1988). Such data-model comparisons are used to test model results with the view that well-tested models will best serve to predict the future global change critical to the habitability of the planet. This procedure is an attempted compromise between two partially conflicting approaches to the scientific study of global change. Reconstructions of past environmental change show how complex, interactive global systems actually functioned. However, the documentation of change does not explain the physical mechanisms inducing that change. Models, such as GCMs, on the other hand, provide physical mechanistic explanations, but only for the idealized assumptions on which the models are based. The GCMs are particularly deficient at incorporating the many complex feedback elements that occur within elements of the hydrological cycle.

Data-based paleohydrological reconstructions have a more fundamental significance than the testing of various idealized models. By reconstructing the workings of the past hydrological processes of the planet one discovers those patterns of operation, anomalous behavior, and puzzling phenomena that are inherent in nature (Baker, 1991). These phenomena cannot be revealed by models that are but artificial simplifications of nature. When the patterns and anomalies are recognized, analyzed as to cause, and understood, the new understanding can be incorporated into the formulation of more realistic models. Thus, in attempting to understand a natural hydrological system dominated by complex feedbacks, there must be continual feedback between paleohydrological reconstruction of the real operation of that system and idealized model-based explanations of system operation. Maintaining the appropriate balance between paleohydrological approaches and predictive model building will be one of the challenges for modern scientific research on global change.

A related problem of overreliance on idealized models for the prediction of long-term hydrological change is that most current models provide information on mean conditions, such as the GCM predictions of mean temperature and precipitation. Aside from issues of the spatial and temporal accuracy of these predictions, there is the question of extreme values and variability of parameters. Variability is of critical importance in river fluxes. As briefly reviewed in this chapter, global fluvial systems have responded to environmental change since the last glaciation with immense variations in water discharge, sediment yield,

and resulting river patterns and sedimentary sequences. In addition to the progressive changes in these parameters, there has also been a clustering of river transfer energy into episodes of intense flooding. At present there are insufficient data with which to assess the role of such flood clustering relative to the usual assumption of the maximization of river work (sediment movement and erosion) by flow events of moderate frequency (Wolman and Miller, 1960). There is also a need to relate changes in atmospheric circulation patterns to the spatial and temporal variability of extreme floods.

The approach to fluvial paleohydrology of IGCP Project 158 and of the INQUA Holocene Commission Working Group on Global Paleohydrology has been to reconstruct river fluxes on a regional scale in drainage basins selected to represent major climatic and hydrological zones. A problem with that strategy is that some rivers may act as better recorders of their past hydrological change than others. For example, the United Kingdom basin chosen for IGCP Project 158 work, the Severn, yielded meager information on its late-glacial and early Holocene paleoflow (Gregory *et al.,* 1987). This contrasts with the abundant paleoflow data generated on the Polish Plain (Korzarski, 1983). The SWD-PSI paleoflood hydrology approach is especially sensitive to the choice of study area. Because some river reaches act as ideal recorders of SWD-PSI data, a major effort should be made to locate the appropriate study sites on the global scale for an optimization of paleoflow information.

With increased societal needs for water there have been major changes in the patterns of water and sediment delivery from rivers. Most spectacular are various large-scale engineering plans that have been proposed for river diversions to supply water for arid regions. Such hypothetical changes as the man-made diversion of Siberian rivers from their Arctic outflow points to arid central Asia could have immense potential for changes in the Earth system. Late Quaternary changes in river systems can serve as natural experiments with which to assess the effects of proposed river diversions or other river mega-engineering projects. Fluvial paleohydrological research should contribute to the basis of understanding long-term river behavior in relation to the global environment so that the consequences of river adjustments will be fully anticipated.

CONCLUSIONS

To understand the complexity of the global earth system, geologists have traditionally sought to reconstruct past earth processes in a manner consistent with the best available physical theory. This is done not only to develop a unique history, but also to characterize the complex Earth systems that cycle over scales of time and space, and defy conventional measurement. Without an understanding of these systems, theoretical modeling is unverified. More important, however, is the recognition of anomalous behavior in the real, model-prototype system that would not have been anticipated in its hypothesized theoretical representation. Such anomalies provide the driving inspiration for scientific discovery.

We are only beginning to formulate a global understanding of river fluxes since the last glaciation. Much of the existing knowledge base has developed from the study of changes in mean conditions of water and sediment discharge interpreted from records in alluvial river valleys. By using regime and sediment transport theories, it has been possible to approximate the magnitudes of change for local examples.

A new approach to fluvial paleohydrology has developed over the past decade through studies of flood slackwater deposits and paleostage indicators (SWD-PSI) at ideal sites; SWD-PSI paleoflood hydrology is especially applicable to arid, tropical, and savanna environments of high variability. The methodology can also be used to achieve remarkably accurate reconstructions of cataclysmic late-glacial floods. By concentrating on extreme flow events. SWD-PSI paleoflood hydrology can provide a new perspective on fluvial changes. Changes in river flow may be related to the extremes of global circulation, including variations in monsoons, tropical cyclones, and temperate-region storm complexes.

Advancement of knowledge on changes in global river fluxes will require an aggressive program of international collaboration. Methods of paleohydrological reconstruction must be used in ways that complement related paleoclimatological work, with both paleoenvironmental data and model-based studies. The importance of this effort is underscored by the key role of river runoff for the future habitability of the Earth.

ACKNOWLEDGMENTS

REFERENCES

Bagnold, R.A. (1966). An approach to the sediment transport problem from general physics, U.S. Geological Survey Professional Paper 422-I, 1-37 .

Baker, V.R. (1973). Paleohydrology and sedimentology of Lake Missoula flooding in eastern Washington, Geological Society of America Special Paper 144, 1-79 .

Baker, V.R. (1974). Paleohydraulic interpretation of Quaternary alluvium near Golden, Colorado, Quaternary Research 4, 95-112 .

Baker, V.R. (1978). Adjustment of fluvial systems to climate and source terrain in tropical and subtropical environments, in Fluvial Sedimentology, A.D. Miall, ed., Memoir 5 , Canadian Society of Petroleum Geologists, Calgary, Alberta, pp. 211-230 .

Baker, V.R. (1983). Large-scale fluvial palaeohydrology, in Background to Palaeohydrology: A Perspective, K.J. Gregory, ed., Wiley, Chichester, pp. 453-478 .

Baker, V.R. (1987a). Paleoflood hydrology and extraordinary flood events, Journal of Hydrology 96, 79-99 .

Baker, V.R. (1987b). Paleoflood hydrology and hydroclimatic change, International Association of Hydrological Sciences Publication 168, 123-131 .

Baker, V.R. (1988a). Palaeoflood hydrology of tropical rivers, in International Seminar on Hydrology of Extremes, National Institute of Hydrology, Roorkee, India, pp. 1-10 .

Baker, V.R. (1988b). Cataclysmic processes in geomorphological systems, Zeitschrift für Geomorphologie Supplement 67, 25-32 .

Baker, V.R. (1989). Magnitude and frequency of paleofloods, in Floods — Their Hydrological, Sedimentological and Geomor-phological Implications, K. Beven and P. Carling, eds., John Wiley & Sons, New York, pp. 171-183 .

Baker, V.R. (1991). A bright future for old flows, in Fluvial Processes in the Temperate Zone During the Last 15,000 Years, L. Starkel, J. Thornes, and K.J. Gregory, eds., John Wiley & Sons, Chichester, pp. 497-520 .

Baker, V.R., and R.C. Bunker (1985). Cataclysmic late Pleistocene flooding from glacial Lake Missoula: A review, Quaternary Science Review 4, 1-41 .

Baker, V.R., and J.E. Costa (1987). Flood power, in Catastrophic Flooding, L. Mayer and D. Nash, eds., Allen and Unwin, Boston, pp. 1-21 .

Baker, V.R., and M.M. Penteado-Orellana (1977). Adjustment to Quaternary climatic change by the Colorado River in central Texas, Journal of Geology 85, 395-422 .

Baker, V.R., and G. Pickup (1987). Flood geomorphology of the Katherine Gorge, Northern Territory, Australia, Geological Society of America Bulletin 98, 635-646 .

Baker, V.R., R.C. Kochel, and P.C. Patton (1979). Long-term flood frequency analysis using geological data, International Association of Hydrological Sciences Publication 128, 3-9 .

Baker, V.R., R.C. Kochel, P.C. Patton, and G. Pickup (1983). Paleohydrologic analysis of Holocene flood slack-water sediments, Special Publication, International Association of Sedimentology 6, 229-239 .

Baker V.R., R. Greeley, P.D. Komar, D.A. Swanson, and R.B. Waitt, Jr. (1987). Columbia and Snake river plains, in Geomorphic Systems of North America, W.L. Graf, ed., Centennial Special 2 , Geological Society of America, Boulder, Colorado, pp. 403-468 .

Baker, V.R., B.N. Bjornstad, A.J. Busacca, K.R. Fecht, E.P. King, U.L. Moody, J.G. Rigby, D.F. Stradling, and A.M. Tallman (1991). The Columbia Plateau, in Quaternary Nonglacial Geology: Conterminous U.S., R.B. Morrison, ed., The Geology of North America K-2, Geological Society of America, Boulder, Colorado, pp. 215-250 .

Baker, V.R., G. Benito, and A.N. Rudoy (1993). Paleohydrology of late Pleistocene superflooding, Altay Mountains, Siberia, Science 259, 348-350 .

Brakenridge, G.R. (1980). Widespread episodes of stream erosion during the Holocene and their climatic cause. Nature 283, 655-656 .

Brakenridge, G.R. (1981). Late Quaternary floodplain sedimentation along the Pomme de Terre River, southern Missouri, Quaternary Research 15, 62-76 .

Broecker, W.S., M. Andree, W. Wolfli, H. Oeschger, G. Bonani, J. Kennett, and D. Peteet (1988). The chronology of the last glaciation: Implications to the cause of the Younger Dryas event, Paleoceanography 3, 1-19 .

Chatters, J.C., and K.A. Hoover (1986). Changing late Holocene flooding frequencies on the Columbia River, Washington, Quaternary Research 26, 309-320 .

Church, M.A. (1978). Palaeohydrological reconstructions from a Holocene valley fill, in Fluvial Sedimentology, A.D. Miall, ed., Memoir 5 , Canadian Society of Petroleum Geologists, Calgary, Alberta, pp. 743-772 .

Church, M., and J.M. Ryder (1972). Paraglacial sedimentation: A consideration of fluvial processes conditioned by glaciation, Geological Society of America Bulletin 83, 3059-3072 .

Church, M.A., and O. Slaymaker (1989). Disequilibrium of Holocene sediment yield in glaciated British Columbia, Nature 337, 452-454 .

Clarke, G.K.C., W.H. Mathews, and R.T. Pack (1984). Outburst floods from glacial Lake Missoula, Quaternary Research 22, 289-299 .

COHMAP (1988). Climatic changes of the last 18,000 years: Observations and model simulations, Science 241, 1043-1052 .

Costa, J.E. (1983). Paleohydraulic reconstruction of flash-flood peaks from boulder deposits in the Colorado Front Range , Geological Society of America Bulletin 94, 986-1004 .

Craig, R.G. (1987). Dynamics of a Missoula flood, in Catastrophic Flooding, L. Mayer and D. Nash, eds., Allen and Unwin, London, pp. 305-332 .

Currey, D.R. (1990). Quaternary palaeolakes in the evolution of semidesert basins, with special emphasis on Lake Bonneville and the Great Basin, U.S.A., Palaeogeography, Palaeoclimatology, Palaeoecology 76, 189-214 .

Dansgaard, W., S.J. Johnson, H.B. Clauson, D. Dahl-Jensen, N. Gundestrup, C.U. Hammer, and H. Oeschger (1986). North Atlantic climatic oscillations revealed by deep Greenland ice cores, in Climate Processes and Climate Sensitivity, Monograph 29 , American Geophysical Union, Washington, D.C., pp. 288-298 .

Denton, G.H., and W. Karlen (1973). Holocene climatic changes, their pattern and possible cause, Quaternary Research 3, 155-205 .

Dury, G.H. (1954). Contributions to a general theory of meandering valleys, American Journal of Science 352, 193-224 .

Dury, G.H. (1965). Theoretical implications of underfit streams, U.S. Geological Survey Professional Paper 452-C, 1-43 .

Dury, G.H. (1985). Attainable standards of accuracy in the retrodiction of palaeodischarge from channel dimensions, Earth Surface Processes and Landforms 10, 205-213 .

Elfstrom, A. (1987). Large boulder deposits and catastrophic floods, Geografiska Ann. 69A, 101-121 .

Ely, L.L., and V.R. Baker (1985). Reconstructing paleoflood hydrology with slackwater deposits: Verde River, Arizona, Physical Geography 6, 103-126 .

Ely, L.L., Y. Enzel, J.E. O'Connor, and V.R. Baker (1992). Paleoflood records and risk assessment: Example from the Colorado River Basin, in Water Resources Engineering and Risk Assessment, J. Ganoulis, ed., Springer-Verlag, Berlin, pp. 105-112 .

Ely, L.L., Y. Enzel, V.R. Baker, and D.R. Cayan (in press). A 5000-year record of extreme floods and climatic change in the southeastern United States, Science.

Enzel, Y., L.L. Ely, P.K. House, V.R. Baker, and R.H. Webb (1993). Paleoflood evidence for a natural upper bound to flood magnitudes in the Colorado River Basin, Water Resources Research 29, 2287-2297 .

Ethridge, F.G., and S.A. Schumm (1978). Reconstructing paleochannel morphologic and flow characteristics: Methodology, limitations and assessment, in Fluvial Sedimentology, A.D. Miall, ed., Memoir 5 , Canadian Society of Petroleum Geologists, Calgary, Alberta, pp. 703-721 .

Fuller, J.E. (1987). Paleoflood hydrology of the alluvial Salt River, Tempe, Arizona, M.S. thesis, University of Arizona, Tucson, 70 pp .

Gillieson, D.D.I. Smith, M. Greenaway, and M. Ellaway (1991). Flood history of the limestone ranges in the Kimberly region, Western Australia, Applied Geography 11 105-123 .

Gregory, K.J. (ed.) (1983). Background to Palaeohydrology: A Perspective, Wiley, Chichester, 486 pp .

Gregory, K.J., J. Lewin, and J.B. Thornes (eds.) (1987). Palaeohydrology in Practice: A River Basin Analysis, Wiley, Chichester, 370 pp .

Griggs, G.B., L.D. Kulm, A.C. Waters, and G.A. Fowler (1970). Deep-sea gravel from Cascadia Channel, Journal of Geology 78, 611-619 .

Grosswald, M.G. (1980). Late Weichselian ice sheet of northern Eurasia, Quaternary Research 13, 1-32 .

Hayden, B.P. (1988). Flood climates, in Flood Geomorphology, V.R. Baker, R.C. Kochel, and P.C. Patton, eds., John Wiley & Sons, New York, pp. 13-26 .

Hirschboeck, K.K. (1987). Catastrophic flooding and atmospheric circulation anomalies, in Catastrophic Flooding, L. Mauer and D. Nash, eds., Allen and Unwin, Boston, pp. 23-56 .

Hirschboeck, K.K. (1991). Climate and floods, in National Water Summary 1988-1989 — Hydrologic Events and Floods and Droughts, U.S. Geological Survey Water-Supply Paper 2375, pp. 67-88 .

Jarrett, R.D. (1991). Paleohydrology and its value in analyzing floods and droughts, in National Water Summary 1988-1989: Hydrologic Events and Floods and Droughts, U.S. Geological Survey Water Supply Paper 237S, pp. 105-116 .

Jarrett, R.D., and H.E. Malde (1987). Paleodischarge of the late Pleistocene Bonneville Flood, Snake River, Idaho, computed from new evidence, Geological Society of America Bulletin 97, 127-134 .

Kale, V.S., and S.N. Rajaguru (1985). Alluvial and sub-alluvial morphology of the western upland rivers of Maharashtra (India), Ann. Nat. Assoc. Geographers (India) 5, 1-9 .

Kale, V.S., and S.N. Rajaguru (1987). Late Quaternary alluvial history of the northwestern Deccan upland region, Nature 325, 612-614 .

Kale, V.S., S. Mishra, Y. Enzel, L. Ely, V.R. Baker, and S.N. Rajaguru (1992). Geomorphic investigations of floods in central Narmada Basin, India, in First National Symposium on Environmental Hydraulics, June, 1992 , Pune, India.

Kehew, A.E. (1982). Catastrophic flood hypothesis for the origin of the Souris spillway, Saskatchewan and North Dakota, Geological Society of America Bulletin 93, 1051-1058 .

Kehew, A.E., and M.L. Lord (1986). Origin and large-scale erosional features of glacial-lake spillways in the northern Great Plains, Geological Society of America Bulletin 97, 162-177 .

Kehew, A.E., and M.L. Lord (1987). Glacier-lake outbursts along the mid-continent margins of the Laurentide ice-sheet, in Catastrophic Flooding, L. Mayer and D. Nash, eds., Allen and Unwin, Boston, pp. 95-120 .

Klemes, V. (1986). Dilettantism in hydrology: Transition or destiny, Water Resources Research 22, 177S-188S .

Klemes, V. (1987). Hydrological and engineering relevance of flood frequency analysis, in Hydrologic Frequency Modeling, V.P. Singh, ed., D. Reidel, Boston, pp. 1-18 .

Klemes, V. (1989). The improbable probabilities of extreme floods and droughts, in Hydrology of Disasters, O. Starosolszky and D.M. Melder, eds., James and James, London, pp. 43-51 .

Knox, J.C. (1983). Responses of river systems to Holocene climates, in Late Quaternary Environments of the United States, Vol. 2 , The Holocene, H.E. Wright, ed., University of Minnesota Press, Minneapolis, pp. 26-41 .

Knox, J.C. (1984). Fluvial responses to small scale climatic changes, in Developments and Applications of Geomorphology, J. E. Costa and P.J. Fleisher, eds., Springer-Verlag, Berlin, pp. 318-342 .

Knox, J.C. (1985). Response of floods to Holocene climate change in the upper Mississippi Valley, Quaternary Research 23, 287-300 .

Knox, J.C. (1993). Large increases in flood magnitude in response to modest changes in climate, Nature 361, 430-432 .

Kochel, R.C., and V.R. Baker (1982). Paleoflood hydrology, Science 215, 353-361 .

Korzarski, S. (ed.) (1983). Palaeohydrology of the Temperate Zone, Quaternary Studies in Poland 4 , Poznan, 261 pp .

Korzarski, S., and K. Rotnicki (1977). Valley floors and changes of river channel patterns in the north Polish Plain during the late Würm and Holocene, Quaestiones Geographicae 4, 51-93 .

Kutzbach, J.E. (1986). The changing pulse of the monsoon, in Monsoons, J.S. Fein and P.L. Stephens, eds., John Wiley & Sons, New York, pp. 247-268 .

Leliavsky, S. (1955). An Introduction to Fluvial Hydraulics, Constable and Co., London, 257 pp .

Lewin, M., G. Macklin, and J.C. Woodward (1991). Late Quaternary fluvial sedimentation in the Voidomatis Basin, Epirus, Greece, Quaternary Research 35, 103-115 .

Lord, M.L., and A.E. Kehew (1987). Sedimentology and paleohydrology of glacial-lake outburst deposits in southeastern Saskatchewan and northwestern North Dakota, Geological Society of America Bulletin 99, 663-673 .

Luo Cheng-Zheng (1987). Investigation and regionalization of historical floods in China, Journal of Hydrology 96, 41-51 .

Maizels, J.K. (1983). Palaeovelocity and palaeodischarge determination for coarse gravel deposits, in Background to Palaeohydrology: A Perspective, K.J. Gregory, ed., John Wiley & Sons, New York, pp. 101-139 .

Malde, H.E. (1968). The catastrophic late Pleistocene Bonneville Flood in the Snake River Plain, Idaho , U.S. Geological Survey Professional Paper 596, 1-52 .

Milliman, J.D., and R.H. Meade (1983). World-wide delivery of river sediment to the oceans, Journal of Geology 91, 1-221 .

Mooley, D.A., and B. Parthasarathy (1984). Fluctuations in all-India summer monsoon rainfall during 1871-1978, Climatic Change 6, 287-301 .

Mueller, E.H., and D.L. Pair (1992). Comment on "Evidence for large-scale subglacial meltwater flood events in southern Ontario and northern New York State," Geology 20, 90-91 .

Nieuwolt, S. (1977). Tropical Climatology, Wiley, London, 207 pp .

O'Connor, J. (1993). Hydrology, hydraulics, and sediment transport of Pleistocene Lake Bonneville flooding on the Snake River, Idaho, in Geological Society of America Special Paper 274, 1-83 .

O'Connor, J.E., and V.R. Baker (1992). Magnitudes and implications of peak discharges from glacial Lake Missoula, Geological Society of America Bulletin 104, 267-279 .

O'Connor, J.E., and R.H. Webb (1988). Hydraulic modeling for paleoflood analysis, the Flood Geomorphology, V.R. Baker, R.C. Kochel, and P.C. Patton, eds., Wiley, N.Y., pp. 393-402 .

Oltman, R.E. (1968). Reconnaissance investigations of the discharge and water quality of the Amazon River, U.S. Geological Survey Circular 552, 1-16 .

Partridge, J.B., and V.R. Baker (1987). Paleoflood hydrology of the Salt River, Arizona, Earth Surface Processes and Landforms 12, 109-125 .

Patton, P.C., V.R. Baker, and R.C. Kochel (1979). Slackwater deposits: A geomorphic technique for the interpretation of fluvial paleohydrology, in Adjustments of the Fluvial System, D.P. Rhodes and G.P. Williams, eds., Kendal/Hunt, Dubuque, Iowa, pp. 225-253 .

Patton, P.C., G. Pickup, and D.M. Proce (1993). Holocene paleofloods of the Ross River, central Australia, Quaternary Research 40, 201-212 .

Pickup, G., G. Allan, and V.R. Baker (1988). History, palaeochannels and palaeofloods of the Finke River, central Australia, in Fluvial Geomorphology of Australia, R.F. Warner, ed., Academic Press, Sydney, pp. 177-200 .

Pitty, A.F. (1971). Introduction to Geomorphology, Methuen and Company, London.

Prell, W.L. (1984). Variation of monsoonal upwelling: A response to changing solar radiation, in Climate Processes and Climate Sensitivity, J. Hansen and T. Takahashi, eds., Maurice Ewing Series No. 5, American Geophysical Union, Washington, D.C., pp. 48-57 .

Rajaguru, S.N., and S.N. Kale (1985). Changes in the fluvial regime of western Maharashtra upland rivers during the late Quaternary, Journal of the Geological Society of India 73, 168-177 .

Riehl, H., and J. Meitin (1979). Discharge of the Nile River: A barometer of short-period climate variations, Science 206, 1178-1179 .

Rotnicki, K. (1983). Modelling past discharges of meandering rivers, in Background to Palaeohydrology, K.J. Gregory, ed., Wiley, Chichester, pp. 321-354 .

Rudoy, A.N. (1988). Regime of glacier-dammed lakes in the intermountain basins of south Siberia, USSR Academy of Sciences: Materials of Glaciological Research 61, 36-42 .

Rudoy, A.N. (1990). Ice flow and ice-dammed lakes of the Altay in the Pleistocene, USSR Academy of Sciences Izvertuya, Seriya geograficheskaya 120, 344-348 .

Rudoy, A.N., and V.R. Baker (1993). Sedimentary effects of cataclysmic glacial outburst flooding, Altay Mountains, Siberia, Sedimentary Geology 85, 53-62 .

Shaw, J. (1989). Drumlins, subglacial meltwater floods, and ocean responses, Geology 17, 853-856 .

Shaw, J., K. Kvill, and B. Rains (1989). Drumlins and catastrophic subglacial floods, Sedimentary Geology 62, 177-202 .

Schumm, S.A. (1965). Quaternary paleohydrology, in The Quaternary of the United States, H.E. Wright and D.G. Frey, eds., Princeton University Press, Princeton, N.J., pp. 783-794 .

Schumm, S.A. (1968). River adjustment to altered hydrologic regimen, Murrumbidgee River and paleochannels, U.S. Geological Survey Professional Paper 598, 1-65 .

Schumm, S.A. (1977). The Fluvial System, John Wiley & Sons, New York.

Schumm, S.A., and G.R. Brakenridge (1987). River responses, in North America and Adjacent Oceans During the Last Deglaciation, W.F. Ruddiman and H.E. Wright, Jr., eds., The Geology of North America K-3, Geological Society of America, Boulder, Colorado, pp. 221-240 .

Shi Fucheng, Yi Yuanjun, and Han Manhua (1987). Investigation and verification of extraordinary large floods on the Yellow River, Journal of Hydrology 96, 69-78 .

Smith, A.M. (1991). Extreme palaeofloods: Their climatic significance and the chances of floods of similar magnitude recurring, South African Journal of Science 87, 219-220 .

Smith, A.M. (1992). Holocene palaeoclimatic trends from palaeoflood analysis, Palaeogeography, Palaeoclimatology, Palaeoecology 97, 235-240 .

Smith, A.M. (1993). Missoula flood dynamics and magnitude inferred from sedimentology of slack-water deposits on the Columbia Plateau, Washington, Geological Society of America Bulletin 105, 77-100 .

Starkel, L. (1983). The reflection of hydrologic changes in the fluvial environment of the temperate zone during the last 15,000 years, in Background to Palaeohydrology, K.J. Gregory, ed., Wiley, Chichester, pp. 213-235 .

Starkel, L. (1993). Late Quaternary continental paleohydrology as related to future environmental change, Global and Planetary Change 7, 95-108 .

Starkel, L., and J.B. Thornes (eds.) (1981). Palaeohydrology of River Basins: Guide to Subproject A, IGCP Project 158, On Palaeohydrological Changes in the Temperate Zone in the

Last 15,000 Years, British Geomorphological Research Group Technical Bulletin 28, 107 pp .

Starkel, L., K.J. Gregory, and J.B. Thornes (eds.) (1991). Fluvial Processes in the Temperate Zones, Wiley, Chichester.

Stedinger, J.R., and V.R. Baker (1987). Surface water hydrology: Historical and paleoflood informations, Reviews of Geophysics 25, 119-124 .

Teller, J.T. (1987). Proglacial lakes and the southern margin of the Laurentide Ice Sheet, in North America and Adjacent Oceans During the Last Deglaciation, W.F. Ruddiman and H.E. Wright, Jr., eds., The Geology of North America, K-3, Geological Society of America, Boulder, Colorado, pp. 39-69 .

Teller, J.T. (1990). Volume and routing of late-glacial runoff from the southern Laurentide Ice Sheet, Quaternary Research 34, 12-23 .

Tricart, J. (1985). Evidence of upper Pleistocene dry climates in northern South America, in Environmental Change and Tropical Geomorphology, I. Douglas and T. Spencer, eds., George Allen and Unwin, London, pp. 197-217 .

Velichko, A.A., L.L. Isayeva, V.M. Makeyev, G.G. Matishov, and M.A. Faustova (1984). Late Plestocene glaciation of the Arctic Shelf, and the reconstruction of Eurasian ice sheets, in Late Quaternary Environments of the Soviet Union, A.A. Velichko, ed., University of Minnesota Press, Minneapolis, pp. 35-44 .

Waitt, R.B. (1985). Case for periodic, colossal jokulhlaups from glacial Lake Missoula, Geological Society of America Bulletin 95, 1271-1286 .

Webb, R.H. (1985). Late Holocene Flooding on the Escalante River, South-Central Utah, Ph.D. dissertation, University of Arizona, Tuscon, 204 pp .

Wells, L. (1987). An alluvial record of El Nino events from northern coastal Peru, Journal of Geophysical Research 92, 14,463-14,470 .

Williams, G.P. (1983). Paleohydrological methods and some examples from Swedish fluvial environments. I. Cobble and boulder deposits, Geografiska Ann. 65A, 227-243 .

Williams, G.P. (1984). Paleohydrological equations for rivers, in Developments Applications of Geomorphology, J.E. Costa and P.J. Fleisher, eds., Springer-Verlag, Berlin, pp. 343-367 .

Williams, M.A.J. (1985). Pleistocene aridity in tropical Africa, Australia, and Asia, in Environmental Change and Tropical Geomorphology, I. Douglas and T. Spencer, eds., George Allen and Unwin, London, pp. 221-233 .

Wohl, E.E. (1988). Northern Australian Paleofloods as Paleoclimatic Indicators, Ph.D. dissertation. University of Arizona, Tucson, 285 pp.

Wohl, E.E. (1992a). Bedrock benches and boulder bars: Floods in the Burdekin Gorge of Australia, Geological Society of America Bulletin 104, 770-778 .

Wohl, E.E. (1992b). Gradient irregularity in the Herbert Gorge of northeastern Australia, Earth Surface Processes and Land-forms 17, 69-84 .

Wohl, E.E., N. Greenbaum, A.P. Schick, and V.R. Baker (in press). Controls on bedrock channel incision along Nahal Paran, Israel, Earth Surface Processes and Landforms.

Wolman, M.G., and J.P. Miller (1960). Magnitude and frequency of forces in geomorphic processes, Journal of Geology 68, 54-74 .

Yarnal, B. (1985). Extratropical teleconnections with El Niño/Southern Oscillation (ENSO) events, Progress in Physical Oceanography 9, 315-352 .

7

Sediment Fluxes Along High-Latitude Glaciated Continental Margins Northeast Canada and Eastern Greenland

JOHN T. ANDREWS
University of Colorado
J. P. M. SYVITSKI
Geological Survey of Canada

ABSTRACT

In the northern hemisphere, glaciated continental margins occur around Greenland, eastern and northern Canada, Norway, Iceland, Spitsbergen, Alaska, and British Columbia, where frequently glaciers and ice sheets terminate(d) at tidewater. The continental shelf may have deep basins parallel to the coast, troughs cut across the shelf, and fiords that extend inland 10 to 100 km from the outer coast. The processes that control the fluxes of sediment to the seafloor during the past deglacial cycle are radically different than those that occurred on continental shelves that lay beyond the limits of glaciation. This is associated with the rate and manner of sediment delivery; the presence of deep basins landward of the shelf break; and a different history of relative sea-level. On time scales of the past 10 ka (ka = 1000 yr), the net flux of sediment to the seafloor can be derived from radiometrically dated cores, or can be modelled. In the eastern Canadian Arctic, the net average net flux to the seafloor varied between 600 and 1300 $kg/m^2/ka$ in the outer fiord basins, to about 400 $kg/m^2/ka$ in shelf/troughs, to 0 to 50 kg/m^2 on the shelf proper. In these fiords, the dominant grain-size delivered to the seafloor is clay, followed by silt and sand. The data suggest that the flux to the seafloor declines exponentially with a "half-distance" of 30 to 40 km. In a large trough off southeast Greenland, the net average flux to the seafloor over the past 8 ka only averaged about 60 $kg/m^2/ka$.

INTRODUCTION

Highly indented fiord coastlines constitute a large proportion of the world's coastline. Fiords (Figure 7.1) are major sediment traps in the terrestrial to deep-sea sediment pathway, and the presence of these basins, landward of the continental shelf, suggests that adjacent shelves and deep-sea basins are presently largely deprived of terrestrial sediment. Based on an estimate of the total volume of later Quaternary (past 100 ka) sediments in fiords, compared to the flux of sediment effluxed from and to the sea during this same interval, fiords have retained 24 percent of the volume of marine sediment deposited over the past 100 ka (Syvitski *et al.,* 1987a, pp. 10-11).

In the past two years, there have been several international symposia on glacial marine sediments and processes, and several major review papers have been published that seek to synthesize our knowledge of these processes and
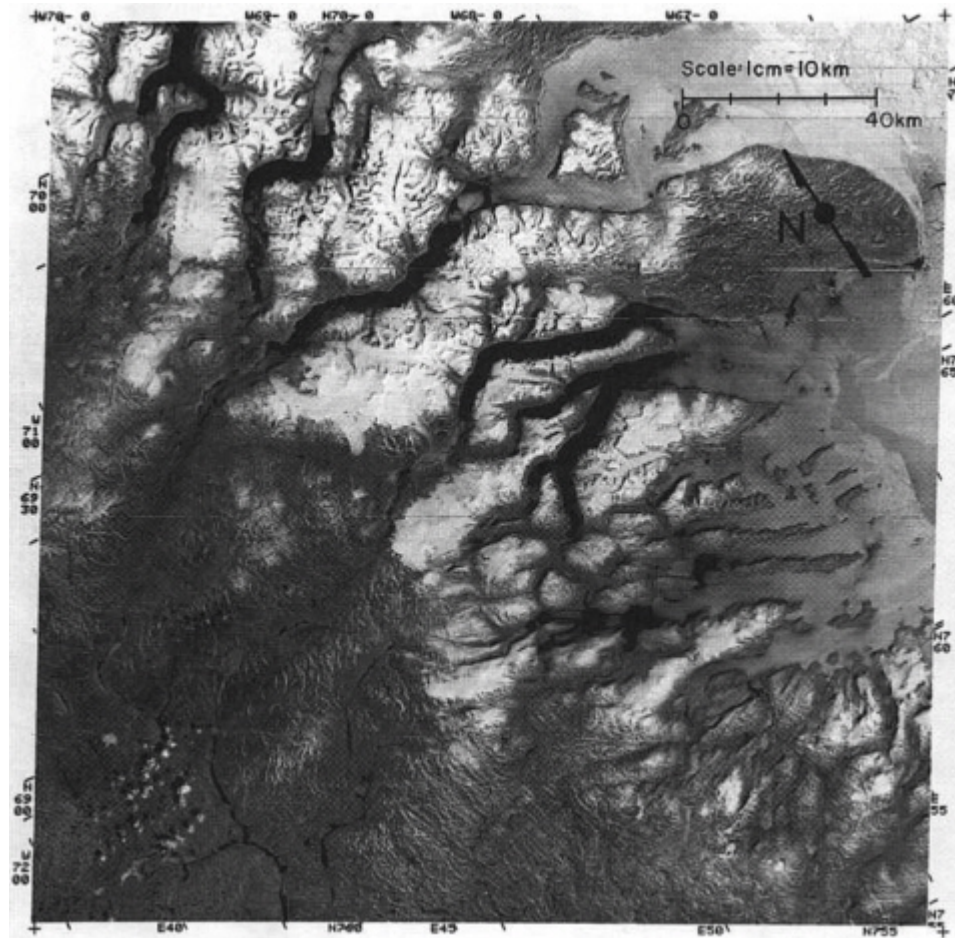
FIGURE 7.1 LANDSAT image of the fiord coast of east Baffin Island, showing the sea ice breaking up (July 22, 1977) and the relatively restricted extent of local ice caps and glaciers.

propose appropriate stratigraphic models (e.g., Andrews and Matsch, 1983; Gilbert, 1983; Molnia, 1983; Elverhoi, 1984; Powell, 1984; Eyles *et al.,* 1985; Dowdeswell, 1987; Powell and Molnia, 1989), yet there is very little information, on a regional scale, of the flux of sediment within the glacial marine environment, especially on time scales of a few thousand years. However, Ruddiman (1977) and Fillon (1985), amongst others, computed the net flux of sand-size particles (ice rafted detritus, IRD) to the North Atlantic deep basins. We confine our discussion, therefore, to areas where we have worked and where such data are available.

This chapter presents data on the flux of sediment to the seafloor along fiord to shelf transects. It thus forms a link between current debates on the efficiency and magnitude of glacial erosion and transfers of sediment to deep sea basins (cf., Laine, 1980; Bell and Laine, 1985; Andrews *et al.,* 1985a). The chapter has two approaches: in the first section we examine the processes that produce sediment along glaciated continental margins and suggest a space-time ranking of these for sediment accumulation. We also examine the climatic and glaciological controls on sediment flux. In the second part, we illustrate some of these aspects by examining two specific regions, the first being the borderland of the eastern Canadian Arctic, fronting Baffin Bay, and the second being part of the East Greenland shelf. The latter area is an analog of the conditions that prevailed in the Canadian Arctic during the last glacial cycle. These areas represent subpolar to polar glaciological environments and contrast (see later) with more active environments in southern Alaska.

OVERALL CONTROLS ON SEDIMENT FLUX

Sediment flux is defined as sediment mass per unit area with respect to time. We normally measure the net flux of sediment to the seafloor, that is kg/m^2 per unit time, hereafter termed $F_n\downarrow$. Consider Figure 7.2 — this shows the direction of sediment fluxes along a fiord to shelf transect. The vertical flux of sediment between two points along this transect is defined as the level of reduced suspended sediment inventory (I in units kg/m^2) throughout the water column between these two points. If $dI/dt = \lambda I$, where λ is a first order removal rate constant, then $F_f\downarrow$, defined as the net downward flux of sediment can be expressed as $F_f\downarrow(x) = F_{f0}e^{-\lambda t}$, where F_{f0} is maximum sedimentation rate at the fiord head (Syvitski *et al.,* 1988).

However, we have an additional flux of sediment ($F_s\downarrow$) being contributed from the shelf (iceberg melting, current resuspension, iceberg ploughing, etc.) and also from local disturbances ($F_1\downarrow$), say between x_3 and x_4 (Figure 7.2), due to gravity flow deposition which delivers sediment to the fiord basins (Syvitski, 1989). Thus, the net sediment accumulation is the resultant of the three sources plus allochthonous (carbon and silica) deposition, minus losses due to erosion (F_r), so that: and over some interval of time the total mass of sediment (kg per meter width per unit time) contributed to the sea-floor would be:
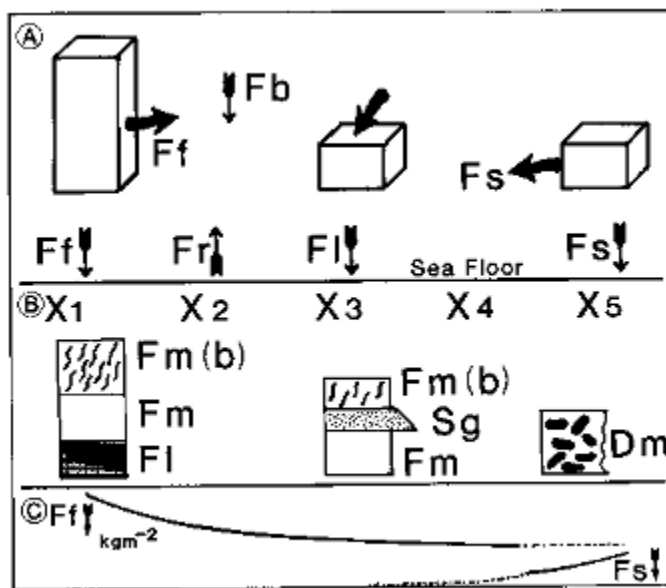
FIGURE 7.2 Diagram illustrating (A) the components in sediment flux along a fiord to shelf transect and (B) the expected sediment types (see text for discussion). The lowermost section (C) schematically shows the expected trends of $F_f\downarrow$ and $F_s\downarrow$, which are the trends in sediment flux from the fiord and shelf, respectively.

$$F_n\downarrow = F_f\downarrow + F_s\downarrow + F_1\downarrow + F_b\downarrow - F_r\uparrow \qquad (7.1)$$

$$T_n\downarrow = \int F_n\downarrow d(x) \qquad (7.2)$$

In this chapter we ignore the carbon flux to the sea floor because, although it is important, it is usually less than 1 percent dry weight of the sediment (Andrews, 1987a; Syvitski *et al.,* 1989, 1990). A potentially more serious matter is the absence of a measure of the biogenic silica flux, although we know from the work of Williams (1988) that this can be substantial.

Two critical factors become important in determining the amount of suspended sediment that escapes from the fiord to the adjacent shelf: (1) the length of the fluvial plume, and (2) the length of the fiord basin. The plume length is primarily a function of the freshwater discharge but the fiord length is an independent variable. For example, the fiords of southwest Greenland are about twice as long as the northeast Baffin fiords, fluvial input is 2 to

5 times larger in southwest Greenland and plume lengths are about twice those observed in Baffin. The net result is that the amount of sediment effluxed from the fiord onto the shelf is about the same in both areas.
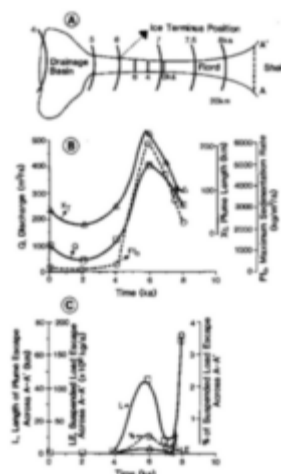
FIGURE 7.3 A. Output from a modeling exercise involving (A) retreat of a fiord glacier through time with a climate equivalent to the eastern seaboard of Baffin Island at present. B. Calculated parameters as a function of time (X T, plume length; Q, discharge; and Ff_0, maximum sediment flux). C. The calculated escape of sediment from the fiord to the shelf across profile A-A' (see Figure 7.3A).

Figure 7.3 is a model run (Syvitski *et al.,* 1988) based on the retreat of a tidewater glacier that started 8 kaBP (before present), was subaerial by 6 kaBP, and finally left the drainage basin less than 4 kaBP. Discharge is based on the present climate of northeast Baffin Island (Figure 7.4) with allowance for ice melt and storage during glacial retreat and the Little Ice Age growth and retreat. From these data the plume length (Figure 7.3B) is calculated as is the maximum fiordhead sedimentation rate, F_{f0}. Figure 7.3C illustrates the length of the plume escaping through section A-A' and the associated volume of sediment (LE) that escapes. Only between 7.5 and 8 kaBP is this escape volumetrically significant, at 3.5 percent of the total fluvial suspended sediment output. Depending on the rate of sediment accumulation, sediment rain-out results in finegrained massive to bioturbated muds (e.g., Hein and Longstaffe, 1985; Syvitski *et al.,* 1989).

The system described on Figure 7.2 results in an exponential decrease in the flux to the seabed along a fiord axis (Elverhoi *et al.,* 1980; Elverhoi, 1984; Pfirman, 1985; Syvitski, 1986; Syvitski *et al.,* 1988). In areas where there is a large number of icebergs drifting along the shelf and into the outer fiords (east Baffin Island and East Greenland) the sediment would coarsen seaward and diamict might be deposited on the shelf because F_n¬ has a significant component of the F_s¬ flux (Figure 7.2)(e.g., Kravitz, 1982). Finally, local debris and mass-movements would result in slumps and/or graded sand beds. Thus, sediment type and
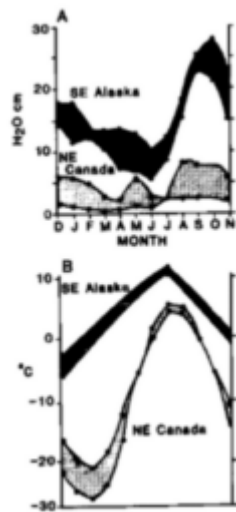
FIGURE 7.4 Climatic range of variables from weather stations along the Baffin Island seaboard compared to climatic data from sites in southeast Alaska (A, precipitation; B, temperature; both monthly averages) in contrasting fiord environments.

the three-dimensional architecture of the basin fills (as portrayed in high resolution seismic profiles) should provide a guide to the processes that resulted in net sediment accumulation at a site (cf., Syvitski, 1989). For example, the difference between draped and ponded sequences indicates a large-scale difference in the dominance of the rain-out of suspended particulates ($F_r\downarrow$) versus the focusing of sediment into basins through various gravity flow processes ($F_1\downarrow$) (Figure 7.2).

Processes

The net sediment flux along glaciated coastlines is a function of (1) local bathymetry and topography; (2) regional extent of glacierization; (3) thermal conditions at the bed and surface of the ice (this controls the manner of sediment supply within the ice and the amount of meltwater that is generated); (4) terrestrial and marine climate, including currents; (5) sea ice and iceberg production and spatial extent; (6) sediment and vegetation cover on land; and (7) relative sea-level history. These controls operate differently through space and time with variations forced by the position of the ice front and the history of relative sea-level.

Bathymetry and Topography Figure 7.5 is a sketch of a glaciated continental borderland, especially those of passive, rifted plate margins. The key bathymetric elements are the fiord basin(s), marginal troughs that lie along geological contacts, and cross troughs that cut across the shelf to the slope. If these were all part of an integrated sediment transport and storage system the cross troughs would head into the fiords; however, as illustrated on Figure 7.6, this is frequently not the case, at least on the shelf fringing east Baffin Island. For example, Figure 7.6 illustrates that the largest fiord in the region is not connected to the adjacent trough. The meaning of this in terms of trough genesis is not clear. The marginal trough (Figure 7.5) is a feature of the Labrador, Norwegian, and West Greenland shelves (Holtedalh, 1958), but they do not occur off Baffin Island. Fiords may or may not have a sill at their mouth (Dowdeswell and Andrews, 1985; Syvitski *et al.* 1987a) and they can consist of a single basin or several basins. The adjacent continental shelves are often marked by distinct "banks" where water depths are <200 m.
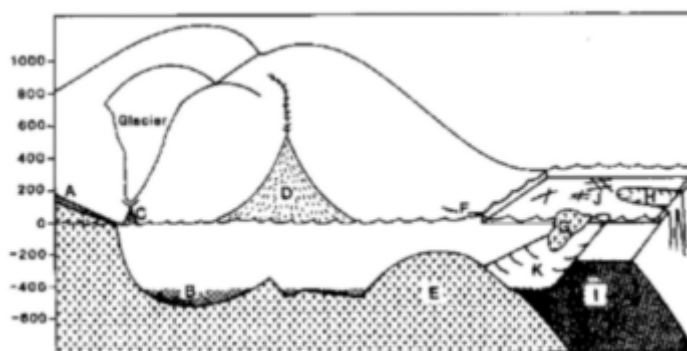
FIGURE 7.5 Schematic sketch of typical features from a fiord head to the adjacent deep-sea basin along a deglaciated coast (NE Canada). A, raised glacial and marine sediment at fiord head; B, basin fill; C and D, coarse fans; E, shield rocks; F, raised beaches and glacial sediments; G, iceberg: H, shelf trough; I, offshore coastal plain sediments; J, iceberg scour marks; K, marginal trough and fill.

Climate and Oceanography Figure 7.4 illustrates the differences in temperature and precipitation between two contrasting glaciated borderlands — one from the eastern Canadian Arctic and the other from southeast Alaska. The former area is characterized by very cold winters, cool summers with average July temperatures of 5° to 7°C, a mean annual temperature (MAT) of -12°C at sea level,
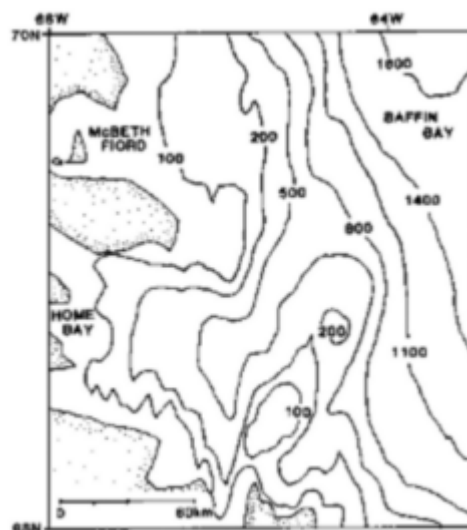
FIGURE 7.6 Bathymetry of the fiord mouths, and shelf in the vicinity of McBeth Fiord, Baffin Island. Note the angle that the shelf troughs make with the fiords. Contours are in meters.

and low annual precipitation receipts of ca. 300 mm. In contrast, the southeast Alaska climate is a cool, wet maritime climate (Figure 7.4). These differences translate into large differences in glaciological regimes, the potential for glacial erosion, and in an order-of-magnitude difference in the volume of meltwater generated by both snow and ice melt (Syvitski *et al.,* 1987a; Powell and Molnia, 1989). An additional major difference between these regimes (Figure 7.4) is that the production of run-off from snow/ice melt and rainfall is restricted to around 90 days in the eastern Canadian Arctic but is potentially year-round in southeast Alaska.

Strong winds are a feature of areas adjacent to ice sheets and glaciers. This, combined with limited vegetation cover, suggests that, in our area of interest, eolian deflation of outwash sediments is a component in highlatitude sediment flux calculations (cf., Gilbert, 1982, 1983; Syvitski and Hein, 1991).

The extent of sea ice (Figure 7.1) and icebergs is extremely different from area to area. The former is related to the air temperature, wind stress, and temperature of the surface layer of the shelf watermass. The size and durability of icebergs is also a matter of air temperature, wind regime, and the character of the source glacier (Dowdeswell and Murray, 1989). Icebergs from fast-moving tidewater glaciers are relatively small, especially compared with the massive icebergs that are produced from outlet glaciers of the Greenland Ice Sheet. A landfast sheet of sea ice during the winter months (Figure 7.1) serves to buffer glacier margins from wave attack, reduces the calving rate, and restricts iceberg passage for several months per year.

Glaciology and Hydrology The critical aspects of glaciology and hydrology for marine sediment flux studies are the mass balance gradient, the thermal conditions at the ice surface and base, the percentage of the basin that is glacierized, and the location and shape of the terminus — does it end in tidewater or on land, and does it have ramp or shelf, or end as a near vertical face? The presence of ice in a drainage basin can extend both the volume of meltwater discharge, by amounts proportional to the area covered by ice, and may also extend the duration of nival and ice associated runoff. However, the origin of sediment carried in the meltwater streams depends on the thermal conditions of the ice body. In temperate areas, with MATs close to 0°C, surface run-off is produced in summer by ablation; this water drains into the glacier and moves toward the ice front in englacial or subglacial conduits. At the base of the glacier, it adds to water already at the bed which has been produced by melting associated with the geothermal heat flux and the frictional heat generated by the ice sliding over its bed. These combined sources result in an annual melt rate at the bed of between <1 mm to several centimeters (Drewry, 1986). By contrast, subpolar environments with MATs << 0°C have meltwater generated on the surface which runs off in supraglacial stream channels on the ice surface. If the supraglacial stream reaches a lateral margin of a glacier it will run along the glacier in a marginal or submarginal drainage channel. Thus, in a temperate glacier, the meltwater reaches the bed of the glacier and can remove fine-grained sediment produced by glacial abrasion and crushing. However, in subpolar glaciers the surface streams are either very clean (if they run over the glacier) or turbid if they can erode sediment along the side of the glacier.

Because of ice convergence into fiords, it is rare to find outlet glaciers reaching the sea that are not at the pressure melting point (PMP) at their beds. Thus, most tidewater glaciers probably discharge water into the sea from basal melt, which rises as a freshwater plume (Pfirman, 1985). Depending on the sediment load, some sediment may be transported via underflows or interflows.

In fiord basins dominated by meltwater there are significant differences between regimes where the fiord is occupied by one or more tidewater glaciers, compared to the situation where the glaciers terminate on land (Syvitski *et al.,* 1988; Syvitski, 1989). In the first situation, sediment deposition is controlled by (1) processes at the ice front (sub-and englacial-meltwater discharge; the flow of supraglacial till, etc.); (2) hemipelagic sedimentation from the fluvial plume; (3) sediment rafting by icebergs and sea ice; and (4) deep-water currents. In contrast, when glaciers end on land, the dominant sediment supplies are from: (1) bedload dumping from the delta front; (2) hemipelagic sedimentation under the seaward flowing river plume; (3) proximal slope bypassing by turbidity currents; and (4) the combined effects of both short- and long-term downslope diffusion of the accreting sediment mass. There is a significant difference in the grain-size distributions between these two cases for the suspended sediment plume (Pfirman, 1985). This is related to the energy loss from a rapidly rising plume (from a subglacial position) compared to the normal fluviodeltaic discharge to the fiord head (Syvitski, 1989). Thus, for a given level of discharge, coarser sediments are deposited closer to the tidewater glacier, whereas equivalent size particles can ride the freshwater surface plume seaward in the fluviodeltaic fiord.

A third glaciological situation exists in true polar climates (i.e., Antarctica), where even in summer no surface melting takes place; basal melting is possible only if the glacier is sliding over its bed.

In the discussion above, we have implicitly assumed that the bulk of glacial sediment is being delivered to the marine environment via meltwater. An alternative delivery system has been proposed, based on theory and limited observation (cf., Boulton and Jones, 1979; Blankenship *et al.,* 1986). This suggests that a glacier may lie on a deformable sediment bed which is transported seaward by

deforming under the ice load. In the Antarctic, where this mechanism has been advocated for a specific ice stream, the deforming sediment is being moved toward the ice front at a rate of >1 km/yr! This process suggests that at the front of fast moving ice streams there may be very large accumulations of ice transported sediment.

Relative Sea-Level History The relative sea-level history against a coast backed by a major continental ice sheet is fundamentally different than that on continental shelves removed from the influence of glacial isostatic depression (e.g., Andrews, 1980; Schlee *et al.,* 1988). This difference is significant in terms of sediment flux. During times of global glaciation, sea-level is lowered by 100 to 120 m on "distant" shelves and the coastal plain sediments are reworked and transported to the shelf edge and beyond (cf., Schlee *et al.,* 1988). In contrast, along glaciated continental margins, *relative* sea-level was 30 to 100 m higher during glacial advances because of isostatic depression. This resulted in large quantities of coarse outwash and deltaic sediments being stored at fiord and bay-heads (Figure 7.7) as the ice retreats inland (Church, 1972; Church and Ryder, 1972; Syvitski *et al.,* 1987a). However, subsequent isostatic recovery was rapid, and rivers cut into these valley/fiord fills (Figure 7.7) resulting in erosion and recycling of outwash and raised glacial marine sediments.

The Deglacial Sediment Flux Cycle The flux of sediment from glaciated margins to the marine environment is a function of five major processes that vary spatially and temporally through a glacial to interglacial cycle, i.e., the past 10 ka (Figure 7.8). This interval includes the period of "paraglaciation" (Church and Ryder, 1972) which, on land, is characterized by the deposition of massive deltas, fans, and outwash trains, and more recently, the interval "neoglaciation" which is associated with the growth and expansion of valley glaciers and ice sheets. Note that in Figure 7.8, we are considering the simplest possible case — a fiord with no significant sidevalley sediment sources.

On Figure 7.8 we show two major variables; the first is glacier extent; the second is the change in relative sea level. The five major processes that contribute to the net sediment flux are: rain-out of suspended sediment from glacial and snow meltwater; the reworking of deltas and outwash trains because of glacial isostatic recovery (Figure 7.7) (associated with a regional *fall* in sea level); rafting from icebergs and sea ice and associated ploughing and disturbance of sediment by reworking (e.g., MacLean, 1985; Josenhans *et al.,* 1986; Praeg *et al.,* 1986; Barnes and Lien, 1988; Pereira *et al.,* 1988); eolian transport (Gilbert, 1982, 1983); and turbidites and debris flows. These processes changed in intensity through the last deglacial cycle (Figure 7.8). The figures on the axes of the sediment processes (10, 1, etc.) represent order of magnitude estimates of the importance of the process to the net $F_n\downarrow$.

An additional factor that is hard to forecast is the effect of earthquakes on sediments. The northeast shelf of Baffin Island is in a high seismicity zone (Adams and Basham, 1989); high magnitude events (for example, the M7.3 event in 1933) could well trigger large slumps and slides throughout the fiord/shelf system.

FIGURE 7.7 Photograph of raised glacial marine sediments that have been eroded by river incision associated with 60 m of glacial isostatic rebound (Home Bay, east Baffin Island) over the past 6 to 8 ka.
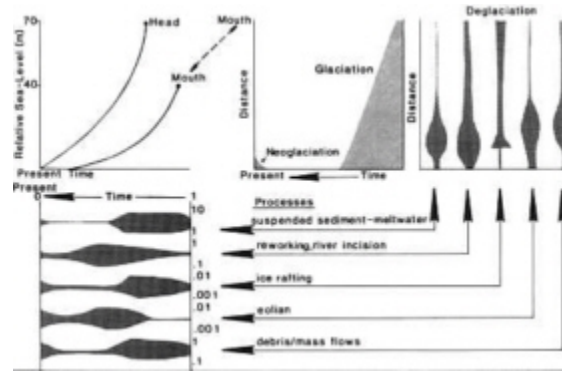
FIGURE 7.8 Sketches of some of the major processes affecting sedimentation along continental glaciated margins such as NE Canada, Greenland, and W. Norway. The rate of sedimentation associated with each is shown in a relative sense versus time and distance from the major sediment source.

DEGLACIAL TO INTERGLACIAL FIORD/SHELF SEDIMENT FLUX

In this section we examine data from the fiords and shelf of the eastern Canadian Arctic (Figures 7.1 and 7.4) and off East Greenland (Figure 7.9) as being broadly representative of both rates and processes in subpolar, arctic conditions. Fluxes in Alaskan fiords are significantly higher (Molnia, 1983; Powell, 1983; Powell and Molnia, 1989).

East Baffin Island

One of the objectives of the Canadian Sedimentology of Arctic Fjords Experiment (SAFE) (Syvitski and Schafer, 1985) was to provide information on modern and late Quaternary sediment processes and fluxes. The various sediment types, or facies, associated with these processes (Figure 7.2) have been identified by Gilbert (1983), Hein and Longstaffe (1985), Syvitski *et al.* (1987b), and Eyles *et al.* (1987), among others. The occurrence of different facies within the fiords, and on the shelf, can be evaluated by a combination of an analysis of high resolution, deep tow seismics (DTS) (e.g., Figure 7.10), and piston coring.

Figure 7.11 shows how the distribution of glaciers and mountains (cf., Figure 7.1) influence the flux of water and sediment from the land to Itirbiling Fiord. The annual present sediment flux into the fiord is estimated at 3.35 million tonnes, of which 83.7 percent is in the form of bedload, 10.7 percent is through eolian transport, and only 5.6 percent is fluvially delivered suspended load (Syvitski, unpubl.). In the inner basin, sedimentation is dominated by gravity flows that are initiated from failure of the delta front, whereas the distal basins are affected by hemipelagic sedimentation of suspended load, eolian sands and silts that have not been scavenged from the surface plumes, and intermittent delivery of mixed grain-size sediments from the melting of icebergs and sea ice. Sediment traps moored in 50 m of water and 0.5 km from the head of Itirbilung Fiord (Figure 7.11) for 39 days in mid- to late summer,
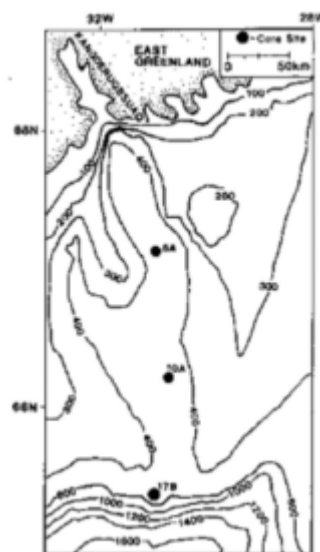
FIGURE 7.9 Map of shelf and trough off East Greenland. Core location is shown and discussed in the text. Contours are in meters.
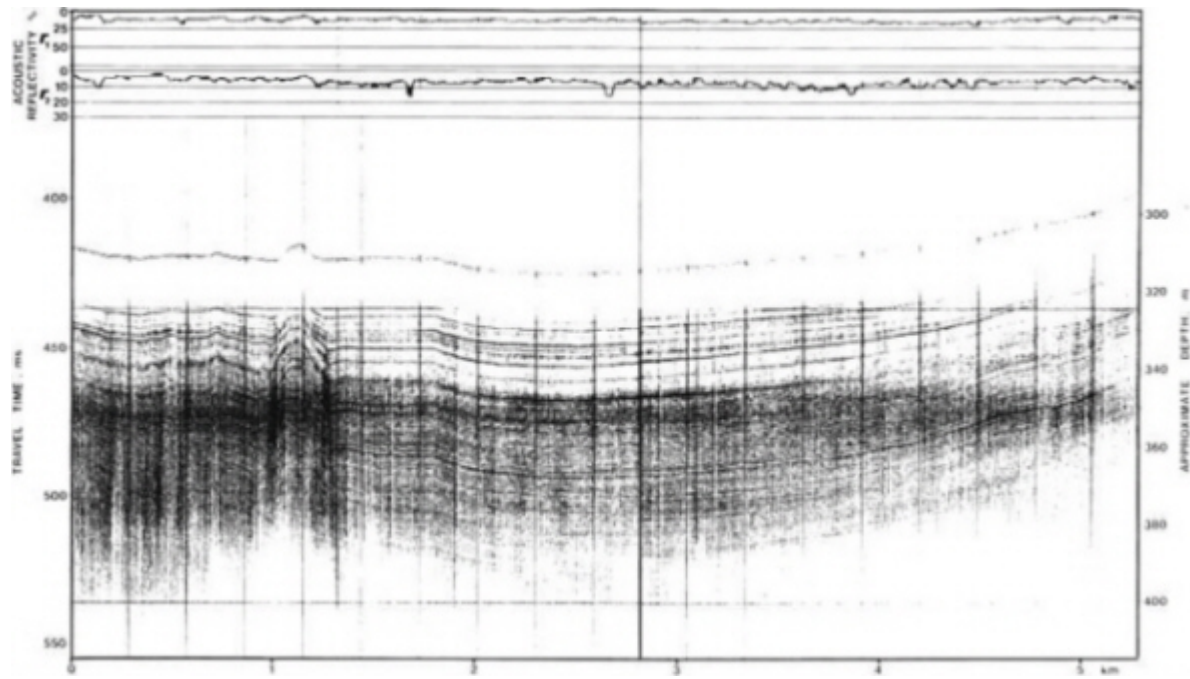
FIGURE 7.10 Huntec DTS record of a fiord basin fill. The record is from McBeth Fiord and shows an acoustically well-stratified sediment with some prominent and continuous reflectors.

1985, collected sediment at a rate of 1.2 kg/m² per day; if we assume this rate applies for a 90-day period, then the "annual" accumulation in the inner basin is 110 kg/m².
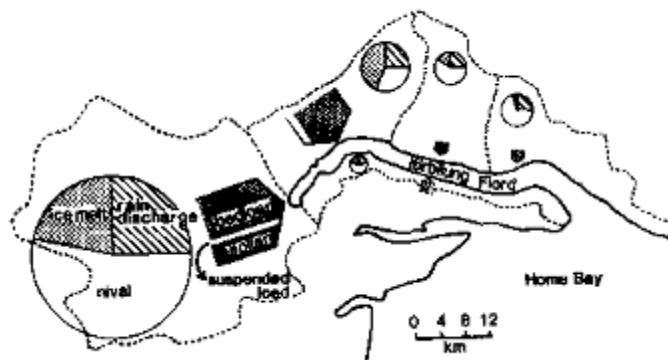
FIGURE 7.11 Itirbilung Fiord, eastern Baffin Island, showing estimated contributions of runoff into the fiord from the different drainage basins and sediment contribution to the fiord.

These estimates (Figure 7.11) reflect current conditions and a fiord dominated by fluvial discharge. However, at 8 to 10 kaBP the fiords of eastern Baffin Island contained large tidewater glaciers and the transition from tidewater to terrestrial glaciers probably occurred ca. 7 kaBP (Andrews, 1990)(see also Figure 7.3A).

In order to determine sediment flux we need information on (1) sediment bulk density, and (2) numeric ages at different levels in cores. The *first* requirement has been met by on-board sampling of sediment in 10 cm Lehigh cores (1 to 3 m length) (Reasoner and Hein, 1984), or by determinations on the piston cores. In the latter we have worked on material specifically sampled for mass physical properties and, in addition, we used sediment collected in 3.15 cc paleomagnetic boxes (cf., Andrews *et al.,* 1986; Andrews and Jennings, 1987) to derive wet volume density (Figure 7.12), which was then converted to dry volume density estimates (Figure 7.13). The *second* requirement is not trivial because the majority of cores from the fiords lacked calcareous foraminifera, so we are unable to date the cores by the accelerator mass spectrometry (AMS) radiocarbon method on 2 to 4 mg samples of hand-picked foraminifera (cf., Andrews *et al.,* 1989a). We had to rely on AMS dates on the acid-insoluble organic matter (AIOM) fraction. We knew from experiments (Andrews *et al.,* 1985b) that these dates were too old; however, a statistical relationship did exist between paired dates on shells and the AIOM fraction. We have used this correction and investigated its applicability by analysis of the geomagnetic secular variations (Andrews *et al.,* 1986) of piston cores. The results indicated that the corrected ¹⁴C dates provided a "reasonable" chronology from 7 to 12 ka. This conclusion was also supported by the pollen and dinoflagellate biostratigraphy (Short *et al.,* 1989). The raw dates and further discussions are included in Jennings (1986), Andrews (1987b; 1990), and Andrews *et al.* (1989a).

Most cores have three ¹⁴C dates that cover the past 10 ka, hence we feel it is most appropriate to consider the sediment flux in appropriate 2 to 5 ka time-slices. Analysis of the contributions of the various measurement errors to errors in estimation indicates that the 95 percent confidence limit in estimating the sediment accumulation (age ± 20 percent and dry volume density ± 10 percent) is ± 14 percent, and no worse than ± 20 percent (Taylor, 1982).

On Figure 7.14 we show a generalized profile for McBeth and Itirbilung fiords (Figure 7.1) and the $F_n\downarrow$ of sediment in the fiord to shelf transects. The data have been divided into four intervals, i.e., the past 10 ka, and then the periods between 8 to 10 kaBP (the glacial/deglacial transition), 5 to 8 kaBP (paraglaciation, i.e., massive meltwater delivery), and 0 to 5 kaBP (neoglaciation). These broad intervals are appropriate given the number of dates per core (about 3) and the problems in radiocarbon dating.

We are now in a position to discuss changes in categories of $F_n\downarrow$; that is, we can convert percentage data on grain size—clay- and silt-size mineralogy (Andrews *et al.,* 1989b)—into fluxes and examine variations during the last deglacial cycle. A critical question is: Can we differentiate the sediment sources by considering changes in specific grain-size, mineral suite, or sediment type?

There are few data on the grain-size characteristics of suspended sediment in glacier meltwater (e.g., Church and Gilbert, 1975; Pfirman, 1985; Gurnell and Clark, 1987; Syvitski *et al.,* 1987b) but an indicator of glacial meltwater activity may be the percentage of coarse silt (Figure 7.15), although this can be influenced by a number of other factors. Coarse silt percentages vary between ca. 2 and 25 percent; there is a consistent difference in the coarse silt seafloor flux between McBeth and Itirbilung fiords (Figure 7.15), although the amount of coarse silt in IT3.1 is markedly different from all other cores. The sample interval employed for the grainsize data on Figure 7.15 is too coarse to be a measure of glacial meltwater variations on a 100-year interval.

Several studies have shown that detrital carbonate is significantly higher on the shelf than in the fiords (Jennings, 1986; Andrews *et al.,* 1989b) and that this reflects the transport of ice eroded sediment from Paleozoic basins in northwest Greenland and the high Canadian Arctic. Carbonates are absent within the fiords and detrital carbonate may reflect a shelf ® fiord sediment transfer (e.g., Jennings, 1986; Andrews *et al.,* 1989).

The 100-km transect from McBeth Fiord (Figure 7.14) includes the outer basin and adjoining shelf. Four cores are available (Table 7.1); the shelf core (HU78-36) has a basal date on shell of 11,770 ± 550 yr (GX-6280) and appears to

have a complete Holocene foraminifera record, although net loss of sediment at times is inferred (Osterman and Nelson, 1989). The fiord head is located 80 km from core HU83-MC4.1 (Figure 7.14). The net total flux of sediment to the seafloor over the past 10 ka varied between 5900 and 950 kg/m^2 with an approximate "half-distance" of 30 km. The $F_{n\downarrow}$ of sand increased between MC4.1 and MC83.6 perhaps suggesting that the sand in the latter core must be derived from the shelf or local sources. During the local glacial/interglacial transition, between 10 and 8 ka. the $F_{n\downarrow}$ at the most ice proximal site, MC4.1, was 1500 kg/m^2 and 1000 kg/m^2 at MC83.6. Clay-size sediment was the major size fraction at MC4.1, whereas at MC83.6 the sediment was about equal in terms of sand/silt/clay. During the next 3 ka, the Laurentide Ice Sheet was melting rapidly across the eastern Canadian Arctic (cf., Dyke, 1974; Dyke and Prest, 1987) and glaciers retreated to the fiord heads and beyond. The fiord to shelf sediment flux gradient of $F_{n\downarrow}$ increased so that the accumulation of 1900 kg/m^2 at MC4.1, and 1500 kg/m^2 at MC7, is matched by only 480 kg/m^2 at MC83.6 (Figure 7.14). Little sand, relative to other sizes, was reaching the seafloor during this period at any site. Finally, local mountain glaciers expanded during the past 5 ka, the so-called "neoglaciation" (Andrews, 1982; Davis, 1985); the supply of sand at MC4.1 shows a dramatic increase (Figure 7.14), which probably represents the input of sediment from local glaciers and glacial fluvial runoff (Andrews, 1990).
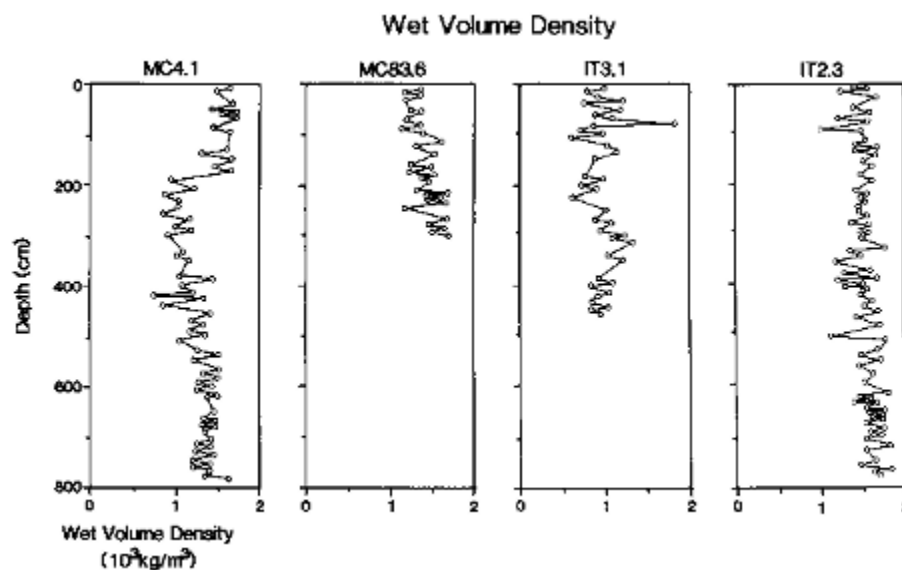
FIGURE 7.12 Downcore variations in wet volume density for fiord cores in McBeth and Itirbilung fiords (see Table 7.1 and Figure 7.1).

The Itirbilung Fiord transect (Figures 7.11 and 7.14) includes a core 20 km from the fiord head and two near the fiord mouth. There is no adjacent shelf core for comparisons although HU78-37 from a trough, just to the south, provides some data (Andrews, 1987b). At HU83-IT2.3, the $F_{n\downarrow}$ at the site over the past 10 ka is 8300 kg/m^2; this is similar to the accumulation of sediment at IT1.1 over the past 4 to 5 ka (Figure 7.14). Even so, the seafloor sediment flux at IT1.1 is a factor of 4 *lower* than that recorded at the sediment trap, some 20 km closer to the delta front.

During neoglaciation the $F_{n\downarrow}$ at IT2.3 amounted to 2750 kg/m^2, comparable to the accumulation at MC4.1 (Figure 7.14). A comparison of IT1.1 and IT2.1 over the past 5 ka indicates that the absolute amount of sand reaching the seafloor declined seaward as did the silt-size material; thus, the sediment became more clay-rich down fiord. The accumulation in the shelf trough at HU78-37 totalled ca. 6000 kg/m^2 for the past 10 ka and 1900 kg/m^2 for the past 5 ka. This is substantially more than at site HU78-36 and indicates a significant difference in $F_{n\downarrow}$ between the shelf proper and troughs/basins within the shelf. An estimate of $T_{n\downarrow}$ for the outer McBeth basins and shelf for the past 10 ka is approximately 120 and 106 kg per meter width (Figure 7.14).
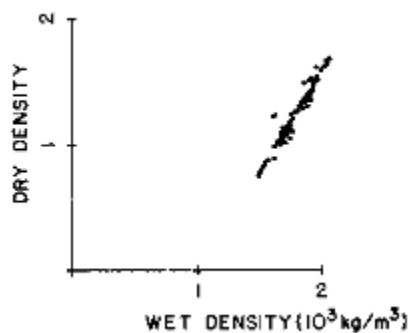
FIGURE 7.13 Relationship between wet and dry volume density determinations on samples from three fiord cores from Baffin Island, NWT, fiords.
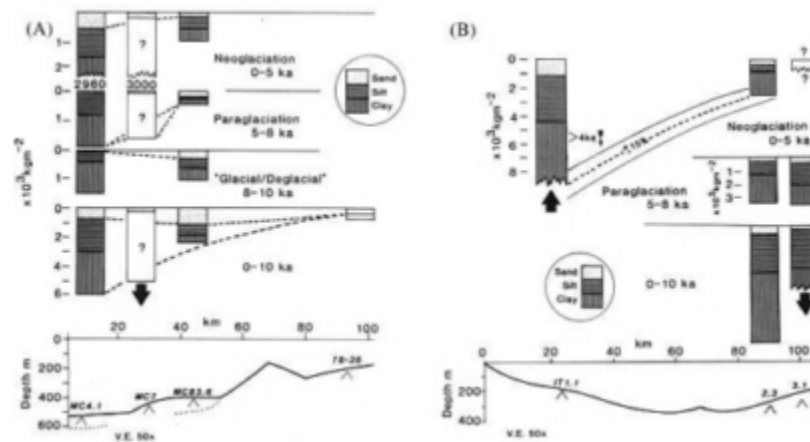
FIGURE 7.14 (A) Diagram of sediment flux variations along McBeth Fiord. The numbers along the profile (Figure 7.14B, e.g., MC7) refer to the number of the core (Table 7.1). Silt and clay content not known for MC7, hence the question mark. (B) Similar data also shown for Itirbilung Fiord. Both profiles start about 70 to 80 km from the respective fiord heads.
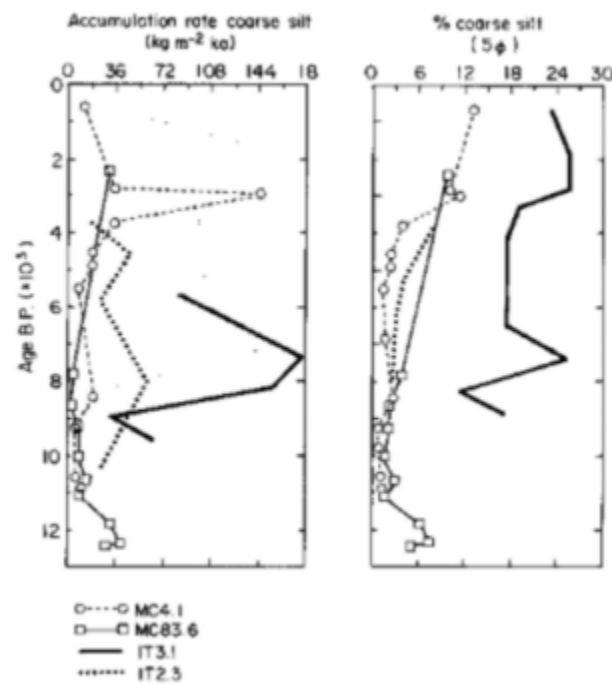
FIGURE 7.15 Downcore variations in the percentage of coarse silt in the <2 mm matrix (right), and the net seafloor flux of this grainsize per 100 yr (left). Core locations are given in Table 7.1.

Southwest Greenland today might be an analog for the Baffin Island region some 8 ka ago. Herman *et al.* (1972) reported that cores from two fiords in front of the ice sheet had about 12 m of accumulation in 5.5 ka. Although sediment densities were not reported, the sediment flux is probably of the order of about 1600 kg/m^2/ka, a figure similar to that observed in the outer Baffin Island fiord basins during deglaciation (Figure 7.14).

Representative $F_n \downarrow$'s for clay-size materials over the past 10 ka are shown as Figure 7.16 for fiord, shelf, and the ODP 645 site in Baffin Bay (cf., Srivastava *et al.,* 1987). The net accumulation of clay-size particles over this interval varies from ca. 4600 in the outer fiords, to 2600 in the shelf troughs, and 1000 kg/m^2 in Baffin Bay. The clay-size mineralogy of samples from all three environments (Andrews *et al.,* 1989b) was studied via standard x-ray diffraction techniques. The dominant clay-mineral species is illite/mica and the net $F_n \downarrow$ of this mineral decreases dramatically from the fiords to the deep sea, with values over 10 ka of 3800, 1700, and 480 kg/m^2, respectively. Quartz and feldspars show much less variation and approximately equal amounts reached the seafloor in the deep sea and shelf troughs. Detrital carbonate, mainly dolomite but with some calcite (Andrews *et al.,* 1989b), reached a peak $F_n \downarrow$ of ca. 250 kg/m^2 on the shelf with

lesser amounts in the fiords and deep sea. These data suggest that the carbonate was brought into the area via the Baffinland Current, probably in the form of both suspended particulates, from meltwater, and as material contained in icebergs.
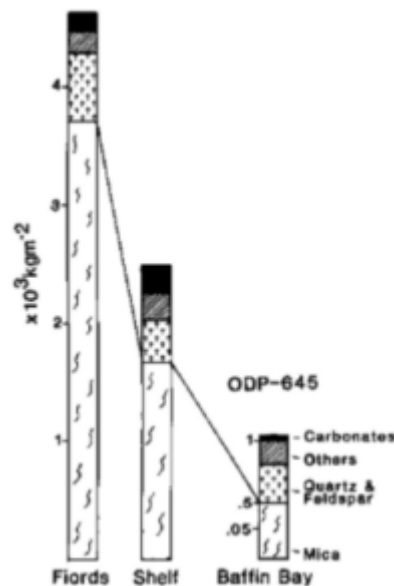
FIGURE 7.16 Seafloor flux $F_n\downarrow$ of clay-size particles and clay-size mineralogy of fiord, shelf, and deep-sea sediments (Baffin Island to Baffin Bay).

Figure 7.17 presents a summary (Andrews, 1987b) for fiord to deep sea $F_n\downarrow$ over the past 8 ka. These data do not include the sites on Figure 7.14, however, they also suggest that the $F_n\downarrow$ decreases by about one-half over a distance of 30 to 40 km (see Figure 7.14).

It must be emphasized that this study considers $F_n\downarrow$ along a narrow strip of the seafloor. Flux calculations, from cores, can be partly checked by the geometries of the acoustic reflectors (Figure 7.10), however, this only provides a two dimensional view of the sediment architecture (e.g., Gilbert, 1985). To be fully representative, so that we can make volume calculations for entire systems, we require cross-fiord and cross-trough seismic stratigraphies.

The East Greenland Margin

Kangderlugssuaq Fiord is a deep re-entry into the heavily glaciated margin of East Greenland. Seaward from the fiord a deep trough (Figure 7.9) cuts across the shelf. In 1988, a WHOI cruise collected a suite of 10-cm diameter gravity cores (1 to 2 m in length) from the trough floor and shelf. Three cores were shipped to the University of Colorado for study (Figure 7.9; Table 7.1). Wet and dry volume densities were measured and a series of basal core dates were obtained on hand-picked foraminifera. Our objective in this ONR supported study was to examine the fiord to deep-sea sediment flux.

The sediments in cores 5A and 10A were principally massive to laminated muds with some dropstones. The lowermost 4 cm in core 10A is a diamict. In deeper water on the slope, the sediment in core 17B was a diamict. Prior to this work we know of no radiocarbon dates from the East Greenland Shelf, although some may exist.

The stonyness of core 17B precluded precise measurements of the dry volume density, but in the other two cores (5A and 10A) it was surprisingly low, with medians of 690 and 860 kg/m³. The AMS basal dates and their depths in the cores (Table 7.2) imply average sediment fluxes during much of the Holocene of 60 kg/m²/ka and 67 kg/m²/ka at sites 5A and 10A, respectively. These initial results give fluxes that are an order of magnitude *less* than the trough cores we have from the eastern Canadian Arctic shelf (Jennings, 1986; Andrews, 1987b; this chapter). At this stage these results are intriguing but need a wider regional context before their value can be adequately assessed; this will come from work on other cores collected during the cruise, plus planned future work on the shelf and in the adjacent fiords. Additional AMS[14]C dates, processed for the core tops, indicate continuous sedimentation to be present.
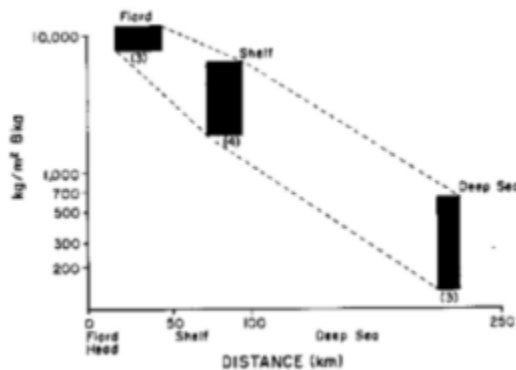
FIGURE 7.17 Sediment flux over the past 8 ka from Baffin Island fiord sites, to shelf-trough sites, to Baffin Bay (from Andrews, 1987b). The numbers in brackets refer to the number of cores used in establishing the range of estimates.

TABLE 7.1 Information on the Cores

Core #	Latitude	Longitude	Water Depth, m	Core Penetration (A)	Core Length (B)	Ratio B/A
78-36	70°0.8.09'	66°48.07'	99	NA	99	NA
MC83.6	69°40.7'	69°09.8'	429	450	306	0.68
MC7	69°37.5'	69°16'	497	NA	1121	NA
MC4.1	69°31.4'	69°57'	549	810	610	0.75
IT3.1	69°17.6'	68°12.3'	365	810	483	0.6
IT2.3	69°17.5'	68°12.3'	410	853	610	0.72
IT1.1	69°20'	69°03.8'	256	900	793	0.88
78-37	68°15.05'	65°12.09'	457	NA	593	NA
East Greenland						
5A	67°05.9'	30°54.5'	707	NA	76	NA
10A	65°12.5	30°39.5'	496	NA	103	NA
17B	65°19.0'	30°59.9'	997	NA	83	NA

TABLE 7.2 Radiocarbon Dates from the East Greenland Shelf

Core #	Depth, m	Laboratory #	Age and Error, yr
5A	0.73 to 0.75	AA-3976	9865 ± 110
10A	110.5 to 102.5	AA-4026	13585 ± 110
17B	0.77 to 0.81	AA-4027	8755 ± 80

CONCLUSIONS

Sediment flux estimates on glacial to interglacial time scales from glaciated continental margins are rare and more studies are required in such areas as Greenland, Spitsbergen, Canada, and Alaska. The sediment flux has contributions from several sources (in a process sense) (Figures 7.2 and 7.8), and distinctions between them in terms of the sediment type are not always obvious. In addition to these different sources, most continental margins have at least a local and a regional sediment provenance—these may be distinguished in some areas on the basis of mineralogies of the different grain-size fractions and/or on the sediment type (Figure 7.16). The most significant scientific obstacle to such studies will continue to be the acquisition of reliable ^{14}C dates. Studies on these time scales should be supplemented, whenever possible, with the deployment of sediment traps to study the nature of the present sediment flux over a period of 1 to 3 years.

In the middle arctic area of western Baffin Bay, on a deglacial/interglacial time scale, the net downward flux of sediment in Baffin Island outer fiord basins is of the order of 600 to 800 kg/m^2/ka, compared with 200 to 300 kg/m^2/ka in the adjacent shelf-troughs (Figure 7.13; Andrews, 1987b). The half-distance for the net accumulation may be of the order of 30 to 40 km. X-radiography and paleomagnetic studies indicate that the dominant sediment flux is associated with the rain-out of sediment from sediment plumes. Preliminary data from an East Greenland shelf-trough gives net accumulation rates of only ca. 60 to 80 kg/m^2/ka, suggesting that (1) little sediment is escaping from the fiords, (2) little sediment is being produced, or (3) most of the sediment is bypassing the trough en route to the deep sea. However, we stress that there is significant spatial and temporal variability in sediment fluxes adjacent to continental glacial margins and, at the moment, generalizations should be made with care.

The sediment flux data reported on in this chapter are largely derived from a number of different sources. There is a critical need to undertake one or more specific transects from fiords out to the adjacent deep sea basins with the intent of studying the sediment flux. If such studies could be combined with long-term sediment trap data then it would be possible to evaluate present and past sediment fluxes along glaciated continental margins. The underlying requirement in all such studies will be availability of accurate and precise ^{14}C age measurements. Rather than the current number of about 3 dates per 10 ka, one date per 1 ka is required to fully evaluate $F_n{\downarrow}$ on glacial to present time scales. In addition, or supplemental to this approach, is the inverse but nonlinear relationship between sediment accumulation and organic carbon content (Andrews, 1987b; Syvitski *et al.,* 1990)—this might allow fine-tuning of sediment accumulation records.

An important requirement is to continue to improve and enhance computer simulations of sediment fluxes (see Figure 7.3) and to integrate them with well designed field experiments, involving sediment trap data, high resolution seismic data (Figure 7.10), and long (20 to 50 m) piston cores.

ACKNOWLEDGMENTS

REFERENCES

Adams, J., and P. Basham (1989). The seismicity and seismotectonics of Canada east of the Cordillera, Geoscience Canada 16, 3-16 .

Andrews, J.T. (1980). Progress in relative sea level and ice sheet reconstructions Baffin Island, N.W.T. for the past 125,000 years, in Earth Rheology, Isostasy, and Eustasy, N.A. Morner, ed., John Wiley, New York, pp. 175-200 .

Andrews, J.T. (1982). Holocene glacier variations in the Eastern Canadian Arctic, Striae 18, 9-14 .

Andrews, J.T. (1987a). Downcore variations in the carbon content of fiord piston cores and association with sedimentation rates, in Sedimentology of Arctic Fjords Experiment: Data Report 3, J.P.M. Syvitski and D.B. Prage, compilers, Canadian Data Report of Hydrography and Ocean Sciences 54, Ch. 12, 19 pp .

Andrews, J.T. (1987b). Late Quaternary marine sediment accumulation in fiord-shelf-deep transects, Baffin Island to Baffin Bay, Quaternary Science Reviews 6, 231-243 .

Andrews, J.T. (1990). Fiord to deep-sea sediment transfers along the Northeastern Canadian continental margin: Models and data, Geographie Physique et Quaternaire 44, 55-70 .

Andrews, J.T., and A.E. Jennings (1987). Influence of sediment source and type on the magnetic susceptibility of fiord and shelf deposits, Baffin Island and Baffin Bay, N.W.T., Canadian Journal of Earth Sciences 24, 1386-1401 .

Andrews, J.T., and C.L. Matsch (1983). Glacial Marine Sediments and Sedimentation: An Annotated Bibliography, Geobooks Ltd., Norwich, U.K., 227 pp .

Andrews, J.T., P.U. Clark, and J.A. Stravers (1985a). The patterns of glacial erosion across the eastern Canadian Arctic, in Quaternary Environments: Baffin Island, Baffin Bay and West Greenland, J.T. Andrews, ed., Allen and Unwin, Boston, pp. 69-92 .

Andrews, J.T., A.J.T. Jull, D.J. Donahue, S.K. Short, and L. E. Osterman (1985b). Sedimentation rates in Baffin Island fiord cores from comparative radiocarbon dates, Canadian Journal of Earth Sciences 22, 1827-1834 .

Andrews, J.T., J.S. Mothersill, and A. Tabrez (1986). Paleomagnetic record, texture, and mineralogy of Late Quaternary fiord sediments, Baffin Island, Arctic and Alpine Research 18, 361-376 .

Andrews, J.T., C.A. Laymon, and W.M. Briggs (1989a). Radiocarbon Date List VI, Baffin Island and III Labrador-Ungava, University of Colorado, Boulder, INSTAAR Occasional Paper No. 46, 85 pp .

Andrews, J.T., A. Geirsdottir, and A.E. Jennings (1989b). Spatial and temporal variations in clay- and silt-size mineralogies of shelf and fiord cores, Baffin Island, Continental Shelf Research 9, 445-463 .

Barnes, P.W., and R. Lien (1988). Icebergs rework shelf sediments to 500 m off Antarctica, Geology 16, 1130-1133 .

Bell, M., and E.P. Laine (1985). Erosion of the Laurentide Ice Sheet by glacial and glaciofluvial processes, Quaternary Research 23, 154-174 .

Blankenship, D.D., S.T. Rooney, R.B. Alley, and C.R. Bentley (1986). Seismic evidence for a deforming and eroding till beneath an active Antarctic ice stream, EOS 67, 946 .

Boulton, G.S., and A.S. Jones (1979). Stability of temperate ice caps and ice sheets resting on beds of deformable sediment, Journal of Glaciology 24, 29-43 .

Church, M. (1972). Baffin Island sandurs: A study of arctic fluvial processes, Geological Survey of Canada Bulletin 216, 208 pp .

Church, M., and R. Gilbert (1975). Proglacial fluvial and lacustrine environments, in Glaciofluvial and Glaciolacustrine Sedimentation, A.V. Jopling and B.C. McDonald, eds., Special Publication 23, Society of Economic Paleontologists and Mineralogists, pp. 22-100 .

Church, M., and J.M. Ryder (1972). Paraglacial sedimentation: A consideration of fluvial processes conditioned by glaciation, Geological Society of America Bulletin 83, 3059-3072 .

Davis, P.T. (1985). Neoglacial moraines on Baffin Island, in Quaternary Environments: Eastern Canadian Arctic, Baffin Bay and Western Greenland, J.T. Andrews, ed., Allen and Unwin, Ondon, pp. 682-718 .

Dowdeswell, J.A. (1987). The processes of glaciomarine sedimentation, Progress in Physical Geography 11, 52-90 .

Dowdeswell, E.K., and J.T. Andrews (1985). The fiords of Baffin Island: Description and classification, in Quaternary Environments: Eastern Canadian Arctic, Baffin Bay and Western Greenland, J. Andrews, ed., Allen and Unwin, London, pp. 682-718 .

Dowdeswell, J.A., and T. Murray (1989). Modeling rates of sedimentation from icebergs (abstract), Glaciomarine Environments: Processes and Sediments, Geological Society of London.

Drewry, D. (1986). Glacial Geologic Processes, Edward Arnold, London, 276 pp .

Dyke, A.S. (1974). Deglacial chronology and uplift history: Northeastern sector, Laurentide Ice Sheet, Occasional Paper No. 12, INSTAAR, University of Colorado, Boulder, 73 pp .

Dyke, A.S., and V.K. Prest (1987). Late Wisconsin and Holocene history of the Laurentide Ice Sheet, Geographie Physique et Quaternaire XLI, 237-264 .

Elverhoi, A. (1984). Glaciogenic and associated marine sediments in the Weddell Sea, fjords of Spitsbergen and the Barents Sea: A review, Marine Geology 57, 53-88 .

Elverhoi, A., O. Liestol, and J. Nagy (1980). Glacial erosion, sedimentation and microfauna in the inner part of Kongsfjorden, Spitsbergen, Norsk Polarinstitutt Skrifter 172, 33-61 .

Eyles, C.H., N. Eyles, and A.D. Miall (1985). Models of glaciomarine sedimentation and their application to the interpretation of ancient glacial sequences, Palaeogeography, Palaeoclimatology, Palaeoecology 51, 15-84 .

Eyles, N., T.E. Day, and A. Gavican (1987). Depositional controls on the magnetic characteristics of lodgement tills and other glacial diamict facies, Canadian Journal of Earth Sciences 24, 2436-2458 .

Fillon, R.H. (1985). Northwest Labrador Sea stratigraphy, sand input and paleoceanography during the last 160,000 years, in Quaternary Environments: Eastern Canadian Arctic, Baffin Bay and Western Greenland, J.T. Andrews, ed., Allen and Unwin, London, pp. 210-247 .

Gilbert, R. (1982). Contemporary sedimentary environments on Baffin Island, N.W.T., Canada, Glaciomarine processes in fiords of eastern Cumberland Peninsula, Arctic and Alpine Res. 14, 1-12 .

Gilbert, R. (1983). Sedimentary processes of Canadian Arctic fiords, Sedimentary Geology 36, 147-175 .

Gilbert, R. (1985). Quaternary glaciomarine sedimentation interpreted from seismic surveys of fiords on Baffin Island, N.W.T., Arctic 38, 271-280 .

Gurnell, A.M., and M.J. Clark (eds.) (1987). Glacio-Fluvial Sediment Transfer, An Alpine Perspective, John Wiley & Sons, New York, 524 pp .

Hein, F.J., and F.J. Lonstaffe (1985). Sedimentologic, mineralogic, and geotechnical descriptions of fine-grained slope and basin deposits, Baffin Island fiords, Geo-Marine Letters 5, 11-16 .

Herman, Y., J.R. O'Neill, and C.L. Drake (1972). Micropaleontology and paleotemperatures of postglacial SW Greenland fjord cores, Acta Universitatis Ouluensis, Series A, Geologica No. 1, University of Oulu, 357-407 .

Holtedahl, H. (1958). Some remarks on the geomorphology of continental shelves off Norway, Labrador, and southeast Alaska, Journal of Geology 66, 461-471 .

Jennings, A.E. (1986). Late Quaternary marine sediments from a transect of fiord and continental shelf environments: A study of piston cores from Clark Fiord and Scott Trough, Baffin Island, M.S. thesis, University of Colorado, Boulder, 245 pp .

Josenhans, H.W., J. Zevenhuizen, and R.A. Klassen (1986). The Quaternary geology of the Labrador Shelf, Canadian Journal of Earth Sciences 23, 1190-1214 .

Kravitz, J.H. (1982). Sediments and sediment processes in Kane Basin, a high arctic glacial marine basin, INSTAAR Occasional Paper 39, University of Colorado, Boulder, 184 pp .

Laine, E.P. (1980). New evidence from beneath the western North Atlantic for the depth of glacial erosion in Greenland -nd North America, Quaternary Research 14, 188-198 .

MacLean, B. (1985). Geology of the Baffin Island shelf, in Quaternary Environments: Eastern Canadian Arctic, Baffin Bay, and Western Greenland, J.T. Andrews, ed., Allen and Unwin, London, pp. 154-177 .

Molnia, B.F., ed. (1983). Glacial-Marine Sedimentation, Plenum, New York.

Osterman, L.E., and A.R. Nelson (1989). Latest Quaternary and Holocene oceanography of the eastern Baffin Island continental shelf, Canada: Benthic foraminiferal evidence, Canadian Journal of Earth Sciences 26, 2236-2248 .

Pereira, C.P.G., C.M.T. Woodworth-Lynas, and J.V. Barrie (1988). Iceberg scour investigations and sedimentology of the Southeast Baffin Island Continental Shelf, Arctic 41, 221-230 .

Pfirman, S.L. (1985). Modern sedimentation in the Northern Barents Sea: Input, dispersal and deposition of suspended sediments from glacial meltwater, Woods Hole Oceanographic Institution 85-4 (Doctoral Dissertation), Woods Hole, MA., 376 pp .

Powell, R.D. (1983). Glacial-marine sedimentation processes and lithofacies of temperate glaciers, Glacier Bay, Alaska, in Glacial-Marine Sedimentation, B.F. Molnia, ed., Plenum, New York, pp. 185-232 .

Powell, R.D. (1984). Glaciomarine processes and inductive lithofacies modeling of ice shelf and tidewater glacier sediments based on Quaternary examples, Marine Geology 57, 1-52 .

Powell, R.D., and B.F. Molnia (1989). Glaciomarine sedimentary processes, facies, and morphology of the south-southeast Alaska shelf and fjords, Marine Geology 85, 359-390 .

Praeg, D.B., B. MacLean, I.A. Hardy, and P.J. Mudie (1986). Quaternary geology of the southeast Baffin Island continental shelf, Geological Survey of Canada Paper 85-14, 13 pp . (with maps).

Reasoner, M.A., and F.J. Hein (1984). Sedimentology and geotechnical properties of surficial bottom sediments, Baffin Island fjords, in Sedimentology of Arctic Fjords Experiment: HU 83-028 Data Report, Volume 2 , J.P.M. Syvitski, compiler, Canadian Data Reports on Hydrography and Ocean Science No. 28, Chapter 11, 111 pp .

Ruddiman, W.F. (1977). Late Quaternary deposition of ice-rafted sand in the subpolar North Atlantic (lat. 40° to 65°), Geological Society of America Bulletin 88, 1813-1827 .

Schlee, J.S., W. Manspeizer, and S.R. Riggs (1988). Paleoenvironments: Offshore Atlantic U.S. margin, in The Geology of North America Vol. 1-2, The Atlantic Continental Margin, Geological Society of America, Boulder, Colorado, pp. 365-385 .

Short, S.K., J.T. Andrews, and W.N. Mode (1989). Modern and late Quaternary pollen spectra from fiord sediments, eastern Baffin Island, Arctic Canada, Marine Micropaleontology 15, 181-202 .

Srivastava, S.P., et al. (1987). Proceedings of the Ocean Drilling Program, Part A-Initial Report, Baffin Bay and Labrador Sea, ODP 105, Texas A&M University, College Station, Texas, 917 pp .

Syvitski, J.P.M. (1986). Sedimentation and accumulation in fluvially-dominated fjords, 15th Arctic Workshop, Abstracts, University of Colorado, Boulder, 68-70 .

Syvitski, J.P.M. (1989). On the deposition of sediment within glacier-influenced fjords: Oceanographic controls, Marine Geology 85, 301-329 .

Syvitski, J.P.M., and F.J. Hein (1991). Sedimentology of an arctic basin: Itirbilung Fiord, Baffin Island, Canada, Geological Survey of Canada Paper 91-11, 66 pp .

Syvitski, J.P.M., and C. Schaefer (1985). Sedimentology of Arctic fjords experiment (SAFE): Project introduction, Arctic 38, 264-270 .

Syvitski, J.P.M., D.C. Burrell, and J.M. Skei (1987a). Fjords, Processes and Products, Springer-Verlag, New York, 379 pp .

Syvitski, J.P.M., R.B. Taylor, and J.A. Stravers (1987b). Suspended sediment loads along the coast of NE Baffin and Bylot islands , in Sedimentology of Arctic Fjords Experiment: Data Report, Volume 3 , J.P.M. Syvitski and D.B. Prage, compilers, Canadian Data Report of Hydrography and Ocean Sciences No. 54, Chapter 4, 20 pp .

Syvitski, J.P.M., J.N. Smith, E.A. Calabrese, and B.P. Boudreau (1988). Basin sedimentation and the growth of prograding deltas, Journal of Geophysical Research 93(C6), 6895-6908 .

Syvitski, J.P.M., G.E. Farrow, R.J.A. Atkinson, P.G. Moore, and J.T. Andrews (1989). Baffin Island fjord macrobenthos: Bottom communities and environmental significance, Arctic 42, 232-247 .

Syvitski, J.P.M., K.W.G. LeBlanc, and R. Cranston (1990). The flux and preservation of organic carbon in Baffin Island fjords, Geological Society of London Special Publication 53, 177-200 .

Taylor, J.R. (1982). An Introduction to Error Analysis, The Study of Uncertainty in Physical Measurements, University Science Books, Mill Valley, California, 270 pp .

Williams, K.M. (1988). Late Quaternary Paleoceanography of the Baffin Bay Region Based on Diatoms, Ph.D. dissertation, University of Colorado, Boulder, 263 pp .

8

Late Quaternary Flux of Eolian Dust to the Pelagic Ocean

DAVID K. REA AND STEVEN A. HOVAN
University of Michigan
THOMAS R. JANECEK
Texas A&M University

ABSTRACT

The eolian flux of terrigenous minerals to the pelagic ocean has been measured in about 30 locations in the Pacific, Atlantic, and Indian Oceans. Dust fluxes vary by three orders of magnitude from more than 1000 $mg/cm^2/kyr$ directly downwind from the major dust sources in China and North Africa to 1 $mg/cm^2/kyr$ over much of the South Pacific and southern Indian Oceans. In both the Atlantic and Pacific oceans there is an order of magnitude reduction in the deposition rates of eolian dust as one proceeds south across the Intertropical Convergence Zone (ITCZ). Dividing the total dust flux value of Prospero (1981) by the area of the global ocean results in an average deposition rate of 200 $mg/cm^2/kyr$, but this value is too low for the nearshore regions and a factor of 4 or 5 high for the pelagic ocean.

Detailed downcore records of eolian flux to the northwest Pacific document much higher fluxes during glacial times and accumulation minima during interglacials; this accumulation pattern matches the loess/soil stratigraphy of central China. Cores raised from just south of the ITCZ in the Pacific exhibit greater dust fluxes during interglacial times, matching the known aridity pattern of northwest South America. We observe a shift from the present southern hemisphere dust flux pattern to that of the northern hemisphere about 300,000 years ago at core RC11-210 at 1.8° N, implying a 5° or greater latitudinal shift in the position of the ITCZ from south to north at the time of the Mid-Brunhes Climate Event.

INTRODUCTION

Terrigenous materials are being supplied to the world's oceans by rivers at a flux rate of about 1.5 to 2 x 10^{16} g/yr (Holland, 1981). Most of this material is trapped in estuaries or on continental shelves and only a minor portion reaches the deep sea. Eolian dust, perhaps only 5 percent of the total lithogenous flux (approximately 0.53 to 0.85 x 10^{15} g/yr, Prospero, 1981), dominates the mineral component of pelagic sediments in regions away from the influence of turbidites, equatorward of the effects of ice rafting and seaward of the influence of hemiplegic deposition (Windom, 1969, 1975; Rea *et al.,* 1985). The eolian input estimate of Prospero (1981) when divided over the 360 x 10^{16} cm^2 of the oceans and marginal seas results in an average dust flux value for the entire ocean of about 200 mg/cm^2/kyr.

Dust is raised by storms from the arid and semi-arid surfaces of continents, elevated to the upper portion of the troposphere, transported global distances by the zonal winds and washed out of the atmosphere by rain. The long-term pattern of this sedimentary process is shown clearly in maps of the quartz content of surficial sediments of the sea floor (Leinen *et al.,* 1986). Regions relatively enriched in quartz, which makes up roughly 10 to 20 percent of the total eolian load, extend downwind from the major deserts of the world—Gobi, Sahara, Arabia, Australia.

The short-term record of dust transport is seasonal. Spring storms are responsible for most of the annual transport. The best record of present-day eolian transport is that developed by Prospero for materials crossing the Atlantic from the Sahara. That record shows an order of magnitude variation in the amount of dust transported in any given year with maxima during the late spring or early summer. On a longer term basis the flux of dust crossing the North Atlantic shows a three- to fivefold increase during the height of the Sahelian droughts in 1973-1974 and 1983-1984, demonstrated times of significantly reduced rainfall (Nicholson, 1985; Middleton, 1985) in comparison to more normal years (Prospero and Nees, 1977, 1986). This sort of seasonality in dust transport with maxima in the late spring occurs wherever dust fluxes have been measured (Parrington *et al.,* 1983; Uematsu *et al.,* 1983; Merrill *et al.,* 1989). Useful summaries of eolian processes and dust deposition have been given by Windom (1975), Prospero (1981), Rea *et al.,* (1985), and Pye (1987).

THE GEOLOGIC RECORD OF DUST DEPOSITION

A Note on Methodology

The mass input of any sedimentary component to the sea floor can be quantified. The parameters necessary to determine the mass accumulation rate (MAR) in g/cm^2/kyr, or flux, of dust are: the linear sedimentation rate (LSR) in cm/kyr, the dry bulk density (DBD) of the sediment in g/cm^3, and the weight percent of the eolian component of the bulk sediment. Eolian flux values are the product of these three. The eolian component itself is isolated from the total sediment by a series of extractions that remove all other sedimentary components, leaving the minerals (Rea and Janecek, 1981). The amount of any volcanic ash remaining after extraction is estimated visually from smear slides and deducted from the total to give values for continentally derived material.

Sediment samples usually span one or two centimeters of any given core and so represent many hundreds to thousands of years of deposition. Furthermore, any initially discrete event or signal is smoothed by the bioturbation process that acts to homogenize the uppermost several centimeters of deep-sea sediments. Short-term climatic variability on time scales of decades to centuries is therefore smoothed and the records we present are representative of truly long-term climatic trends and events. Our working assumption, based largely on the data of Prospero on transport from Africa (Prospero, 1981; Prospero and Nees, 1986), is that the amount of dust transported to the oceans is a function of source area aridity; drier, less vegetated regions provide more dust to the atmosphere than do moist, well vegetated regions. This assumption is also consistent with information available for the pedology of the great loess-soil sequences in China (Kukla, 1987; Kukla and An, 1989) and the distal record of those sequences (Hovan *et al.,* 1989). The supply of dust to the oceans is independent of the intensity of transporting winds (Chuey *et al.,* 1987), that aspect of eolian deposition is recorded by the grain size variation of the dust (Rea *et al.,* 1985; Pisias and Rea, 1988).

Geographic Variation in Eolian Fluxes

The input rate of dust to the pelagic oceans today (Holocene) ranges through three orders of magnitude, from low values of 1 or 2 mg/cm^2/kyr in the center of the South Pacific to more than 1000 mg/cm^2/kyr just downwind from the North African and Asian source regions. There are perhaps 35 locations in all the oceans where flux values for clearly pelagic eolian minerals have been determined (Figure 8.1; Table 8.1), locations more than 500 of 1000 km offshore and thus beyond the effective range of hemipelagic deposition. All values calculated for near continent regions may include a significant hemipelagic component. When compared with information from nearby sediment traps or the data from island-based collectors, the dust flux values from sediment cores agree to within the combined errors of the two kinds of measurements (Rea *et al.,* 1985).
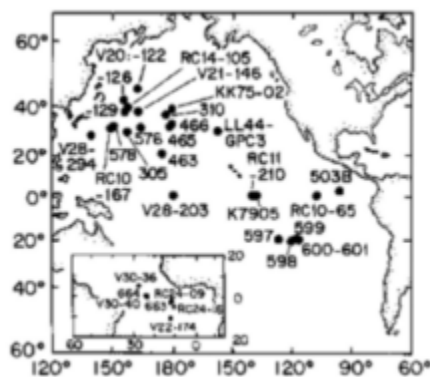
FIGURE 8.1 Locations of Pacific and Atlantic Ocean cores discussed in text.
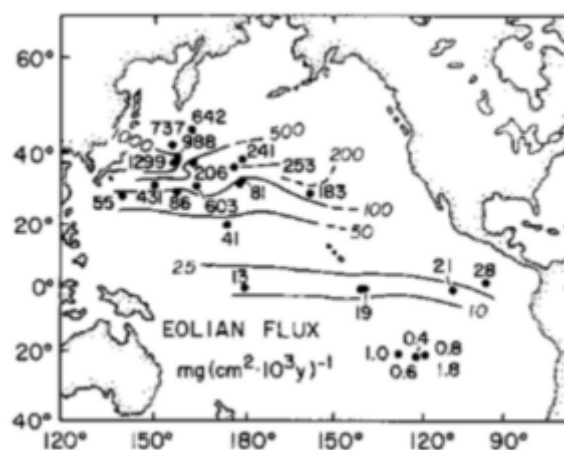
FIGURE 8.2 Pleistocene-Holocene eolian flux to the Pacific Ocean.

The most flux data exist for the North Pacific where essentially all of the eolian dust deposited comes from central and western China and Mongolia. That material is transported to the east by the westerlies and the westerly jet stream, then drifts south towards the equator and dominates eolian deposition all the way south to the Intertropical Convergence Zone (Merrill *et al.,* 1989). Flux rates decline all along this transport path (Figure 8.2).

Rea and Leinen (1988) reported on the late Glacial to Holocene eolian records of a suite of six cores along a latitudinal profile extending from 28.4°N to 46.6°N between 155° and 160°E. Data from those cores (Figure 8.3) show distinct latitudinal variations in dust flux with a present-day maximum of about 1000 mg/cm^2/kyr at 38° to 40°N and flux values falling off to the north and south. The latitudinal position of the flux maxima has remained unchanged through the last 30,000 years, although the amount has varied (Rea and Leinen, 1988). Farther east, at the same latitude of 37 to 40°N and between 174 and 179°E, the flux of dust in uppermost samples (i.e., Pleistocene, not Holocene) of DSDP and piston cores is approximately 250 mg/cm^2/kyr, a significant decline in about 1500 km of transport distance.

To the south of the main region of the westerlies, the eolian fluxes in the central North Pacific decline to less than 100 mg/cm^2/kyr at about 30 to 35°N, depending on longitude. Flux values from three equatorial cores whose late Glacial and Holocene records were studied in detail, all from about 1°N and spaced between 109 and 179°W, remain quite constant at 10 to 20 mg/cm^2/kyr over the past 30 kyr (Figure 8.4). The Holocene flux value from DSDP Core 503B at about 4°N, 96°W, somewhat closer to the presumed South American source area, is slightly greater (Rea *et al.,* 1986).

We have determined the flux of eolian dust to the South Pacific for five of the DSDP Leg 92 drill sites which were spaced along 19°S from 130 to 117°W (Figure 8.1; Bloomstine and Rea, 1986). The flux value of the uppermost sample from each of these cores averaged 1 mg/cm^2/kyr and was never greater than 1.8 mg/cm^2/kyr. Eolian fluxes to the South Pacific are very low and have been so at least since the Oligocene (Rea and Bloomstine, 1986). Results from the southern Indian Ocean indicate similarly low fluxes for most of the Cenozoic (Hovan and Rea, 1991).

The Pacific data are adequate to construct a map of the flux of eolian dust to the ocean (Figure 8.2). The data mapped (Table 8.1) include both Holocene and whole-Pleistocene values so the map does not represent a true (i.e., restricted) time slice. Nevertheless the primary flux patterns are clear. High eolian accumulation rates near Asia decrease to the east along a latitude band approximately 35 and 45°N from over 1000 to less than 250 mg/cm^2/kyr in the central North Pacific. Isopleths of eolian flux trend east-west, matching the pattern of present-day transport (Merrill *et al.,* 1989) and the pattern of mineralogy of sea-floor surface sediments (Leinen *et al.,* 1986). There is an order of magnitude decline in dust input along about 30° N from the high values to the north to values of a few tens of mg/cm^2/kyr in the northern subtropics. Another order of magnitude decline occurs at the Intertropical Convergence Zone, where the rainfall associated with the equatorial low serves as an effective barrier to the interhemispherical transport of dust.

TABLE 8.1 Core Locations and "Surfical" (Holocene Average or Youngest Pleistocene) Eolian Flux Values (in mg/cm^{2}/kyr).

Core	Reference	Latitude	Longitude	Flux	Comment
V20-122	1	6.6°N	161.7°E	642	Holocene
V20-126	1	42.2°N	155.9°E	737	Holocene
RC14-105	1	39.7°N	157.5°E	988	Holocene
V-129	1	37.7°N	156.6°E	1299	Holocene
RC10-167	1	33.4°N	150.4°E	431	Holocene
V28-294	1	28.4°N	140.0°E	55	Holocene
V21-146	2	37.7°N	163.0°E	206	Holocene
KK75-02	3	38.6°N	179.3°E	241	Holocene
DSDP 310	4	36.9°N	176.9°E	253	Pleistocene
DSDP 466	5	34.2°N	179.3°E	81	Pleistocene
DSDP 578	6	33.9°N	151.6°E	1790	Probably hemipelagic
DSDP 465	5	33.8°N	178.9°E	9	Unreliable sediment rate
DSDP 576	6	32.4°N	164.3°E	603	Pleistocene
DSDP 305	4	32.0°N	157.8°E	86	Pleistocene
DSDP 463	7	21.4°N	174.7°E	41	Pleistocene
LL44-GPC3	8	30.3°N	157.8°W	183	Pleistocene
RC11-210	9	1.8°N	140.0°W	nd	Near K7905-16GC
DSDP 503B	10	4.1°N	95.6°W	28	Holocene
V28-203	11	1.0°N	179.4°W	13	Holocene
K7905-16GC	11	1.1°N	138.9°W	19	Holocene
RC10-65	11	0.7°N	108.6°W	21	Holocene
DSDP 597	12	8.8°S	129.8°W	1.0	Pleistocene
DSDP 598	12	19.0°S	124.7°W	0.6	Pleistocene
DSDP 599	12	19.5°S	119.9°W	0.4	Pleistocene
DSDP 600C	12	18.9°S	116.8°W	0.8	Pleistocene
DSDP 601	12	18.9°S	116.9°W	1.8	Pleistocene
V30-36	13	5.4°S	27.3°W	nd	
V30-40	13	0.2°S	23.1°W	450	Holocene
RC24-09	13	1.9°S	11.4°W	474	Holocene
RC24-16	13	5.0°S	10.2°W	89	Holocene
V22-174	13	10.8°S	12.0°W	38	Holocene
ODP 664	14	0.1°N	23.2°W	450	Pleistocene
ODP 663A	14	1.2°S	11.9°W	380	Pleistocene
RC27-61	15	16.6°S	59.9°E	500	Holocene
ODP 756B	11	27.4°S	87.6°E	0.3	Holocene

Note: References to original data are: 1. Rea and Leinen (1988); 2. Hovan *et al*. (1989); 3. Janecek (1983); 4. Rea and Janecek (1982); 5. Rea and Harrsch (1981); 6. Janecek (1985); 7. Rea and Janecek (1981); 8. Janecek and Rea (1983); 9. Chuey *et al*. (1987); 10. Rea *et al*. (1986); 11. Rea, unpublished data; 12. Bloomstine and Rea (1986); 13. Janecek, unpublished data; 14. Ruddiman *et al*. (1989); 15. Clemens and Prell (1990).

The flux of dust to the Atlantic has been measured in several cores, most of which are downwind from the Sahara (Table 8.1). Holocene flux values in cores well away from the problems attendant to continental margin sedimentation are 400 to 500 mg/cm^2/kyr in the region between the equator and about 10°N. There is a marked drop-off south of the equator to values of about 90 mg/cm^2/kyr at 5°S and about 40 mg/cm ^{2}/kyr at 11° S, an order of magnitude reduction in values, a similar amount to the trans-equatorial flux reduction in the Pacific. The westward moving dust plume from the deserts of North Africa is centered at about 20° N (Sarnthein *et al.,* 1981; Leinen *et al.,* 1986), so flux values greater than 500 mg/cm^2/kyr might be expected at that latitude.
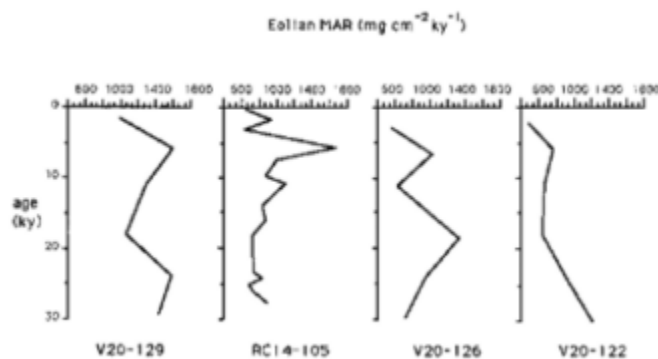
FIGURE 8.3 Late Glacial and Holocene eolian fluxes in four Northwest Pacific cores.
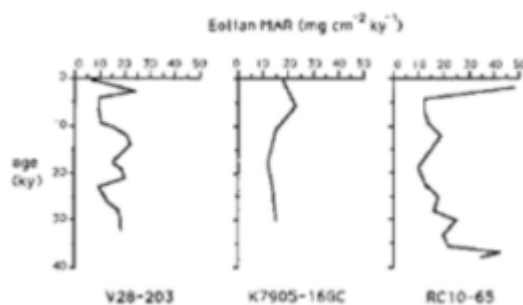
FIGURE 8.4 Late Glacial and Holocene eolian fluxes in three Equatorial Pacific cores.
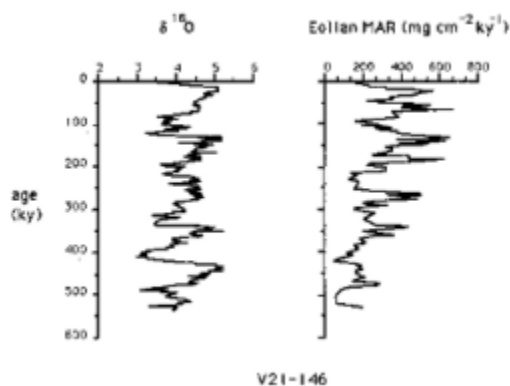
FIGURE 8.5 Eolian flux to North Pacific core V21-146 during the past 530,000 years. Left: benthic $\delta^{18}O$ record, glacial aged (positive $\delta^{18}O$) peaks to the right; right: flux record.

The Downcore Record of Quaternary Eolian Deposition

The best record of eolian flux from the North Pacific ocean has been developed for core V21-146 raised from 3968 meters depth at 37.7°N, 163.0°E, about 3500 km downwind from the dust-generating regions of China (Figure 8.5; Hovan *et al.,* 1989, 1991). That core has a detailed $\delta^{18}O$ record derived from benthic foraminifera, which can be linked to the SPECMAP $\delta^{18}O$ time scale (Imbrie *et al.,* 1984), providing the temporal basis for the eolian flux analyses. During the last 530,000 yr, the flux of dust to core V21-146 has averaged about 250 mg/cm^2/kyr, ranging from a low of about 55 to a peak value of about 670 mg/cm^2/kyr. There is a distinct correlation between flux maxima and times of glaciation as indicated by the $\delta^{18}O$ record; on the average, flux values increase by a factor of 3.9 from interglacial minima to glacial-aged maxima (Figure 8.5). Furthermore, the dust flux variations in V21-146 also correlate with the loess-soil stratigraphy of the China Loess Plateau (Kukla, 1987; Kukla and An, 1989). The correlation of periods of low flux to times of soil development and of times of high flux to periods of loess activity permits us to make a direct tie between this classic continental record of Quaternary climates and the $\delta^{18}O$ record of climate change using the information from core V21-146 (Hovan *et al.,* 1989, 1991).

A longer-term trend of increasing dust flux to the North Pacific in younger sediments during the past 500,000 yr is apparent (Figure 8.5). This observation, which suggests increasing late Pleistocene aridity in the eolian source region, is consistent with the observations of Pye and Li (1989) of increased rates of dust accumulation in the Xifeng loess sequence.

Equatorial core RC11-210 (1.8°N, 140.0°W, 4420 m), from the east-central Pacific south of the Intertropical Convergence Zone, provides a detailed, 946,000-yr-long record of paleoclimatic proxy indicators (Figure 8.6; Chuey *et al.,*

1987; Pisias and Rea, 1988; Rea *et al.,* 1991). To the east, the uppermost hydraulic piston cores from DSDP Site 503B (4.0° N, 95.6° W, 3672 m) provide a somewhat less detailed record of the past 420,000 yr (Figure 8.6; Rea *et al.,* 1986). At RC11-210 eolian dust accumulated during the late Pleistocene at rates of 4 to 90 mg/cm^2/kyr (the high values at the top of the core may be spurious; the sharp peak at 75 kyr is an ash layer, see discussion in Chuey *et al.,* 1987). Flux maxima occur during both interglacial, Stages 7, 15 and perhaps 19, and glacial, Stages 10 and 12, times. At 503B the flux pattern is similar, maxima occur in interglacial Stages 5 and 7, and glacial Stage 10. The shift in the flux pattern from interglacial maxima to glacial maxima occurs about 300,000 yr ago, the time of the Mid-Brunhes Climate Event (Chuey *et al.,* 1987; Pisias and Rea, 1988).
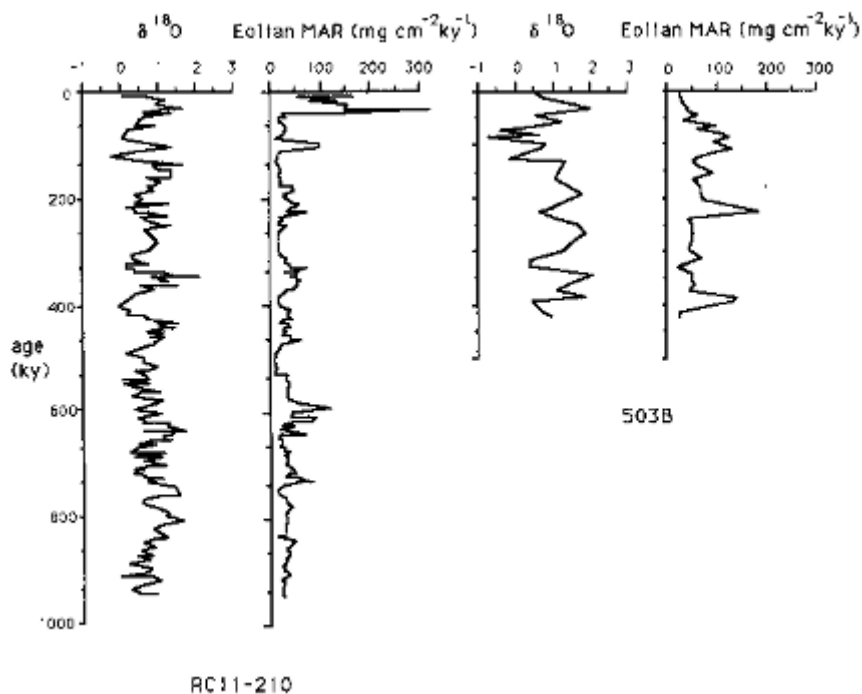
FIGURE 8.6 Late Pleistocene eolian flux to Equatorial Pacific cores RC 11-210 (left) and DSDP 503B (right). Planktic δ^{18}O records; glacial aged (positive δ^{18}O) peaks to the right.
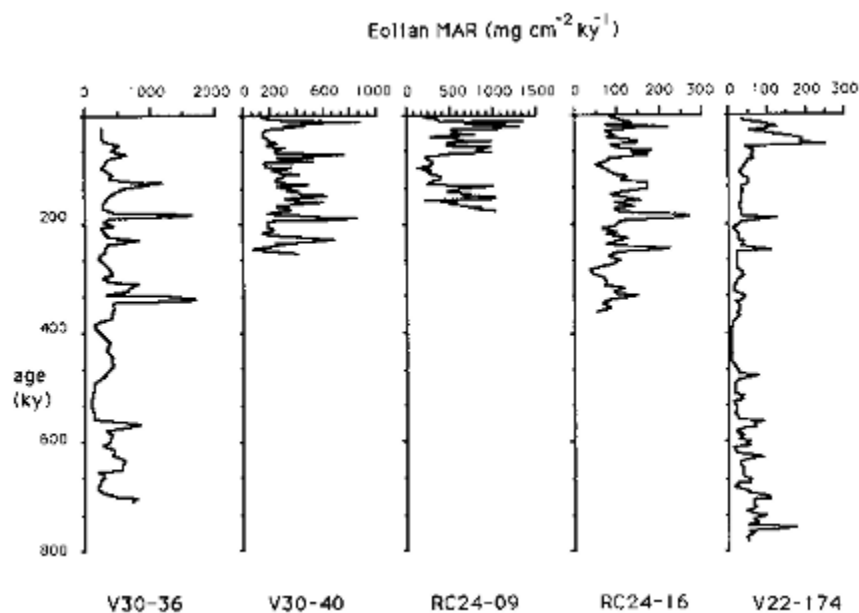
FIGURE 8.7 Late Pleistocene eolian flux to Equatorial Atlantic cores V30-36, V30-40, RC24-09, RC24-16, and V22-174. Note that flux scales vary.

Five piston cores raised from the Equatorial Atlantic between about 5° N and 11° S provide a record of eolian dust flux to that part of the ocean over the past 300,000 yr (Figures 8.1 and 8.7). Flux values at ODP drillsites north of the ITCZ have averaged 400 to 500 mg/cm^2/kyr for the past 0.5 myr and may have been 50 percent or more higher in earlier portions of the Pleistocene (Ruddiman *et al.,* 1989). The piston cores appear to show an irregular pattern of heightened flux of dust during both the younger portions of

glacial stages and occasionally during interglacial periods. Pokras and Mix (1985, 1987) have studied the flux of the windblown freshwater diatom *Melosira* to core V30-40. Their data do not match the dust flux patterns shown on Figure 8.7; the diatom fluxes may be recording the initial drying and deflation of African lakes at the onset of arid conditions (Pokras and Mix, 1987). The decrease in dust flux by a factor or eight to ten to the south of the Intertropical Convergence Zone persists throughout the downcore records.

Estimating the long-term flux of volcanogenic material to the ocean is more difficult. Studies of ash layers are common but provide information on discrete events and not the ongoing, on geologic time scales, influx of ash and other volcanic debris to the deep sea. A geochemical approach to this problem has been taken recently by Olivarez (Olivarez, 1989; Olivarez *et al.,* 1991), who used methods of multivariate analysis to apportion the assemblage of rare earth elements (REE) in the eolian material between continental and oceanic crust (presumably volcanic) end members. She found that near the west Pacific island arcs, the ocean-crust component was perhaps 20 to 25 percent of the REE assemblage, declining to 5 to 10 percent in the central North Pacific. The REE abundance patterns of the low dust-flux cores along the equator commonly indicate 30 to 50 percent of the oceanic crust end member. Although not definitive, these results are indicative of an important background of disseminated volcanic material entering the ocean via the wind. Quantification is problematic; Olivarez' data suggest that volcanogenic flux values might be as much as 10 to 30 percent of those shown on Figure 8.2, with the greater values nearer the volcanic arcs of the Pacific rim. Partitioning and provenance of the eolian material is an ongoing research topic.

DISCUSSION

In the introduction we noted that the average flux of eolian dust to the ocean was 200 mg/cm^2/kyr. The data presented here, however, shows that this value is exceeded only in regions immediately downwind from important dust sources, China, North Africa, and Arabia. All the remaining pelagic ocean has fluxes of only a few tens of mg/cm^2/kyr, and the entire South Pacific and probably the southern Indian Ocean receives almost no dust. For the pelagic ocean, therefore, the average value of eolian flux is far too high, probably by a factor of four or five. This does not negate the value of the total flux number, 0.7 x 10^{15} g/yr, because just as for rivers, most of the dust carried to the oceans will be deposited within a few hundred kilometers of the shoreline and become indistinguishable from the hemipelagic and turbidite materials accumulating at those locations at much larger rates. The reader should be aware, however, that over most of the open sea the input of dust to the ocean is no more than a few tens of mg/cm^2/kyr, and that this value is much less in the southern hemisphere (Figure 8.2, Table 8.1).

The provenance of dust in Pacific equatorial cores is a significant problem. If we infer a southern hemisphere source for these cores presently south of the Intertropical Convergence Zone, then the flux records of Site 503B and RC11-210 may be related to the paleoclimatology of the northern Andes. Pollen data from that region show that throughout the Quaternary the Andean lakes were full during glacial times and dry salars or playas during interglacial times (Hooghiemstra, 1984; van der Hammen, 1985). This is consistent with the eolian flux data at 503B, which show interglacial flux maxima during Stages 5 and 7. The shift in accumulation maxima from the assumed southern hemisphere pattern of interglacial maxima to the known northern hemisphere pattern of glacial-aged maxima implies a quasi-permanent shift in the latitude of the Intertropical Convergence Zone at the time of the Mid-Brunhes Climate Event, from an earlier more southerly location to a younger position further north. The location RC11-210 constrains this latitudinal shift in the position of the ITCZ to be at least 5° .

ACKNOWLEDGMENTS

REFERENCES

Bloomstine, M.K., and D.K. Rea (1986). Post-middle Oligocene eolian deposition from the trade winds of the southeast Pacific, in Initial Reports of the Deep Sea Drilling Project 92 , M. Leinen, D.K. Rea et al., U.S. Government Printing Office, Washington, D.C., pp. 331-340 .

Chuey, J.M., D.K. Rea, and N.G. Pisias (1987). Late Pleistocene paleoclimatology of the central Equatorial Pacific: A quantitative record of eolian and carbonate deposition, Quaternary Research 28, 323-339 .

Clemens, S.C., and W.L. Prell (1990). Late Pleistocene variability of Arabian Sea summer-monsoon winds and continental aridity: Eolian records from the lithogenic component of deep-sea sediments, Paleoceanography 5, 109-145 .

Holland, H.D. (1981). River transport to the Oceans, in The Sea, Volume 7 , The Oceanic Lithosphere, C. Emiliani, ed., John Wiley and Sons, New York, pp. 763-800

Hooghiemstra, H. (1984). Vegetational and Climatic History of the High Plain of Bogota, Columbia: A Continuous Record of the Last 3.5 Million Years, J. Cramer, Vaduz, Liechenstein, 368 pp .

Hovan, S.A., and D.K. Rea (1991). The post-Eocene record of eolian deposition at ODP Sites 752, 754, and 756, eastern Indian Ocean, in Proceeding of the Ocean Drilling Program, Scientific Results, 121 , J. Pierce, J. Weissel et al., eds., Ocean Drilling Program, College Station, Texas, pp. 219-228 .

Hovan, S.A., D.K. Rea, N.G. Pisias, and N.J. Shackleton (1989). A direct link between the China loess and marine $\delta^{18}O$ records: Aeolian flux to the north Pacific, Nature 340, 296-298 .

Hovan, S.A., D.K. Rea, and N.G. Pisias (1991). Late Pleistocene continental climate and oceanic variability recorded in northwest Pacific sediments, Paleoceanography 6, 349-370 .

Imbrie, J., J.D. Hays, D.G. Martinson, A. McIntyre, A.C. Mix, J.J. Morley, N.G. Pisias, W.G. Press, and N.J. Shackleton (1984). The orbital theory of Pleistocene climate: Support from a revised chronology of the marine $\delta^{18}O$ record, in Milankovitch and Climate Understanding the Response to Orbital Forcing, Part 1, A. Berger, J. Imbrie, J. Hays, G. Kukla, and B. Saltzman, eds., D. Reidel, Dordrecht, pp. 269-305 .

Janecek, T.R. (1983). The History of Eolian Sedimentation and Atmospheric Circulation During the Late Cenozoic, unpub. Ph.D. dissertation, University of Michigan, Ann Arbor, 176 pp .

Janecek, T.R. (1985). Eolian sedimentation in the northwest Pacific Ocean: A preliminary examination of the data from Deep Sea Drilling Project Sites 576 and 578, in Initial Reports of the Deep Sea Drilling Project 86 , G.R. Heath, L.H. Burckle et al., U.S. Government Printing Office, Washington, D.C., pp. 589-603 .

Janecek, T.R., and D.K. Rea (1983). Eolian deposition in the northeast Pacific Ocean: Cenozoic history of atmospheric circulation, Geological Society of America Bulletin 94, 730-738 .

Kukla, G. (1987). Loess stratigraphy in central China, Quaternary Science Reviews 6, 191-219 .

Kukla, G., and Z. An (1989). Loess stratigraphy in central China, Palaeogeography, Palaeoclimatology, Palaeoecology 72, 203-225 .

Leinen, M., D. Cwienk, G.R. Heath, P.E. Biscaye, V. Kolla, J. Thiede, and J.P. Dauphin (1986). Distribution of biogenic silica and quartz in recent deep-sea sediments, Geology 14, 199-203 .

Merrill, J.T., M. Uematsu, and R. Bleck (1989). Meteorological analysis of long range transport of mineral aerosols over the North Pacific, Journal of Geophysical Research 94, 8584-8598 .

Middleton, N.J. (1985). Effect of drought on dust production in the Sahel, Nature 316, 431-434 .

Nicholson, S.E. (1985). Sub-Saharan rainfall 1981-1984, Journal of Climatology and Applied Meteorology 24, 1388-1391 .

Olivarez, A.M. (1989). Investigations of the Geochemistry of the Rare Earth Elements in the Exogenic Cycle, unpublished Ph.D. thesis, University of Michigan, Ann Arbor, 193 pp .

Olivarez, A.M., R.M. Owen, and D.K. Rea (1991). Geochemistry of eolian dust in Pacific pelagic sediments: Implications for paleoclimatic interpretations, Geochimica et Cosmochimica Acta 55, 2147-2158 .

Parrington, J.R., W.H. Zoller, and N.K. Aras (1983). Asian dust: Seasonal transport to the Hawaiian Islands, Science 220, 195-197 .

Pisias, N.G., and D.K. Rea (1988). Late Pleistocene paleoclimatology of the central Equatorial Pacific: Sea-surface response to the southeast tradewinds, Paleoceanography 3, 21-37 .

Pokras, E.M., and A.C. Mix (1985). Eolian evidence for spatial variability of Late Quaternary climates in tropical Africa, Quaternary Research 24, 137-149 .

Pokras, E.M., and A.C. Mix (1987). Earth's precession cycle and Quaternary climatic change in tropical Africa, Nature 326, 486-487 .

Prospero, J.M. (1981). Eolian transport to the world ocean, in The Sea, Volume 7 , The Oceanic Lithosphere, C. Emiliani, ed., John Wiley and Sons, New York, pp. 801-874 .

Prospero, J.M., and R.T. Nees (1977). Dust concentrations in the atmosphere of the equatorial North Atlantic: Possible relationships to the Sahalian droughts, Science 196, 1196-1198 .

Prospero, J.M., and R.T. Nees (1986). Impact of North African drought and El Niño on mineral dust in the Barbados trade winds, Nature 320, 735-738 .

Pye, K. (1987). Aeolian Dust and Dust Deposits, Academic Press, London, 334 pp .

Pye, K., and P.Z. Li (1989). Late Pleistocene and Holocene aeolian dust deposition in North China and the Northwest Pacific Ocean, Palaeogeography, Palaeoclimatology, Palaeoecology 73, 11-23 .

Rea, D.K., and M.K. Bloomstine (1986). Neogene history of the South Pacific tradewinds: Evidence for hemispherical asymmetry of atmospheric circulation, Palaeogeography, Palaeoclimatology, Palaeoecology 55, 55-64 .

Rea, D.K., and E.C. Harrsch (1981). Mass accumulation rates of the non-authigenic, inorganic, crystalline (eolian) component of deep sea sediments from the Hess Rise, Deep Sea Drilling Project Sites 464, 465, and 466, in Initial Reports of the Deep Sea Drilling Project 62 , J. Thiede, T.L. Vallier et al., U.S. Government Printing Office, Washington, D.C., pp. 661-668 .

Rea, D.K., and T.R. Janecek (1981). Mass accumulation rates of the non-authigenic, inorganic, crystalline (eolian) component of deep sea sediments from western Mid-Pacific mountains, Deep Sea Drilling Project Site 463 , in Initial Reports of the Deep Sea Drilling Project 62 , J. Thiede, T.L. Vallier et al., U.S. Government Printing Office, Washington, D.C., pp. 653-659 .

Rea, D.K., and T.R. Janecek (1982). Late Cenozoic changes in atmospheric circulation deduced from North Pacific eolian sediments, Marine Geology 49, 149-167 .

Rea, D.K., and M. Leinen (1988). Asian aridity and the zonal westerlies: Late Pleistocene and Holocene record of eolian deposition in the northwest Pacific Ocean, Palaeogeography, Palaeoclimatology, Palaeoecology 66, 1-8 .

Rea, D.K., M. Leinen, and T.R. Janecek (1985). Geologic approach to the long-term history of atmospheric circulation, Science 227, 721-725 .

Rea, D.K., L.W. Chambers, J.M. Chuey, T.R. Janecek, M. Leinen, and N.G. Pisias (1986). A 420,000-year record of cyclicity in oceanic and atmospheric processes from the eastern Equatorial Pacific, Paleoceanography 1, 577-586 .

Rea, D.K., N.G. Pisias, and T. Newberry (1991). Late Pleistocene paleoclimatology of the central Equatorial Pacific: Flux patterns of biogenic sediments, Paleoceanography 6, 227-244 .

Ruddiman, W.F., M. Sarnthein, J. Backman, J. Baldauf, W. Curry, L.M. Dupont, T. Janecek, E.M. Pokras, M.E. Raymo, B. Stabell, R. Stein, and R. Thiedemann (1989). Late Miocene to Pleistocene evolution of climate in Africa and the lowlatitude Atlantic: Overview of Leg 108 results, in Proceedings of the Ocean Drilling Program, Scientific Results 108, W.F. Ruddiman, M. Sarnthein et al., eds., Ocean Drilling Program, College Station, Texas, pp. 463-484 .

Sarnthein, M., G. Tetzlaff, B. Koopmann, K. Wolter, and U. Pflaumann (1981). Glacial and interglacial wind regimes over the eastern subtropical Atlantic and north-west Africa, Nature 293, 193-196 .

Uematsu, M., R.A. Duce, J.M. Prospero, L. Chen, J.T. Merrill, and R.L. McDonald (1983). Transport of mineral aerosol from Asia over the North Pacific Ocean, Journal of Geophysical Research 88, 5343-5352 .

van der Hammen, T. (1985). The Plio-Pleistocene climatic record of the tropical Andes, Journal of the Geological Society of London 142, 483-489 .

Windom, H.L. (1969). Atmospheric dust records in permanent snowfields: Implications to marine sedimentation, Geological Society of America Bulletin 80, 761-782 .

Windom, H.L. (1975). Eolian contributions to marine sediments, Journal of Sedimentary Petrology 45, 520-529 .

9

Particle Fluxes in the Ocean and Implications for Sources and Preservation of Ocean Sediments

JACK DYMOND
Oregon State University
MITCHELL LYLE
Lamont-Doherty Earth Observatory

ABSTRACT

Measurements of the settling particle flux throughout the water column enable estimates of the rain and recycling of elements and biogenic compounds within the oceans. On 10 of 11 open-ocean sites the rain rate and burial rates of refractory elements (Al, Fe, and Ti) are approximately equal. Poor agreement between rain and burial of refractory elements at the Hatteras Abyssal Plain may be due to deep lateral inputs of particulate debris to the site. The balance between rain and burial of refractory elements suggests similar comparisons for the labile components should provide accurate estimates of their extent of recycling. The degree of preservation of organic matter, opal, and carbonate computed from the rain/burial comparison is highly variable at the different oceanographic settings. The percentage of organic carbon varies from less than 1 percent at a low productivity mid-ocean site to approximately 30 percent in a site adjacent to the continental slope. The preservation correlates with the accumulation rate of the sediments. Opal preservation varies in a similar manner; however, the degree of preservation appears to correlate with the opal rain rate. Carbonate preservation correlates most strongly with water depth and possibly to the ratio of organic carbon to carbonate in the raining particles.

Strong offshore decrease in carbon rain rate and preservation demonstrate the importance of the continental margin as a region of enhanced organic carbon burial. These effects produce a factor of 60 change in carbon burial rate over a 600 km offshore transect in the North East Pacific. Some transport of particles to the deep basins appears to take place by a sediment focusing processes whereby multiple resuspension events move material laterally and down slope from the continental shelf and slope.

Eolian inputs can be inferred from particle fluxes at sites distant from the continental margins. These studies demonstrate that the Equatorial Pacific, which is under the influence of Trade winds, has relatively low fluxes. Measurements from the Nares Abyssal Plain in the Atlantic, however, indicate that this site is receiving important inputs of aluminosilicate debris from African deserts.

INTRODUCTION

Measurements of settling particle flux not only clarify a variety of oceanic biogeochemical processes but also aid the interpretation of the sedimentary record. Particle settling is the primary mechanism for transferring dissolved and suspended materials from the water column to the sediments; however, scavenging and recycling alters the flux and composition of raining particles. Consequently, the burial rates of elements and compounds generally do not equal the particulate rain rate.

A major focus of this paper will be the comparison between the burial rate of materials that form the sediment record and the rain rate of particles that settle through the water column. From this comparison we can determine the rate of recycling or benthic flux of materials that settle to the seafloor. In effect, the benthic flux is the exchange rate of solutes between the sediment and the overlying water column. This exchange transforms raining particulate material into the sedimentary record. In its simplest form the benthic equation is:

Rain rate of any particulate component =

Burial rate of that component + Benthic flux

The rain rate is the particulate flux that reaches the bottom for any component, and the burial rate is the preservation rate of that component in the sediment.

The direct measurement of particle flux has followed important developments in marine technology. Deployment and recovery of deep ocean moorings, which position particle collectors throughout the water column, are now routine. A variety of these particle collectors (commonly called sediment traps) are in current use (Soutar *et al.,* 1977; Blomqvist and Hakanson, 1981; Dymond *et al.,* 1981; Gardner, 1980; Honjo and Doherty, 1988). Most are cylinders or funnels in which particles enter through a baffle at the top and settle into a sample cup where a bactericide is maintained at a concentration capable of inhibiting decomposition of the sample. Many designs have timer-controlled sample changers that can collect a time series of settling particles over preset intervals.

Sediment traps work as collectors of settling particles because large, rapidly settling forms dominate the particle flux in the oceans (McCave, 1975). A number of recent studies have shown that these large particles are either amorphous aggregates of smaller particles commonly called marine snow (Alldredge and Silver, 1988) or zooplankton fecal pellets ((Urrere and Knauer, 1981; Pilskaln and Honjo, 1987). As a result of the rapid settling, a variety of sediment trap designs have similar efficiencies for collecting settling particles in the low current regime of the open ocean. These large particles settle through the entire water column of typical ocean depths (5000 m) in one to two months.

METHODS

In this study we will summarize and evaluate the particle flux measurements made with sediment traps developed at Oregon State University between 1980 and 1988 (Table 9.1). The OSU trap is a single-cone modification of a design originally developed by Andrew Soutar (Soutar *et al.,* 1977). It features all plastic or fiberglass construction, a two-to-one height to diameter cone, a one cm by five cm baffle at the top of the cone, and a 10 cm wide lip at the top of the cone that limits turbulence at the mouth of the cone. The trap has evolved from a five-cup, sequential collector to the current model that has a 15-cup collector for enhanced temporal resolution of the particle flux. In

TABLE 9.1 Location and Date of Sediment Trap Experiments

Site	Latitude (N)	Longitude (W)	Depth (m)	Date of Experiment
Atlantic				
HAP	32.73	70.82	5400	6/7/82 – 4/28/83
NAP	23.20	63.98	5847	8/21/83 – 9/27/84
Pacific				
MFZ	39.49	127.69	4230	9/9/83 – 9/1/84
JDF	47.97	128.10	2200	9/9/84 – 8/10/85
NS	42.09	125.77	2829	9/22/87 – 9/16/88
MW	42.19	127.58	2830	9/28/87 – 9/14/88
G	41.55	132.00	3664	9/25/87 – 9/23/88
H	6.57	92.77	3565	9/20/80 – 10/17/81
M	8.83	103.98	3150	9/12/80 – 10/23/81
S	11.06	140.14	4620	12/29/82 – 2/14/84
C	1.04	138.94	4445	12/23/82 – 5/3/85

this study, however, we will report only average fluxes for the time intervals of the trap deployments. In general, the deployment periods are for one year (Table 9.1), the minimum deployment necessary to encompass the known seasonal flux changes (Deuser and Ross, 1980).
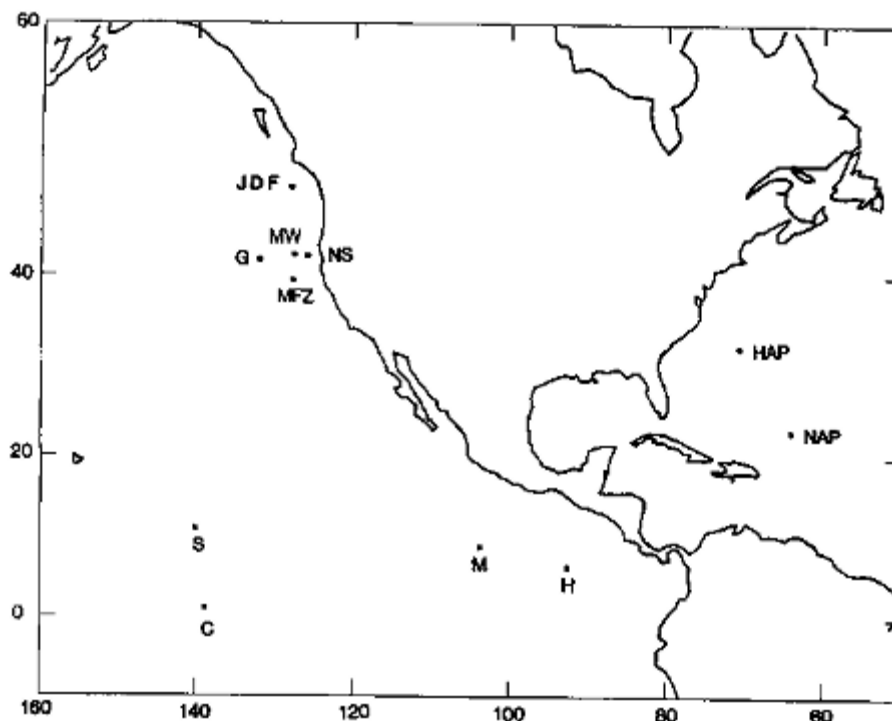
FIGURE 9.1 Locations of sediment trap moorings used in this study.

Sodium azide concentrations of 15 g/l in the sample cups preserve the trap samples. Azide is an effective bactericide, and because of the high alkalinity of the cup solutions, $CaCO_3$ tests (even aragonite) are very well preserved. Fischer *et al.* (1983) discusses the sample preparation procedures in detail. Organic carbon and $CaCO_3$ data were measured by acid evolution of CO_2 and detection with a LECO carbon analyzer (Weliky *et al.,* 1983). Atomic absorption spectrophotometry and instrumental neutron activation were used for all other analyses.

We report particle fluxes and burial rates for 11 sites (Figure 9.1; Tables 9.2-9.4). There are four equatorial Pacific sites (H, M, S, and C). Flux data from sites H and M have previously been reported in Dymond and Lyle, 1985; Murphy and Dymond, 1984; Fischer *et al.,* 1986; Walsh *et al.,* 1988a, b. Data from sites C and S have been reported in Dymond and Collier, 1988. There are five sites off the west coast of the United States. MFZ is a California Current site just north of the Mendocino Fracture Zone (Fischer *et al.,* 1983). Nearshore (NS), Midway (MW), and Gyre (G) form a California Current transect (42° N) from very productive waters influenced by coastal upwelling to the relatively unproductive, central gyre. JDF is located on the Endeavour Segment of the Juan de Fuca Ridge, a site of present day, intense hydrothermal discharge. Although the primary purpose of this mooring was definition of processes effecting the hydrothermal particle flux (Dymond and Collier, 1988; Dymond and Roth, 1988; Roth and Dymond, 1989), three sediment traps were placed above the hydrothermal effluent plume. These data define the biological and upper water column inputs to this part of the ocean. Two sites are in the Atlantic. Hatteras Abyssal Plain (HAP) is approximately 300 km off the east coast of the United States. Particle flux data from this site have been reported in Heggie *et al.* (1987). Nares Abyssal Plain (NAP) is a deep water site in the western Atlantic (Thomson *et al.,* 1984).

Definition of particulate rain rate to the sea floor requires data on the particulate flux variations with depth. Dissolution and decomposition of sinking particles remove labile components. Heterotrophic organisms consume the settling detritus, metabolize a portion of the organic matter, and repackage remaining inorganic and nonnutritious components into rapidly sinking fecal pellets. In addition, inclusion of clay-sized particles into large marine snow aggregates enhances the flux of fine particles and alters the composition of settling particles. Horizontal advection and lateral down slope transport from continental margins also modify the flux and composition of the settling material. Distinguishing between distal and local resuspension effects is necessary to determine the rain rate to the sediment. Distal resuspension by nepheloid transport, contour currents, or turbidity currents may be sources of biogenic and nonbiogenic components to a site. Locally resuspended material collected in a sediment trap, however,

represents an artificial flux. The trap intercepts the cycling of particles from the bottom into the water column and back to the bottom. This process increases the residence time of settling particles in the water column (Walsh *et al.,* 1988b), but not the particulate flux to the bottom.

TABLE 9.2 Bulk Sedimentation Data

Site	Sedimentation Rate[a]	Mass Accumulation Rate[b]	Total Rain Rate[b]	% Preserved	Recycled Flux[b]
Atlantic					
HAP	10	4,500	2000	225	-2,500
HAP	1	650	1190	55	540
Pacific					
MFZ	5.9	3,240	3,970	82	730
JDF	1.6	840	2,500	34	1,660
NS	19	9,690	19,010	51	9,320
MW	11	4,440	6,050	73	1,650
G	1.3	650	1,030	63	380
H	0.66	110	2,550	4	2,440
M	1.0	288	1,980	15	1,692
S	0.1	32	1,030	3	998
C	1.7	848	3,701	23	2,854

[a] Units of cm/1000 yr

[b] Units of mg/cm^2/yr.

TABLE 9.3 Refractory Element Fluxes

	A1			Fe			Ti		
Site	Rain Rate	Burial Rate	% Preserved	Rain Rate	Burial Rate	% Preserved	Rain Rate	Burial Rate	% Preserved
Atlantic									
HAP	47	312	664	25	171	684	2.28	18.51	812
NAP	52.4	59.8	114	29.5	33.1	112	3.01	3.43	114
Pacific									
MFZ	220	254	115	135	162	120	12	15	125
JDF	30.6	29.1	95	19.3	44.7	232	—	—	—
NS	940	746	79	—	—	—	46	52	113
MW	200	308	154	—	—	—	11	30	273
G	20	34	170	—	—	—	—	—	—
H	7	6.4	91	3.75	5.4	144	0.74	0.4	54
M	15.1	14.2	94	15.7	20.3	129	0.85	0.97	114
S	1.8	2.1	117	1.01	1.3	129	—	0.12	—
C	5.41	4.8	89	2.61	3.2	123	—	0.21	—

NOTE: All rates are in units of mg/cm^2/yr.

These difficulties cannot be overcome by mooring a single trap within the water column. Studies that involve deployment of 3-4 traps within the bottom 1000 m, however, indicate that local resuspension is not significant at elevations a few hundred meters above bottom (Dymond *et al.,* 1981; Fischer, 1984; Walsh *et al.,* 1988b). In this paper we will use particulate flux measurements from traps above the resuspension zone (Figure 9.2) to extrapolate the rain rate to bottom depths.

Temporal variations in the particle flux provide another complication to estimating the particulate rain to the bot

tom. The scales of variation range from individual bloom events (Limpitt 1985) to seasonal (Deuser and Ross, 1980) and even interannual scales. Consequently, studies that are shorter than one year are likely to result in erroneous estimates of the average particulate rain rate. Moreover, data for a single year at any given site will not resolve the importance of interannual variability such as those caused by ENSO events (Dymond and Collier, 1988).

TABLE 9.4 Biogenic Component Fluxes

| Site | ORGANIC CARBON | | | | CaCO₃ | | | | OPAL | | | |
	Rain Rate	Burial Rate	% Preserved	Recycled Flux	Rain Rate	Burial Rate	% Preserved	Recycled Flux	Rain Rate	Burial Rate	% Preserved	Recycled Flux
Atlantic												
HAP	76.4	18.7	24	58	1,105	948	86	157	180	135	75	45
NAP	48.3	1.93	4	46	482	36.6	8	445	106	1	1	105
Pacific												
MFZ	127	25	20	102	550	57	10	493	850	102	12	748
JDF	109	12.8	12	96	1,170	185	16	985	728	74	10	791
NS	490	130	27	360	1,490	80	5	1,410	4,772	850	18	3,992
MW	220	50	23	170	910	100	11	810	1,663	200	12	1,463
G	90	3.5	4	87	420	20	5	400	330	22	7	308
H	89	0.83	1	88	659	1	0	1,268	388	16	4	372
M	138	3.8	3	134	2,093	42.2	6	617	711	30	4	681
S	30	0.15	1	30	542	0.3	0	542	345	6	2	339
C	130	2.59	2	127	2,093	64.2	31	1,451	1,069	113	11	956

Note: All rates have units of mg/cm²/yr.
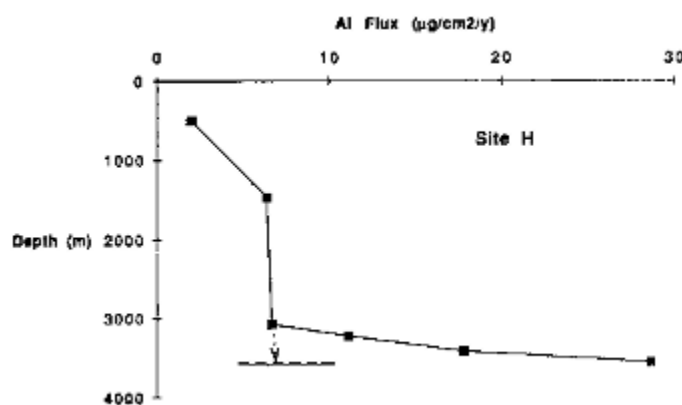
FIGURE 9.2 Particulate aluminum flux variations with water depth at site H in the eastern Equatorial Pacific. The very strong increase in flux below a depth of 3100 m is thought to be due to local resuspension of previously deposited sediments. The dashed horizontal line indicates the bottom depth at the site. The dotted arrow indicates the extrapolation procedure used to define the rain rate to the bottom at this site.

Determination of the accumulation rate of sediments may also have difficulties. Ideally, we would like to compare sedimentation rates measured in the uppermost portion of the sediment to bring the time scales of burial fluxes and sediment trap measurements more in accord. Although the best coring technology can sample the upper few centimeters of sediment, bioturbation is a consistent feature of the upper 10 cm of deep sea sediments. Consequently, dating techniques generally integrate over time scales greater than 10^4 yr and include perturbations due to the most recent glacial-interglacial transition. In this study we will use a variety of techniques (^{230}Th,^{14}C and oxygen isotopic stratigraphy) to define the sedimentation rate.

REFRACTORY ELEMENT RAIN AND BURIAL FLUXES

Certain elements found in the particulate load of the oceans are carried in unreactive phases. For example, aluminum, iron, titanium, scandium, and thorium are dominantly in aluminosilicate debris and oxide phases that undergo little dissolution or transformation between their entry to the oceanic system and burial in sediments. For these elements the burial rate should be equal to the rain rate.

At most sites fluxes of refractory elements increase with depth in the water column. Aluminum is an example (Figure 9.3); a similar pattern exists for other refractory elements (Fe, Ti, Sc, and Th). The cause of the increase in refractory element fluxes could be: (1) resuspension of sediments and down slope movement of particles or (2) aggregation of fine

clays and other aluminosilicates by settling organic matter. Probably both processes are important.

The conservative character of refractory elements provides a test for the validity of a comparison between rain rate measured by sediment trap fluxes and burial rates in the underlying sediments. If the burial rate of a refractory element does not equal its rain rate to the bottom, there is good reason to question the comparison of more labile elements as well. For all sites except HAP the burial fluxes of Al and Fe are within a factor of two of the rain rates (Table 9.3). We discuss reasons for the HAP discrepancies below. Except for HAP the small differences between rain and burial rates for refractory elements are probably a consequence of comparing rain rates from a single year to the 103 to 105 yr time scale that is integrated by sediment accumulation rate measurements. Some differences could be due to imperfect collection efficiencies by sediment traps. If this effect was important, however, it should produce consistently higher or lower rain rates compared to burial rates. Also, trapping efficiency estimates for traps similar to those used in this study approach 100 percent (Bacon *et al.,* 1985).

The rain rate of particulate aluminum varies by a factor of 500 in our study (Table 9.3). Near shore sites generally have higher rain rates than more open ocean sites. Riverine aluminosilicate inputs could cause such a pattern. The Multitracers Transect (sites NS, MW, and Gyre) provides a clear demonstration of the decrease in flux with increasing distance from the continental margin. The total rain rate varies by a factor of 20 over the 600 km transect. Aluminum rain rates, which primarily indicate the extent of continental aluminosilicate input, vary by a factor of nearly 50 across this transect.
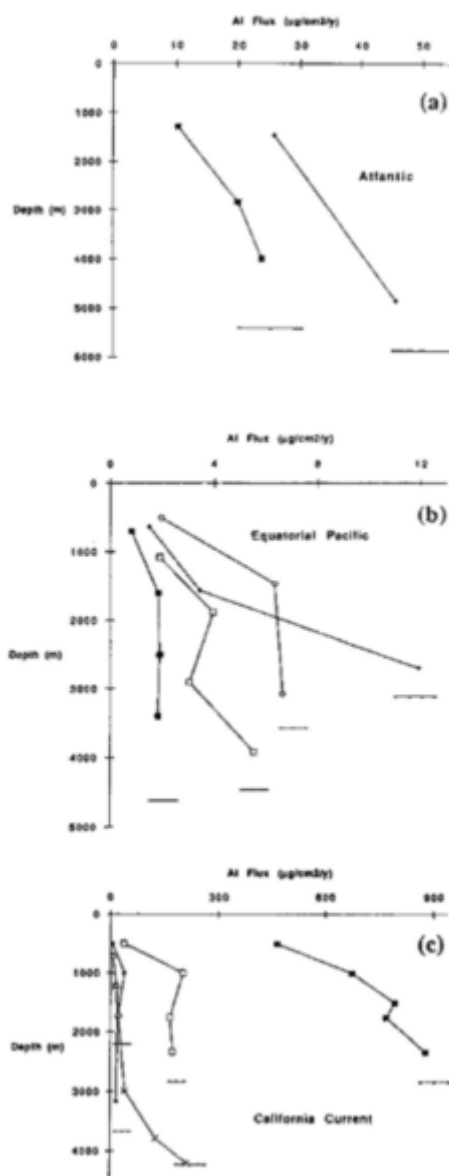
FIGURE 9.3 (a) Particulate aluminum flux variations with water depth at Atlantic sites used in this chapter. The squares denote the HAP site; diamonds indicate the NAP site. The horizontal lines mark the depth of the bottom for each site. (b) Particulate aluminum variations with depth at Equatorial Pacific sites. Open diamonds are for site H; filled diamonds are site M; open squares are site C; filled squares are site S. (c) Particulate aluminum flux variations with water depth at California Current sites. Filled squares are Nearshore; open squares are Midway; filled diamonds are Gyre; x denotes MFZ; open triangles are for ER.

BIOGENIC RAIN AND BURIAL FLUXES

At most sites biogenic debris dominates the settling particle flux. This is the case even for the particulate debris that reaches the bottom (Tables 9.2 and 9.4), despite the decomposition and dissolution that occurs throughout the water column. Assuming the biogenic fraction is composed of only carbonate, opal, and organic matter (2.5 times organic carbon), this fraction comprises 40 to 94 percent of the rain rate at the sites studied. Only at the relatively near shore sites in the California (NS and MFZ) is the total rain rate composed of less than 50 percent biogenic debris. The Equatorial Pacific sites, which contain 74 to 94 percent biogenic debris, are the most biogeneousrich of the 11 sites.

Several studies have attempted to relate rates of primary production to the flux of particulate organic carbon measured using sediment traps (Suess, 1980; Betzer *et al.,* 1984; Pace *et al.,* 1987). These results indicate that particle flux through the water column is a function of primary productivity and that this particulate flux decreases strongly with increasing depth. Presumably the decrease in particulate organic carbon with depth is a consequence of decomposition by bacteria and metabolism by zooplankton of carbon in of settling particles. The relationships exhibited by Figure 9.4 suggest that approximately 1 percent of the carbon fixed in the euphotic zone reaches depths as great as three kilometers. Recently, Silver and Gowing (1991) suggest that living organisms, which enter sediment traps (swimmers), can strongly influence the changes in carbon flux observed in the upper 1000 meters of the ocean and relationships such as shown in Figure 9.4.

The concept of "new" productivity is particularly relevant to the magnitude of particulate flux. New productivity is that portion of the total primary production that results from influx of new nutrients to euphotic zone (Dugdale and Goering, 1967). If the input of nutrients to the euphotic zone by upwelling, stream input, and atmospheric sources is balanced by an export flux due to the settling of particulate organic matter (Eppley and Peterson, 1979), measurement of POM fluxes can be used to estimate new productivity within the ocean. Low productivity regions of the oceans appear to have a major fraction (>80 percent) of total primary productivity supported by organic matter recycling. In contrast, much of the primary production in highly productive continental margins (˜ 50 percent) is new production (Platt and Harrison, 1985). One consequence of higher ratios of new to total primary productivity in more productive sites is that the rain rates of organic matter magnify the pattern of primary productivity variations. Thus, all other factors being equal, the carbon burial rate in sediments underlying high productivity sites should
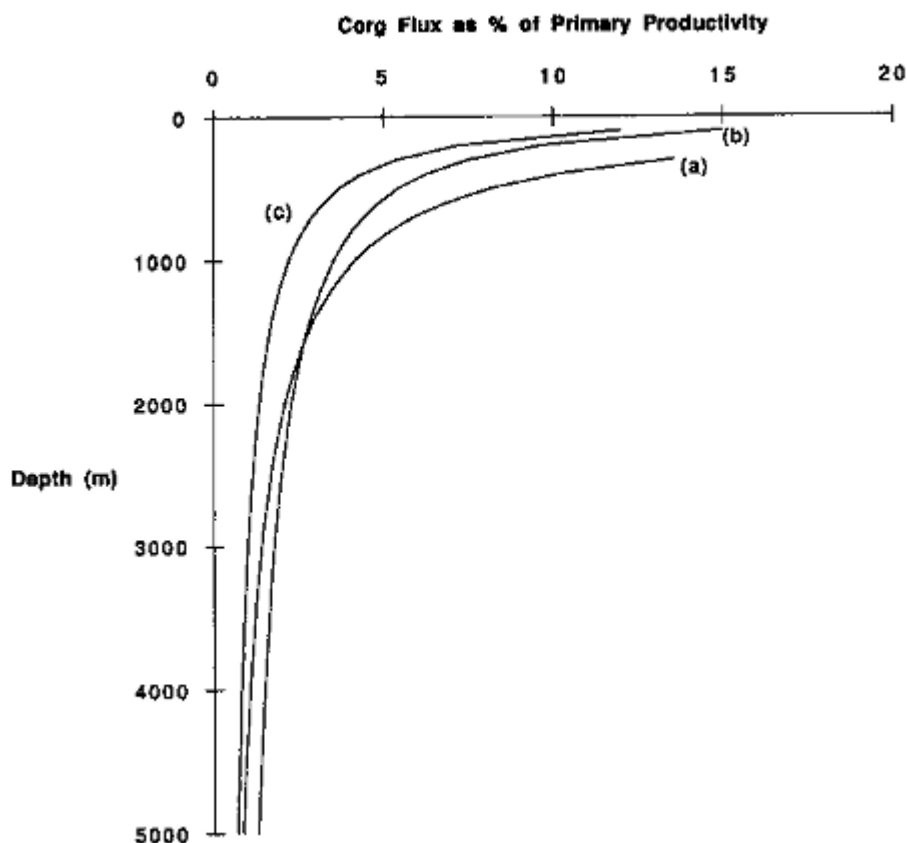
FIGURE 9.4 Particulate organic carbon flux as a percentage of primary productivity plotted against water depth. Curve (a) is from Suess (1980); curve (b) is from Betzer et al. (1984); curve (c) is from Pace et al. (1987).

be a larger fraction of primary productivity than at unproductive sites.
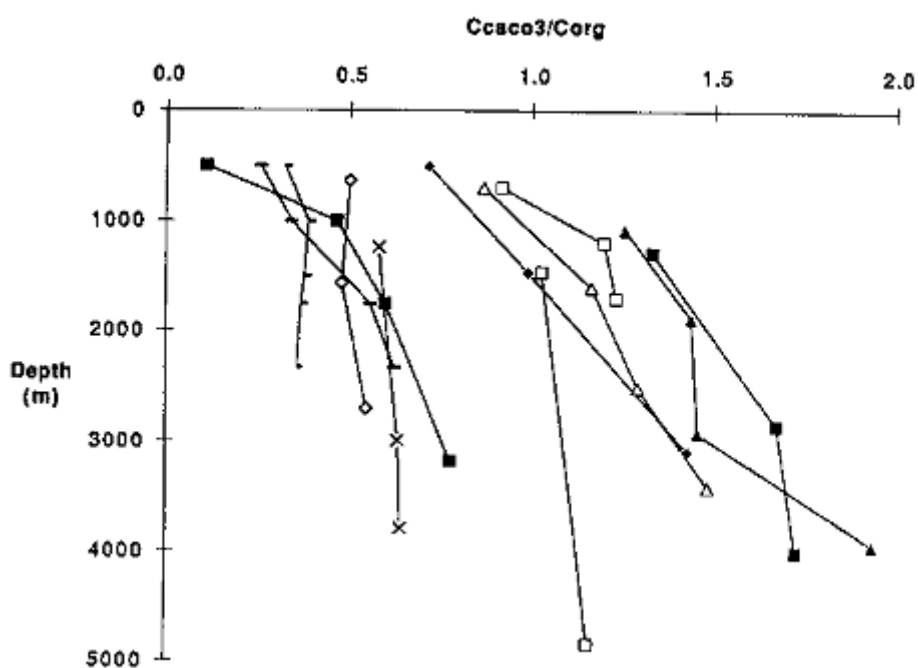
FIGURE 9.5 The ratio of carbonate carbon to organic carbon versus depth at all sites. Filled squares are HAP; open squares are NAP; filled diamonds are H; open diamonds are M; filled triangles are C; open triangles are S; x's are MFZ; small dashes are NS; large dashes are MW; filled squares are G; open squares are ER.

Because temporal variations in new production are a consequence of changes in external forcing agents (wind intensity, continental erosional rates), particle flux and sediment burial fluxes can be used to define changes in oceanographic conditions over a range of temporal scales. Moreover, the flux of particulate organic matter settling from the euphotic zone is one mechanism by which carbon is transferred from the upper ocean to the deep ocean. This process is largely responsible for the low carbon dioxide content in the atmosphere relative to what would be expected for equilibrium with the ocean atmosphere system (Broecker and Peng, 1982). Berger et al. (1988) suggest this process transfers 4-5 gigaton of carbon each year to the deep ocean.

The composition of settling biogenic particles can also affect atmospheric CO_2 (Dymond and Lyle, 1985). In particular the ratio of carbonate carbon to organic carbon influences the impact of the organic matter fluxes. This is because the settling of $CaCO_3$ is an alkalinity flux that has the effect of adding CO_2 to the atmosphere. Figure 9.5 summarizes the carbonate carbon to organic carbon variations at each site. In general there is an increase in this ratio with increasing water depth, an indication that organic carbon is recycled more rapidly than $CaCO_3$.

ORGANIC CARBON PRESERVATION

Organic carbon preservation in the pelagic sites (greater than 500 km from a continental margin) is low (Table 9.4). For these sites the average burial rate of organic carbon is less than 5 percent of the extrapolated rain to the sea floor. The sites near continental margins, however, have much higher preservation, as can be observed in a profile combining all of the northeast Pacific moorings (Figure 9.6). For sites less than 300 km from the coastline, greater than 20 percent of the rain rate is preserved. Preservation at the more distant sites drops to levels we have observed elsewhere in our pelagic mooring locations.

Relatively high preservation levels may not be uncommon near continental margins. Jahnke (1986) observed approximately a 50 percent preservation of the organic carbon rain in Santa Monica Basin. Similar high levels of carbon preservation have been compiled for other Southern California basins (Emerson, 1985). High apparent preservation could be due to deep lateral inputs of particulate organic matter (Jahnke et al., 1990). Other possible explanations for high preservation near the continents include the presence of refractory terrestrial organic matter in the organic fraction, the loss of an extremely labile fraction of organic carbon from the sediment trap material after collection, or a coupling between sedimentary mass accumulation rate and the preservation of the organic carbon fraction.

We can test the possibility for a significant terrestrial component in the organic fraction for the Multitracers sites in the California Current. There we have analyses of the lipid fraction in the surface sediments and can use the abundance of terrestrial plant wax alkanes to estimate the total terrestrial input to each site. We achieve this through abundance measurements made by Prahl and Carpenter

(1984) of these biomarkers with respect to total terrestrial organic carbon carried in the Columbia River. Measurement of the biomarker in the sediment (F. Prahl, unpublished) can then be multiplied by this factor in order to get an estimate of the total terrestrial organic carbon in the sample. This approach suggests no variation in the proportion of terrestrial organic carbon along the mooring transect, from 100 km from the coast to 700 km. In each case, the organic fraction consistently had a model terrestrial organic carbon fraction of about 20 percent. Thus, variations in the terrestrial organic carbon fraction cannot explain the decrease in preservation offshore.
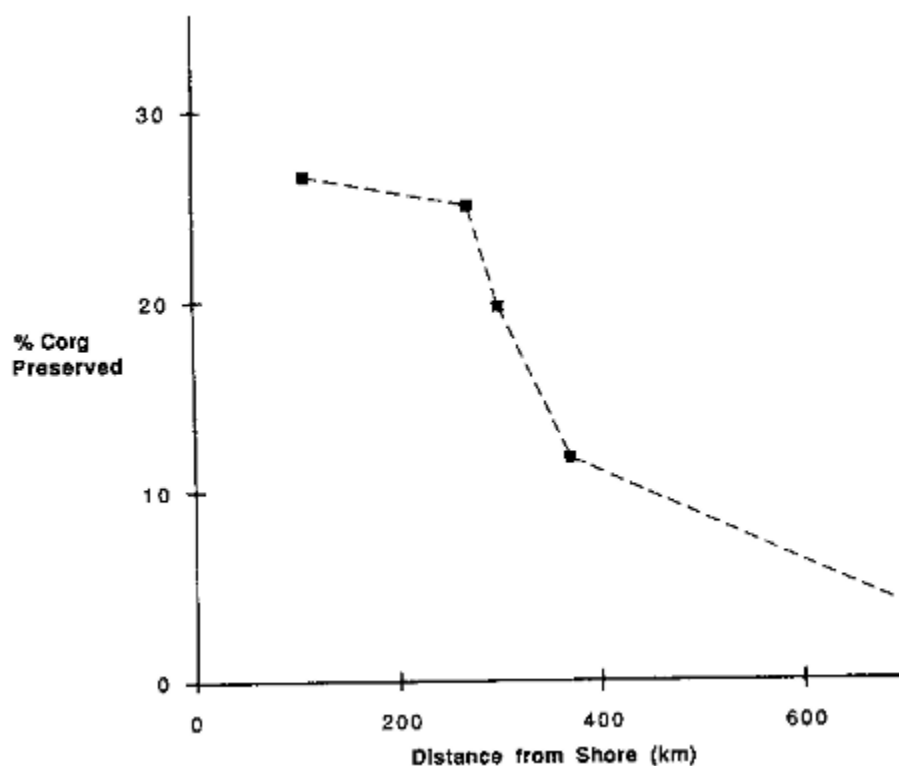
FIGURE 9.6 The percentage of the organic carbon rain rate that is preserved in the sediments versus distance from shore for the California Current sites.

The high preservation rates of organic carbon might be a consequence of underestimating the rain rate to the sediments. One possibility of error is that a portion of the settling organic matter dissolves upon entering the trap cups. Significant fractions of particulate P, N, and organic carbon enter into the trap solutions (Knauer, *et al.,* 1984; Karl, 1989; Dymond and Collier, 1989). Unfortunately, we cannot completely evaluate this effect because we do not have data on the dissolved organic carbon in most of our trap cups. Data that are available, however, suggest that the soluble fraction of the particulate organic matter is greatest at shallow depths (R.W. Collier, unpublished data). At depths of 81000 m the soluble fraction is approximately 50 percent of the total carbon flux and decreases to approximately 20 percent at greater depths (Dymond and Collier, 1989). Consequently, this effect could not account for the factor of 10 change in preservation observed on the Multitracers (NS to Gyre) transect. Moreover, the soluble loss of organic carbon would have to be greater in the near shore traps compared to central ocean traps to explain the observed gradient in preservation. There is no reason to suspect that near shore organic particles are more vulnerable to soluble loss than particles collected in the offshore traps.

High apparent preservation rates can be achieved near continental margins if organic material has been transported to the depositional site by deep lateral advection. A marked increase in the organic carbon flux with water depth would support this hypothesis. Data from the Multitracers transect, however, show relatively small increases of trapped organic carbon flux through the water column (Figure 9.7). Thus, if lateral transport has been important for the organic carbon flux, it must be occurring deeper than the deepest traps on our moorings, nominally 500 m above the seafloor. Because the measured rain rates of aluminum in NS and MFZ traps agree within a factor of two with the aluminum burial rates (Table 9.3), major near bottom inputs seem unlikely for these sites. Significant aluminosilicate contributions should accompany any deep inputs of particulate organic carbon.

Finally, as suggested by Heath *et al.* (1977), Muller and Suess (1979), Henrichs and Reeburgh (1987), and

Ingall and vanCappellen (1990), variations in sediment accumulation may affect the preservation of organic matter in the sediments. Emerson (1985), however, has argued that the residence time for organic carbon is too short for sediment accumulation rates to have any effect on the organic carbon preservation. Nevertheless, the correlation between organic carbon preservation and mass accumulation rate of the sediments (Figure 9.8) is significant ($R^2 = 0.80$). Perhaps these observations can be reconciled with the carbon degradation model of Emerson (1985) if organic carbon has a broad range of reactivities. If so, the relatively short residence time for organic carbon (~ 100 yr) would be a consequence of a mixture of highly labile organic matter and refractory organic matter with degradation constants sufficiently large that the sedimentation rate has an influence on the extent of preservation. In a more recent paper, Emerson and Hedges (1988) state that if organic carbon rain to sediments has a refractory component with a residence time of thousands of years, its concentration in sediments would be sensitive to sedimentation rate. Alternatively, Emerson (1985) suggests that bottom-water oxygen content and bioturbation rates are important controls on organic carbon preservation. Although we would not expect much variation of bottom
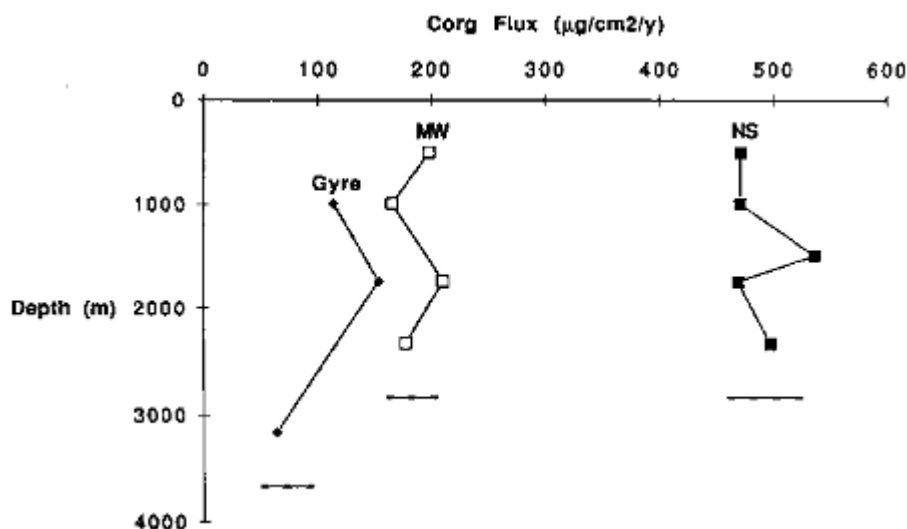
FIGURE 9.7 Variations in the particulate organic carbon flux with depth at the three sites comprising the Multitracers transect across the California current.
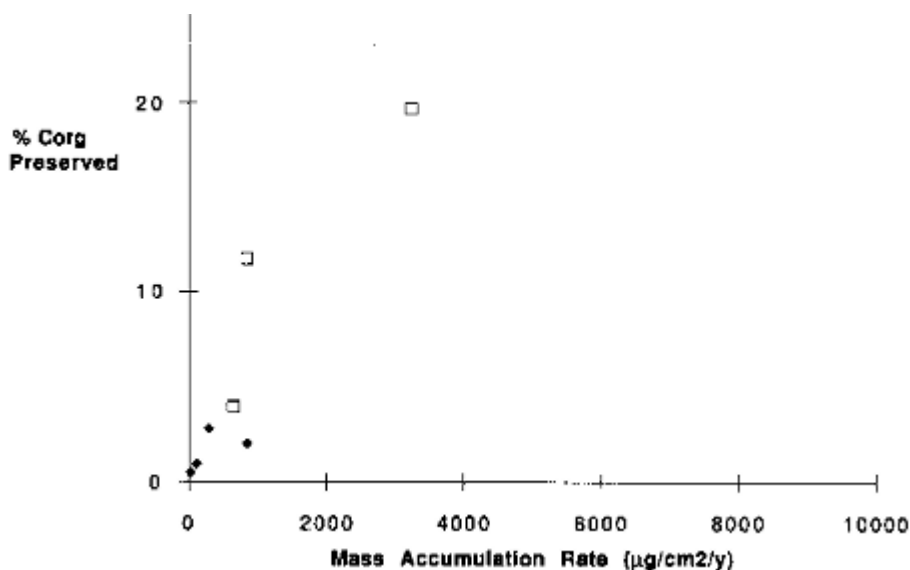
FIGURE 9.8 The percentage of organic carbon rain rate that is preserved versus the mass accumulation rate at that site. Filled square is Nares Abyssal Plain; open squares are California Current sites; diamonds are Equatorial Pacific Sites.

water oxygen along the latitudinal Multitracers transect, there may be variations in the bioturbation rate. It seems reasonable that the abundance of benthic fauna (and thus, bioturbation) correlates with organic carbon rain rate, which decreases strongly offshore. If this were the case, one would expect the organic carbon preservation rate to show a relationship to the carbon rain rate. The correlation between these two variables is weaker ($R^2 = 0.55$; Figure 9.9) than the correlation between carbon preservation and mass accumulation rate.
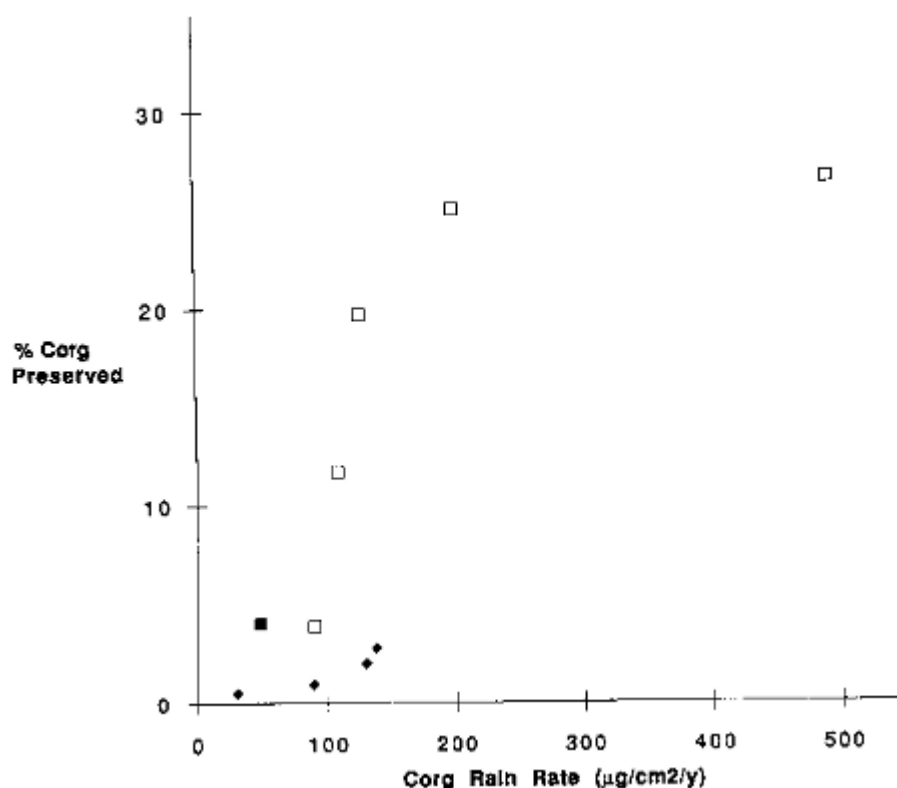
FIGURE 9.9 The percentage of organic carbon rain rate that is preserved versus the rain rate of organic carbon. Filled square is Nares Abyssal Plain; open squares are California Current sites; diamonds are Equatorial Pacific Sites.

CALCITE PRESERVATION

Calcite preservation in sediments is most strongly affected by the depth dependent changes in calcite saturation in the oceans. The effect is apparent at the northeast Pacific sites where the water depth ranges from 2200 to 4200 m. Above about 2200 m roughly 1/3 of the total calcite falling through the water column is preserved. Below this depth less than 10 percent survives in the sediments. There is no significant correlation between mass accumulation rate and preservation of $CaCO_3$ for these sites.

The $CCaCO_3/Corg$ of the raining debris may also effect the degree of preservation of $CaCO_3$. The production of CO_2 from organic matter decomposition (Emerson, 1981) will enhance $CaCO_3$ dissolution within the sediments. The effects of metabolic CO_2 production are a function of the $CCaCO_3/Corg$ of the biogenic particles reaching the seafloor. This effect may account for the relatively low preservation at the Nearshore site that has the lowest rain rate $CCaCO_3/Corg$ (Figure 9.5) and the lowest preservation of those California Current sites of similar depth (Table 9.4).

OPAL PRESERVATION

The percentage of opal preserved ranges from 1 to 20 percent at the sites shown in Table 9.4. Broecker and Peng (1982) have proposed an opal dissolution model in which the rain rate of opal provides an important control on the degree of preservation. With this model sites of high rain rate will not experience as large as fractional loss of the raining opal as sites with low opal rain rates. Thus, dissolution effects should enhance differences in the primary rain rate. Our data suggest higher preservation with greater rain rate of opal (Figure 9.10). The Broecker and Peng modeling of dissolution, however, assumes a constant rate of dissolution of pure opaline materials. This dissolution factor, which can be computed from the data in Tables 9.2 and 9.4, ranges from rates of 1000 to 12,000 $\mu g/cm^2/yr$. The Nearshore site has the highest dissolution factor. Variation in the rate of dissolution is not surprising since the nature of opaline debris ranges from robust radiolarian and diatom forms to more easily soluble silicoflagellates.
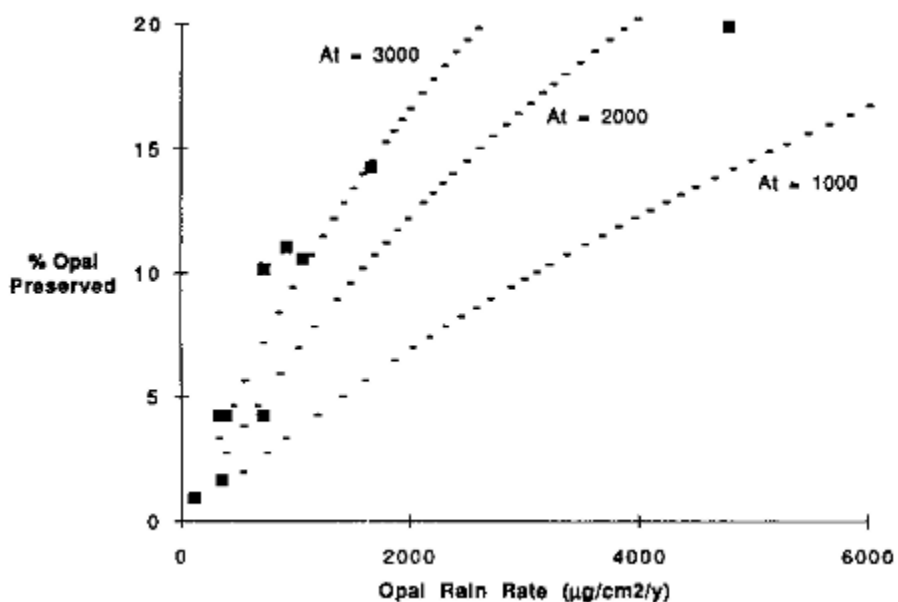
FIGURE 9.10 The percentage of opal rain rate that is preserved versus the opal rain rate. The dashed lines indicate the model opal preservation estimates of Broecker and Peng (1982). Their model suggests that the preservation is proportional to the opal rain rate, the dissolution rate of pure opal, and the burial rate of non-opal materials. The effects of different non-opal accumulation rates are shown (At = 1000, 2000, and 3000 μg/cm^2/yr). For all of the model lines a pure opal dissolution rate of 3000 μg/cm^2/yr was used.

THE RELATIONSHIP BETWEEN ALUMINOSILICATE AND BIOGENIC RAIN RATES

The aggregation of clays into larger, more rapidly settling particles is necessary to account for the discrete patterns of clay mineral distributions in deep ocean sediments. The direct relationship between the flux of organic carbon and aluminosilicate debris (Honjo, 1982; Deuser *et al.,* 1983) indicates some biogenic aggregation mechanism. Indiscriminate filtering of zooplankton, which repackage fine-grained aluminosilicate debris into rapidly sinking fecal pellets, could account for the carbon-aluminosilicate relationship. Alternatively, organic-rich flocs or marine snow may incorporate fine, inorganic particles. Although correlation between aluminosilicate or alumi
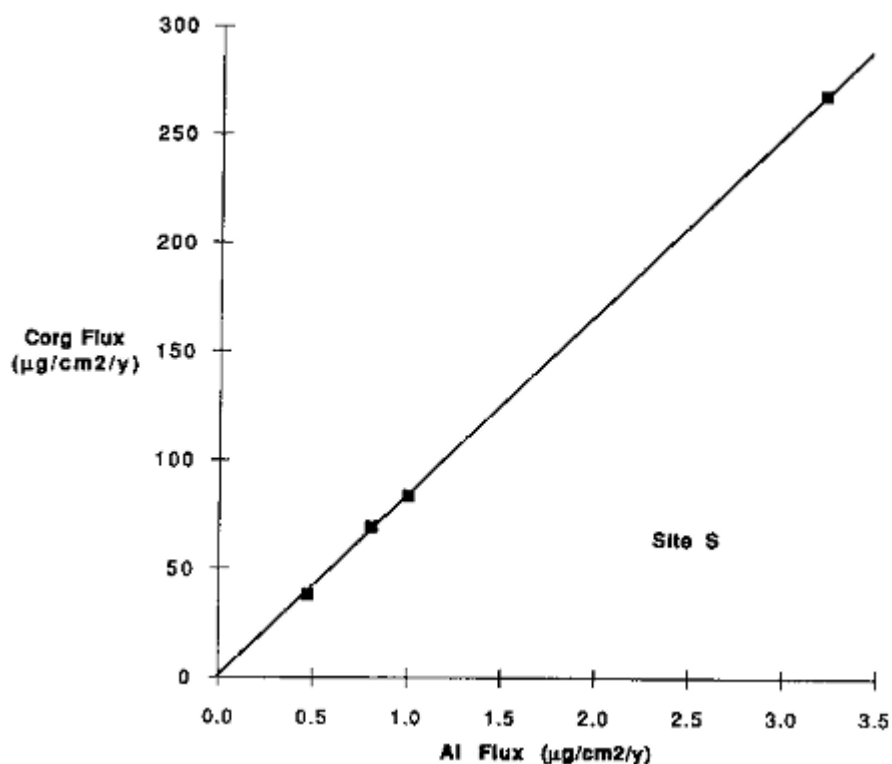
FIGURE 9.11 Organic carbon flux versus Al flux for site S samples. Only samples from the uppermost trap (700 m) deployed at this site were used. The different samples shown are the seasonal cups, which for S was only four samples.

nium fluxes and the flux of organic carbon (Figure 9.11) is apparent at any given site, a single relationship does not fit for all oceanic sites. Figure 9.12 demonstrates more than a factor of 100 range in Corg/Al values for settling particles in the oceans. Sites near continental sources have Corg/Al values that are less than one; in contrast, the ratio for Equatorial Pacific particles is approximately 100. These variations indicate that Corg and Al fluxes define a common carrier rather than a direct functional relationship. Zooplankton filtering or other aggregation processes may be responsible for the relationship, however, the available aluminosilicate debris is strongly dependent on location.

The strong correlation between the fluxes of particulate organic carbon and aluminum at any given site suggests an alternative means for computing the degree of preservation at the various sites. If the flux of aluminum to the bottom is conservative and the Corg/Al of the raining material remains constant over the time interval integrated by sediment burial rate data, the following relationship is valid:

Similar relationships can be written for any of the labile components of the particulate rain.

This approach overcomes problems that result from errors in the mass accumulation rate or trap efficiency. It is functionally equivalent to computing a correction factor for the rain rates that would make the rain rates of Al the same as the burial rate in sediments. Figure 9.13 demonstrates the change in the labile/Al ratio with depth for two sites and compares the ratio with that observed in the sediments. In Table 9.5 we have compiled the degree of preservation of Corg, CaCO₃, and opal computed by this ratio-to-Al approach. In general, this means of computing the degree of preservation agrees very well with the preservation of biogenic component computed by comparison of the rain rate and the burial fluxes (Figure 9.14).

For the Hatteras Abyssal Plain site (HAP) the ratio and the flux method do not agree. The rain rate/burial rate comparison indicates 24 and 90 percent preservation of organic carbon and CaCO₃ respectively (Table 9.3). In contrast, the preservation computed by the ratio-to-Al method is 4 percent for organic carbon and 11 percent for CaCO₃ (Table 9.5). Since the burial and rain rates of refractory element at HAP do not agree, we suspect the ratio method provides more accurate estimates of preservation at this site.

At HAP the burial flux of Al, Fe, and Ti exceeds the rain rate of these elements by nearly an order of magnitude
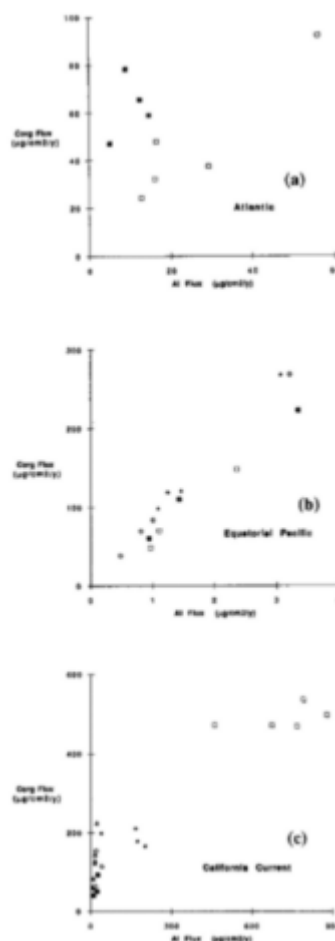
FIGURE 9.12 Organic carbon flux versus Al flux. (a) Atlantic sites; (b) Equatorial Pacific; (c) California Current. Only the uppermost samples at each site were used for this comparison and the trap depths range from 500 to 1500 m.

(Table 9.4). In addition, the mass accumulation rate is more than a factor of two greater than the total rain rate (Table 9.2). Several possibilities can account for this observation: (1) near bottom, down slope sediment transport from the nearby continental margin is a major source of deposition at this site; (2) episodic inputs of sediments are not measured by short-term trap experiments; (3) major errors exist in the sediment accumulation rates at this site. The third possibility seems unlikely because the sedimentation rates at this site are very well constrained by ^{14}C age determinations on several cores (Dickson, 1985). Neither of the other possibilities, however, can be elimi
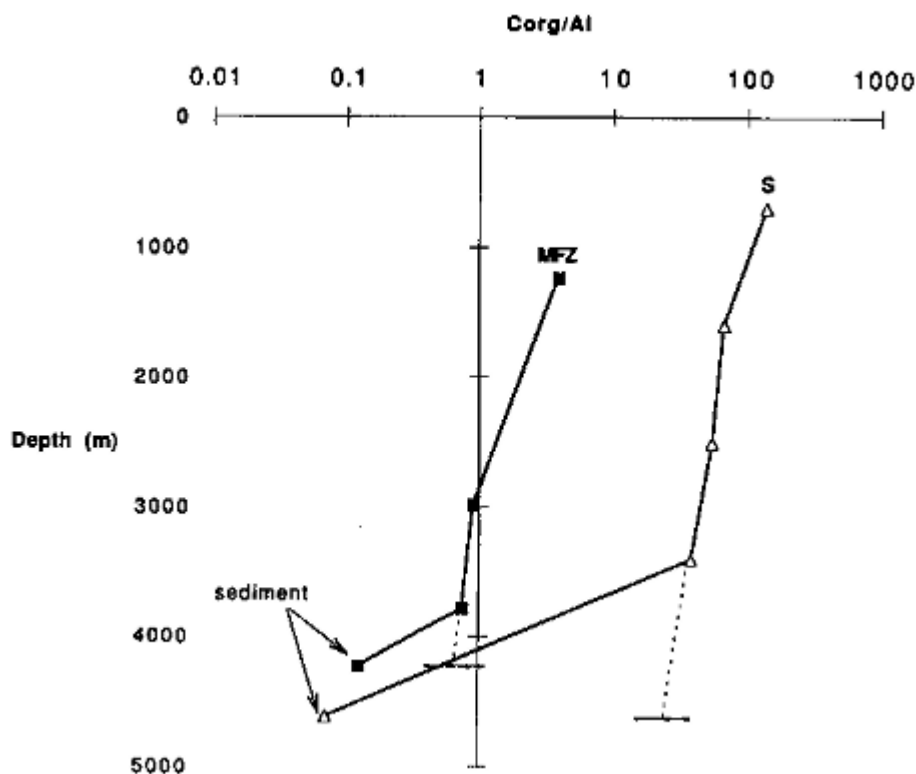
FIGURE 9.13 Changes in the particulate carbon to Al ratios with water depth for two representative sites. The deepest sample at each site is the ratio observed in sediments at the site. The horizontal dashed line indicates the bottom depth; the sloping dashed line indicates an extrapolation of the ratio to the bottom.

TABLE 9.5 Percentage of Rain Rate of Biogenic Components Preserved in the Sediment as Computed from Rations to Aluminim

Site	ORGANIC CARBON			CaCO₃			OPAL		
	C_{org}/A 1 (rain)	$C_{org}/A1$ (burial)	% Preserved (ratio)	$CaCo_3/A1$ (rain)	$CaCO_3/A1$ (burial)	% Preserved (ratio	Opal/A1 (rain)	Opal/A1 (burial)	% Preserved (ratio)
Atlantic									
HAP	1.6	0.1	3.7	23.5	3.0	12.9	3.8	0.4	11
NAP	0.9	0.0	3.5	9.2	0.6	6.7	2.0	0.0	0.83
Pacific									
MFZ	0.6	0.1	17	2.5	0.2	9.0	3.9	0.4	10.4
JDF	3.6	0.4	12.3	38.2	6.4	17	24	2.5	10.7
NS	0.5	0.2	33	1.6	0.1	6.8	5.1	1.1	22.5
MW	1.1	0.2	15	4.6	0.3	7.1	8.3	0.6	7.8
G	4.5	0.1	2.3	21.0	0.6	2.8	17	0.6	3.9
H	12.7	0.1	1.0	181.3	0.2	0.1	55	2.6	4.6
M	9.1	0.3	2.9	43.6	3.0	6.8	47	2.1	4.5
S	16.70	0.1	0.4	301.1	0.1	0.05	192	2.7	1.4
C	24.0	0.5	2.2	386.9	133.8	35	198	24	11.9

nated. At this site we also deployed some traps within 50 m of the bottom (Dymond, unpublished data). These traps had 10 to 20 times greater flux than the rain rates indicated in Table 9.2. Although this observation could be explained by local resuspension, the enhanced near bottom particle flux could also be due to lateral, near bottom advection, and thus, explain the rain rate/burial mismatch. Episodic flux events can not be ruled out. Turbidite inputs and benthic storms (Gardner and Sullivan, 1981), which occur in this general region of the Atlantic Ocean, could be a dominant source of sediments and yet not be observed in our short-term experiment.

An important implication of the observed mismatch between rain rate and burial rate of refractory elements is that labile components are probably also introduced by whatever process deposited the excess refractory elements. Thus, computations of the degree of preservation based on rain/burial comparisons are very likely to be erroneous. Computations of preservation based on the ratios-to-Al may be less effected by deep or episodic inputs since the labile-to-Al ratios in these sources are likely to be similar to the extrapolated ratios used in our calculations.

INFLUENCE OF THE CONTINENTAL MARGINS

The biogenic fluxes and preservation rates that we have computed indicate the importance of continental margins as a major removal site of biogenic material from the ocean. The large decrease in rain rate of biogenic material combined with the apparently greater preservation of these components (particularly organic carbon and opal) in sites near the continent result in very high burial rates. For example the burial rate of organic carbon and opal decrease by a factor of approximately 60 over the 600 km long Multitracers Transect (Table 9.4). The carbon burial rate at the Nearshore site is approximately 1000 times greater than that at site S, a central Pacific site that probably has organic carbon burial rates similar to red clay areas beneath the Pacific and Indian Ocean central gyre regions. These results are compatible with the global compilations of Berner (1982) and Romankevich (1984) that suggest more than 80 percent of the carbon burial in the oceans occurs at continental margins.

Because of the high rain rate of carbon near continental margins, these sites are also very important contributors of
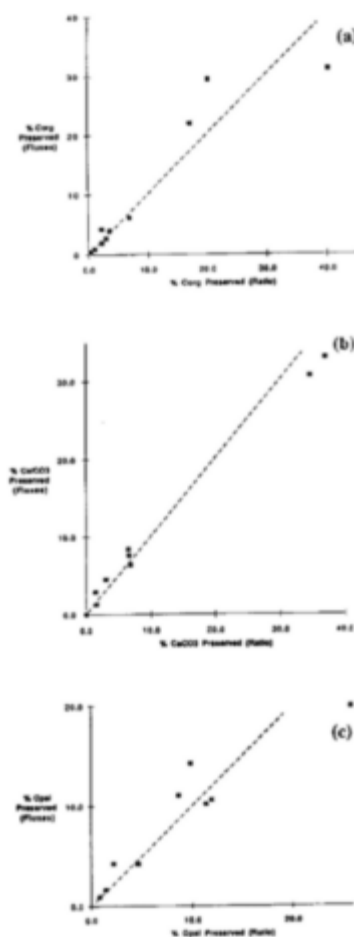
FIGURE 9.14 A comparison between the extent of preservation of (a) organic carbon, (b) CaCO$_3$, and (c) opal computed by two methods. The fluxes method compares the rain and burial fluxes of carbon. The ratio method compares the carbon-to-Al ratio in settling particles and bottom sediments.

the benthic flux to the bottom waters, despite their better preservation. The benthic flux decreases by a factor of six along the 600 km transect from our Nearshore site to the Gyre site (Table 9.4). These trap estimates of benthic flux and the decrease offshore are similar to estimates made from bottom chamber experiments (Smith and Hinga, 1983) off the southern California margin.

Resuspension and down slope movement of particles may be an important mechanism for transporting materials from the continental margins to the deep ocean basins. Variations in the flux of Al with depth are evidence for such a sediment-focusing mechanism. For the sites far from a continental margin such as Gyre, S and C there is little or no increase in Al flux with increasing water depth (Figure 9.3). In the Nearshore, Midway, and the MFZ sites, however, the flux of aluminum increases one to two orders of magnitude more rapidly with increasing depth (Figure 9.3). Since diagenesis of raining particles results in enrichments of aluminosilicates compared to biogenic components, sediment resuspension and down slope transport will be most effective in transporting aluminum and aluminosilicate-associated elements.

There is evidence that resuspension of shelf sediments is an important process for those sites within the California Current. This high energy continental margin experiences frequent winter storms that are known to produce wave-induced ripple marks to a depth of 200 m water depth (Komar *et al.,* 1972). Kulm *et al.,* 1975 suggest silt and clay accumulate on the Oregon shelf in the summer months and are resuspended and transported offshore in the winter. Moreover, because of the high biological productivity stimulated by summer upwelling, the same process may be an important means of exporting carbon and other bioactive elements. Time series measurements at the Nearshore site demonstrate surprisingly high organic carbon fluxes in the winter months (Collier *et al.,* 1989), a time expected to have low primary productivity. It is currently unknown whether this winter flux of carbon is the result of shelf resuspension or a winter productivity bloom. It is clear that the significance of shelf resuspension and off shore transport to the global carbon cycling is undefined and controversial (Walsh *et al.,* 1981; Rowe *et al.,* 1986).

EOLIAN SOURCES

It is probable that the source of particulate aluminosilicate flux observed at sites distant from continents is predominantly eolian. If we assume the eolian dust input has an Al content typical of igneous and sedimentary rocks, the total input can be compared to other estimates of the eolian fluxes. A variety of crustal rocks have Al contents of approximately 8 percent (Poldervaart, 1955), suggesting the estimated rain of aluminosilicate debris reaching the bottom at the Equatorial Pacific sites S and C is 23 and 77 μg/cm^2/yr respectively. Possibly only fluxes measured in the upper water column represent eolian inputs. Consequently, for sites S and C the eolian inputs estimated from Al fluxes measured at a depth of approximately 1000 m (Figure 9.3) are approximately 20 μg/cm^2/yr. This estimate is very similar to the Holocene atmospheric dust input determined by acid treating equatorial sediment cores (Rea *et al.,* Chapter 8, this volume). A similar computation for Gyre, another open-ocean site in the Pacific, suggests approximately 200 μg/cm^2/yr of eolian debris reaches this location. This estimate compares favorably with the sediment-based estimate of Janecek and Rea (1983) for sites in the central and eastern North Pacific that lie beneath the Westerly flow from Asian deserts.

Data from the Nares Abyssal Plain suggest that eolian sources are more important here than for any of our Pacific sites. Although this site is more than 1000 km from the nearest continental margin, the aluminum rain rate is higher than that measured for the more near shore HAP site. The aluminum flux measured at a depth of 1465 m (Figure 9.3) suggests a total eolian flux of over 300 μg/cm^2/yr. This site lies within the region of the Atlantic affected by Trade winds that sweep the African deserts and carry dust across the Atlantic Ocean (Prospero, 1981).

CONCLUSIONS

Biological debris dominates the settling particle flux in most open ocean sites. This flux of material is not only an important mechanism for transferring carbon to the deep ocean but also is linked to the removal of aluminosilicate material of continental origin. Comparison between the rain rate of aluminosilicates reaching the seafloor and their burial rate in the sediments indicates that sediment trap studies provide a valid approach for studying the recycling of biogenic elements at the seafloor.

The preservation of organic carbon appears to depend upon the sediment accumulation rate. The processes that account for this relationship are uncertain. Defining the factors that control the preservation of organic carbon is important for interpreting the sedimentary record and for estimating the extent of carbon removal from the ocean system.

Opal preservation appears to be related to the opal rain rate reaching the ocean floor. One consequence of this relationship is that burial rate patterns in sediments will magnify the patterns of opal production in the upper water column. In contrast, water depth strongly affects carbonate preservation.

Continental margins are sites of very high rain rates of biogenic and aluminosilicate debris, and the fluxes of these materials decrease very rapidly with increasing distance

from shore. This observation coupled with a decrease in organic preservation with distance indicates that continental margins are very important sites of carbon removal from the ocean. Some of the rain of carbon in the basins adjacent to margins may come from export of carbon that was fixed and temporally deposited on continental shelves and slopes.

REFERENCES

Alldredge, A.L., and M.W. Silver (1988). Characteristics, dynamics and significance of marine snow, Progress in Oceanography 20, 41-82 .

Bacon, M.P., C.A. Huh, A.P. Fleer, and W.G. Deuser (1985). Seasonality in the flux of natural radionuclides and plutonium in the deep Sargasso Sea, Deep-Sea Research 32, 273-286 .

Berger, W.H., K. Fischer, C. Lai, and G. Wu (1988). Ocean carbon flux: Global maps of primary production and export production, in Biogeochemical Cycling and Fluxes Between the Deep Euphotic Zone and Other Oceanic Realms, C. R. Agegian, ed., NOAA National Undersea Research Program, Research Report 88-1, pp. 131-176 .

Berner, R.A. (1982). Burial of organic carbon and pyrite sulfur in the modern ocean: Its geochemical and environmental significance, American Journal of Science 282, 451-473 .

Betzer, P.R., W.J. Showers, E.A. Laws, C.D. Winn, G.R. DiTullio, and P.M. Kroopnick (1984). Primary productivity and particle fluxes on a transect of the Equator at 153° W in the Pacific Ocean, Deep-Sea Research 31, 1-11 .

Blomqvist, S., and L. Hakanson (1981). A review on sediment traps in aquatic environments, Arch. Hydrobiology 91, 101-132 .

Broecker, W.S., and T.H. Peng (1982). Tracers in the Sea, Eldigio, New York, pp. 47-94 .

Collier, R., J. Dymond, N. Pisias, and M. Lyle (1989). Effects of seasonal oceanographic cycles on the paleoceanography record: Initial results from the MULTITRACERS experiment. EOS 70, 365 .

Deuser, W.G., and E.H. Ross (1980). Seasonal change in the flux of organic carbon to the deep Sargasso Sea, Nature 283, 364-365 .

Deuser, W.G., P.G. Brewer, T.D. Jickells, and R.F. Commeau (1983). Biological control of the removal of abiogenic particles from the surface ocean, Science 219, 388-391 .

Dickson, S. (1985). Late Quaternary evolution of the northern Hatteras Abyssal Plain. M. Sc. Thesis, University of Rhode Island, Kingston.

Dugdale, R.C., and J.J. Goering (1967). Uptake of new and regenerated forms of nitrogen in primary productivity, Limnology and Oceanography 12, 196-206 .

Dymond, J. (1984). Sediment traps, particle fluxes, and benthic boundary layer processes, in Global Ocean Flux Study, Proceedings of a Workshop, National Academy Press, Washington, D.C., pp. 260-284 .

Dymond, J., and M. Lyle (1985). Flux comparisons between sediments and sediment traps in the eastern tropical Pacific: Implications for atmospheric CO_2 variations during the Pleistocene, Limnology and Oceanography 30, 699-712 .

Dymond, J., and S. Roth (1988). Plume dispersed hydrothermal particles: A time-series record of settling flux from the Endeavour Ridge using moored sensors, Geochimica et Cosmochimica Acta 52, 2525-2536 .

Dymond, J., and R. Collier (1988). Biogenic particle fluxes in the equatorial Pacific: Evidence for both high and low productivity during the 1982-1983 El Niño, Global Biogeochemical Cycles 2, 129-137 .

Dymond, J., and R. Collier (1989). The easily soluble fraction of the settling particle flux, in Global Ocean Flux Study, Proceedings of a Workshop, National Academy Press, Washington, D.C., pp. 84-85 .

Dymond, J., K. Fischer, M. Clauson, R. Cobler, W. Gardner, M. J. Richardson, W. Berger, A. Soutar, and R.A. Dunbar (1981). A sediment trap inter-comparison study in the Santa Barbara Basin, Earth and Planetary Science Letters 53, 409-418 .

Emerson, S. (1981). Carbon fluxes at the sediment-water interface of the deep-sea: Calcium carbonate preservation. Journal of Marine Research 39, 139-162 .

Emerson, S. (1985). Organic carbon preservation in marine sediments, The Carbon Cycle and Atmospheric CO_2: Natural Variations Archean to Present, E.T. Sundquist and W.S. Broecker, eds., American Geophysical Union, Washington D.C., pp. 78-89 .

Emerson, S., and J.I. Hedges (1988). Processes controlling the organic carbon content of open ocean sediments, Paleoceanography 3, 621-634 .

Eppley, R.W., and B.J. Peterson (1979). Particulate organic matter flux and planktonic new production in the deep ocean, Nature 282, 677-680 .

Fischer, K.J. (1984). Particle Fluxes to the Eastern Tropical Pacific Ocean — Sources and Processes, Ph.D. Thesis, Oregon State University, Corvallis, 241 pp .

Fischer, K., J. Dymond, C. Moser, D. Murray, and A. Matherne (1983). Seasonal variation in particulate flux in an offshore area adjacent to coastal upwelling, in Coastal Upwelling, Part A., E. Suess and J. Thiede, eds., Plenum Publishing Corp., New York, pp. 209-224 .

Fischer, K., J. Dymond, M. Lyle, A. Soutar, and S. Rau (1986). The benthic cycle of copper: Evidence from sediment trap experiments in the eastern tropical North Pacific Ocean, Geochimica et Cosmochimica Acta 50, 1535-1543 .

Gardner, W.D. (1980). Field assessment of sediment traps, Journal of Marine Research 38, 41-52 .

Gardner, W.D., and L.G. Sullivan (1981). Benthic storms: Temporal variability in a deep-ocean nepheloid layer, Science 213, 329-331 .

Heath, G.R., T.C. Moore, Jr., and J.P. Dauphin (1977). Organic carbon in deep-sea sediments, in The Fate of Fossil Fuel CO_2 in the Oceans, N.R. Andersen and A. Malahoff, eds., Plenum Publishing Corp., New York, pp. 605-625 .

Heggie, D., C. Maris, A. Hudson, J. Dymond, R. Beach, and J. Cullen (1987). Organic carbon oxidation and preservation in NW Atlantic continental margin sediments, in Geology and Geochemistry of Abyssal Plains, P.P.E. Weaver and J. Thomson, eds., Geological Society Special Publication No. 31, 215-236 .

Henrichs, S.M., and Reeburgh (1987). Anaerobic mineralization of marine sediments organic matter: Rates and the role of anaerobic processes in the oceanic carbon economy, Geomicrobiology Journal 5, 191-237 .

Honjo, S. (1982). Seasonality and interaction of biogenic and lithogenic particulate flux at the Panama Basin, Science 218, 516-518 .

Honjo, S., and K.W. Doherty (1988). Large aperture time-series oceanic sediment traps: Design objectives, construction and application, Deep-Sea Research 35, 133-149 .

Ingall, E.D., and P. vanCappellen (1990). Relationship between sedimentation rates and burial of organic phosphorous and organic carbon in marine sediments, Geochimica et Cosmochimica Acta 54, 373-386 .

Jahnke, R.A. (1986). Pelletal phosphorite precipitation in Peru continental margin sediments, EOS 67 , 1007 .

Jahnke, R.A., C.E. Reimers, and D.B. Craven (1990). Intensification of recycling of organic matter at the sea floor near ocean margins, Nature 348, 50-54 .

Janecek, T.R., and D.K. Rea (1983). Eolian deposition in the northeast Pacific Ocean: Cenozoic history of atmospheric circulation, Geological Society of America Bulletin 94, 730-738 .

Karl, D. (1989). The measurement of total C, N and P flux, in Global Ocean Flux Study, Proceedings of a Workshop, National Academy Press, Washington, D.C., pp. 68 .

Knauer, G.A., D.M. Karl, J.H. Martin, and C.N. Hunter (1984). In-situ effects of selected preservatives on total carbon, nitrogen and metals collected in sediment traps, Journal of Marine Research 42, 445-462 .

Komar, P., R.H. Neudeck, and L.D. Kulm (1972). Observations and significance of deep-water oscillatory ripple marks on the Oregon continental shelf, in Shelf Sediment Transport, Swift, Duane and Pilkey, eds., Dowden, Hutchinson and Ross, Inc., Stroudsburg, Pa., pp. 601-619 .

Kulm, L.D., R.C. Roush, J.C. Harlett, R.H. Neudeck, D.M. Chambers, and E.J. Runge (1975). Oregon continental shelf sedimentation: Interrelationships of facies distribution and sedimentary processes, Journal of Geology 83, 145-175 .

Lampitt, R.S. (1985). Evidence for the seasonal deposition of detritus to the deep-sea floor and its subsequent resuspension, Deep-Sea Research 32, 885-897 .

McCave, I.N. (1975). Vertical flux of particles in the ocean, Deep-Sea Research 22, 491-502 .

Murphy, K., and J. Dymond (1984). Rare earth element fluxes and geochemical budget in the eastern equatorial Pacific , Nature 307, 444-447 .

Muller, P.J., and E. Suess (1979). Productivity, sedimentation rate, and sedimentary organic matter in the oceans: I. Organic carbon preservation, Deep-Sea Research 26A, 1347-1362 .

Pace, M., G.A. Knauer, D.M. Karl, and J.H. Martin (1987). Particulate matter fluxes in the ocean: A predictive model, Nature 325, 803-804 .

Pilskaln, C.H., and S. Honjo (1987). The fecal pellet fraction of biogeochemical particle fluxes to the deep sea, Global Biogeochemical Cycles 1, 31-48 .

Platt, T., and W.G. Harrison (1985). Reconciliation of carbon and oxygen fluxes in the upper ocean, Deep-Sea Research 33, 273-276 .

Poldervaart, A. (1955). Chemistry of the Earth's Crust, in Crust of the Earth, A. Poldervaart, ed., Geological Society of America Special Paper 62, pp. 119-144 .

Prahl, F., and R. Carpenter (1984). Hydrocarbons in Washington coastal sediments, in Estuarine and Coastal Shelf Science 18, 703-720 .

Prospero, J.M. (1981). Eolian transport to the world ocean, in The Sea, Volume 7 , The Oceanic Lithosphere, C. Emiliani, ed., John Wiley and Sons, New York, pp. 801-874 .

Romankevich, E.A. (1984). Geochemistry of Organic Matter in the Oceans. Springer-Verlag, New York.

Roth, S.E., and J. Dymond (1989). Transport and settling of organic material in a deep-sea hydrothermal plume: Evidence from particle flux measurements, Deep-Sea Research 36, 1237-1254 .

Rowe, G.T., S. Smith, P. Falkowski, T. Whitledge, R. Theroux, W. Proehl, and H. Ducklow (1986). Do continental shelves export organic matter? Nature 324, 559-561 .

Silver, M.W., and M.M. Gowing (1991). The "particle" flux: Origins and biological components, Progress in Oceanography 26, 75-113 .

Smith, K.L., and K.R. Hinga (1983). Sediment community respiration in the deep sea, in The Sea, Volume 8 , G.T. Rowe, ed., John Wiley and Sons, Inc., New York, pp. 331-370 .

Suess, E. (1980). Particulate organic carbon flux in the oceans-surface productivity and oxygen utilization, Nature 288, 260-263 .

Soutar, A., S.A. Kling, P.A. Crill, E. Duffrin, and K.W. Bruland (1977). Monitoring the marine environment through sedimentation, Nature 266, 136-139 .

Thomson, J., M.S.N. Carpenter, S. Colley, T.R.S. Wilson, H. Elderfield, and H. Kennedy (1984). Metal accumulation rates in northwest Atlantic pelagic sediments, Geochimica et Cosmochimica Acta 48, 1935-1948 .

Urrere, M.A., and G.A. Knauer (1981). Zooplankton fecal pellet fluxes and vertical transport of particulate organic material in the pelagic environment, Plankton Research 3, 369-387 .

Walsh, I.K., G.T. Rowe, R.L. Iverson, and C.P. McRoy (1981). Biological export of shelf carbon as a neglected sink of the global CO_2 cycle, Nature 291 .

Walsh, I., K. Fischer, D. Murray, and J. Dymond (1988a). Evidence for resuspension of rebound particles from near-bottom sediment traps, Deep-Sea Research 35, 59-70 .

Walsh, I., J. Dymond, and R. Collier (1988b). Rates of recycling of biogenic components of settling particles in the ocean derived from sediment trap experiments, Deep-Sea Research 35, 43-58 .

Weliky, K., E. Suess, C.A. Ungerer, P.J. Muller, and K. Fischer (1983). Problems with accurate carbon measurements in marine sediments and water column particulates: A new approach, Limnology and Oceanography 28, 1252-1259 .

10

Seafloor Diagenetic Fluxes

W.R. MARTIN AND F.L. SAYLES
Woods Hole Oceanographic Institution

INTRODUCTION

Early diagenesis is an important contributor to the oceanic cycles of many components of seawater. In many cases, the flux across the sediment-water interface resulting from early diagenesis is comparable to input rates to the ocean from other sources. In the cases of many bioactive elements, the early diagenetic flux is considerably larger than, for instance, the riverine input to the ocean, as early diagenesis is intimately involved in the rapid cycling of these elements within the ocean. However, a general characteristic of early diagenetic fluxes, both for bioactive components of seawater and for the major seawater ions, is that they affect oceanic concentrations on long time scales, ranging from 10^4 to 10^7 years.

The study of early diagenesis is important to the study of ocean hisory, as early diagenetic reactions play an important role in fixing sediment composition. Diagenetic fluxes exceed burial rates for the major bioactive elements: about 90 percent of the organic carbon rain to the sea floor degrades during early diagenesis; over 60 percent of the biogenic silica, and about 80 percent of the $CaCO_3$ reaching the sea floor dissolve. Thus, variations in diagenetic reaction rates can have disproportionately large effects on sedimentary concentrations and accumulation rates of these components.

It is important to recognize that, at the present time, any analysis of the role of early diagenesis in oceanic processes is data-limited. The spatial coverage of measurements is limited; more importantly, the interpretation of results often depends on the measurement technique used. For this reason, we begin our evaluation of early diagenetic fluxes with a review of measurement techniques and uncertainties. Then, we examine the ways in which early diagenesis affects the modern oceanic cycles of the major seawater ions, carbon, and silicon; and we examine its effects on the sedimentary record of ocean history as it is interpreted using organic carbon, $CaCO_3$, and opal data.

THE MEASUREMENT OF BENTHIC FLUXES

The most sensitive indicators of early diagenetic reactions are the fluxes of dissolved reactants or products across the sediment-water interface. If the sedimentary system is in quasi-steady state over the time scale of the reaction of interest, the benthic fluxes of the reactants and/or products provide a measure of the reaction rate, integrated over the sediment column. Several considerations are essential to an evaluation of benthic flux measurements. Among the most important are the possibility of measurement artifacts, the resolution of the measurement method relative to the characteristic length or time of the

reaction being monitored, and the importance of model assumptions to the flux calculation.

Most benthic flux estimates made to date have been obtained by applying transport models to concentration versus depth profiles of pore water solutes. An important feature of these estimates is that they are only as accurate as the transport parameters needed to convert the concentration measurements into flux estimates. In pelagic sediments, the dominant transport process is molecular diffusion; here, accurate estimates of sediment diffusivity and porosity near the sediment-water interface are required. In continental margin sediments, solute transport is enhanced over that due to diffusion by biologically and physically driven irrigation, and models applied to pore water profiles must include independent estimates of the effects of these processes (Aller, 1980b; Christensen *et al.,* 1984). Benthic flux estimates that are less dependent on transport models are obtained through the use of benthic flux chambers. In these experiments, sediments and a small volume of overlying water are enclosed for incubation periods of hours to about a month, and changes in concentration of diagenetic products or reactants in the overlying water are monitored. It appears that, with the possible exception of reactions with scale lengths on the order of a millimeter, the assumptions leading from these measurements to benthic flux estimates are reasonably robust (e.g., Bender *et al.,* 1989). In the special case of rapid reactions occurring primarily within one or two millimeters of the sediment-water interface, neglect of the diffusive sublayer at the sediment-water interface may lead to erroneous flux estimates (Boudreau and Guinasso, 1982). Benthic flux estimates based on flux chamber experiments are probably preferable to pore water profile based estimates because, in most cases, the estimates are essentially model-independent.

A second consideration that is important to evaluating benthic flux estimates is the resolution of the method used. For pore water profile based estimates, accurate flux calculations depend on the relationship between the length scale over which the diagenetic reaction occurs in the sediments and the sampling length scale. Because many reactions occur on length scales of millimeters to one or two centimeters in many locations (Emerson and Bender, 1981; Bender and Heggie, 1984; Reimers, 1987; Bender *et al.,* 1989), sampling resolution is an important limitation of many pore water based flux estimates. "Traditional" core sectioning and centrifuging/squeezing methods have been used with a resolution of 0.5 to 2 cm. In situ sampling methods based on "harpoon"-type samplers (Sayles *et al.,* 1973b), while free of the artifacts associated with core recovery, have been limited to a sampling resolution of 2 to 5 cm. Recently, two methods capable of in situ measurement of several pore water components have begun to be used: electrode techniques for the measurement of dissolved oxygen and pH (Revsbech *et al.,* 1980; Reimers *et al.,* 1986; Archer *et al.,* 1989), and whole-core squeezers for measuring solutes whose concentration is not changed by disturbances of ion exchange equilibria on very short time scales (minutes) (Bender *et al.,* 1987; Martin *et al.,* 1988; Bender *et al.,* 1989). Both of these methods are capable of millimeter-scale resolution. We compare the resolution of several of these techniques in Figure 10.1. For flux chamber based estimates, one must consider whether the experiment length is sufficient to produce a measurable concentration change in the solution component of
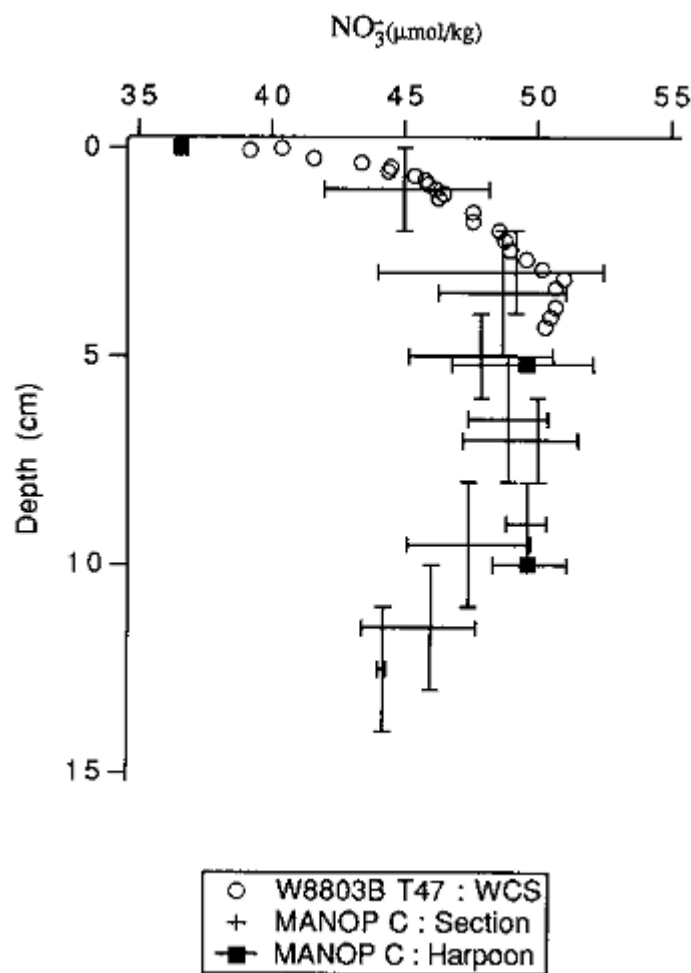
FIGURE 10.1 A comparison of the depth resolution of different pore water sampling techniques. Samples are from the eastern equatorial Pacific. The vertical bars on the section/centrifuge samples represent the sampling interval; the horizontal bars represent the range of values measured in the different cores samples. All MANOP data are from Jahnke et al. (1982b). The wholecore squeezer samples (open circles) are not strictly comparable to the section/centrifuge (crosses) or in situ (closed circles) samples; they were taken at the same latitude as the others but somewhat to the east of them and were taken several years later. Nonetheless, the concentrations are comparable, and the resolution comparison should be valid.

interest. Ultimately, experiment length is limited by the need to maintain incubation conditions close to those of the steady state sediment system. In most sediments, experiment length is limited by changes in the bottom water oxygen concentration or by the availability of labile organic matter in the closed system; these limitations make it difficult to measure fluxes of slowly reacting components of the system, particularly if they are present at high concentrations in bottom water. Thus, fluxes of major ions, and, to a lesser extent, ΣCO_2, are difficult to measure using benthic flux chambers.

Because the changes in concentration that must be resolved to estimate benthic fluxes are often small, samples must be artifact-free. Artifacts introduced in the recovery of cores from the seafloor are known to significantly alter pore water concentrations for many of the major species of interest here. These artifacts occur as a result of warming during recovery and can strongly affect the major cations through ion exchange reactions (Mangelsdorf *et al.,* 1969; Bischoff *et al.,* 1970; Sayles *et al.,* 1973a). De-pressurization during recovery of cores from the deep sea can also introduce artifacts through $CaCO_3$ precipitation, substantially changing ΣCO_2, alkalinity, and Ca^{2+} concentrations (Murray *et al.,* 1980; Emerson *et al.,* 1982). It is these problems that led to the development of in situ pore water sampling techniques (Barnes, 1973; Sayles *et al.,* 1973b). Comparisons of profiles obtained by in situ and shipboard techniques have shown that shipboard techniques can be used for measuring dissolved oxygen, nitrate, and silicate; they do not appear to be suitable for phosphate measurement (Jahnke *et al.,* 1982b). Because benthic flux chamber measurements are typically carried out in situ, they are free of artifacts due to shipboard separation of pore waters from the solid phases of sediments.

Sampling resolution, measurement artifacts, and transport model assumptions affect fluxes calculated from different measurement techniques to varying extents. There is another important class of model assumptions which affect all flux calculations equally. These assumptions result from our limited knowledge of diagenetically important chemical reactions. The outstanding example, one which will be important to our subsequent discussion, is the calculation of the rate of organic carbon degradation at the sea floor. Because of the difficulty of making artifact-free measurements of dissolved inorganic (and organic) carbon in pore waters, benthic organic carbon degradation rates are often estimated based on fluxes of nitrate and oxygen across the deep sea sediment-water interface, and on fluxes of sulfate in nearshore sediments. Translations of these measurements into organic carbon fluxes require assumptions about the oxidation/reduction stoichiometry of organic carbon degradation reactions (see Table 10.1). The oxidation states of C, N, and H in organic matter are generally represented by assuming the elements are present as CH_2O and NH_3. All of the the organic C is assumed to be oxidized to CO_2; depending on the environmental redox potential, N is oxidized to NO_3^- (oxic degradation) or N_2 (denitrification and Mn reduction), or released as NH_3 (Fe reduction, sulfate reduction) (Froelich *et al.,* 1979). Takahashi *et al.* (1985) have called into question the assumptions about the oxidation states of the reactants, par

TABLE 10.1 Organic Matter Degradation Reactions

O_2 Reduction

a. No $CaCO_3$ dissolution:
$(CH_2O)_{106}(NH_3)_{16}(H_3PO_4) + 138\ O_2 \rightarrow$
$106\ HCO_3^- + 16\ NO_3^- + HPO_4^{2-} + 124\ H^+ + 16\ H_2O$

b. With $CaCO_3$ dissolution:
$(CH_2O)_{106}(NH_3)_{16}(H_3PO_4) + 138\ O_2 + 124\ CaCO_3 \rightarrow$
$230\ HCO_3^- + 16\ NO_3^- + HPO_4^{2-} + 124\ Ca^{2+} + 16\ H_2O$

Nitrate Reduction

a. No $CaCO_3$ dissolution:
$(CH_2O)_{106}(NH_3)_{16}(H_3PO_4) + 94.4\ NO_3^- \rightarrow$
$13.6\ CO_2 + 92.4\ HCO_3^- + 55.2\ N_2 + HPO_4^{2-} + 84.8\ H_2O$

b. With $CaCO_3$ dissolution:
$(CH_2O)_{106}(NH_3)_{16}(H_3PO_4) + 94.4\ NO_3^- + 13.6\ CaCO_3 \rightarrow$
$119.6\ HCO_3^- + 55.2\ N_2 + HPO_4^{2-} + 13.6\ Ca^{2+} + 71.2\ H_2O$

Mn Reduction

a. No $CaCO_3$ equilibrium:
$(CH_2O)_{106}(NH_3)_{16}(H_3PO_4) + 236\ MnO_2 + 364\ H^+ \rightarrow$
$236\ Mn^{2+} + 106\ HCO_3^- + 8\ N_2 + HPO_4^{2-} + 260\ H_2O$

b. With $CaCO_3$ equilibrium:
$(CH_2O)_{106}(NH_3)_{16}(H_3PO_4) + 236\ MnO_2 + 364\ Ca^+ + 258\ HCO_3^- \rightarrow$
$236\ Mn^{2+} + 364\ CaCO_3 + 8\ N_2 + HPO_4^{2-} + 260\ H_2O$

Fe Reduction

a. No $CaCO_3$ equilibrium:
$(CH_2O)_{106}(NH_3)_{16}(H_3PO_4) + 212\ Fe_2O_3 + 756\ H^+ \rightarrow$
$424\ Fe^{2+} + 106\ HCO_3^- + 16\ NH_4^+ + HPO_4^{2-} + 424\ H_2O$

b. With $CaCO_3$ equilibrium:
$(CH_2O)_{106}(NH_3)_{16}(H_3PO_4) + 212\ Fe_2O_3 + 756\ Ca^{2+} + 650\ HCO_3^- \rightarrow$
$424\ Fe^{2+} + 756\ CaCO_3 + 16\ NH_4^+ + HPO_4^{2-} + 424\ H_2O$

Sulfate Reduction

a. No $CaCO_3$ equilibrium:
$(CH_2O)_{106}(NH_3)_{16}(H_3PO_4) + 53\ SO_4^{2-} \rightarrow$
$106\ HCO_3^- + 16\ NH_4^+ + HPO_4^{2-} + 53\ HS^- + 39\ H^+$

b. With $CaCO_3$ equilibrium:
$(CH_2O)_{106}(NH_3)_{16}(H_3PO_4) + 53\ SO_4^{2-} + 39\ CaCO_3 \rightarrow$
$145\ HCO_3^- + 16\ NH_4^+ + HPO_4^{2-} + 53\ HS^- + 39\ Ca^{2+}$

ticularly of organic H: using data taken on isopycnal surfaces in the upper water column, they have shown that the Redfield O_2:C ratio may underestimate the true ratio (they estimate 172:122 ± 18 versus 138:106 in the Redfield scheme). In addition, several workers have measured substantial gradients of dissolved organic carbon and nitrogen across the sediment-water interface, both in continental margin and deep-sea sediments (Suess *et al.,* 1980; Elderfield, 1981; Heggie *et al.,* 1987): in several cases, DOC gradients an order of magnitude larger than the inorganic carbon gradients. Unfortunately, the diffusivity of DOC in marine sediments is unknown, and these gradients cannot be translated into fluxes. Existing estimates of the diffusivity of DOC indicate that it may be less than an order of magnitude smaller than that of dissolved inorganic carbon (Mackin, 1986); thus, it cannot be assumed that all organic C is oxidized to CO_2 during degradation, and DOC cannot be ignored in the sedimentary carbon budget.

Assumptions about the C:N:P ratio in degrading organic matter are often made when a local, measurement-based estimate is not available. In fact, organic matter composition varies over significant ranges, and accurate calculation of carbon fluxes requires that this compositional variability be taken into account. C:N ratios of degrading organic matter have been estimated by measurements of solid phase elemental ratios (Table 10.2), yielding a range of about a factor of 2, from 6.6 to 12 (compared to the Redfield ratio of 6.6). Sediment trap measurements made by Honjo (1980) and by Martin *et al.* (1987) show that the C:N ratio at a site increases systematically with depth; Honjo's results also show that sedimentary organic matter has C:N systematically greater than that of the organic matter in deep sediment traps at the same locations (Table 10.2). Thus, organic matter appears to be fractionated during degradation, with N being recycled more rapidly than C (Suess and Muller, 1980; Martin *et al.,* 1987). For that reason, C:N of the solid phase may not be the best measure of C:N of the degrading organic matter. Several workers have used ratios of pore water constituents, usually O_2 and NO_3^- in oxic pelagic sediments, coupled with assumptions about redox stoichiometry, to derive C:N ratios (Berner, 1977). This procedure has yielded a range similar to that of the solid phase analyses, C:N » 7 to 12 (Table 10.2). We conclude that carbon fluxes calculated from NO_3^- profiles will be systematically low if organic matter is assumed to have Redfield composition, and that an uncertainty of up to ± 50 percent may be introduced if the C:N ratio is not estimated at the measurement site.

In considering the sedimentary dissolution of $CaCO_3$, we must also consider the stoichiometric relationship between organic carbon degradation and $CaCO_3$ dissolution. Several lines of evidence indicate that, in the presence of $CaCO_3$ in sediment, organic matter produced CO_2 reacts essentially to completion and the stoichiometry as given in Table 10.1 is a reasonable representation of O_2 oxidation

TABLE 10.2 C:N Ratios

Location	C:N	Sources[a]
A. Solid Phase Analysis		
U.S. Atlantic Coast Continental Margin	7.6 50 8.3	1
Hatteras Continental Rise	8.6 ± 0.1, 8.4 ± 0.3	2
Hatteras Abyssal Plain	7.0 ± 0.7, 5.4 ± 1.9, 6.6 ± 0.8	2
Bermuda Rise	6.6 ± 0.8	2
Sargasso Sea	5200 m trap: 7.4; sediment: 8.0	3
Equatorial Atlantic	5000 m trap: 10.5; sediment: 12	3
Pacific Gyre	5600 m trap: 9.6; sediment: 11	3
B. Pore Water DO_2/DNO_3^- and $-DO_2/DSCO_2 = 138:106$		
Central Equatorial Pacific	8.1 ± 2.2	4
Eastern Equatorial Pacific	7	5
Subtropical South Pacific	12	6
Eastern Equatorial Pacific,		
10°S to 11°N	7.6 ± 1.9	7
C. Nearshore sediments: SO_4^{2-} reduction rate/NH_4^+ production rate and $-DSCO_2/DSO_4^{2-} = 2$		
Long Island Sound	5.5 to 10.7	8

[a] Sources (see references): 1—Premuzic *et al.* (1982); 2—Heggie *et al.* (1987); 3—Honjo (1980); 4—Grundmanis and Murray (1982); 5—Jahnke *et al.* (1982b); 6—Bender *et al.*, 1985/1986); 7—Martin, Bender, Leinen, unpub. data; 8—Aller (1980a).

and CaCO$_3$ dissolution. Sayles (1981) and Emerson *et al.* (1982) both have shown that the observed relationship between Ca^{2+} and alkalinity is that predicted by the stoichiometry of Table 10.1. The ratio of ΣCO_2 to alkalinity is similarly that which is predicted. Finally, the isotopic composition of the ΣCO_2 added to the pore solutions requires a stoichiometry at least close to that predicted (McCorkle *et al.,* 1985), although Sayles and Curry (1988) conclude that dissolution is perhaps 25 percent less than the predicted value. The relatively small departures from ideal stoichiometry reported by Sayles and Curry notwithstanding, it appears that the dissolution of CaCO$_3$ can be calculated from ΣCO_2 fluxes with reasonable accuracy.

It is clear that the calculation of early diagenetic fluxes depends to a significant degree on the measurement techniques used and on assumptions about the physical and chemical processes determining the fluxes. Any assessment of the importance of early diagenetic fluxes in surficial geochemical budgets must take the effects of experimental limitations and model assumptions into account. Because of the limited use of flux chambers and fine-resolution pore water sampling devices to date, most of the fluxes we discuss below were obtained with resolution-limited pore water sampling techniques. Fluxes of the major ions and estimates of calcium carbonate dissolution rates are based on in situ techniques, with a resolution of 2 to 5 cm, because of shipboard sampling artifacts for these components. For this reason, our flux estimates must be considered to be lower limits of the true fluxes.

EARLY DIAGENESIS AND MODERN OCEANIC CYCLES

Early diagenetic fluxes fulfill two roles in the modern oceanic cycles of the elements we are considering. For some, the reactions represent a primary input or removal term in the oceanic budget: they are a source of new dissolved material to seawater, or they remove solutes directly from seawater. Na, K, and Mg are affected in this way. For others, early diagenesis forms a part of the element's internal oceanic cycle: material that is fixed into the solid phase in the oceanic water column undergoes degradation during early diagenesis such that a significant portion is recycled back to the water column. The small fraction of the rain of these elements to the sea floor that survives degradation during early diagenesis represents a slow leak from the oceanic cycle. The bioactive elements fall into this category: C, Si, and Ca.

Na, K, and Mg

The early diagenesis of aluminosilicate minerals in oceanic sediments is characterized by the uptake of K$^+$ and Mg^{2+} from seawater, and by the addition of Na$^+$ and protons to seawater (Sayles, 1979). The reaction rate is slow enough that the resultant change in the composition of the sediments is not measurable; but the reaction rates can be determined by precise, artifact-free measurements of dissolved fluxes across the sediment-water interface. Sayles (1979; 1981) has estimated benthic fluxes from in situ sampled pore waters, using model fits to the pore water concentration versus depth data, at a large number of stations in the temperate north and south Atlantic, the Caribbean Sea, and the southern ocean between Africa and Antarctica. Representative data are shown in Figure 10.2. It is important to note that the first sample is at 5 cm below the sediment-water interface. The changes with depth of the Na$^+$, K$^+$, and Mg^{2+} concentrations appear to be slow enough for this relatively poor resolution not to affect the calculated fluxes greatly, but the fluxes will tend to represent lower limits on the early diagenetic reaction rates. The results of these studies are summarized in Table 10.3. The importance of these fluxes in the oceanic budgets of Na, K, and Mg can be estimated by integrating the fluxes, weighting global sediments crudely as 30 percent "margin" and 70 percent "central" (Table 10.4). In the case of Mg and K, early diagenetic reactions remove the elements from seawater at rates that are very nearly equal to their input rates from rivers; and Na is added to seawater at a rate comparable to its river input. There is little doubt that diagenetic fluxes are important to the oceanic cycles of these components of sea water. The time scale of changes in oceanic concentrations of these components that would result from changes in diagenetic processes is slow: the oceanic reservoir for each element is in excess of 10^{19} moles, giving them residence times with respect to diagenetic fluxes of millions of years.

C, Ca, and Si

Carbon, calcium, and silicon show broadly similar behavior in the oceans. Each is fixed into the solid phase by organisms living in the surface ocean: carbon by reduction during photosynthesis, calcium and silicon by precipitation to form the tests of planktonic organisms. The C, Ca, and Si rich particles degrade as they fall through the water column, and degrade further at the surface of the sediments. The result is that a slow input to the oceans, from rivers, and, to a lesser extent for Si and Ca, from seafloor hydrothermal activity, is balanced by a slow loss via burial in sediments; and rapid cycling between dissolved and particulate forms takes place within the oceans. Early diagenesis is an important part of the internal cycles of these elements.

We illustrate this behavior in Tables 10.5 and 10.6. The residence times of all of these elements are long
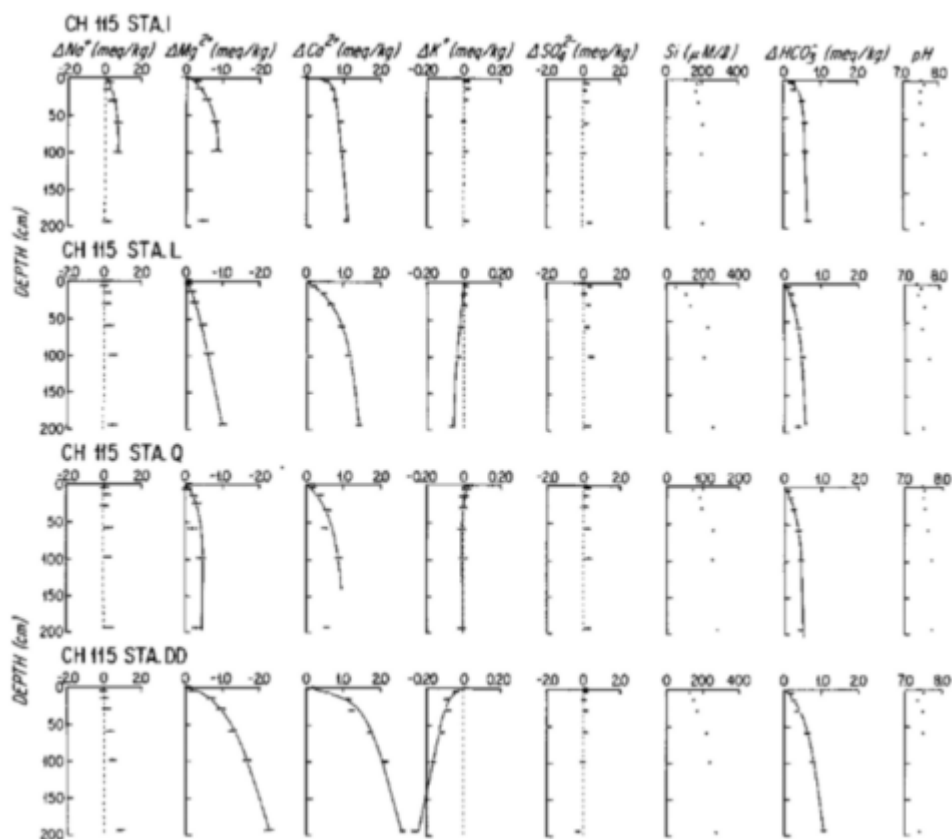
FIGURE 10.2 Profiles of the major components of seawater in the pore waters of marine sediments from subtropical South Atlantic. Stations I-Q are on the flanks of the Mid-Atlantic Ridge; Station DD is from the continental rise off Brazil. The solid lines are the analytical representation of the data from which fluxes were calculated.

relative to the ocean's mixing time of about 1000 years, ranging from 20,000 years for Si to 130,000 years for C and 10^6 years for Ca. They are fixed into particles in the surface ocean at a much faster rate: Ca at a rate 5 times faster than its input and burial rates, Si 25 times faster, and C 350 times faster. C, the most rapidly cycled of the three, is effectively remineralized in the surface ocean, and the fraction of primary production that reaches the sea floor is only about 2 percent in the deep sea (Smith and Hinga, 1983; Jahnke and Jackson, 1987), and 10 percent on the continental margins (Henrichs and Reeburgh, 1987). Si is the next most rapidly remineralized, as the surface ocean is highly undersaturated with respect to the solid phase present (Hurd, 1972): it has been estimated that about 55 percent of the biogenic silica precipitated in the surface ocean redissolves in the water column (e.g., Calvert, 1983), most of it in the surface ocean (Edmond, 1974). In contrast, the surface ocean is supersaturated with respect to the important $CaCO_3$ minerals. While the deep ocean is undersaturated with respect to aragonite, large areas of the sea floor underlie water columns that are saturated with respect to calcite throughout their length. The proportion of the $CaCO_3$ fixed in the surface ocean that reaches the sea floor is variable (e.g., Honjo, 1980; Dymond and Collier,

1988, Walsh *et al.,* 1988), but $CaCO_3$ is the most slowly cycled of the three biogenic sediment components.

TABLE 10.3 Fluxes of Major Components of Seawater Across the Sediment-Water Inferface Estimated from In-Situ Sample Pore Water Profiles

	Units of mEq/yr					
	Na	Mg	Ca	K	HCO_3	Sources[a]
Continental Margins Areas						
Northwest Atlantic (6)[b]	3.5	-4.0[c]	8.2	-0.2	10.3	2,3
Southwest Atlantic (4)	0.7	-3.1	5.1	-0.7	3.8	1
Caribbean (7)	2.1	-5.4	5.4	-0.1	5.8	1
South African (4)	9.8	-10.0	13.0	-0.3	10.2	2
East Equatorial Pacific (2)	—	—	9.9	—	17.7	3
Average	3.7	-5.6	7.8	-0.6	8.4	
Central Areas						
Carbonate Rich (8)						
North Atlantic (6)	4.0	-4.0	6.3	-0.2	8.4	2
South Atlantic (9)	0.9	-1.5	2.8	-0.4	2.8	1
Average	2.1	-2.5	3.4	-0.3	5.0	
Biogenic SiO_2 Rich						
Indian Ocean (7)	1.2	1.5	1.8	-0.04	3.1	2

[a] Sources (see references): 1—Sayles (1979); 2—Sayles (1981); 3—Sayles and Curry (1988).

[b] Number of stations used in average.

[c] Negative numbers refer to a flux into the sediment from the overlying water.

TABLE 10.4 Diagenetic Fluxes Between Sediment and the Oceans. Estimated from In-Situ Pore Water Profiles

	Units of 10^{18} mEq/yr				
	Na	Mg	Ca	K	HCO_3
"Margin" Areas	3.6	-5.4	7.5	-5.8	8.1
Central Areas	4.3	-5.2	6.9	-6.6	10.4
Total	7.9	-10.6	14.4	-1.1	18.5
River Flux[a]	8.3	11.7	27.2	1.3	33.3

[a] Cation data from Martin and Meybeck (1979); HCO_3^- from Meybeck (1982).

The order of importance of early diagenesis to the internal cycles of the elements is, then, Ca > Si > C. We have estimated the involvement of early diagenesis by comparing its rate to the rate of formation of the solid phase in the surface ocean (Table 10.6). For carbon, we have calculated the early diagenetic flux as the difference between the rain rate to the sea floor and the burial rate, with the rain rate estimated from surface water productivity and compilations of benthic flux measurements for the deep sea (Smith and Hinga, 1983; Jahnke and Jackson, 1987), and a water column particle degradation model for coastal regions (Henrichs and Reeburgh, 1987). For Ca and Si, we show two estimates: in each case, the lower of the two is derived from compilations of pore water profile based benthic flux measurements, and the higher value is derived from steady-state ocean models. Both estimates are uncertain. Those based on benthic fluxes are lower limits, and are likely to be underestimates. This is especially true for Ca, since the pore water sampling was by coarse-resolution, in situ methods (Sayles, 1979, 1981), whereas the $CaCO_3$ dissolution rate in surficial sediments is very rapid (Keir, 1983). Our estimates for the rate of benthic degradation of solid phase organic carbon, $CaCO_3$, and SiO_2 relative to the rates of formation of the solids: about 4 percent of the organic carbon formed annually degrades in the sediments, 5 to 40 percent of the SiO_2, and 10 to 80 percent of the $CaCO_3$. For the latter two, and especially for $CaCO_3$, the lower estimate is probably unrealistic. Early diagenesis is a minor player in the cycling within the ocean of organic carbon, but is quantitatively significant both for $CaCO_3$ and SiO_2.

Early diagenetic reactions are clearly important determinants of the loss rates of all three elements from the oceans. Over 90 percent of the organic carbon rain to the sea floor degrades during early diagenesis, as do 30 to 80 percent of the $CaCO_3$ rain and 50 to 90 percent of the SiO_2 rain. Thus, the rates of early diagenetic reactions are generally larger than burial rates. If other parts of the oceanic cycles remain constant, changes in the rates of early diagenetic reactions must be reflected in changing burial rates.

TABLE 10.5 Oceanic Residence Times: C, Ca and Si

		Carbon	Ca	Si
Reservoir size (moles)	HCO_3	3×10^{18} (1)	1.5×10^{19} (1)	1.4×10^{17} (1)
	DOC	1×10^{17} (2)		
Burial rate (moles/yr)	$CaCO_3$	1×10^{13} (3)	1.4×10^{13} (3)	7×10^{12} (5)
	Org. C	1×10^{13} (4)		
Residence time burial (yrs)		130,000	10^6	20,000
Residence time: diagenetic flux (yrs)		20,000	0.3×10^6 50 2×10^6	1,500 to 18,000

Note: DOC = dissolved organic carbon.
Sources: (1) Broecker and Peng (1982); (2) Druffel *et al.* (1989), unpublished manuscript), Williams and Druffel (1987); (3) Forelich *et al.* (1982); (4) Berner (1982); (5) Ledford-Hoffman *et al.* (1986).

TABLE 10.6 Internal Oceanic and Early Diagenesis: C[org], CaCO[3], and SiO[2]

	Organic Carbon (1)				
	Open Ocean	Coastal	Total	$CaCo_3$ (2)	SiO_2 (3)
Fixation in solid phase, Surface clean (moles/yr)	3×10^{15}	8×10^{14}	3.8×10^{15}	7×10^{13}	1.7×10^{14}
Flux to sediment/water Interface (moles/yr)	7×10^{13}	9×10^{13}	1.6×10^{14}	(>2.1 TO <7) $\times 10^{13}$	(>1.5 TO 8) $\times 10^{13}$
Burial (moles/yr)	1×10^{12}	9×10^{12}	1×10^{13}	1.4×10^{13}	7×10^{12}
Fraction of rain to the Seafloor that is recycled	98%	90%	93%	>30 TO <80%	>53 TO 91%
Early diagenetic flux/rate of fixation	2.3%	10%	4%	>10 TO <80%	>5 TO 43%

Sources: (1) Berner (1982), Smith and Hinga (1983), Jahnke and Jackson (1987), Martin *et al.* (1987); (2)Li *et al.* (1969), Forelich *et al.* (1982); (3) Calvert (1983), Ledford-Hoffman *et al.* (1986).

Spatial Variability in Early Diagenetic Reaction Rates

There are significant spatial variations in the benthic degradation/dissolution rates of organic carbon, $CaCO_3$, and SiO_2. Quantitative evaluations of the spatial variability of benthic fluxes must take into account many factors affecting reactivity, which we will consider later. With the possible exception of $CaCO_3$, however, there is an underlying correlation between the rain rate to the sea floor and the benthic flux (Reimers, 1989). For the major seawater ions involved in reactions of aluminosilicate minerals (Na, K, Mg), this correlation shows in the fact that the fluxes from sediments adjacent to continental sources of sediment are roughly twice as large as those from areas remote from land masses. The lowest fluxes are observed in sediments composed largely of biogenic silica, in the high latitude Indian Ocean (Table 10.3). For organic carbon, benthic degradation rates have been measured along transects moving away from the continental margins in the North Atlantic and North Pacific, and have been found to decrease systematically moving away from the continent, as does the surface water productivity (Smith and Hinga, 1983; Jahnke and Jackson, 1987). Benthic organic carbon degradation rates also have been measured across the equatorial high productivity zone in the Pacific, and they show a distinct maximum at the equator, where productivity is highest (Martin *et al.,* 1988). Calvert (1983) has compared maps of the rate of extraction of Si from surface waters (Lisitzin *et al.,* 1967) to maps of the asymptotic dissolved SiO_2 concentration in sediment pore waters in the Atlantic Ocean. The latter quantity can be considered a rough indicator of benthic flux variations. There is a reasonable correlation, as values of both quantities increase moving toward the African coast in the equatorial Atlantic and moving northward north of about 35° N. Like the organic carbon degradation rate, the SiO_2 dissolution rate shows a distinct maximum at the equator in the eastern Pacific (Martin *et al.,* 1988).

The Oxidants for Organic Matter Degradation: O2, N, and S

There is another group of bioactive elements, the oxidants required for organic matter oxidation (O_2, SO_4^{3-}, and NO_3^-; see Table 10.1), which are removed directly from seawater by early diagenetic reactions. The net rate of loss of SO_4^{3-} from seawater due to sulfate reduction during organic matter diagenesis is about 0.5×10^{12} moles/yr (Berner, 1982), a rate which is comparable to, but smaller than, the input rate of SO_4^{3-} to the oceans by rivers and its removal by hydrothermal activity (Edmond *et al.,* 1979). The residence time of S in the oceans with respect to these processes is long, on the order of 10^7 years. Oceanic dissolved O_2 and fixed nitrogen levels may be affected on shorter time scales. Jahnke and Jackson (1987), for instance, used a compilation of benthic flux measurements to conclude that most of the oxygen consumption occurring below 3 km in the oceans is driven by sedimentary organic carbon degradation; and Emerson *et al.* (1987) inferred from determinations of the amount and lifetime of reactive organic carbon in pelagic sediments that increases in the sedimentary organic carbon degradation rate during the last glacial (due to increases in the sedimentary organic carbon concentration) could have had a significant influence on deep ocean apparent oxygen utilization rates. Sedimentary organic carbon degradation may also have important effects on the oceanic nitrogen cycle. In continental margin sediments, oxygen is often depleted during early diagenesis, and denitrification begins (Table 10.1). NO_3^- consumed during denitrification most likely is reduced to N_2 (Bender *et al.,* 1977; Froelich *et al.,* 1979; Goloway and Bender, 1982; Jahnke *et al.,* 1982a), and the N released from organic matter during denitrification and sulfate reduction also may ultimately be oxidized from NH_3 to N_2. Thus, organic matter degradation is a fixed nitrogen sink; in fact, some recent estimates of denitrification on continental shelves exceed estimates of inputs of fixed nitrogen to the ocean plus oceanic nitrogen fixation (Codispoti and Christensen, 1985; Christensen *et al.,* 1987).

In this section, we have illustrated the roles of early diagenetic reactions in modern oceanic geochemical cycles. In the case of the elements affected by aluminosilicate mineral alteration reactions, early diagenesis is a primary source of the element to seawater (Na) or sink from seawater (K, Mg). For the bioactive elements, C, Ca, and Si, early diagenesis is an active player in the cycling of the elements within the ocean and an important determinant of loss rates from the ocean. For the major ions of seawater, the residence times of the elements with respect to input or loss due to early diagenesis are on the order of millions of years. The bioactive elements, C and Si, appear to have shorter residence times with respect to early diagenesis, about 10^4 years. The oxidants used during organic matter degradation are consumed during early diagenesis: for O_2 and fixed nitrogen, the consumption rates may be rapid enough to affect oceanic distributions on thousand to ten thousand year time scales.

EARLY DIAGENETIC FLUXES AND THE SEDIMENTARY RECORD

Introduction

In the preceding section we showed that, as a general rule, diagenetic fluxes are small in the sense that changes in them affect oceanic geochemical cycles on time scales of tens of thousands of years. The significance of early diagenesis to the study of shorter-term processes (i.e., processes with time scales of hundreds to a few thousand years) lies in the fact that the history of past climatic change is an important source of information about the causes and effects of future change. Temporal variability in the concentrations and accumulation rates of the biogenic components of marine sediments are a key source of information on changes in oceanic and atmospheric conditions on the thousand to ten thousand year time scale of the events governing glacial-to-interglacial transitions. Because early diagenetic reactions at the surface of sediments may affect the relationship of observed concentrations and accumulation rates to oceanic and atmospheric conditions, correct interpretation of the sedimentary record requires an understanding of the relationships between rain rates to the sea floor, conditions at the surface of the sediments, and the ultimate concentrations and accumulation rates of sediment components.

The role of early diagenesis in fixing sediment accumulation rates can be viewed in terms of a simple mass balance model. In steady state, the rain rate of a sediment component to the sea floor (R) must equal the sum of its degradation/dissolution rate (F) and its burial rate (B). Then, defining the burial efficiency (E) as the fraction of the rain to the sea floor that is preserved,

$$E = \frac{B}{R} = 1 - \frac{F}{R}. \qquad (10.1)$$

If E is constant, or if burial rates are much larger than reaction rates, then early diagenetic reactions have little effect on burial rates, and the latter are easily translated into rain rates to the sea floor. We have shown already that this is not true for organic carbon, $CaCO_3$, and SiO_2 (Table 10.6): early diagenetic reaction rates are much greater than burial rates for organic carbon, and significantly larger for SiO_2 and $CaCO_3$. Burial rates are slow relative to reaction rates for these biogenic materials, and the relationship between

burial rates and rain rates is no longer simple. A numerical example illustrates the point. If 95 percent of the rain of, for instance, organic carbon is degraded during early diagenesis (F/R=0.95), then a 5 percent reduction in F due to a change in the sedimentary environment (F/R=0.9) will cause a doubling of the fraction of the rain that is preserved: the accumulation rate will double with no change in the rain rate. Although early diagenetic reactions affect oceanic concentrations of the chemical species of interest here only on long time scales, they cannot be ignored when sedimentary concentrations are considered: an understanding of early diagenetic reactions is essential to the interpretation of the sedimentary record.

Variations in Burial Efficiency in Marine Sediments: CaCO$_3$, SiO$_2$, and Organic Carbon

The simple mass balance of Eq. (10.1) hides the complexity of the relationships that determine burial efficiency for biogenic materials: relationships between solid phase reactivity, the chemical and biological environment of the sediments, and the transport processes that operate within the sediment column. The relationships can be demonstrated using simple diagenetic models, but application of the models to the problem of predicting spatial and temporal variability in burial efficiency, as well as to the more difficult problem of estimating burial efficiency variations through time from the sedimentary record, requires a wealth of data about early diagenesis. The data base does not yet exist. In the following paragraphs, we will review existing knowledge and present a framework for the examination of relevant sedimentary properties.

Measuring burial efficiencies is a difficult problem. It requires measurement of two of the three variables in Eq. (10.1), coupled with a steady-state assumption. All of the measurement uncertainties we mentioned previously—sampling resolution, stoichiometric uncertainties, possible sampling artifacts—apply to the benthic reaction rate determinations we will use. Additional uncertainties arise from the varying temporal resolution of the different measurements. Sediment trap based rain rate measurements typically average over a one or two year period. Because of the rate at which benthic organic carbon degradation and silica dissolution occur, benthic flux measurements of species involved in these reactions, and also in carbonate dissolution, are averaged over periods which may range from years to hundreds of years. The resolution of burial rate (accumulation rate) measurements is determined by sediment mixing, and can be limited to 103 to 104 years (Dymond and Lyle, 1985). Thus, comparisons of these different measurements must be interpreted with some caution. Where possible, we apply calculations from different pairs of measurements in order to compare results.

CaCO$_3$

The simplest case among the three we examine is CaCO$_3$. Sedimentary CaCO$_3$ dissolves when the pore waters surrounding it are undersaturated with respect to the mineral phase (calcite or aragonite). By most accounts, resaturation is very rapid. Keir (1983), for example, estimated rate constants for dissolution of about 1000 percent/day. Recently, Archer *et al.* (1989) have estimated that the rate constant is 10 to 100 times slower; this is still rapid on the time scale of early diagenesis. The result of the rapidity of CaCO$_3$ dissolution in undersaturated pore waters is that transport processes within the sediment column are of secondary importance in determining calcite burial efficiency.

Dissolution in sediments occurs for two reasons: because the sediments lie underneath undersaturated bottom water, and in response to acids released by the oxidation of organic matter by O$_2$ (see the stoichiometry in Table 10.1). If only the first process is operating, dissolution will cease within a few millimeters of the sediment/water interface. The effects of the second process are to drive dissolution at water depths shallower than the CaCO$_3$ saturation horizon and beneath the level in the sediments where the pore waters would reach saturation in the absence of organic carbon oxidation. Emerson and Bender (1981) used kinetic models of CaCO$_3$ preservation and dissolution to suggest that it could lead to dissolution as much as 1000 m above the saturation horizon; Sayles (1981) used measurements of Ca^{2+} fluxes from sediments to demonstrate the occurrence of dissolution as much as 1500 m above saturation horizon in the North Atlantic. We will use calculations of the burial efficiency for CaCO$_3$ to evaluate the importance of dissolution due to the introduction of acids from the oxidation of organic matter in the sediments and to demonstrate the variability in burial efficiency. The data are shown in Table 10.7, which lists burial efficiencies along with the carbonate content of the sediments and the method used for the calculation.

The stations in the Atlantic at which E is estimated all lie above the lysocline. Two stations lie on the continental margin, the rest in the deep Northwest Atlantic. All stations show dissolution of a significant fraction of the CaCO$_3$ rain to the sea floor, with the largest fractional dissolution (50 to 74 percent) occurring in margin sediments. The average fractional dissolution for deep Atlantic stations is lower, 20 percent. However, these values were obtained by in situ sampling techniques with limited resolution near the sediment-water interface; as a result, the benthic Ca^{2+} flux, and therefore the CaCO$_3$ dissolution rate, may be underestimated by more than a factor of two. Since all of these stations lie above the saturation horizon, all dissolution is due to the effects of organic matter oxidation, emphasizing the importance of this process.

TABLE 10.7 Fluxes of CaCO[3]

Location	Water Depth (m)	Depth Relative to Lysocline[a]	CaCO₃ Rain (μM/cm²/yr)	CaCO₃ Dissolution Flux (μM/cm²/yr)	Percent Dissolved[b]	Sedo, emt % CaCO₃	Type of Data Used in Estimates[c]
Pacific Ocean							
Site M	3100	≤	6.6[d]	6.2[d]	94	3 to 5[d]	1
				11.8[e]	180		2
Site H	3600	>	12.8[d]	12.8[d]	»100	<1[d]	1
				11.9[e]	93		2
Site C	4450	>	23[f]	16[g]	70	≈80	1
				20[h]	89		2
				23[i]	100		3
Site S	4900	>	7.3[f]	7.3[f]	100	<1	1
			7.3[f]	1.8[h]	25		2
				7[i]	≈100		3
California borderland							
San Pedro Basin		>	29[j]	11[k]	38		3
San Nicholas Basin		>	51[j]	22[k]	43		3
Atlantic Ocean							
SEEP I (margin, U.S. East Coast)	400 to 2750	<	29[l]	14[l]	50		1
NW Atlantic margin (41°30'N, 63°20'W) 3480		<	6.8[m]	5.0[m]	74	43	4
NW Atlantic (average 9 stations)<4200		<	19[n]	3.8[o]	20	40 to 60[o]	4

Notes:

[a] <, ≤ and > represent water depths of less than, less than or equal to, and greater than the lysocline, respectively.

[b] Percent of CaCO₃ rain estimated to dissolve at or below the sediment-water interface.

[c] Method used in calculating the Dissolution Flux; 1—particle rain, burial; 2—particle rain, diagenetic flux, (NO_3-); 3—particle rain, diagenetic flux (O_2); 4—diagenetic flux, burial (Ca^{+2}) [d] Dymond and Lyle (1985); sediment trap data, 1-yr duration, burial rates from radioisotope dating.

[e] Bender and Heggie (1984); estimates of TCO_2 produced are from models of NO_3 profiles in the pore water.

[f] Dymond and Collier (1988); sediment trap, duration = 2 yrs at Site C, 1 yr at Site S. Site C values were 7 and 23 1 μM/cm²/yr in years 1 and 2, respectively. The first year was influenced by a strong ENSO event and the authors consider 23 μM/cm²/yr a more representative value. We have used this value in calculations. Since percent CaCO₃ » 0 at Site S, total dissolution flux must equal rain.

[g] Value calculated using burial flux of 7 μM/cm²/yr from Lyle et al. (1988).

[h] Bender and Heggie (1984) report a range of fluxes for TCO_2 derived from the oxidation of organic carbon estimated from NO_3 profiles.

[i] Emerson (1985) provides estimates of organic carbon oxidized from models of O_2 microelectrode profiles in the pore water. The flux across the interface is assumed to be the integrated reaction rate, i.e., steady state.

[j] Values for rain are the sum of estimates of the dissolution flux and burial flux. For stations where bottom waters are undersaturated, as the San Pedro and San Nichollas station, rain rate values are a minimum. The data are from Berelson et al. (1987).

[k] Diagenetic flux is estimated from a model of CaCO₃ dissolution that makes a number of assumptions regarding dissolution kinetics and depth in sediment to saturation; see Berelson et al. (1987) for details. The carbon oxidation rate is based on O_2 consumption rates measured in situ with a benthic lander.

[l] Average sediment-trap particle fluxes and CaCO₃ accumulation in sediment from Biscaye et al. (1988). Transect is located south of Cape Code; water depths of 500 to 2750 m.

[m] Diagenetic flux based upon Ca^{2+} flux of Sayles and Curry (1988) for two separate stations. Burial calculated from percent CaCO₃ profile in sediments that exhibits sharp drop in CaCO₃ (43 percent to 15 percent between 5 and 8 cm) typical of the interglacial-glacial transition in the north Atlantic. The transition at 11,000 yr is assumed to be at 6.5 cm, the porosity is 73 (±1) percent (unpublished data).

[n] Calculated from a burial rate of 15 μM/cm²/yr recalculated from the data of Turekian (1965) and Bacon (1984) for cores in the general area of the pore water studies (12 below).

[o] Average value of diagenetic flux for nine stations in the northwest Atlantic from Sayles (1981). Estimates based on Ca^{2+} fluxes determined by in situ water sampling.

The Pacific stations, with the exception of MANOP M, lie below the lysocline. It is immediately apparent that fractional dissolution at these sites, with the exception of the California borderland, is greater than at the Atlantic sites. Estimates range from 70 to 100 percent (except for one low estimate for MANOP S). The lower value at the California borderland site (Berelson *et al.,* 1987) is surprising, and contrasts to the conclusion of Berger (1970), who found that 85 percent of foraminifera shells reaching the sediments there dissolved, even at depths as shallow as a few hundred meters on the slope of the Santa Barbara basin. The Pacific results argue for the importance of dissolution below the saturation horizon. The results tend to indicate that dissolution is occuring deep enough within the sediments to be measured by limited-resolution pore water profiles. At all the MANOP sites, estimates are based both on the particle rain/burial and particle rain/diagenetic flux pairs, and they agree well (again, the low estimate based on NO_3^- profiles at MANOP S is an exception). In addition, the pore water based estimates are calculated from organic matter oxidation stoichiometry, and so do not include dissolution as a result of undersaturated bottom waters. If the sediment trap based estimates of rain rates do not underestimate the true rain rate of $CaCO_3$, then we must conclude that, even at these sites below the lysocline, dissolution due to metabolic acids is an important process.

SiO_2

The driving force for biogenic silica dissolution in marine sediments is similar to that for $CaCO_3$: pore waters are undersaturated with respect to the solid phase present. There are two important differences, however: seawater is universally undersaturated with respect to amorphous silica (Hurd, 1972), and pore waters rarely reach saturation; and the rate of dissolution is significantly slower for biogenic silica, occurring on a time scale of years to tens of years in sediments, compared to minutes to days for $CaCO_3$. The result of these differences is that sediment mixing plays a more important role in determining silica preservation.

In laboratory experiments, it has been shown that the dissolution of opaline tests in seawater depends on the concentration of opal surface exposed to the seawater, on several details of surface characteristics, and on the degree of saturation of the water with respect to amorphous silica (Hurd and Theyer, 1975; Hurd, 1983). Marine pore waters rarely reach saturation with respect to amorphous silica (about 1000 µM at 3° C: Hurd and Theyer, 1975). However, pore waters do approach asymptotic dissolved silica concentrations in the upper 50 to 150 cm of the sediments. The values vary from little over 100 µM in sediments underlying unproductive surface waters (Bender *et al.,* 1985/86; Sayles, 1979), to values of up to 580 µM below the equatorial upwelling region in the eastern Pacific (Jahnke *et al.,* 1982b), and to values in excess of 750 µM in the siliceous oozes of the southern ocean (Sayles, 1981). Schink *et al.* (1975) have explained this variability in asymptotic pore water values in terms of a kinetic model based on the rate law of Hurd (1972). According to this model, the asymptotic $[SiO_2]$ results from a balance between supply to the sediments and loss to overlying water. The balance depends on the rain rate of opal to the sea floor, the rate of opal dissolution, and the bioturbation mixing coefficient. Opal burial efficiency must also depend on these factors.

TABLE 10.8 Biogenic Silica Mass Balances: Percent Preservation

Location	Percent Opal	Percent Dissolved
MANOP C[a]	15	91
MANOP S[b]	16	>85
Southern California borderland[c]	3.5 to 6.0	90
Antarctic continental shelf[d]		
Sulzberger Bay	2	50
South central Ross Sea	24	<25

[a] Lyle *et al.* (1988); Martin *et al.* (1988)

[b] Dymond and Collier (1988); Martin *et al.* (1988)

[c] Berelson *et al.* (1987)

[d] Ledford-Hoffman *et al.* (1986)

The data for calculating biogenic silica burial efficiencies are limited, but enough exist to illustrate its variability. In Table 10.8, we list calculations for five sites from the eastern equatorial Pacific, the California borderland, and the Antarctic continental shelf. Fractional dissolution varies substantially, from about 90 percent in eastern equatorial Pacific sediments to values as low as 25 percent on the Antarctic continental shelf. Clearly, the highest preservation rates occur on the Antarctic shelf (>50 percent of the rain is preserved). This is consistent with the fact that about 75 percent of the opal accumulation in marine sediments occurs in the deep ocean surrounding Antarctica and on the Antarctic continental shelf (Ledford-Hoffman *et al.,* 1986).

Organic Carbon

The study of organic carbon diagenesis is complicated by the wide variety of compounds grouped under the heading. Its bulk reactivity varies with the source of the organic matter, as different compounds have differing susceptibilities to degradation in sediments (e.g., Emerson and Hedges, 1988); in addition, the composition of or

ganic matter varies with its age, so that reactivity varies with depth below the sediment-water interface even at a given site (Middelberg, 1989). As a result of its varying composition and of the dependence of reactivity on environmental factors, organic carbon reactivity varies over several orders of magnitude. A compilation by Emerson and Hedges (1988) shows that the mean lifetime of the organic matter increases systematically with the age of the organic matter considered. They noted values of 0.1 years or less for fresh phytoplankton, years to tens of years for surficial sediments, hundreds of years for intermediate depth sediments (the upper 20 cm of the sediment column), and 106 years for very deep sediments.

Further complicating organic matter diagenesis is the existence of a suite of chemical reactions, with different thermodynamic driving forces, to accomplish organic matter degradation. They are shown in Table 10.1, in the order of their occurrence with increasing depth below the sediment-water interface. Although some details of the stoichiometry of the table are uncertain, the general validity of the model is well established. The suite of redox reactions leaves well-documented traces in pore waters. Oxic degradation is marked by oxygen consumption and NO_3^- production (with consumption indicated by positive curvature of the pore water profile, production by negative curvature: Berner, 1980), denitrification by NO_3^- consumption, Mn and Fe reduction by production of the dissolved reduced metal ion, and sulfate reduction by SO_4^{3-} consumption and NH_3 production. The reactions have been documented, through pore water profiles, benthic flux measurements, and sediment incubations, in pelagic (Froelich *et al.,* 1979; Jahnke *et al.,* 1982a), hemipelagic (Klinkhammer, 1980), and nearshore sediments (Elderfield *et al.,* 1981).

The relative importance of the different electron acceptors depends on several factors: order of use, differing reactivities of organic matter exposed to the different electron acceptors, availability, and oxidizing capacity. The effect of these factors is that organic carbon degradation by dissolved oxygen accounts for about 90 percent of the organic carbon degradation in marine sediments (Henrichs and Reeburgh, 1987). In general, in pelagic and hemipelagic sediments of the eastern equatorial Pacific and the equatorial and northwest Atlantic, 90 to 99 percent of the organic carbon degradation is by O_2, most of the rest being done by nitrate reduction (Jahnke *et al.,* 1982a; Bender and Heggie, 1984; Sayles and Curry, 1988). Sulfate reduction occurs at rapid rates in shallow areas on the continental margins, but since these areas cover less than 10 percent of the sea floor, it is responsible for only a small fraction of the total organic carbon oxidized (Jorgensen, 1982). Jahnke *et al.* (1982b) and Henrichs and Reeburgh (1987) have pointed out that, although the secondary oxidants are responsible for only a small fraction of sedimentary organic carbon remineralization, they oxidize an amount of carbon approximately equal to that preserved in sediments. Thus, they may exert an important influence on the proportion of the organic carbon rain that is preserved. The importance of sulfate reduction lies in the fact that it occurs to a significant extent on continental margins, where the bulk of organic carbon burial in marine sediments takes place (Berner, 1982).

Organic carbon burial efficiency varies because of varying composition of the degrading organic matter pool, and also because of variations in electron acceptor availability. Although fresh organic matter appears to be degraded almost equally efficiently using either O_2 or SO_4^{3-} as an electron acceptor (Westrich and Berner, 1984), there is ample evidence to indicate that the concentration of dissolved oxygen in bottom water influences the extent of degradation of organic matter in marine sediments. The evidence takes the form of observations of enhanced burial efficiency in sediments underlying anoxic bottom waters (Canfield, 1989); an observation that the oxidation of organic carbon that had been deposited at depth by a turbidite flow is limited by the rate of diffusion of O_2 into the sediments, despite the presence of other oxidants (Wilson *et al.,* 1985); and predictions based on modeling studies and organic carbon preservation variations in the California borderlands (Emerson, 1985).

A further factor affecting organic carbon burial efficiency, which we examine below, is the relationship of transport away from the sediment-water interface by burial and mixing to degradation reactions. The result of the interactions of the various factors is that organic carbon burial efficiency varies over a wide range in marine sediments. One recent compilation (Henrichs and Reeburgh, 1987) shows a range of burial efficiencies from a few tenths of a percent in pelagic sediments of the eastern tropical Pacific to about 80 percent in coastal sediments at Cape Lookout Bight on the North Carolina coast. Henrichs and Reeburgh (1987) demonstrate a positive correlation between burial efficiency and bulk sedimentation rate, which results in the following pattern: burial efficiency generally increases from pelagic values of 0.6 to 16 percent, to values of 8 to 28 percent on the continental slopes, to 8 to 79 percent in shelf and estuarine sediments.

Discussion

Despite the uncertainties in the calculation of burial efficiencies, the first order result of measurements made to date is that the burial efficiency of organic carbon, $CaCO_3$, and opal is highly variable. The implication of this result is that, in order to interpret temporal variations in burial rates of these three components in terms of rain rates to the sea floor

and variations in sedimentary environments, it is necessary to understand the causes of the burial efficiency variations. Perhaps the simplest case is $CaCO_3$, because of the rapidity of the resaturation of pore waters with respect to the mineral phase. Even here, however, there is a complication: from the compilation presented here, we can conclude that reactions within the sediments account for 40 to 75 percent of $CaCO_3$ dissolution at the sea floor, and a substantial fraction must be due to the acid introduced into pore waters by oxic degradation of organic matter. Thus, quantitative interpretations of $CaCO_3$ preservation depend on an understanding of organic matter diagenesis. Opal diagenesis has been found to depend on a variety of factors, including rain rate variations, reactivity variations, and rates of sediment mixing (Schink *et al.,* 1975). Organic carbon diagenesis depends on the same factors, but has added uncertainties due to the complexity of the material and the range of reactions responsible for its degradation. To enhance the accuracy and usefulness of paleoceanographic reconstructions based on concentrations and accumulation rates of biogenic sediment components, we must have adequate data on early diagenetic reactions and a framework for evaluating the data. We present such a framework in the next section.

A Model Including Transport and Reaction Effects: The Case of Organic Carbon

In steady state, the distribution of organic carbon with depth below the sediment-water interface is determined by a balance between transport processes, which tend to aid the preservation of organic carbon, and chemical reactions, which consume it. The relationships between the processes can be understood by considering a simple system in which organic carbon decays with a first-order rate constant, k, to a depth X_{rxn} below the sediment-water interface; is mixed, within a layer X_{mix} thick, by a quasi-Fickian diffusion process described by mixing coefficient, D_B; and is buried at sedimentation rate, w. The mean lifetime of the organic carbon is $1/k$. It takes a length of time, X_{rxn}/w, for a particle to be transported through the reaction zone by sedimentation; and a length of time that is proportional to $X_{rxn}^{2/D}{}_B$ to be transported by mixing through the reaction zone. The competition between transport and reaction is clear: the thicker the reaction zone, and the slower the sedimentation and mixing rates, the longer a particle resides in the reaction zone, and the less likely it is to survive degradation. Preservation is enhanced by a thin reaction zone, rapid sedimentation and mixing, and low reactivity. A final factor is the thickness of the mixed layer. Mixing will clearly be most effective at sequestering organic carbon when X_{mix} exceeds X_{rxn}.

We formalize these arguments in the model described by Eq. (10.3). We assume that the sedimentary system is in steady state on the time scale of organic carbon degradation reactions; and take porosity and the sedimentation rate (w) to be constant. To enhance the model's generality, we allow both the organic carbon degradation rate constant (k) and the bioturbation mixing coefficient (D_B) to decrease as the depth below the sediment-water interface increases:

$$k = k_0 \exp\left(-\frac{x}{k_1}\right) \qquad (10.2)$$

and

$$D_B = D_B^0 \exp\left[-\left(\frac{x}{\bar{x}}\right)^2\right].$$

In this formulation, k_1 corresponds roughly to X_{rxn}, x to X_{mix}. In keeping with the findings of Berner (1980) and Boudreau and Westrich (1984), we assume that organic carbon degradation is first order with respect to the sedimentary organic carbon concentration. The decrease of k as depth below the sediment-water interface increases is consistent with the "multi-G" model of Berner (Berner, 1980; Westrich and Berner, 1984; Emerson *et al.,* 1987; Middelberg, 1989). Our representation of the depth dependence of the mixing coefficient follows the model of Christensen (1982). We apply a mass balance condition at the sediment-water interface ($x=0$), and specify that degradation reactions cease at some depth below the interface. In equation form (Berner, 1980), with C the sedimentary organic carbon concentration and R the organic carbon rain rate,

$$\frac{\partial C}{\partial t} = 0 = \frac{\partial}{\partial x}\left[D_B(x)\frac{\partial C}{\partial x} - wC\right] - k(x)C$$

$$\left(D_B\frac{\partial C}{\partial x} + wC\right) = R$$

$$\left(\frac{\partial C}{\partial x}\right)_{x \to \infty} = 0.$$

To examine the sensitivity of the organic carbon burial efficiency to model parameters, we transform the differential equation and boundary conditions into dimensionless variables (Table 10.9). The first, P_1, measures the depths to which mixing and reaction are important: the larger is P_1, the further organic carbon can be mixed below the layer in the sediments in which rapid degradation reactions occur. P_2 is a dimensionless transport parameter: the larger it is, the more effective burial is, relative to mixing, at sequestering organic carbon below the reactive layer of the sediments. P_3 is a dimensionless reaction parameter: as it increases, the degradation rate increases relative to the rate at which organic carbon is mixed through the

reactive layer. The output of the model is a dimensionless concentration parameter; when multiplied by the ratio, P_2/P_3, it is equal to the burial efficiency (E in the mass balance above).

TABLE 10.9 Organic Preservation Model: Parameters

Parameter	Explanation
A. Input Parameters	
k_0, k_1	Describe the reaction rate of organic carbon, $k(x) = k_0 e^{-x/k_1}$. k_0 in yr^{-1}, k_1 in centimeters
$D_B{}^0$, x	Describe the bioturbation mixing rate, $D_B = D_B{}^0 \exp(-x^2/\&sign;^2)$. $D_B{}^0$ in cm^2/yr, x in centimeters
w	sedimentation rate, cm/yr
B. Dimensionless Variables for Model Calculations	
$P_1 = x/k_1$	The ratio of the scale lengths describing the mixing coefficient and degradation rate profiles
$P_2 = wk_1/D_B{}^0$	The dimensionless transport parameter. Interpreted as the ratio of the mean length of time for mixing through the reaction layer ($k_1{}^2/D_B{}^0$) to the mean length of time for burial through that layer (k_1/w)
$P_3 = k_0 k_1{}^2/D_B{}^0$	The dimensionless reaction parameter. The ratio of the mean length of time for mixing through the reaction layer to the mean lifetime of the organic carbon with respect to degradation ($1/k_0$)

We have applied the model to four oceanic sediments to test its ability to predict organic carbon burial efficiencies. The results are preliminary: the model requires that pore water nutrient, ΣCO_2, and/or O_2 data and solid phase organic carbon data be available for the determination of the degradation rate constant (pore water data to furnish the rate, solid phase data to convert the rate into a first-order degradation rate constant); and that sedimentation rate and bioturbation mixing rate data (we have used ^{210}Pb measurements) be available. The needed information exists at only a few sites. The results are in Table 10.10. The trend in burial eficiencies is reproduced by the model, with the highest E at the southern California borderland site, a high value at the other continental margin site (Buzzards Bay, Massachusetts), and much lower values at the tropical Pacific (MANOP) sites, the lowest value occurring at the site that is farther from the equator. At the individual sites, the agreement between calculated and measured burial efficiencies is probably within the uncertainty in the data.

We examine the effects of the individual sedimentary parameters in the organic carbon burial efficiency contour map of Figure 10.3. The contours were calculated from an 11 x 11 grid of solutions to Eq. (10.3); the solutions had been obtained by varying P_2 and P_3 systematically, with P_1 held constant at a value of 2.5. Contours are shown for two regions: those in the upper left are roughly representative of "pelagic" sedimentary environments, those in the middle and lower right correspond roughly to "continental margin" sediments. Within each region of the plot, successive contours represent a doubling of the burial efficiency. The effects of varying individual parameters are shown by the two clusters of arrows. Starting from the center of each cluster, each arrow shows the effect on E of doubling one model parameter. Varying the bioturbation mixing coefficient ($D_B{}^0$) has almost no effect at the high sedimentation rates characteristic of margin sediments: its arrow is almost parallel to the constant-E contours. At lower (pelagic) sedimentation rates (the cluster in the upper left), mixing has greater effect, with preservation increasing as the mixing rate increases. Doubling the sedimentation rate leads to a nearly proportional increase in burial efficiency. Both reaction parameters, k_0, which represents the absolute degradation rate, and k_1, which is related to the distance below the sediment-water interface over which organic carbon degradation reactions are important, significantly influence organic carbon preservation. Doubling either causes a proportionate decrease in E under continental margin conditions; their effects, especially that of the reaction scale length, are enhanced in pelagic sediments. The plot does not show the effect of varying the thickness of the mixing zone relative to the reaction zone, as parameter P_1 is held constant. Variations in P_1 have little effect at higher values of E; their effect at lower E can be seen by comparing the value plotted for MANOP C ("MC" in the figure), calculated using $P_1 = 2.5$, to the value obtained for the measured P_1 ($P_1 = 7$). The E value in the figure is low by about a factor of two: at low sedimentation rates, mixing is the most effective means of sequestering organic carbon, and increasing the depth below the interface to which mixing occurs causes corresponding increases in burial efficiency.

The model we have shown is a framework for the analysis of burial efficiencies of biogenic sediment components: it defines the sedimentary environment in terms of five measurable parameters. In order to be useful, it must be accompanied by information on the interrelationships between the parameters, and on how they are affected by changing oceanic conditions. One example of the application of the model is a comparison of the two equatorial Pacific sites included in our data set (MANOP C and MANOP S). The most important differences between the two sites are the higher sedimentation rate and reaction rate constant at MANOP C. If the only change were the increased sedimentation rate, burial efficiency would be ten times higher at site C than at site S. However, the reaction rate constant is also higher at site C, and as a

result, the net increase in E is only a factor of 2 to 3. This observation is in agreement with the correlations noted by Emerson (1985), using data from these sites and others: the rain rate of organic carbon to the sea floor increases with the bulk sedimentation rate, and the degradation rate constant varies with the rain rate. Thus, the model confirms the importance of variations in reactivity in determining the relationship between organic carbon burial efficiency and bulk sedimentation rate.
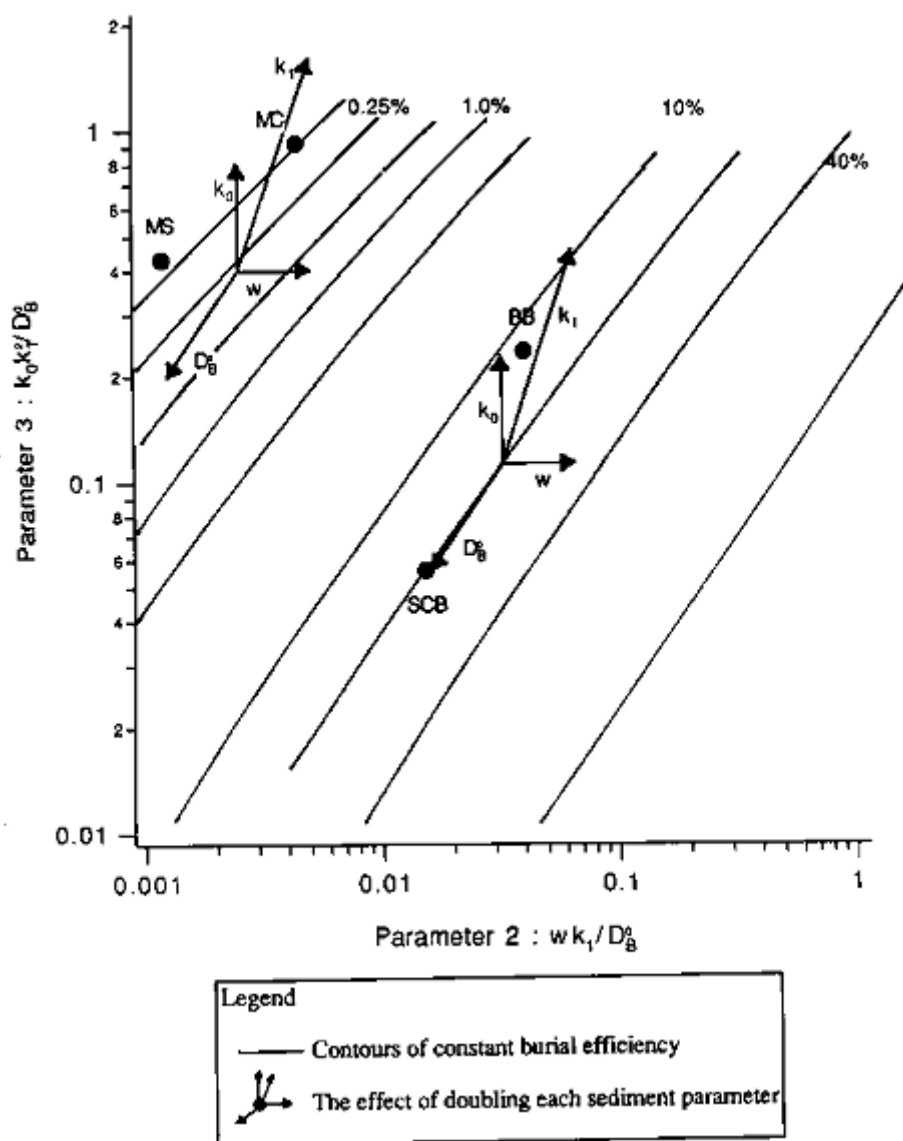
FIGURE 10.3 The sensitivity of organic carbon burial efficiency to changes in sediment parameters. Shown are contours of constant organic carbon burial efficiency, as a function of the model dimensionless transport parameter, T_m/T_b (parameter #2), and reaction parameter, T_m/T_r (parameter #3), with model parameter #1, x/k_1, held constant at 2.5. Sites at which model calculations were compared to measured burial efficiencies (see Table 10.10) are shown by the closed circles. The two pelagic sediment sites are MANOP S (MS) and MANOP C (MC); the two continental margin sites are in Buzzards Bay, Massachusetts (BB), and in the San Clemente Basin (SCB) in the southern California borderland. The two clusters of vectors show the effects of organic carbon burial efficiency of varying the sediment parameters. Details are described in the text.

Our data set includes two continental margin sites, one in a shallow, coastal sediment (Buzzards Bay, Massachusetts), and a second in the California borderland, underlying poorly oxygenated bottom water (San Clemente Basin, with bottom water $[O_2]$ = 56 umol/kg). A comparison of these sites (Table 10.10) shows a lower burial efficiency in Buzzards Bay, despite its more rapid mixing and sedimentation rates. Changes in reaction rate constants are important: the rate constant at the sediment-water interface is about 50 percent higher at the Buzzards Bay site; more importantly, the rate constant decreases more slowly with depth there. Several factors could contribute to the differences. Oxygen penetrates to only about 5 mm below the sediment-water interface at the San Clemente Basin site (Reimers, 1987); in Buzzards Bay, Mn profiles show that oxygen diffusing across the sediment-water interface reaches similar depths (Martin, 1985), but irrigation is significant to depths of 20 cm in the warm months (Martin and Sayles, 1987), and it may supply O_2 to regions well below the sediment-water interface. In addition, there is a larger supply of fresh organic matter to the sediments at the shallow Buzzards Bay site, making secondary oxidants more effective (Westrich and Berner, 1984; Emerson and

Hedges, 1988); the average temperature is higher in Buzzards Bay; and the "quality" of the organic matter may differ between the two sites. At these continental margin sites, as at the two equatorial Pacific sites, reactivity has an important influence on the burial efficiency versus sedimentation rate relationship.

TABLE 10.10 Sample Calculations

	Input Parameters				Model Parameters			Results		
Site	k_0(yr^{-1})	K_1 (cm)	w (cm/yr)	D_B^0(cm^2/yr)	x (cm)	P1	P2	P3	E_{calc} (%)	E_{meas} (%)
Buzzards Bay	0.073[a]	4[a]	0.05[a]	5[b]	10[b]	2.5	0.040	0.234	12	7.4[a]
SCB	0.056[c]	1[c]	0.015[d]	1[d]	6[d]	6	0.015	0.056	21	22[c] , [d]
"MC"	0.30[e]	0.7[e]	0.001[f]	0.16[g]	5[g]	7.1	0.00438	0.919	0.3	1[h]
"MS"	0.03[e]	1.2[e]	0.0001[f]	0.10[g]	3[g]	2.5	0.0012	0.43	0.1	0.5[h]

Data Sources
[a] McNichol *et al.* (1988)
[b] Martin and Sayles (1987)
[c] Bender *et al.* (1989)
[d] R. Anderson, unpublished data
[e] W. Martin, M. Bender, and M. Leinen, unpublished data (see Martin *et al.*, 1988)
[f] Emerson *et al.* (1987)
[g] Cochran (1985)
[h] Bender and Heggie (1984)

Burial efficiencies are easy to model because the effects of transport processes are simple: increasing transport rates leads to increasing preservation rates. Unfortunately, accumulation rates (which are simply related to rain rates: see Eq. (10.1)) are difficult to measure, and sedimentary concentrations are often used in paleoceanographic models. The effects of transport processes on concentrations are complex: they tend to increase concentrations by enhancing preservation, but tend to decrease them by dilution (that is, the supply of, for instance, organic carbon to the sediments may be constant, but, because the organic carbon is buried or mixed more rapidly, it is spread through a thicker sediment layer). At low sedimentation rates, the preservation effect dominates, and increasing sedimentation tends to increase concentrations. At higher sedimentation rates, the dilution effect dominates, and increases tend to decrease concentrations. The concentration enhancement effect of increasing sedimentation rate is smaller, the more rapid the mixing coefficient and the thicker the mixed layer (Figure 10.4). Thus, in addition to the effects of varying reactivities, models relying on sedimentary concentrations to recreate rain rate variations to the sea floor must account for the complex effects of variable burial and mixing rates.

CONCLUSIONS

We have considered the roles played by early diagenetic reactions in the oceanic cycles of the major seawater ions, Na^+, K^+, Mg^{2+}, Ca^{2+}, and SO_4^{3-}, and in the cycles of two additional major players in oceanic biological cycles, C and Si. The elements whose cycles are controlled by nonbiological reactions—Na, K, and Mg—are characterized by long oceanic residence times and diagenetic reactions that are slow in the sense that modest changes in their rates will affect oceanic cycles on time scales in excess of 10^6 years. Nonetheless, early diagenetic reactions are important, as they result in fluxes that are similar in magnitude to the other sources and sinks of the elements to and from seawater. Early diagenesis plays a larger role in the cycles of the biologically active elements, C, Ca, and Si. Diagenetic cycling rates are rapid with respect to the rates of riverine and hydrothermal input and burial in sediments. Residence times of the elements in seawater with respect to inputs resulting from early diagenesis are about 10^4 years for C and Si, nearly 10^6 years for Ca. Early diagenetic reaction rates are greater than burial rates: thus, they may exert important control over the rates of burial of the biogenic sediment components, organic carbon, calcite, and opal.

The burial efficiency of the biogenic sediment components—that is, the fraction of the rain to the sea floor that is preserved to become part of the sedimentary record—varies substantially in the oceans for each component. This last fact has two implications: early diagenesis must be understood to infer rain rates (hence, make paleoceanographic reconstructions) from sediment concentration and accumulation rate data; and early diagenesis must be understood to infer variations in diagenetic reaction rates from the sedimentary record. We have presented a framework for examining spatial, and ultimately temporal, variations in the early diagenesis of organic carbon. The framework needs to be extended to include the other biogenic sediment components, both individually and in an integrated early diagenetic model. There is a need for a greatly expanded data set to determine the interactions between the different parameters affecting diagenetic reaction rates: rain rates to the sea floor, reactivities, and sedimentation and sediment mixing rates.
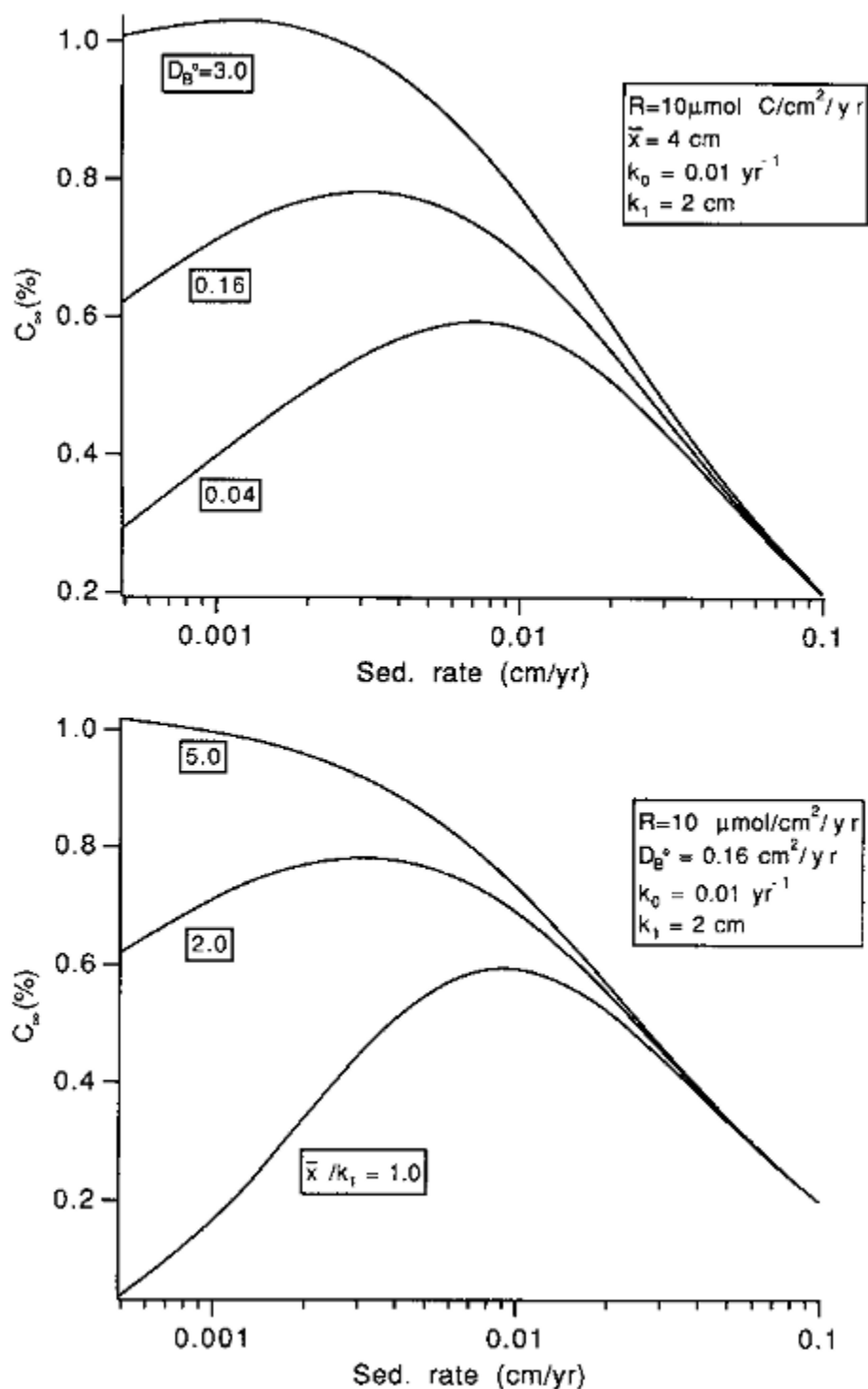
FIGURE 10.4 The effects of changes in the mixing rate parameters on the $C\infty$ versus sedimentation rate w relationship. $C\infty$ represents the organic carbon concentration in accumulating sediment, in percent on a dry weight basis. In the top figure, x/k_1 is held constant at 2.0 and the mixing rate coefficient, $D_B{}^0$ is allowed to vary; in the bottom figure, $D_B{}^0$ is constant at 0.16, while x/k_1 is varied. For both, the rain rate to the sediment-water interface is 10μmol C/cm ^{2}/yr; the organic carbon degradation rate at $x=0$ (k_0) is 0.01 per year, and k_1 is 2 cm.

ACKNOWLEDGMENTS

REFERENCES

Aller, R.C. (1980a). Diagenetic processes near the sediment-water interface of Long Island Sound. I. Decomposition and nutrient element geochemistry (S, N, P), in Estuarine Physics and Chemistry: Studies in Long Island Sound, B. Saltzman, ed., Academic Press, New York, pp. 237-349 .
Aller, R.C. (1980b). Quantifying solute distributions in the bioturbated zone of marine sediments by defining an average microenvironment, Geochimica et Cosmochimica Acta 44, 1955-1965 .

SEAFLOOR DIAGENETIC FLUXES

Archer, D., S. Emerson, and C.R. Smith (1989). Dissolution of calcite in deep-sea sediments: pH and O_2 microelectrode results, Geochimica et Cosmochimica Acta 53(11), 2831 .

Bacon, M.P. (1984). Glacial to interglacial changes in carbonate and clay sedimentation in the Atlantic Ocean estimated from Th-230 measurements, Isotope Geoscience 2, 97-111 .

Barnes, R.O. (1973). An in situ interstitial water sampler for use in unconsolidated sediments, Deep-Sea Research 20, 1125-1128 .

Bender, M.L., K.A. Fanning, P.N. Froelich, G.R. Heath, and V. Maynard (1977). Interstitial nitrate profiles and oxidation of sedimentary organic matter in the Eastern Equatorial Atlantic, Science 198, 605-609 .

Bender, M.L., and D.T. Heggie (1984). Fate of organic carbon reaching the deep sea floor: A status report, Geochimica et Cosmochimica Acta 48, 977-986 .

Bender, M.L., A. Hudson, D.W. Graham, R.O. Barnes, M. Leinen, and D. Kahn (1985/1986). Diagenesis and convection reflected in pore water chemistry on the western flank of the East Pacific Rise, 20° south , Earth and Planetary Science Letters 76, 71-83 .

Bender, M., W. Martin, J. Hess, F. Sayles, L. Ball, and C. Lambert (1987). A whole-core squeezer for interstitial pore-water sampling, Limnology and Oceanography 32(6), 1214-1225 .

Bender, M., R. Jahnke, R. Weiss, W. Martin, D. Heggie, J. Orchardo, and T. Sowers (1989). Organic carbon oxidation and benthic nitrogen and silica dynamics in San Clemente Basin, a continental borderland site, Geochimica et Cosmochimica Acta 53, 685-697 .

Berelson, W.M., D.E. Hammond, and K.S. Johnson (1987). Benthic fluxes and the cycling of biogenic silica and carbon in two southern California borderland basins, Geochimica et Cosmochimica Acta 51, 1345-1363 .

Berger, W.H. (1970). Planktonic foraminifera: selective solution and the lysocline, Marine Geology 8, 111-138 .

Berner, R.A. (1977). Stoichiometric models for nutrient regeneration in anoxic sediments, Limnology and Oceanography 22(5), 781-786 .

Berner, R.A. (1980). Early Diagenesis: A Theoretical Approach, Princeton University Press, Princeton, N.J.

Berner, R.A. (1982). Burial of organic carbon and pyrite sulfur in the modern ocean: Its geochemical and environmental significance, American Journal of Science 282, 451-573 .

Biscaye, P.E., R.F. Anderson, and B.L. Deck (1988). Fluxes of particles and constituents to the eastern United States continental slope and rise: SEEP-1, Continental Shelf Research 8(5-7), 855-904 .

Bischoff, J.L., R.E. Greer, and A.O. Luistro (1970). Composition of interstitial waters of marine sediments: Temperature of squeezing effect, Science 167, 1245-1246 .

Boudreau, B.P., and N.L. Guinasso, Jr. (1982). The influence of a diffusive sublayer on accretion, dissolution, and diagenesis at the sea floor, in The Dynamic Environment of the Ocean Floor, K.A. Fanning and F.T. Manheim, eds., Lexington Books, Lexington, Mass., 502 pp .

Boudreau, B.P., and J.T. Westrich (1984). The dependence of bacterial sulfate reduction on sulfate concentration in marine sediments, Geochimica et Cosmochimica Acta 48, 2503-2516 .

Broecker, W.S., and T.H. Peng (1982). Tracers in the Sea, Eldigio, New York, pp. 47-94 .

Calvert, S.E. (1983). Sedimentary geochemistry of silicon, in Silicon Chemistry and Biogeochemistry, Academic Press, London, pp. 143-186 .

Canfield, D.E. (1989). Sulfate reduction and oxic respiration in marine sediments: implications for organic carbon preservation in euxinic environments, Deep-Sea Research 36(1), 121-138 .

Christensen, E.R. (1982). A model for radionuclides in sediments influenced by mixing and compaction, Journal of Geophysical Research 87(C1), 566-572 .

Christensen, J.P., A.H. Devol, and W.M. Smethie, Jr. (1984). Biological enhancement of solute exchange between sediments and bottom water on the Washington continental shelf, Continental Shelf Research 3, 9-23 .

Christensen, J.P., W.M. Smethie, and A.H. Devol (1987). Benthic nutrient regeneration and denitrification on the Washington continental shelf, Deep-Sea Research 34(5/6), 1027-1047 .

Cochran, J.K. (1985). Particle mixing rates in sediments of the eastern equatorial Pacific: Evidence from ^{210}Pb,^{239}, ^{240}Pu, and ^{137}Cs distributions at MANOP sites , Geochimica et Cosmochimica Acta 49, 1195-1210 .

Codispoti, L.A., and J.P. Christensen (1985). Nitrification, denitrification, and nitrous oxide cycling in the eastern tropical Pacific Ocean, Marine Chemistry 16, 277-300 .

Dymond, J., and M. Lyle (1985). Flux comparisons between sediments and sediment traps in the eastern tropical Pacific: Implications for atmospheric CO_2 variations during the Pleistocene, Limnology and Oceanography 30(4), 699-712 .

Dymond, J., and R. Collier (1988). Biogenic particle fluxes in the equatorial Pacific: Evidence for both high and low productivity during the 1982-1983 El Niño, Global Biogeochemical Cycles 2(2), 129-137 .

Edmond, J.M. (1974). On the dissolution of carbonate and silicate in the deep ocean, Deep-Sea Research 21, 455-480 .

Edmond, J.M., C. Measures, R.E. McDuff, L.H. Chan, R. Collier, R., B. Grant, L.I. Gordon, and J.B. Corliss (1979). Ridge crest hydrothermal activity and the balances of the major and minor elements in the ocean: The Galapagos data, Earth and Planetary Science Letters 46, 1-18 .

Elderfield, H. (1981). Metal-organic associations in interstitial waters of Narragansett Bay sediments, American Journal of Science 281, 1184-1196 .

Elderfield, H., N. Luedtke, R.J. McCaffrey, and M. Bender (1981). Benthic studies in Narragansett Bay, American Journal of Science 281, 768-787 .

Emerson, S. (1985). Organic carbon preservation in marine sediments, in The Carbon Cycle and Atmospheric CO_2: Natural Variations Archean to Present, American Geophysical Union, Washington, D.C.

Emerson, S., and M.L. Bender (1981). Carbon fluxes at the sediment-water interface of the deep sea: Calcium carbonate preservation, Journal of Marine Research 39, 139-162 .

Emerson, S., and J.I. Hedges (1988). Processes controlling the organic carbon content of open ocean sediments, Paleoceanography 3(5), 621-634 .

Emerson, S., V. Grundmanis, and E. Graham (1982). Carbonate chemistry in marine pore waters: MANOP sites C and S, Earth and Planetary Science Letters 61, 220-232 .

Emerson, S., C. Stump, P.M. Grootes, M. Stuiver, G.W. Farwell, and F.H. Schmidt (1987). Estimates of degradable organic carbon in deep-sea surface sediments from ^{14}C concentrations, Nature 329, 51-53 .

Froelich, P.N., G.P. Klinkhammer, M.L. Bender, N.A. Luedtke, G.R. Heath, D. Cullen, P. Dauphin. D. Hammond, B. Hartman, and V. Maynard (1979). Early oxidation of organic matter in pelagic sediments of the eastern equatorial Atlantic: Suboxic diagenesis, Geochimica et Cosmochimica Acta 43, 1075-1090 .

Froelich, P.N., M.L. Bender, N.A. Luedtke, G.R. Heath, and T. DeVries (1982). The marine phosphorous cycle, American Journal of Science 282, 474-511 .

Goloway, F., and M. Bender (1982). Diagenetic models of interstitial nitrate profiles in deep sea suboxic sediments, Limnology and Oceanography 27(4), 624-638 .

Grundmanis, V., and J.W. Murray (1982). Stoichiometry of decomposing organic matter in aerobic marine sediments, Geochimica et Cosmochimica Acta 46, 1101-1121 .

Heggie, D., C. Maris, A. Hudson, J. Dymond, R. Beach, and J. Cullen (1987). Organic carbon oxidation and preservation in NW Atlantic continental margin sediments, in Geology and Geochemistry of Abyssal Plains, pp. 215-236 .

Henrichs, S.M., and W.S. Reeburgh (1987). Anaerobic mineralization of marine sediment organic matter: Rates and the role of anaerobic processes in the oceanic carbon economy, Geomicrobiology Journal 5(3/4), 191-237 .

Honjo, S. (1980). Material fluxes and modes of sedimentation in the mesopelagic and bathypelagic zones, Journal of Marine Research 38(1), 53-97 .

Hurd, D.C. (1972). Factors affecting solution rate of biogenic opal in seawater, Earth and Planetary Science Letters 15, 411-417 .

Hurd, D.C. (1983). Physical and chemical properties of siliceous skeletons, in Silicon Chemistry and Biogeochemistry, Academic Press, London.

Hurd, D.C., and F. Theyer (1975). Changes in the physical and chemical properties of biogenic silica from the central equatorial Pacific, 1, Solubility, specific surface area, and solution rate constants of acid-cleaned samples, in Analytical Methods in Oceanography, American Chemical Society, Washington, D.C.

Jahnke, R.A., and G.A. Jackson (1987). Role of sea floor organisms in oxygen consumption in the deep North Pacific Ocean, Nature 329, 621-623 .

Jahnke, R.S., R. Emerson, and J.W. Murray (1982a). A model of oxygen reduction, denitrification, and organic matter mineralization in marine sediments, Limnology and Oceanography 27, 610-623 .

Jahnke, R.S., D. Heggie, S. Emerson, and D. Graham (1982b). Pore waters of the central Pacific Ocean: Nutrient results, Earth and Planetary Science Letters 61, 233-256 .

Jorgensen, B.B. (1982). Mineralization of organic matter in the sea bed—the role of sulphate reduction, Nature 296, 643-645 .

Keir, R.S. (1983). Variation in the carbonate reactivity of deep-sea sediments: Determination from flux experiments, Deep-Sea Research 30, 279-296 .

Klinkhammer, G.P. (1980). Early diagenesis in sediments from the eastern equatorial Pacific, II, Pore water metal results, Earth and Planetary Science Letters 49, 81-101 .

Ledford-Hoffman, P.A., D.J. DeMaster, and C.A. Nittrouer (1986). Biogenic silica accumulation in the Ross Sea and the importance of Antarctic continental-shelf deposits in the marine silica budget, Geochimica et Cosmochimica Acta 50, 2099-2110 .

Li, Y-H., T. Takahashi, and W.S. Broecker (1969). Degree of saturation of $CaCO_3$ in the oceans, Journal of Geophysical Research 74, 5507-5525 .

Lisitzin, A.P., Y.A. Belyayev, Y.A. Bogdanov, and A.N. Bogoyavlensky (1967). Distribution, relationships and forms of silicon suspended in waters of the world ocean, International Geology Review 9, 604-623 .

Lyle, M., D.W. Murray, B.P. Finney, J. Dymond, J.M. Robbins, and K. Brooksforce (1988). The record of late Pleistocene biogenic sedimentation in the eastern tropical Pacific Ocean, Paleoceanography 3, 39-59 .

Mackin, J.E. (1986). The free-solution diffusion coefficient of boron: Influence of dissolved organic matter, Marine Chemistry 20, 131-140 .

Mangelsdorf, P.C., Jr., T.R.S. Wilson, and B. Daniell (1969). Potassium enrichments in interstitial waters of recent marine sediments, Science 165, 171-174 .

Martin, J.H., G.A. Knauer, D.M. Karl, and W.W. Broenkow (1987). VERTEX: Carbon cycling in the northeast Pacific, Deep-Sea Research 34(2), 267-285 .

Martin, J.M., and M. Meybeck (1979). Elemental mass balance of material carried by major world rivers, Marine Chemistry 7, 173-206 .

Martin, W.R. (1985). Transport of Trace Metals in Nearshore Sediments, PhD Thesis, M.I.T./W.H.O.I. Joint Program in Oceanography.

Martin, W.R., and F.L. Sayles (1987). Seasonal cycles of particle and solute transport processes in nearshore sediments: Rn-222/Ra-226 and Th-234/U-238 disequilibrium at a site in Buzzards Bay, MA., Geochimica et Cosmochimica Acta 51, 927-943 .

Martin, W.R., and M.L. Bender (1988). The variability of benthic fluxes and sedimentary remineralization rates in response to seasonally variable organic carbon rain rates in the deep sea: A modeling study, American Journal of Science 288, 561-574 .

Martin, W.R., M. Bender, M. Leinen, and J. Orchardo (1988). Benthic fluxes of NO_3, SiO_2, and O_2 across the equatorial high productivity zone at 135° W, EOS 69(44), 1264 .

McCorkle, D.C., S.R. Emerson, and P.D. Quay (1985). Stable carbon isotopes in marine pore waters, Earth and Planetary Science Letters 74, 13-26 .

McNichol, A.P., C. Lee, and E.R.M. Druffel (1988). Carbon cycling in coastal sediments: 1. A quantitative estimate of the remineralization of organic carbon in the sediments of Buzzards Bay, MA., Geochimica et Cosmochimica Acta 52, 1531-1543 .

Meybeck, M. (1982). Carbon, nitrogen, and phosphorous transport by world rivers, American Journal of Science 282, 401-450 .

Middelberg, J.J. (1989). A simple rate model for organic matter decomposition in marine sediments, Geochimica et Cosmochimica Acta 53, 1577-1581 .

Murray, J.W., S. Emerson, and R.A. Jahnke (1980). Pressure effect on the alkalinity of deep-sea interstitial water samples, Geochimica et Cosmochimica Acta 44, 963-972 .

Premuzic, E.T., C.M. Benkovitz, J.S. Gaffney, and J.J. Walsh (1982). The nature and distribution of organic matter in the surface sediments of world oceans and seas, Organic Geochemistry 4, 63-77 .

Reimers, C.E. (1987). An in situ microprofiling instrument for measuring interfacial pore water gradients: Methods and oxygen profiles from the North Pacific Ocean, Deep-Sea Research 34(12), 2019-2035 .

Reimers, C.E. (1989). Control of benthic fluxes by particulate supply, in Productivity in the Ocean: Present and Past, W.H. Berger, V.S. Smetacek, and G. Wefer, eds., John Wiley and Sons, London, pp. 217-233 .

Reimers, C.E., K.M. Fischer, R. Merewether, K.L. Smith, Jr., and R.A. Jahnke (1986). Oxygen microprofiles measured in situ in deep ocean sediments, Nature 320, 741-744 .

Revsbech, N.P., J. Sorensen, T.H. Blackburn, and J.P. Lomholt (1980). Distribution of oxygen in marine sediments measured with microelectrodes, Limnology and Oceanography 25(3), 403-411 .

Sayles, F.L. (1979). The composition and diagenesis of interstitial solutions—I. Fluxes across the seawater-sediment interface in the Atlantic Ocean, Geochimica et Cosmochimica Acta 43, 527-545 .

Sayles, F.L. (1981). The composition and diagenesis of interstitial solutions—II. Fluxes and diagenesis at the water-sediment interface in the high latitude north and South Atlantic, Geochimica et Cosmochimica Acta 45, 1061-1086 .

Sayles, F.L., and W.B. Curry (1988). $\delta^{13}C$, TCO_2, and the metabolism of organic carbon in deep sea sediments, Geochimica et Cosmochimica Acta 52, 2963-2978 .

Sayles, F.L., F.T. Manheim, and L.S. Waterman (1973a). Interstitial water studies on small core samples, Leg 15, in Initial Reports of the Deep Sea Drilling Project 15 , B. Heezen et al., ed., U.S. Government Printing Office, Washington, D.C., pp. 33-54 .

Sayles, F.L., T.R.S. Wilson, D.N. Hume, and P.C. Mangelsdorf (1973b). In situ sampler for marine sedimentary pore waters: Evidence for potassium depletion and calcium enrichment, Science 181, 154-156 .

Schink, D.R., N.L. Guinasso, Jr., and K.A. Fanning (1975). Processes affecting the concentration of silica at the sedimentwater interface of the Atlantic Ocean, Journal of Geophysical Research 80(21), 3013-3031 .

Smith, K.L., Jr., and K.R. Hinga (1983). Sediment community respiration in the deep sea, in The Sea, John Wiley & Sons, New York.

Suess, E., and P.J. Muller (1980). Productivity, sedimentation rate and sedimentary organic matter in the oceans, II. Elemental fractionation. Colloques Internationaux du C.N.R.S.—Biogeochemie de la Matiere Organique a l'Interface Eau-Sediment Marin 293, 17-26 .

Suess, E., P.J. Muller, H.S. Powell, and C.E. Reimers (1980). A closer look at nitrification in pelagic sediments, Geochemical Journal 14, 129-137 .

Takahashi, T., W.S. Broecker, and S. Langer (1985). Redfield ratio based on chemical data from isopycnal surfaces, Journal of Geophysical Research 90 (C4), 6907-6924 .

Turekian, K.K. (1965). Some aspects of the geochemistry of marine sediments, in Chemical Oceanography, J.P. Riley and G. Skirrow, eds., Academic Press, New York, pp. 81-126 .

Walsh, I., J. Dymond, and R. Collier (1988). Rates of recycling of biogenic components of settling particles in the ocean derived from sediment trap experiments, Deep-Sea Research 35, 43-58 .

Westrich, J.T., and R.A. Berner (1984). The role of sedimentary organic matter in bacterial sulfate reduction: The G model tested, Limnology and Oceanography 29(2), 236-249 .

Williams, P.M., and R.R.M. Druffel (1987). Radiocarbon in dissolved organic matter in the central North Pacific Ocean, Nature 330, 246-248 .

Wilson, T.R.S., J. Thomson, S. Colley, D.J. Hydes, N.C. Higgs, and J. Sorensen (1985). Early organic diagenesis: The significance of progressive subsurface oxidation fronts in pelagic sediments, Geochimica et Cosmochimica Acta 49, 811-822 .

Index